

THE FLOW OF NON-NEWTONIAN FLUIDS THROUGH  
POROUS MEDIA

Thesis for the Degree of Ph. D.  
MICHIGAN STATE UNIVERSITY  
HEE CHUNG PARK  
1972



3 1293 01747 8755

JHE 5



This is to certify that the

thesis entitled

THE FLOW OF NON-NEWTONIAN FLUIDS  
THROUGH POROUS MEDIA

presented by

HEE CHUNG PARK

has been accepted towards fulfillment  
of the requirements for

PH.D. degree in CHEMICAL ENGINEERING

*Martin C. Hawley*

Major professor

Date May 18, 1972

SEP 21 2004

## ABSTRACT

### THE FLOW OF NON-NEWTONIAN FLUIDS THROUGH POROUS MEDIA

By

Hee Chung Park

The Ergun equation is widely used to relate pressure drop to volumetric flow rate of Newtonian fluids in packed beds. In this study the Ergun equation was extended to non-Newtonian fluids by using an effective viscosity in place of the Newtonian viscosity. The effective viscosity was calculated based on the result of a hydrodynamic analysis of the capillary model of the packed bed using the appropriate constitutive equation for each non-Newtonian fluid.

Measurements of pressure drops and corresponding flow rates were made for several concentrations of aqueous solutions of three polymers (polyacrylamide, polyvinylpyrrolidone, and polymethylcellulose) flowing through packed beds, and the rheological properties of these aqueous polymer solutions were determined with a Weissenberg rheogoniometer.

The Sprigg's four-parameter model was selected to characterize the rheological properties of aqueous

solutions of polyacrylamide because these solutions exhibited viscoelastic behavior. The average percent deviation in the apparent viscosities between values predicted from the model and experiment for 103 data points was 3.4% for shear rates in the range 0.00675 to 851.0  $\text{sec}^{-1}$  for concentrations of 0.50, 0.25, 0.10, and 0.05 weight percent. The pressure drop-flow rate data for aqueous solutions of polyacrylamide were correlated very well by the Ergun equation whose effective viscosity was calculated based on the result of a hydrodynamic analysis of the capillary model of the packed bed using the Sprigg's model. The average percent deviation between the experimental values of friction factor and the corresponding values from the Ergun equation was 5.7% for 117 experimental points with the Sprigg's model. The corresponding deviations for the power-law model and the Ellis model were 19.1% and 9.3%, respectively.

Meter's four-parameter model was selected to characterize the rheological properties of aqueous solutions of polyvinylpyrrolidone because these solutions were purely viscous having both upper and lower limiting viscosities. The average percent deviation in the apparent viscosities between values predicted from the model and experiment for 98 data points was 2.1% for shear rates in the range 0.02689 to 1076.0  $\text{sec}^{-1}$  for concentrations of 4.0, 3.0, 1.0, and 0.5 weight percent. Large

deviations between experimental values of friction factor and those from the Ergun equation occurred for effective Reynolds numbers greater than one. A new correction parameter  $(D_p G_o / M(1 - \epsilon) \eta_o) (G_o \lambda / \rho D_p)$  was used to account for the deviation. Agreement was excellent after correction. The average percent deviation between the experimental values of friction factor and the corresponding values from the Ergun equation was 10.8% for 87 experimental points; before correction the deviation was greater than 60%.

The Herschel-Bulkley three-parameter model was used to characterize the rheological properties of aqueous solutions of polymethylcellulose because these solutions exhibited yield stresses with non-linear flow curves. The average percent deviation in the apparent viscosities between values predicted from the model and experiment for 72 data points was 1.7% for shear rates in the range 1.076 to 851.0  $\text{sec}^{-1}$ , for concentrations of 0.3 and 0.5 weight percent of each of two different molecular weights. The pressure drop-flow rate data for aqueous solutions of polymethylcellulose were correlated very well by the Ergun equation using the Herschel-Bulkley model for effective viscosity calculation. The average percent deviation between the experimental values of friction factor and the corresponding values from the Ergun equation was 8.2% for 139 experimental points.

Polymer solutions are adequately represented by the capillary model of the packed bed for effective Reynolds numbers less than one. The pressure drop-flow rate data for non-Newtonian fluids is not correlated very well by the Ergun equation for effective Reynolds numbers greater than one. It appears as though an improvement in the model for packed beds is required in order to account for inertial effects and surface effects of polymer solutions. Past investigators have used the power-law and the Ellis model to calculate the effective viscosity for packed beds. However, this work has shown that considerable improvement in accuracy of the friction factor predictions can be accomplished by using the rheological model which characterizes the shear stress-shear rate relationship with minimum error for calculating the effective viscosity for packed beds.

THE FLOW OF NON-NEWTONIAN FLUIDS  
THROUGH POROUS MEDIA

By

Hee Chung Park

A THESIS

Submitted to  
Michigan State University  
in partial fulfillment of the requirements  
for the degree of

DOCTOR OF PHILOSOPHY

Department of Chemical Engineering

1972

G 76070

To my brother

Hee Bock

## ACKNOWLEDGMENTS

No man of science is likely to achieve anything great, unless he brings to his work a zeal comparable with that of religion, and unless he is prepared to follow truth wherever it leads him. But zeal without strict discipline of the intellect will get him nowhere.

The author wishes to express his sincere appreciation to his major professor, Dr. M. C. Hawley, for providing his thoughtful guidance, genuine wisdom, and encouragement throughout the course of this investigation, and also for his painstaking review of this manuscript. He also wishes to extend his thanks to Dr. R. F. Blanks whose discussions and suggestions concerning the molecular aspects of polymer solution behavior have furthered the author's understanding of the physical phenomena observed in this investigation. Sincere appreciation is extended, also, to Dr. B. J. Meister of Dow and the Dow Chemical Company for the technical assistance and for furnishing the polymers and the Weissenberg Rheogoniometer used in this investigation. Other guidance committee members, Drs. M. H. Chetrick, C. M. Cooper, D. A. Anderson, and

R. H. Wasserman, are also deeply appreciated for their concern and interest in this investigation.

Finally, the author wishes to thank his wife, Inoak, for her patience, understanding, and encouragement in the entire period of his study.

## TABLE OF CONTENTS

Chapter	Page
1. INTRODUCTION . . . . .	1
2. RHEOLOGY . . . . .	6
2.1 Time-independent Non-Newtonian Fluids . . . . .	7
2.2 Time-dependent Non-Newtonian Fluids. . . . .	10
2.3 Viscoelastic Fluids . . . . .	12
2.4 Definitions of Material Functions . . . . .	14
2.5 Generalized Newtonian Fluids . . . . .	14
2.6 Specific Rheological Equation of State. . . . .	18
2.7 Linear Response of Viscoelastic Fluids. . . . .	22
2.8 Non-linear Response of Viscoelastic Fluids . . . . .	25
3. POROUS MEDIA PARAMETERS FOR VARIOUS CONSTITUTIVE EQUATIONS. . . . .	51
4. POLYACRYLAMIDE SYSTEM . . . . .	56
4.1 Chemistry . . . . .	56
4.2 Physical Properties . . . . .	58
4.3 Solution Preparation. . . . .	59
4.4 Rheology. . . . .	61
4.5 The Flow of Non-Newtonian Fluids Through Porous Media. . . . .	100
4.6 Conclusions. . . . .	118
5. POLYVINYLPIRROLIDONE SYSTEM . . . . .	120
5.1 Chemistry . . . . .	120
5.2 Physical Properties . . . . .	122
5.3 Rheology. . . . .	125
5.4 The Flow of Non-Newtonian Fluids Through Porous Media. . . . .	133
5.5 Conclusions. . . . .	142

Chapter	Page
6. POLYMETHYLCELLULOSE SYSTEM . . . . .	146
6.1 Chemistry . . . . .	146
6.2 Physical Properties. . . . .	148
6.3 Solution Preparation . . . . .	152
6.4 Rheology . . . . .	153
6.5 The Flow of Non-Newtonian Fluids Through Porous Media . . . . .	161
6.6 Conclusions . . . . .	169
7. CONCLUSIONS AND RECOMMENDATIONS . . . . .	172
7.1 Conclusions . . . . .	172
7.2 Recommendations . . . . .	177
NOMENCLATURE . . . . .	179
BIBLIOGRAPHY . . . . .	183
APPENDICES	
Appendix	
A. Development of Packed Bed Equations . . . . .	190
B. Viscometric Experiment: Detailed Description, Weissenberg Rheogoniometer. . . . .	234
C. Flow Experiment: Detailed Description . . . . .	252
D. Summary of Viscometric Data Steady State Shear Stress Measurement. . . . .	260
E. Summary of Viscometric Data Steady State Normal Stress Measurement . . . . .	264
F. Summary of Viscometric Data $H(\tau)$ , Relax- ation Time Spectrum vs. $t$ , Time . . . . .	266
G. Model Independent Parameters . . . . .	270
H. Model Independent Stress Parameters . . . . .	272
I. Summary of Viscometric Data and Ellis Model Calculation . . . . .	275

Appendix	Page
J. Summary of Viscometric Data and Power-Law Model Calculation . . . . .	279
K. Summary of Viscometric Data and Spriggs Model Calculation . . . . .	283
L. Summary of the Viscometric Data and Bird-Carreau Model Calculation . . . . .	291
M. Summary of the Constant Flow Rate Experiment Data and Newtonian Fluid Calculation .	295
N. Summary of the Constant Flow Rate Experiment Data and Power-Law Model Calculation .	296
O. Summary of the Constant Flow Rate Experiment Data and Ellis Model Calculation . .	300
P. Summary of the Constant Flow Rate Experiment Data and Sprigg's Model Calculation .	304
Q. Summary of Viscometric Data and Meter Model Calculation . . . . .	308
R. Summary of the Constant Flow Rate Experiment Data and Meter's Model Calculation. .	312
S. Summary of Viscometric Data and Herschel-Bulkley Model Calculation . . . . .	316
T. Summary of the Constant Flow Rate Experiment Data and Herschel-Bulkley Model Calculation . . . . .	320

## LIST OF TABLES

Table		Page
2.4-1	Summary of Definitions of Material Functions . . . . .	15
2.8-1	Components of $\Delta V$ . . . . .	28
2.8-2	Components of $V \cdot \nabla \tau$ . . . . .	29
2.8-3	Simple Shear Flow Notation . . . . .	30
3-1	Porous Media Parameters . . . . .	54
4.4-1	Power-law Parameters for Polyacrylamide Solutions as Obtained from a Weissenberg Rheogoniometer at 21°C. . . . .	86
4.4-2	Ellis Parameters for Polyacrylamide Solutions as Obtained from a Weissenberg Rheogoniometer at 21°C. . . . .	88
4.4-3	Spriggs 4-Constant Model Parameters for Polyacrylamide Solutions as Obtained from a Weissenberg Rheogoniometer at 21°C . . . . .	89
4.4-4	Bird-Carreau Model Parameters for Polyacrylamide Solutions as Obtained from a Weissenberg Rheogoniometer at 21°C. . . . .	99
4.4-5	Bird-Carreau Model Parameters for Polyacrylamide Solutions as Obtained from a Weissenberg Rheogoniometer at 21°C. . . . .	101
4.5-1	Summary of Experimental Data for Power-law Modification . . . . .	112
4.5-2	Summary of Experimental Data for Ellis Model Modification . . . . .	114
4.5-3	Summary of Experimental Data for Spriggs Model Modification . . . . .	115

Table	Page
4.5-4	Summary of Error Analysis . . . . . 117
5.3-1	Meter Model Parameters for PVP Solutions as Obtained from a Weissenberg Rheogoniometer at 21°C . . . . . 132
5.4-1	Summary of Experimental Data for PVP Solutions. . . . . 144
6.2-1	Viscosities of Methylcellulose of Various Molecular Weights . . . . . 150
6.4-1	Herschel-Bulkley Model Parameters for PMC Solutions as Obtained from a Weissenberg Rheogoniometer at 21°C . . . . . 159
6.5-1	Summary of Experimental Data for Herschel- Bulkley Modification . . . . . 170
B-1	Torsion Bar Calibration. . . . . 242
B-2	Normal Force Spring Calibration . . . . . 246
B-3	Gap Setting. . . . . 247
B-4	Rotation Shear Rates for Various Platens . . 250
D-1	Results for the Weissenberg Rheogoniometer for 0.50% Polyacrylamide Solution at 21°C . 260
D-2	Results for the Weissenberg Rheogoniometer for 0.25% Polyacrylamide Solution at 21°C . 261
D-3	Results for the Weissenberg Rheogoniometer for 0.10% Polyacrylamide Solution at 21°C . 262
D-4	Results for the Weissenberg Rheogoniometer for 0.05% Polyacrylamide Solution at 21°C . 263
E-1	Results for the Weissenberg Rheogoniometer for 0.50% Polyacrylamide Solution at 21°C . 264
E-2	Results for the Weissenberg Rheogoniometer . 265
F-1	Results of the Viscometric Experiments for 0.5% Separan Solution at 21°C . . . . . 266
F-2	Results of the Viscometric Experiments for 0.25% Separan Solution at 21°C. . . . . 267

Table		Page
F-3	Results of the Viscometric Experiments for 0.10% Separan Solution at 21°C . . . . .	268
F-4	Results of the Viscometric Experiments for 0.05% Separan Solution at 21°C . . . . .	269
G-1	Model Independent Parameters for 0.50% Separan Solution at 21°C . . . . .	270
G-2	Model Independent Parameters for 0.25% Separan Solution at 21°C . . . . .	270
G-3	Model Independent Parameters for 0.10% Separan Solution at 21°C . . . . .	271
G-4	Model Independent Parameters for 0.05% Separan Solution at 21°C . . . . .	271
H-1	Model Independent Stress Parameters for 0.5% Polyacrylamide Solution at 21°C . . . . .	272
H-2	Model Independent Stress Parameters for 0.25% Polyacrylamide Solution at 21°C. . . . .	273
H-3	Model Independent Stress Parameters for 0.1% Polyacrylamide Solution at 21°C . . . . .	274
H-4	Model Independent Stress Parameters for 0.05% Polyacrylamide Solution at 21°C. . . . .	274
I-1	Results for the Weissenberg Rheogoniometer for 0.50% Polyacrylamide Solution at 21°C. . . . .	275
I-2	Results for the Weissenberg Rheogoniometer for 0.25% Polyacrylamide Solution at 21°C. . . . .	276
I-3	Results for the Weissenberg Rheogoniometer for 0.10% Polyacrylamide Solution at 21°C. . . . .	277
I-4	Results for the Weissenberg Rheogoniometer for 0.05% Polyacrylamide Solution at 21°C. . . . .	278
J-1	Results for the Weissenberg Rheogoniometer for the 0.5% Polyacrylamide Solution at 21°C. . . . .	279

Table		Page
J-2	Results for the Weissenberg Rheogoniometer for the 0.25% Polyacrylamide Solution at 21°C . . . . .	280
J-3	Results for the Weissenberg Rheogoniometer for 0.10% Polyacrylamide Solution at 21°C . . . . .	281
J-4	Results for the Weissenberg Rheogoniometer for 0.05% Polyacrylamide Solution at 21°C . . . . .	282
K-1	Results for the Weissenberg Rheogoniometer for 0.50% Polyacrylamide Solution at 21°C . . . . .	283
K-2	Results for the Weissenberg Rheogoniometer for 0.25% Polyacrylamide Solution at 21°C . . . . .	284
K-3	Results for the Weissenberg Rheogoniometer for 0.10% Polyacrylamide Solution at 21°C . . . . .	285
K-4	Results for the Weissenberg Rheogoniometer for 0.05% Polyacrylamide Solution at 21°C . . . . .	286
K-5	Results for the Weissenberg Rheogoniometer for 0.50% Polyacrylamide Solution at 21°C.	287
K-6	Results for the Weissenberg Rheogoniometer for 0.25% Polyacrylamide Solution at 21°C.	288
K-7	Results for the Weissenberg Rheogoniometer for 0.10% Polyacrylamide Solution at 21°C.	289
K-8	Results for the Weissenberg Rheogoniometer for 0.05% Polyacrylamide Solution at 21°C.	290
L-1	Results for the Weissenberg Rheogoniometer for 0.50% Polyacrylamide Solution at 21°C.	291
L-2	Results for the Weissenberg Rheogoniometer for 0.25% Polyacrylamide Solution at 21°C.	292
L-3	Results for the Weissenberg Rheogoniometer for 0.10% Polyacrylamide Solution at 21°C.	293

Table		Page
L-4	Results for the Weissenberg Rheogoniometer for 0.05% Polyacrylamide Solution at 21°C.	294
M-1	Results for the Constant Flow Rate Experi- ments for Newtonian (Distilled Water) Fluid at 21°C . . . . .	295
N-1	Results for the Constant Flow Rate Experi- ments for 0.50% Polyacrylamide Solution at 21°C . . . . .	296
N-2	Results for the Constant Flow Rate Experi- ments for 0.25% Polyacrylamide Solution at 21°C . . . . .	297
N-3	Results for the Constant Flow Rate Experi- ments for 0.10% Polyacrylamide Solution at 21°C . . . . .	298
N-4	Results for the Constant Flow Rate Experi- ments for 0.05% Polyacrylamide Solution at 21°C . . . . .	299
O-1	Results for the Constant Flow Rate Experi- ments for 0.5% Polyacrylamide Solution at 21°C . . . . .	300
O-2	Results for the Constant Flow Rate Experi- ments for 0.25% Polyacrylamide Solution at 21°C . . . . .	301
O-3	Results for the Constant Flow Rate Experi- ments for 0.10% Polyacrylamide Solution at 21°C . . . . .	302
O-4	Results for the Constant Flow Rate Experi- ments for 0.05% Polyacrylamide Solution at 21°C . . . . .	303
P-1	Results for the Constant Flow Rate Experi- ments for 0.50% Polyacrylamide Solution at 21°C . . . . .	304
P-2	Results for the Constant Flow Rate Experi- ments for 0.25% Polyacrylamide Solution at 21°C . . . . .	305

Table		Page
P-3	Results for the Constant Flow Rate Experiments for 0.10% Polyacrylamide Solution at 21°C . . . . .	306
P-4	Results for the Constant Flow Rate Experiments for 0.05% Polyacrylamide Solution at 21°C . . . . .	307
Q-1	Results for the Weissenberg Rheogoniometer for 4.0% PVP Solution at 21°C. . . . .	308
Q-2	Results for the Weissenberg Rheogoniometer for 3.0% PVP Solution at 21°C. . . . .	309
Q-3	Results for the Weissenberg Rheogoniometer for 1.0% PVP Solution at 21°C. . . . .	310
Q-4	Results for the Weissenberg Rheogoniometer for 0.5% PVP Solution at 21°C. . . . .	311
R-1	Results for the Constant Flow Rate Experiments for 4.0% PVP Solution at 21°C. . . . .	312
R-2	Results for the Constant Flow Rate Experiments for 3.0% PVP Solution at 21°C. . . . .	313
R-3	Results for the Constant Flow Rate Experiments for 1.0% PVP Solution at 21°C. . . . .	314
R-4	Results for the Constant Flow Rate Experiments for 0.50% PVP Solution at 21°C . . . . .	315
S-1	Results for the Weissenberg Rheogoniometer for 0.05% PMC 400 Solution at 21°C . . . . .	316
S-2	Results for the Weissenberg Rheogoniometer for 0.3% PMC 400 Solution at 21°C . . . . .	317
S-3	Results for the Weissenberg Rheogoniometer for 0.5% PMC 25 Solution at 21°C. . . . .	318
S-4	Results for the Weissenberg Rheogoniometer for 0.3% PMC 25 Solution at 21°C. . . . .	319
T-1	Results for the Constant Flow Rate Experiments for 0.50% PMC 400 Solution at 21°C . . . . .	320
T-2	Results for the Constant Flow Rate Experiments for 0.30% PMC 400 Solution at 21°C . . . . .	321

Table		Page
T-3	Results for the Constant Flow Rate Experiments for 0.50% PMC 25 Solution at 21°C .	322
T-4	Results for the Constant Flow Rate Experiments for 0.30% PMC 25 Solution at 21°C .	323

## LIST OF FIGURES

Figure		Page
2.1-1	Flow Curves for Various Types of Time Independent Fluid . . . . .	11
2.2-1	Flow Curves for Thixotropic and Theoplectic Fluids in Single Continuous Experiments . . . . .	13
4.3-1	Schematic Diagram of the Stock Solution Preparation . . . . .	60
4.4-1	Reservoir Platen Arrangement . . . . .	64
4.4-2	Start-Up Experiment . . . . .	65
4.4-3	Shear Stress-Shear Rate Data for Aqueous Separan Ap 30 Solutions . . . . .	68
4.4-4	Non-Newtonian Viscosity of Separan Ap 30 Solutions. . . . .	69
4.4-5	Primary Normal Stress Difference Coefficient of Separan Ap 30 Solutions . . . . .	70
4.4-6	Relaxation Spectrum of Separan Ap 30 Solutions. . . . .	71
4.4-7	$\eta_0$ , Zero-Shear Viscosity, vs. C, Concentration . . . . .	77
4.4-8	$S_w$ , Recoverable Shear Strain, vs. $\dot{\gamma}$ , Shear Rate . . . . .	81
4.4-9	$G_w$ , Shear Modulus, vs. $\dot{\gamma}$ , Shear Rate . . . . .	83
4.4-10	Model Independent Parameter $\theta/\eta$ vs. $\dot{\gamma}$ . . . . .	85

Figure	Page
4.4-11	$(\tau_{12}(t)/\tau_{12}(0))$ , Unsteady State Shear Stress, vs. $t$ , Real Time for Polyacrylamide Solutions . . . . . 91
4.5-1	Schematic Diagram of the Equipment . . . . . 103
4.5-2	$f^*$ , Friction Factor vs. $N_{Re}$ , Reynolds Number for Newtonian Fluid . . . . . 106
4.5-3	Pressure Drop-Flow Rate Correlation for Flow of 0.50% Aqueous Solutions of Separan Ap 30 Through Packed Beds . . . . . 107
4.5-4	Pressure Drop-Flow Rate Correlation for Flow of 0.25% Aqueous Solutions of Separan Ap 30 Through Packed Beds . . . . . 108
4.5-5	Pressure Drop-Flow Rate Correlation for Flow of 0.10% Aqueous Solutions of Separan Ap 30 Through Packed Beds . . . . . 109
4.5-6	Pressure Drop-Flow Rate Correlation for Flow of 0.05% Aqueous Solutions of Separan Ap 30 Through Packed Beds . . . . . 110
4.5-7	The Effects of the Wall Correction Factor in Friction Factor-Reynolds Number Correlation for .50% Separan Ap 30 Solution . . . . . 111
5.3-1	Shear Stress-Shear Rate Behavior for Four Aqueous Solutions of PVP . . . . . 128
5.3-2	Non-Newtonian Viscosity for Four Aqueous Solutions of PVP . . . . . 129
5.3-3	Comparison of Experimental and Calculated Values of the Apparent Viscosity for Four Aqueous Solutions of PVP . . . . . 131
5.4-1	Pressure Drop-Flow Rate Correlation for Flow of 4.0% PVP Solutions Through Packed Beds . . . . . 136
5.4-2	Pressure Drop-Flow Rate Correlation for Flow of 3.0% PVP Solutions Through Packed Beds . . . . . 137

Figure	Page
5.4-3 Pressure Drop-Flow Rate Correlation for Flow of 1.0% PVP Solutions Through Packed Beds . . . . .	138
5.4-4 Pressure Drop-Flow Rate Correlation for Flow of 0.5% PVP Solutions Through Packed Beds . . . . .	139
5.4.5 Pressure Drop-Flow Rate Correlation for Flow of PVP Solutions Through Packed Beds. . . . .	143
6.2-1 Viscosity of Polymethylcellulose of Various Molecular Weights. . . . .	149
6.2-2 Typical Moisture Absorption of Methocel Products at Relative Humidity Shown at 20°C. . . . .	151
6.4-1 Shear Stress-Shear Rate Behavior for Four Aqueous Solutions of Polymethylcellulose.	157
6.4-2 Non-Newtonian Viscosity for Aqueous Solutions of Polymethylcellulose . . . .	158
6.4-3 Comparison of Experimental and Calculated Values of the Apparent Viscosity for Aqueous Solutions of Polymethylcellulose.	160
6.5-1 Pressure Drop-Flow Rate Correlation for Flow of 0.5% PMC 400 Solutions Through Packed Beds . . . . .	164
6.5-2 Pressure Drop-Flow Rate Correlation for Flow of .3% PMC 400 Solutions Through Packed Beds . . . . .	165
6.5-3 Pressure Drop-Flow Rate Correlation for Flow of 0.5% PMC 25 Solutions Through Packed Beds . . . . .	166
6.5-4 Pressure Drop-Flow Rate Correlation for Flow of 0.3% PMC 25 Solutions Through Packed Beds . . . . .	167
6.5-5 Pressure Drop-Flow Rate Correlation for Flow of Aqueous Solutions of Polymethylcellulose Through Packed Beds . . . .	168

Figure	Page
A.3-1 Cylindrical Shell of Fluid Over Which Momentum Balance is Made to Get the Velocity Profile . . . . .	199
A.3-2 Momentum Flux and Velocity Distributions in Flow in Cylindrical Tubes . . . . .	202
A.4-1 Stress Acting on a Cylindrical Element of Fluid of Radius R in Steady Flow. . . . .	212
A.5-1 Packing of Uniform Spheres . . . . .	233
A.5-1 Pore Space in Packing of Uniform Spheres . . . . .	233
A.5-2 Pendular Ring Between Two Spheres . . . . .	233
B.1 Typical Arrangement of the Weissenberg Rheogoniometer. . . . .	235
B.2 Arrangement of Normal Force Measurement . . . . .	243
B.3 Schematic Diagram of Normal Force Measurement System . . . . .	244
B.4 Correction Terms for Normal Stress Difference . . . . .	251
C.1 Brooks-Mite Rotometer . . . . .	255

## CHAPTER 1

### INTRODUCTION

The aims of this work were to measure and correlate friction factor data for the flow of non-Newtonian fluids through porous media and to characterize non-Newtonian fluids by a rheological equation of state more generally applicable than the commonly used power-law model. Rheological measurements were made on a number of rather different types of non-Newtonian fluids and several rheological models were compared and criticized in view of experimental data. Non-Newtonian fluids were categorized as: (a) purely viscous, (b) with yield stresses and non-linear flow curves, and (c) viscoelastic.

Many studies of the flow of fluids through porous media have been concerned with Newtonian fluids; i.e., fluids for which the relation between shear stress and shear rate is a simple proportionality. This includes gases and most homogeneous, non-polymeric liquids. In many branches of engineering one is faced with design problems for non-Newtonian fluids; i.e., fluids for which the relation between shear stress and shear rate is not

a simple proportionality. Suspensions and solutions of polymers are examples of this latter class of fluids. The vast majority of these "non-linear" fluids show a decrease of apparent viscosity with increasing shear rates.

The open literature was essentially devoid of any studies on the flow of non-Newtonian fluids through porous media until recently. During the past few years a number of papers in this area have appeared. Several different approaches were taken to treat the experimental flow data. Bird and Sadowski [1] and Sadowski [2, 3] correlated a friction factor with a modified Reynolds number. The correlation was based on Darcy's law and the Ellis equation for non-Newtonian fluids. Christopher and Middleman [4] and Marshall and Metzner [5] used a similar approach except that they used the power-law model for non-Newtonian fluids. Gregory and Griskey [6] developed a friction factor versus Reynolds number correlation based on the Mooney-Rabinowitch equation.

Chemical engineers have traditionally been employed in industries involving the manufacture of products from raw materials by chemical reactions and physical changes. The activities of many chemical engineers in industry involve the development of processes and the design and operation of production facilities. A major portion of the skills required by the engineer engaged in these activities is obtained through study of the transport

processes of mass, heat, and momentum. In particular, an understanding of fluid flow and the behavior of fluids in process equipment is a basic element of modern engineering training.

The flow of polymeric fluids is an important aspect of engineering science in the polymer industry. The conversion of high polymers to useful products by operations such as extrusion, molding, mixing, and calendaring constitutes a new and challenging branch of technology of polymeric fluids called polymer processing. This development has led to a demand for scientific engineering research into the area of polymeric fluid behavior, including synthetic polymers as well as natural polymers such as proteins, cellulose, and natural rubber.

Knowledge of flow of fluids through porous media is basic for many scientific and engineering applications. It is essential to the individual problems of such diversified fields as soil mechanics, ground water hydrology, industrial filtration of polymer solutions and slurries, ceramic engineering, and the movement of aqueous polymer solutions through sand in secondary oil operations. To the chemical engineer, such knowledge forms the basic background for the design of packed towers and reactors containing granular catalysts.

The impetus for this investigation is both of a practical and of a fundamental nature. There is interest

in the secondary recovery of oil from underground reservoirs by displacement of the oil with non-Newtonian fluids. Non-Newtonian fluid flow in liquid-solid chromatographic separations is common in the pharmaceutical industry. Very small concentrations of high molecular weight polymers will increase the solution viscosities to values greater than those for the reservoir oils.<sup>1</sup> Models which have been used to describe non-Newtonian fluid behavior have been tested in relatively simple flow geometries. A test of these models for a very complex flow geometry, such as that which exists in a packed bed, may lead to more confidence in the application of the models to any arbitrary flow geometry. These problems will be discussed in Chapter 2.

In order to construct a tractable mathematical model of the complicated flow system involved, it is necessary to resort to a number of simplifications. If the viscosity of the fluid is properly characterized, traditional treatments for the study of the fluid flow in porous media may be adequate.

The following assumptions were made for the present investigation:

- a. The fluid was treated as an incompressible and a continuous medium in which each point had a flow-path.

---

<sup>1</sup>Typical reservoir oil viscosities are generally less than 100 c.p. (Muskat, 1949, p. 96).

- b. The porous medium was isotropic, homogeneous, and of regular geometry.
- c. The flow of the fluids was isothermal and single-phase.
- d. The external forces on the fluids were homogeneous and time independent.
- e. For simplicity the gravity term was neglected.
- f. The inertia terms are omitted from the equations of fluid motion.
- g. Different parts of one sample were macroscopically identical. This means that a fluid particle proceeding through the porous medium found the same total probability for displacement along all points of its path.

The analysis for this investigation included the characterization of the non-Newtonian fluids with an appropriate rheological equation of state and the development of the Ergun equation, derived from the equations of motion and the rheological equation of state for an appropriate model of the packed bed.

## CHAPTER 2

### RHEOLOGY

The subject of non-Newtonian flow is a subdivision of rheology, "the science of flow and deformation of matter." In this chapter the equations of change and several rheological equations of state will be presented. Emphasis will be placed on the several "generalized Newtonian models" as well as the empirical viscoelastic rheological equations of state of Spriggs and Bird-Carreau.

The word fluid does not have a precise meaning. It may be said that the essential property of fluids is the absence of preferred configurations. Therefore, a fluid may be defined as that substance whose configuration can not be distorted. Some dictionaries define fluid as a substance capable of flowing.

Non-Newtonian fluids are defined as materials which do not conform to a direct proportionality between shear stress and shear rate. Because of negative definition of non-Newtonian behavior, an infinite number of possible rheological relationships exist for this class

of fluids and, as yet, no single equation has been proven which can describe exactly the shear rate-shear stress relationships of all such materials over all ranges of shear rates. As a result non-Newtonian fluids are classified in the following manner [120]:

1. Time-independent fluids . . . those for which the rate of shear at a given point is solely dependent upon the instantaneous shear stress at that point.
2. Time-dependent fluids . . . those for which the shear rate is a function of both magnitude and the time lapse between consecutive applications of shear stress.
3. Viscoelastic fluids . . . those that show partial elastic recovery upon removal of a deforming shear stress. Such materials possess properties of both fluid and elastic solids.

## §2.1 Time-independent Non-Newtonian Fluids

These purely viscous fluids are usually classified into two groups, fluids with yield stresses and fluids without yield stresses.

### §2.1.1 Fluids with Yield Stresses

The physical behavior of fluids with yield stresses is usually explained in terms of an internal

structure in three dimensions which is capable of preventing movement for values of shear stress less than the yield value,  $\tau_y$ . For  $\tau_{yx} > \tau_y$ , the internal structure collapses completely, allowing shearing movement to occur. When  $\tau_{yx} < \tau_y$ , the internal structure is considered to be reformed virtually instantaneously.

Examples of fluids with yield stresses may be found in the following materials: certain plastic melts, oil drilling mud, ores, sand in water, coal, cement, rock and chalk slurries, grain water suspension, chocolate mixtures, tooth paste, peat slurries, margarine and shortenings, greases, aqueous thorium oxide slurries, soap and detergent slurries, and paper pulp.

### §2.1.2 Fluids Without Yield Stresses

#### A. Pseudoplastic Fluids

The majority of non-Newtonian materials are found in this category. A logarithmic plot of  $\tau_{yx}$  vs.  $dv_x/dy$  for these materials is often found to be linear over a wide range of shear rates. Fluid dispersions of asymmetric molecules or particles are probably characterized by extensive entanglement of the particles when the fluid is at rest. Progressive disentanglement should occur under the influence of shearing forces, the particles tending to orient themselves in the direction of shear. This orienting influence is proportional to shear rate

and is opposed by the randomly disorienting effects of Brownian movement [7], the extent of which is determined only by the temperature of a given fluid.

Pseudoplastic behavior would also be consistent with the existence of highly solvated molecules or particles in the dispersion. Progressive shearing away of solvated layers with increasing shear rate would result in decreasing interaction between the particles (because of their smaller effective size) and consequent reduction in apparent viscosity.

Examples of pseudoplastic fluids may be found in the following materials: rubber solutions, adhesives, certain polymer solutions or melts, greases, starch suspensions, cellulose acetate solutions used in rayon manufacturing, mayonnaise, soap, detergent slurries, paper pulp, napalm, paints and dispersion media in certain pharmaceutical fluids.

#### B. Dilatant Fluids

Two phenomena have been observed with dilatant materials [8, 9]. Volumetric dilatancy denotes an increase in total volume under shear, whereas rheological dilatancy refers to an increase in apparent viscosity with increasing shear rate. It is this latter property which is usually associated with dilatant fluids, although these materials are far less common than pseudoplastic fluids.



Examples of materials which have been found to exhibit both volumetric and rheological dilatancy include the following materials: aqueous suspensions of titanium dioxide, some gum arabic and borax solutions, some corn flour and sugar solutions, starch, potassium silicate, gum arabic in water, quicksand, wet beach sand, many deflocculated pigment dispersions containing high suspension concentrations, solids such as mica, powdered quartz, and iron powder in low viscosity liquids.

Flow curves for various types of time-independent fluids and models relating  $\tau_{yx}$  to  $dv_x/dy$  are shown in Figure 2.1-1.

## §2.2 Time-dependent Non-Newtonian Fluids

These materials are usually classified into two groups, thixotropic fluids and rheopectic fluids, depending upon whether the shear stress decreases with time at a given shear rate and constant temperature.

### §2.2.1 Thixotropic Fluids

These substances exhibit a reversible decrease in shear stress with time at a certain rate of shear and fixed temperature. Flow curves for thixotropic fluids in continuous experiments in which the shear rate is steadily increased from zero to a maximum value and then immediately

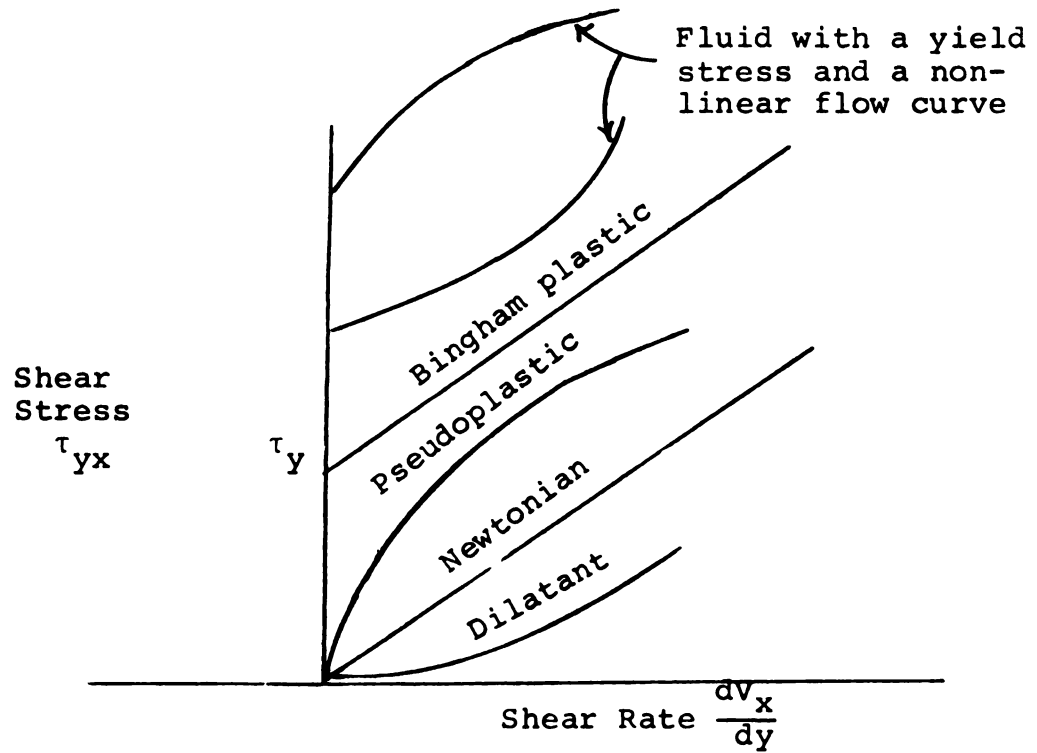


Figure 2.1-1 Flow Curves for Various Types of Time-independent Fluid

decreased steadily towards zero form a hysteresis loop as shown in Figure 2.2-1.

Examples of thixotropic properties have been found in the following materials: some solutions or melts of high polymers, oil well drilling muds, greases, margarine and shortening, printing inks, and many food materials.

### §2.2.2 Rheopectic Fluids

These materials, occasionally referred to as antithixotropic fluids, are relatively rare in occurrence. They exhibit a reversible increase in shear under isothermal conditions.

Rheopectic behavior is often explained in terms analogous to those used to account for dilatancy but in this case with more prolonged time periods for the structural changes involved. Although for some of these examples rheopexy is confined to moderate rates of shear, rheopectic characteristics have been observed in the following materials: bentonite clay suspensions, vanadium pentoxide suspensions, gypsum suspensions, certain soils, and dilute suspensions of ammonium oleate.

### §2.3 Viscoelastic Fluids

These materials exhibit both viscous and elastic properties. Oldroyd [10, 11] has shown that dispersions of one Newtonian fluid in another may lead to emulsions

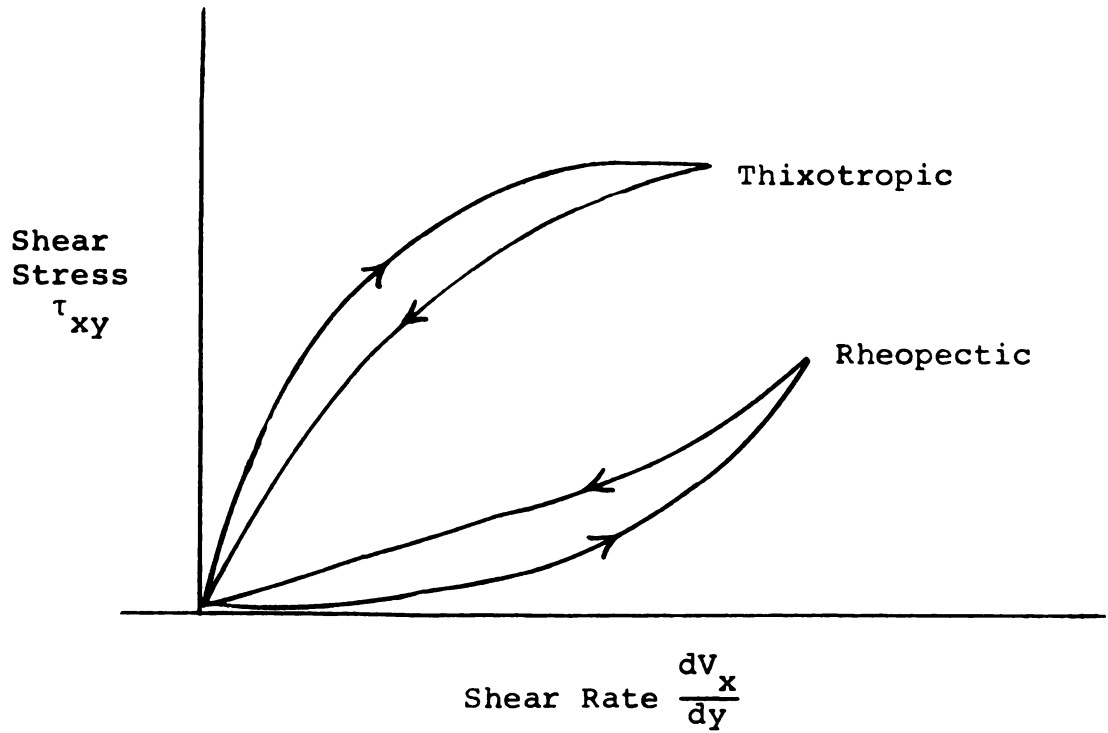


Figure 2.2-1 Flow Curves for Thixotropic and Rheopectic Fluids in Single Continuous Experiments

possessing both viscous and elastic characteristics. More discussions about viscoelasticity will be given in sections 6, 7, and 8.

#### §2.4 Definitions of Material Functions

Some investigators have defined various measurable material functions based on their experiments [14, 15, 16, 17]. The tube-flow experiment suggests the definition of a non-Newtonian viscosity  $\eta(\dot{\gamma})$ . The study of Weissenberg effects has led to the definition of a primary normal stress coefficient  $\theta(\dot{\gamma})$  and a secondary normal stress coefficient  $\beta(\dot{\gamma})$ . The oscillatory flow experiments have suggested the definition of the complex viscosity  $\eta^*(\omega)$  with its real and imaginary contributions  $\eta'(\omega)$  and  $\eta''(\omega)$ .

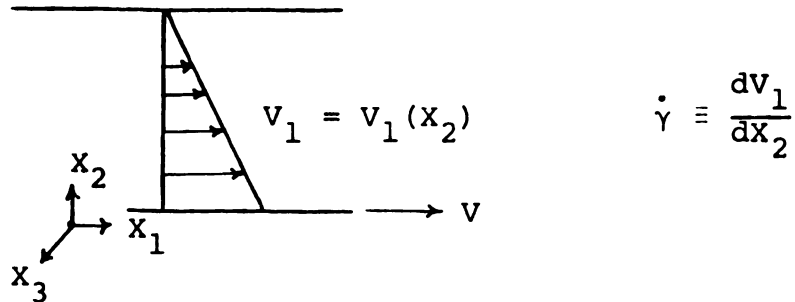
It is convenient to summarize the definition of these material functions at this point in terms of flow between two infinite flat plates. Such a summary is given in Table 2.4-1.

#### §2.5 Generalized Newtonian Fluids

In order to characterize the nature of different fluids, one introduces a rheological equation of state, or constitutive equation, which identifies the basic properties of the fluids. In particular, one must specify a relation between the deviatoric part of the shear stress tensor,  $\tau_{ij}$ , and the shear rate tensor  $e_{ij}$ .

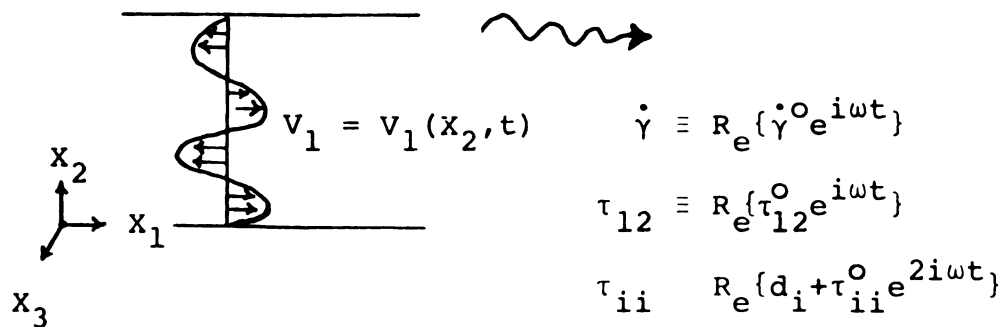
TABLE 2.4-1 Summary of Definitions of Material Functions

## 1. Steady Shear Flow



- a. Viscosity:  $\eta(\dot{\gamma}) \equiv \tau_{12}/(-\dot{\gamma})$
- b. Normal Stress Functions:  $\theta(\dot{\gamma}) \equiv (\tau_{11} - \tau_{22})/(-\dot{\gamma}^2)$   
 $\beta(\dot{\gamma}) \equiv (\tau_{22} - \tau_{33})/(-\dot{\gamma}^2)$

## 2. Small Amplitude Sinusoidal Oscillations



- a. Complex Viscosity  $\eta^*(\omega) \equiv \eta'(\omega) - i\eta''(\omega) \equiv \tau_{12}^0/(-\dot{\gamma}^0)$
- b. Complex Normal Stress Coefficients:  
 $\theta^*(\omega) \equiv \theta'(\omega) - i\theta''(\omega) \equiv (\tau_{11}^0 - \tau_{22}^0)/(-\dot{\gamma}^0)^2$   
 $\beta^*(\omega) \equiv \beta'(\omega) - i\beta''(\omega) \equiv (\tau_{22}^0 - \tau_{33}^0)/(-\dot{\gamma}^0)^2$
- c. Normal Stress Displacement Functions:  
 $\theta^d \equiv \text{Re}\{d_1 - d_2\}/-|\dot{\gamma}^0|^2$   
 $\beta^d \equiv \text{Re}\{d_2 - d_3\}/-|\dot{\gamma}^0|^2$

Consider a fluid placed in the region between two parallel plates which extend infinitely. The upper plate is held fixed, whereas the lower one is made to move with a constant velocity (see Table 2.4-1). The force per unit area in the x-direction required to maintain this motion is proportional to the velocity gradient:

$$\tau_{yx} = -\mu dv_x/dy \quad (2.5-1)$$

and the proportionality constant  $\mu$  is called the viscosity. This relation is called "Newton's law of viscosity." All the gases and simple liquids whose behaviors follow this relationship are called Newtonian fluids. It is also known that, if one can assume that the fluid is incompressible, then for motions more complicated than that above, Eq. (2.5-1) can be generalized to give [12]:

$$\begin{aligned} \tau_{ij} &= -\mu \left( \frac{\partial v_j}{\partial x_i} + \frac{\partial v_i}{\partial x_j} \right) \\ &= -2\mu e_{ij} \end{aligned} \quad (2.5-2)$$

which serves to define the quantities  $e_{ij}$ : in Eq. (2.5-2) it is understood that  $i$  and  $j$  can be  $x$ ,  $y$ , or  $z$ .

Reiner [18] suggested a most useful and practical constitutive relation which is so-called "generalized Newtonian fluid,"

$$\tau_{ij} = -2\eta e_{ij} \quad (2.5-3)$$

This relation is a simplification of the Reiner-Rivlin-Prager relation [19, 20]

$$\tau_{ij} = -\eta e_{ij} - \eta_c \Sigma_k e_{ik} e_{kj} \quad (2.5-4)$$

where  $\eta$  and the "cross viscosity"  $\eta_c$  are, in general, functions of the scalar invariants of the  $e$  tensor:

$$e_I = (e:\delta) = \Sigma_i e_{ii} \quad (2.5-5)$$

$$e_{II} = (e:e) = \Sigma_i \Sigma_j e_{ij} e_{ji} \quad (2.5-6)$$

$$e_{III} = \det e = \Sigma_i \Sigma_j \Sigma_k \epsilon_{ijk} e_{li} e_{2j} e_{3k} \quad (2.5-7)$$

Eq. (2.5-4) is the most general relation between  $\tau_{ij}$  and  $e_{ij}$  which does not involve space time derivative of either  $\tau_{ij}$  or  $e_{ij}$ . The exclusion of time effects restricts the relation to inelastic fluids.

The reduction of Eq. (2.5-4) to Eq. (2.5-3) depends upon several assumptions. First, in all cases, the fluid must be considered to be incompressible; therefore the first invariant  $e_I$  is identically equal to zero. Second, cross viscosity effects must be neglected, i.e.,  $\eta_c = 0$ . There is little known about cross viscosity effects. Some investigators [21, 22] have assumed  $\eta_c$  to be constant. Leigh [23], however, has shown that thermodynamic principles require that  $\eta_c$  not be a constant. Most investigators are content to ignore this

function. Third, it must be assumed that there exists no functional dependence of the viscosity  $\eta$  on the third invariant  $e_{III}$ . There is little known about the effect of  $e_{III}$  on fluid flow. In simple flow geometries, e.g., flow through a tube or a slit, the third invariant is identically zero.

## §2.6 Specific Rheological Equation of State

Numerous empirical functions of the form of Eq. (2.5-3) have been presented in the literature. Any proposed rheological model should represent the actual behavior of a fluid with accuracy, convenience, and simplicity. No known model describes the behavior of all non-Newtonian fluids with a reasonable number of constants. Different models may be necessary to describe different fluids or even the same fluid under different conditions. The best relationship for a given fluid is not necessarily known until an experiment is made on the fluid to relate  $\tau_{ij}$  and  $e_{ij}$ .

The power-law model is a rheological equation of state which is used widely [12],

$$\tau_{ij} = - \left\{ K \left( \frac{e:e}{2} \right)^{\frac{n-1}{2}} \right\} e_{ij} \quad (2.6-1)$$

where  $K$  and  $n$  are two positive fluid parameters determinable from viscometric experiments. When  $n = 1$  and  $K = \mu$ , this model becomes Newton's law of viscosity. This model

does not describe the limiting viscosity at zero shear rate  $\eta_0$ , the limiting viscosity at infinite shear rate  $\eta_\infty$ , and the relaxation time  $\lambda$ . It is also subject to Reiner's [19] "dimension objection" since the dimension of  $K$  will vary with the value of  $n$ .

Nonetheless, the model generally gives an adequate description of fluid behavior over an intermediate range of shear rates. Because of its mathematical simplicity, the power-law model has been used extensively by several investigators. It was used by Lyche and Bird [24] to extend the Graetz-Nusselt problem in heat transfer theory to non-Newtonian fluids. It was also used for an exact analysis of laminar tube and annular flow by Fredrickson and Bird [25], in an approximate analysis of flow around a sphere by Tomita [26] and Slattery [27], in a variational analysis of flow by Bird [28] and Schechter [29], and in laminar nonisothermal flow by Hanks and Christiansen [30], and in correlation of a friction factor with a modified Reynolds number by Christopher and Middleman [4], and Marshall and Metzner [5].

Ellis [19] and, more recently, Gee and Lyon [31], for plastic melts, proposed the following three-parameter model,

$$e_{ij} = - \left\{ \phi_0 + \phi_1 \left( \frac{\tau_{ij}}{2} \right)^{\frac{\alpha-1}{2}} \right\} \tau_{ij} \quad (2.6-2)$$

where  $\phi_0$ ,  $\phi_1$ , and  $\alpha$  are the fluid parameters. The Ellis model does not describe the limiting viscosity at infinite shear rate  $\eta_\infty$ , but more important is the fact that it describes the limiting viscosity at zero shear rate  $\eta_0 = 1/\phi_0$  for polymer solutions.

An alternate form for Eq. (2.6-2) has been suggested by Bird, viz.,

$$e_{ij} = - \frac{1}{\eta_0} \left\{ 1 + \left( \frac{\sqrt{1/2}(\tau:\tau)}{\tau_{1/2}} \right)^{\alpha-1} \right\} \tau_{ij} \quad (2.6-3)$$

where  $\eta_0$ ,  $\tau_{1/2}$ , and  $\alpha$  are the fluid parameters. The shear stress  $\tau_{1/2}$  is that value of shear stress for which the corresponding non-Newtonian viscosity has dropped off to one-half of the value of the limiting viscosity at zero shear rate  $\eta_0$ . The introduction of the fluid parameter  $\tau_{1/2}$  enabled the elimination of the dimensional objection to Eq. (2.6-2). Slattery and Bird [32] used the Ellis model to predict the drag coefficients for flow around a sphere. They found that the three-parameter model in Eq. (2.6-3) provided a better description of non-Newtonian behavior than the two-parameter power-law model. Ree and Eyring [33] discussed several successful applications of Eq. (2.6-3) to polymeric and colloidal systems. The application of this model to various flow geometries (McEachern [34], for flow through tube, and Ziegenhagen [35], for flow around sphere) led to very formidable mathematical expressions of the flow behavior.

A four-parameter generalization of the Ellis model, in which there is limiting viscosities at both zero shear rate and infinite shear rate, is that proposed by Meter [36]

$$\tau_{ij} = - \left[ \eta_{\infty} + \frac{\eta_0 - \eta_{\infty}}{1 + \left[ \frac{\sqrt{\frac{1}{2}(\tau:\tau)}}{\tau_m} \right]^{\alpha-1}} \right] e_{ij} \quad (2.6-4)$$

where  $\eta_0$ ,  $\eta_{\infty}$ ,  $\tau_m$ , and  $\alpha$  are the fluid parameters. The Meter's model in Eq. (2.6-4) may be thought of as an extension of the Peek-Mclean model ( $\alpha = 2$ ) [37] and the Reiner-Phillippoff model ( $\alpha = 3$ ) [19, 38]. The parameter  $\tau_m$  is the value of the shear stress for which the corresponding non-Newtonian viscosity has dropped off to the arithmetic mean of the limiting viscosities, i.e., to the value of  $\frac{1}{2}(\eta_0 + \eta_{\infty})$ . The constant  $\alpha$  indicates the abruptness of the transition from  $\eta_0$  to  $\eta_{\infty}$ . Meter [39] has successfully applied this model to the description of the turbulent flow through tubes of seven hydroxyethyl-cellulose solutions. For many fluids,  $\eta_{\infty}$  is at least an order of magnitude smaller than  $\eta_0$  so that Eq. (2.6-4) can be rewritten as:

$$e_{ij} = - \frac{1}{\eta_0} \left[ 1 + \left( \frac{\sqrt{\frac{1}{2}(\tau:\tau)}}{\tau_m} \right)^{\alpha-1} \right] \left[ \sum_{j=0}^{\infty} \left( - \frac{\eta_{\infty}}{\eta_0} \left( \frac{\sqrt{\frac{1}{2}(\tau:\tau)}}{\tau_m} \right)^{\alpha-1} \right)^j \right] \tau_{ij} \quad (2.6-5)$$

by rearranging and then expanding in powers of  $\eta_\infty/\eta_0$ . In this form, the Meter's model may be considered to be the Ellis model with a small perturbation on it. Equations (2.6-4) and (2.6-5) reduce to Newton's law for the limit in which  $\tau_m$  approaches infinity.

Herschel and Bulkley [40, 41] proposed a three-parameter model

$$\tau_{ij} - \tau_y = \left[ \mu_0 \left( \frac{e:e}{2} \right)^{\frac{1-m}{2}} \right]^{\frac{1}{m}} e_{ij} \quad (2.6-6)$$

where  $\tau_y$ ,  $\mu_0$ , and  $m$  are the fluid parameters. This model is the combination of the Bingham plastic model and the power-law model. In evaluating the parameters in this model, the yield stress  $\tau_y$  is first read from the flow curve. Parameters  $m$  and  $\mu_0$  are then obtainable from the slope and intercept of a logarithmic plot of  $-dv_z/dr$  vs.  $\tau_{rz} - \tau_y$ . There are not many applications of this model reported in the literature.

## §2.7 Linear Response of Viscoelastic Fluids

Although the generalized Newtonian theory, in its various forms, describes non-Newtonian fluid behavior quite well, it fails to predict the normal stress effects and the viscoelastic effects associated with time-dependent phenomena.

Normal stress effects were demonstrated by Weissenberg's [42] experiments in which various types of fluids

were sheared in a gap between two concentric cylinders. Greensmith and Rivlin [43], for a modified parallel-plate viscometer, found that the fluid, in manometer tubes placed at various radii into the fixed plate of the viscometer, tended to rise in the center manometer tubes, while the second plate rotated at a constant angular velocity. Markovitz and Williamson [44] noted the same effect for a modified cone-and-plate viscometer. Transient and dynamic (oscillatory) experiments [45] exhibit behavior, for viscoelastic fluids, which are not predicted by the generalized Newtonian theory.

Linear behavior is defined as that in which the measured value of a material property is unaffected by a change in magnitude of shear stress and shear rate. Within the framework of linear behavior and sinusoidal shearing, a significant achievement of molecular theory exists. Zimm [46], Rouse [47], and Bueche [48] have all proposed theories which relate the response of dilute polymer solutions to such parameters  $c$  (number-concentrations of solute molecules),  $T$  (absolute temperature),  $\eta_0$  (solution viscosity at zero shear rate), and  $\eta^{(s)}$  (solvent viscosity, Newtonian). Theoretical similarities between all three involve the assumptions:

1. Dilution to the extent that solute molecules have no direct interaction with each other.

2. "Segmented necklace" structural model, highly flexible to the point that a Gaussian distribution describes relative positions of the segments along the molecular chain.
3. Responsiveness to the random restorative forces of entropy, i.e., Brownian motion.

From these and other postulates, a differential equation can be written to describe a balance between distorting and restoring forces acting on the cooperating segments of the entire molecules. Rouse and Zimm obtained solutions expressible in terms of the complex viscosity<sup>1</sup>  $\eta^*(\omega)$ :

$$\eta^* - \eta(s) = CkT \sum_{p=1}^N \frac{\lambda_p}{1 + i\omega\lambda_p} \quad (2.7-1)$$

where  $\lambda_p$  is the relaxation time of the p'th mode of motion, and k is Boltzmann's constant. The Rouse assumption of a "free-draining" molecular coil led to:

$$\lambda_p = \left[ \frac{6(\eta_0 - \eta(s))}{\pi^2 CkT} \right]^{1/2} \equiv \left[ \lambda_R \right] \frac{1}{p} \quad (2.7-2)$$

---

<sup>1</sup>Complex notation is a convenience for manipulating simultaneously two separate equations: one describing the component of stress in-phase with the shear, the other describing the out-of-phase component. Thus we assume  $\tau_{12} = \text{Re}\{\tau_{12}^0 e^{i\omega\tau}\}$  and  $e_{12} = \text{Re}\{e_{12}^0 e^{i\omega\tau}\}$  in which  $\tau_{12}^0$ ,  $e_{12}^0$  are complex amplitudes and  $\omega = 2\pi f$  is the radian frequency. Then we define:

$$\eta^*(\omega) \equiv \tau_{12}^0 / e_{12}^0 \equiv \eta'(\omega) - i\eta''(\omega)$$

where  $\lambda_R$  is the longest relaxation time constant. Zimm's introduction of hydrodynamic interaction between segments gave the result:

$$\lambda_p = \left[ \lambda_R \right] \frac{1.71}{\Lambda_p} \quad (2.7-3)$$

where the  $\Lambda_p$  are numerical solutions to a complicated equation. Bueche's concepts, similar to those of Rouse, produced a slightly different expression with relaxation times twice the magnitude of Rouse's.

## §2.8 Non-linear Response of Viscoelastic Fluids

In recent years several models have been proposed which describe non-Newtonian viscosity, normal stresses, and oscillatory phenomena of viscoelastic fluids [49, 50, 51, 52, 53]. Most of these theories have been partially successful in describing some of the observed features of viscoelastic phenomena. Naturally none of them seems to be able to simulate, without ambiguity, all features of viscoelastic phenomena and certain other effects observed in complex fluids. Most of these theories and special cases of the more general theories are naturally subject to certain assumptions. Typical assumptions include:

1. An absence of peculiarities within the fluid or between the fluid and the confining boundaries which would cause the no-slip criterion to be violated.

2. No preferred orientation by the fluid with respect to the confining boundaries.
3. Absence of a yield stress.
4. No time-dependent behavior of the type referred to as thixotropy, rheopexy, etc.
5. The fluid is a continuum rather than a collection of discrete particles.

Molecular theories have also been developed which attempt to portray certain viscoelastic phenomena and non-Newtonian viscosity behavior in terms of inter- and intramolecular forces, polydispersity, coil rigidity, network and entanglement effects, and other morphological parameters [54, 55, 56].

Models of great generality, and great complexity, have been proposed by Rivlin and Erickson [57], in terms of functions of time rather than time constants, and by Coleman and Noll [14, 15], in terms in functionals evaluated at different times.

#### §2.8.1 Sprigg's Four-parameter Model

Spriggs proposed [58] a non-linear extension of the generalized Maxwell model as a constitutive equation for viscoelastic fluids. The non-linear operator which is a special case of the one used by Oldroyd in formulating his 8-constant model [11] is given by

$$F_{\epsilon} \tau = \frac{D\tau}{Dt} - (1 + \epsilon)(e \cdot \tau + \tau \cdot e - \frac{2}{3} t_r(\tau \cdot e) \delta) \quad (2.8-1)$$

where

$$\frac{D\tau}{Dt} = \frac{\partial \tau}{\partial t} + V \cdot \nabla \tau + \omega \cdot \tau - \tau \cdot \omega \quad (2.8-2)$$

Here  $2e \equiv \nabla V + (\nabla V)^T$ ,  $2\omega \equiv \nabla V - (\nabla V)^T$  and  $\epsilon$  is an adjustable dimensionless parameter. The components of  $\nabla V$  and  $V \cdot \nabla \tau$  in rectangular, cylindrical, and spherical coordinates are tabulated in Tables 2.8-1 and 2.8-2. Simple shear flow notation is also tabulated in Table 2.8-3.

In terms of operator  $F_{\epsilon}$  defined in Eq. (2.8-1), the extension of the generalized Maxwell model is given by

$$\tau^p + \lambda_p F_{\epsilon} \tau^p = -2\eta_p e \quad (2.8-3)$$

$$\tau = \sum_{p=1}^{\infty} \tau^p \quad (2.8-4)$$

where  $\lambda_p$  and  $\eta_p$  are constants which characterize the linear viscoelastic behavior of the fluid. The  $\tau^p$  are given an interpretation in the "spring and dashpot" theory of linear viscoelasticity [59]. The components of  $\tau^p$  are differentiated and integrated in the same manner as the component of  $\tau$ .

If one lets

$$\lambda_p \equiv \lambda p^{-\alpha} \quad (2.8-5)$$

TABLE 2.8-1 Components of  $\Delta V$ 


---



---

 Rectangular Coordinate  $(x, y, z)$ 

$$\nabla V = \begin{bmatrix} \frac{\partial V_x}{\partial x} & \frac{\partial V_y}{\partial x} & \frac{\partial V_z}{\partial x} \\ \frac{\partial V_x}{\partial y} & \frac{\partial V_y}{\partial y} & \frac{\partial V_z}{\partial y} \\ \frac{\partial V_x}{\partial z} & \frac{\partial V_y}{\partial z} & \frac{\partial V_z}{\partial z} \end{bmatrix}$$

Cylindrical Coordinate  $(r, \theta, z)$ 

$$\nabla V = \begin{bmatrix} \frac{\partial V_r}{\partial r} & \frac{\partial V}{\partial r} & \frac{\partial V_z}{\partial r} \\ \frac{1}{r} \frac{\partial V_r}{\partial \theta} - \frac{V_\theta}{r} & \frac{1}{r} \frac{\partial V_\theta}{\partial \theta} + \frac{V_r}{r} & \frac{1}{r} \frac{\partial V_z}{\partial \theta} \\ \frac{\partial V_r}{\partial z} & \frac{\partial V_\theta}{\partial z} & \frac{\partial V_z}{\partial z} \end{bmatrix}$$

Spherical Coordinate  $(r, \theta, \phi)$ 

$$\nabla V = \begin{bmatrix} \frac{\partial V_r}{\partial r} & \frac{\partial V_\theta}{\partial r} & \frac{\partial V_\phi}{\partial r} \\ \frac{1}{r} \frac{\partial V_r}{\partial \theta} - \frac{V_\theta}{r} & \frac{1}{r} \frac{\partial V_\theta}{\partial \theta} + \frac{V_r}{r} & \frac{1}{r} \frac{\partial V_\phi}{\partial \theta} \\ \frac{1}{r \sin \theta} \frac{\partial V_r}{\partial \phi} - \frac{V_\phi}{r} & \frac{1}{r \sin \theta} \frac{\partial V_\theta}{\partial \phi} - \frac{V_\phi}{r} \cot \theta & \frac{1}{r \sin \theta} \frac{\partial V_\phi}{\partial \phi} + \frac{V_r}{r} + \frac{V_\theta}{r} \cot \theta \end{bmatrix}$$

TABLE 2.8-2 Components of  $V \cdot \nabla \tau$ For Symmetrical Rectangular Coordinate  $(x, y, z)$ 

$$V \cdot \nabla = V_x \frac{\partial}{\partial x} + V_y \frac{\partial}{\partial y} + V_z \frac{\partial}{\partial z}, \quad (V \cdot \nabla \tau)_{ij} = (V \cdot \nabla) \tau_{ij}$$

$$V \cdot \nabla \tau = \begin{bmatrix} (V \cdot \nabla) \tau_{xx} & (V \cdot \nabla) \tau_{xy} & (V \cdot \nabla) \tau_{xz} \\ (V \cdot \nabla) \tau_{yx} & (V \cdot \nabla) \tau_{yy} & (V \cdot \nabla) \tau_{yz} \\ (V \cdot \nabla) \tau_{zx} & (V \cdot \nabla) \tau_{zy} & (V \cdot \nabla) \tau_{zz} \end{bmatrix}$$

For Cylindrical Coordinate  $(r, \theta, z)$ 

$$V \cdot \nabla = V_r \frac{\partial}{\partial r} + \frac{V_\theta}{r} \frac{\partial}{\partial \theta} + V_z \frac{\partial}{\partial z}$$

$$V \cdot \nabla \tau = \begin{bmatrix} (V \cdot \nabla) \tau_{rr} - 2 \frac{V_\theta}{r} \tau_{r\theta} & (V \cdot \nabla) \tau_{r\theta} + \frac{V_\theta}{r} (\tau_{rr} - \tau_{\theta\theta}) & (V \cdot \nabla) \tau_{rz} - \frac{V_\theta}{r} \tau_{\theta z} \\ (V \cdot \nabla) \tau_{r\theta} + \frac{V_\theta}{r} (\tau_{rr} - \tau_{\theta\theta}) & (V \cdot \nabla) \tau_{\theta\theta} + 2 \frac{V_\theta}{r} \tau_{r\theta} & (V \cdot \nabla) \tau_{\theta z} + \frac{V_\theta}{r} \tau_{rz} \\ (V \cdot \nabla) \tau_{rz} - \frac{V_\theta}{r} \tau_{\theta z} & (V \cdot \nabla) \tau_{\theta z} + \frac{V_\theta}{r} \tau_{rz} & (V \cdot \nabla) \tau_{zz} \end{bmatrix}$$

For Spherical Coordinate  $(r, \theta, \phi)$ 

$$V \cdot \nabla = V_r \frac{\partial}{\partial r} + \frac{V_\theta}{r} \frac{\partial}{\partial \theta} + \frac{V_\phi}{r \sin \theta} \frac{\partial}{\partial \phi}$$

$$V \cdot \nabla \tau = \begin{bmatrix} A & B & C \\ B & D & E \\ C & E & F \end{bmatrix}$$

$$A = (V \cdot \nabla) \tau_{rr} - 2 \frac{V_\theta}{r} \tau_{r\theta} - 2 \frac{V_\phi}{r} \tau_{r\phi}$$

$$B = (V \cdot \nabla) \tau_{r\theta} + \frac{V_\theta}{r} (\tau_{rr} - \tau_{\theta\theta}) - \frac{V_\phi}{r} (\tau_{\theta\phi} + \tau_{r\phi} \cot \theta)$$

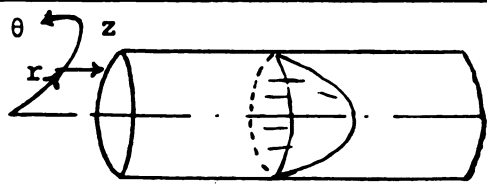
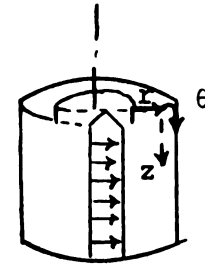
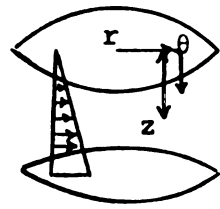
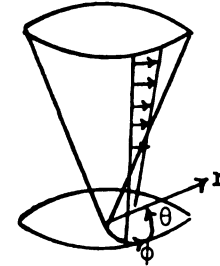
$$C = (V \cdot \nabla) \tau_{r\phi} + \frac{V_\phi}{r} [(\tau_{rr} - \tau_{\phi\phi}) + \tau_{r\theta} \cot \theta] - \frac{V_\theta}{r} \tau_{\theta\phi}$$

$$D = (V \cdot \nabla) \tau_{\theta\theta} + 2 \frac{V_\theta}{r} \tau_{r\theta} - 2 \frac{V_\phi}{r} \tau_{\theta\phi} \cot \theta$$

$$E = (V \cdot \nabla) \tau_{\theta\phi} + \frac{V_\phi}{r} [\tau_{r\theta} + (\tau_{\theta\theta} - \tau_{\phi\phi}) \cot \theta] + \frac{V_\theta}{r} \tau_{r\phi}$$

$$F = (V \cdot \nabla) \tau_{\phi\phi} + 2 \frac{V_\phi}{r} \tau_{r\phi} + 2 \frac{V_\theta}{r} \tau_{\theta\phi} \cot \theta$$

TABLE 2.8-3 Simple Shear Flow Notation

Flow Geometry	Coordinate Notation		
	1	2	3
 <p>1. Poiseuille Flow</p>	$z$	$r$	$\theta$
 <p>2. Couette Flow</p>	$\theta$	$r$	$z$
 <p>3. Parallel Plate Torsion</p>	$\theta$	$z$	$r$
 <p>4. Cone and Plate Torsion</p>	$\phi$	$\theta$	$r$

and

$$\eta_p \equiv \eta_0 \lambda^p / \sum_{p=1}^{\infty} p^{-\alpha} \quad \lambda_p = \frac{\eta_0}{p^\alpha Z(\alpha)} \quad (2.8-6)$$

where  $Z(\alpha) = \sum_{p=1}^{\infty} p^{-\alpha}$  denotes the Riemann zeta-function [60], then, expressions for the material functions  $\eta^*$ ,  $\theta^*$ ,  $\theta^d$ ,  $\beta^*$ ,  $\beta^d$ ,  $\eta$ ,  $\theta$ , and  $\beta$  can be derived in terms of four parameters: (1) a zero-shear viscosity  $\eta_0$ , (2) a characteristic time  $\lambda$ , (3) a dimensionless parameter  $\alpha$  which describes the slope of  $\log \eta'$  vs.  $\log \omega$  and  $\log \eta$  vs.  $\log \dot{\gamma}$  plots in the "power-law" region, and (4) a dimensionless parameter  $\epsilon$  which accounts for deviations from the Weissenberg [61] hypothesis that  $\tau_{22} - \tau_{33} = 0$ .

#### §2.8.1.1 Derivation of Material Functions

For simple shearing motion, the velocity field has the form  $V_1 = V_1(X_2, t)$ ,  $V_2 = 0$ ,  $V_3 = 0$ . Then the only non-vanishing components of the  $e$  and  $\omega$  tensors are  $e_{12} = e_{21} = \omega_{21} = -\omega_{12} = \dot{\gamma}/2$ , where  $\dot{\gamma} \equiv dV_1/dX_2$ . For the  $\tau$  tensor one has  $\tau_{12} = \tau_{21}$  and  $\tau_{13} = \tau_{31} = \tau_{23} = \tau_{32} = 0$ . Then Eq. (2.8-3) becomes:

$$\begin{aligned}
& (1 + \lambda_p \frac{\partial}{\partial t}) \begin{bmatrix} \tau_{11}^P & \tau_{12}^P & 0 \\ \tau_{12}^P & \tau_{22}^P & 0 \\ 0 & 0 & \tau_{33}^P \end{bmatrix} + \frac{\dot{\gamma}}{2} \lambda_p \begin{bmatrix} -(\frac{8}{3} + \frac{2}{3}\epsilon)\tau_{12}^P & -\epsilon\tau_{11}^P - (2+\epsilon)\tau_{22}^P & 0 \\ -\epsilon\tau_{11}^P - (2+\epsilon)\tau_{22}^P & (\frac{4}{3} - \frac{2}{3}\epsilon)\tau_{12}^P & 0 \\ 0 & 0 & \frac{4}{3}(1+\epsilon)\tau_{12}^P \end{bmatrix} \\
& = -\eta_p \begin{bmatrix} 0 & \dot{\gamma} & 0 \\ \dot{\gamma} & 0 & 0 \\ 0 & 0 & 0 \end{bmatrix} \tag{2.8-7}
\end{aligned}$$

From this matrix

$$\tau_{12}^P + \lambda_p \frac{\partial \tau_{12}^P}{\partial t} - \lambda_p (\epsilon\tau_{11}^P + (2+\epsilon)\tau_{22}^P) \frac{\dot{\gamma}}{2} = -\eta_p \dot{\gamma} \tag{2.8-8}$$

$$\tau_{11}^P + \lambda_p \frac{\partial \tau_{11}^P}{\partial t} - \lambda_p (\frac{8}{3} + \frac{2}{3}\epsilon)\tau_{12}^P \frac{\dot{\gamma}}{2} = 0 \tag{2.8-9}$$

$$\tau_{22}^P + \lambda_p \frac{\partial \tau_{22}^P}{\partial t} + \lambda_p (\frac{4}{3} - \frac{2}{3}\epsilon)\tau_{12}^P \frac{\dot{\gamma}}{2} = 0 \tag{2.8-10}$$

$$\tau_{33}^P + \lambda_p \frac{\partial \tau_{33}^P}{\partial t} + \lambda_p (\frac{4}{3} + \frac{4}{3}\epsilon)\tau_{12}^P \frac{\dot{\gamma}}{2} = 0 \tag{2.8-11}$$

Since  $\tau_{11} + \tau_{22} + \tau_{33} = 0$ , only three of these equations are independent.

### A. Non-Newtonian Viscosity and Normal Stresses

For steady simple shearing,  $\partial\tau_{ij}/\partial t = 0$ ,  $i, j = 1, 2, 3$ , then Equations (2.8-8) through (2.8-11) become:

$$\tau_{12}^p - \lambda_p (\epsilon\tau_{11}^p + (2+\epsilon)\tau_{22}^p) \frac{\dot{\gamma}}{2} = -\eta_p \dot{\gamma} \quad (2.8-12)$$

$$\tau_{11}^p - \lambda_p \left(\frac{8}{3} + \frac{2}{3}\epsilon\right) \tau_{12}^p \frac{\dot{\gamma}}{2} = 0 \quad (2.8-13)$$

$$\tau_{22}^p + \lambda_p \left(\frac{4}{3} - \frac{2}{3}\epsilon\right) \tau_{12}^p \frac{\dot{\gamma}}{2} = 0 \quad (2.8-14)$$

$$\tau_{33}^p + \lambda_p \left(\frac{4}{3} + \frac{4}{3}\epsilon\right) \tau_{12}^p \frac{\dot{\gamma}}{2} = 0 \quad (2.8-15)$$

From Equations (2.8-12), (2.8-13), and (2.8-14)

$$\tau_{12}^p = -\frac{\eta_p \dot{\gamma}}{1 + (c\lambda_p \dot{\gamma})^2} \quad (2.8-16)$$

where  $c$  is a shift factor and defined as:

$$c^2 = \frac{2 - 2\epsilon + \epsilon^2}{3} \quad (2.8-17)$$

Then from Equations (2.8-5), (2.8-6), and (2.8-16) the non-Newtonian viscosity can be obtained as:

$$\begin{aligned} \eta(\dot{\gamma}) &\equiv \tau_{12}/(-\dot{\gamma}) = \sum_{p=1}^{\infty} \frac{\eta_p}{1 + (c\lambda_p \dot{\gamma})^2} \\ &= \frac{\eta_0}{Z(\alpha)} \sum_{p=1}^{\infty} \frac{p^\alpha}{p^{2\alpha} + c^2 \lambda^{2\alpha} \dot{\gamma}^2} \end{aligned} \quad (2.8-18)$$

From Equations (2.8-13), (2.8-14), and (2.8-16)

$$\tau_{11}^p - \tau_{22}^p = - \frac{2 \lambda_p \eta_p \dot{\gamma}^2}{1 + (c\lambda_p \dot{\gamma})^2} \quad (2.8-19)$$

Then from Equations (2.8-5), (2.8-6), and (2.8-19) the primary normal stress coefficient can be obtained as:

$$\begin{aligned} \theta(\dot{\gamma}) &\equiv (\tau_{11} - \tau_{22})/(-\dot{\gamma}^2) \\ &= \frac{2 \lambda \eta_0}{Z(\alpha)} \sum_{p=1}^{\infty} \frac{1}{p^{2\alpha} + c^2 \lambda^2 \dot{\gamma}^2} \end{aligned} \quad (2.8-20)$$

From Equations (2.8-14), (2.8-15), and (2.8-16)

$$\tau_{22}^p - \tau_{33}^p = - \frac{\epsilon \lambda_p \eta_p \dot{\gamma}^2}{1 + (c\lambda_p \dot{\gamma})^2} \quad (2.8-21)$$

Then from Equations (2.8-5), (2.8-6), and (2.8-21) the secondary normal stress coefficient can be obtained as:

$$\begin{aligned} \beta(\dot{\gamma}) &\equiv (\tau_{22} - \tau_{33})/(-\dot{\gamma}^2) \\ &= \frac{\epsilon \lambda \eta_0}{Z(\alpha)} \sum_{p=1}^{\infty} \frac{1}{p^{2\alpha} + c^2 \lambda^2 \dot{\gamma}^2} \end{aligned} \quad (2.8-22)$$

## B. Oscillatory Shear Stresses and Normal Stresses

Assume that the amplitude of the shearing vibrations is small enough that the terms of order  $\dot{\gamma}^3$

can be neglected. Since  $\tau_{ij} = 0(\dot{\gamma}^2)$ , from Eq. (2.8-8) predicted  $\tau_{12}$  varies linearly with  $\dot{\gamma}$ .

Let:

$$\dot{\gamma} = \text{Re} \{ \dot{\gamma}^0 e^{i\omega t} \} \quad (2.8-23)$$

$$\tau_{12} = \text{Re} \{ \tau_{12}^0 e^{i\omega t} \} \quad (2.8-24)$$

Then:

$$\begin{aligned} \tau_{12} \dot{\gamma} &= \text{Re} \{ \tau_{12}^0 e^{i\omega t} \} \text{Re} \{ \dot{\gamma}^0 e^{i\omega t} \} \\ &= \frac{1}{2} \text{Re} \{ \tau_{12}^0 \dot{\gamma}^0 e^{2i\omega t} + \tau_{12}^0 \overline{\dot{\gamma}^0} \} \end{aligned} \quad (2.8-25)$$

Substituting Equations (2.8-23), (2.8-24), and (2.8-25) into Eq. (2.8-8) and equating terms with a similar time-dependence by removing Re- operator gives

$$\tau_{12}^{po} = - \frac{\eta_p \dot{\gamma}^0}{1 + i\omega\lambda_p} \quad (2.8-26)$$

From Equations (2.8-5), (2.8-6), and (2.8-26) the complex viscosity  $\eta^*(\omega)$  is given as:

$$\begin{aligned} \eta^*(\omega) &\equiv \eta'(\omega) - i\eta''(\omega) \equiv \tau_{12}^0 / (-\dot{\gamma}^0) \\ &= \sum_{p=1}^{\infty} \frac{\eta_0}{p^\alpha \Gamma(\alpha)} \left[ \frac{1}{1 + \omega^2 \lambda_p^2} - i \frac{\omega \lambda_p}{1 + \omega^2 \lambda_p^2} \right] \end{aligned} \quad (2.8-27)$$

Therefore,

$$\eta'(\omega) = \frac{\eta_0}{Z(\alpha)} \sum_{p=1}^{\infty} \frac{p^\alpha}{p^{2\alpha} + \omega^2 \lambda^2} \quad (2.8-28)$$

$$\eta''(\omega) = \frac{\eta_0}{Z(\alpha)} \sum_{p=1}^{\infty} \frac{\omega \lambda}{p^{2\alpha} + \omega^2 \lambda^2} \quad (2.8-29)$$

From Equations (2.8-4), (2.8-9), (2.8-10), (2.8-11), and (2.8-26) the predicted oscillatory normal stress must be of the form:

$$\tau_{jj} = \text{Re} \{ d_j + \tau_{jj}^0 e^{2i\omega t} \} \quad j = 1, 2, 3 \quad (2.8-30)$$

Substituting Equations (2.8-23), (2.8-24), (2.8-25), and (2.8-30) into Equations (2.8-9), (2.8-10), and (2.8-11) and equating terms with a similar time-dependence by removing Re- operator gives:

$$\tau_{11}^{po} (1 + i2\omega\lambda p) = \frac{4 + \epsilon}{6} \lambda_p \tau_{12}^{po} \dot{\gamma}^0 \quad (2.8-31)$$

$$\tau_{22}^{po} (1 + i2\omega\lambda p) = - \frac{2 - \epsilon}{6} \lambda_p \tau_{12}^{po} \dot{\gamma}^0 \quad (2.8-32)$$

$$\tau_{33}^{po} (1 + i2\omega\lambda p) = - \frac{1 + \epsilon}{3} \lambda_p \tau_{12}^{po} \dot{\gamma}^0 \quad (2.8-33)$$

$$d_1^p = \frac{4 + \epsilon}{6} \lambda_p \tau_{12}^{po} \dot{\gamma}^0 \quad (2.8-34)$$

$$d_2^p = - \frac{2 - \epsilon}{6} \lambda_p \tau_{12}^{po} \dot{\gamma}^0 \quad (2.8-35)$$

$$d_3^p = - \frac{1 + \varepsilon}{3} \lambda_p \tau_{12}^{po} \bar{\dot{\gamma}}^o \quad (2.8-36)$$

From Equations (2.8-26), (2.8-31), and (2.8-32)

$$\tau_{11}^{po} - \tau_{22}^{po} = - \frac{\lambda_p \eta_p (\dot{\gamma}^o)^2}{(1 + i\omega\lambda_p)(1 + 2i\omega\lambda_p)} \quad (2.8-37)$$

Hence, from Equations (2.8-5), (2.8-6), and (2.8-37) the primary complex normal stress coefficient  $\theta^*(\omega)$  is given as:

$$\begin{aligned} \theta^*(\omega) &\equiv \theta'(\omega) - i\theta''(\omega) \equiv (\tau_{11}^o - \tau_{22}^o) / (-\dot{\gamma}^o)^2 \\ &= \frac{\eta_o \lambda}{Z(\alpha)} \sum_{p=1}^{\infty} \frac{p^{2\alpha} - 2\omega^2 \lambda^2 - i3\omega \lambda p^\alpha}{(p^{2\alpha} + \omega^2 \lambda^2)(p^{2\alpha} + 4\omega^2 \lambda^2)} \quad (2.8-38) \end{aligned}$$

Therefore,

$$\theta'(\omega) = \frac{\eta_o \lambda}{Z(\alpha)} \sum_{p=1}^{\infty} \frac{p^{2\alpha} - 2\omega^2 \lambda^2}{(p^{2\alpha} + \omega^2 \lambda^2)(p^{2\alpha} + 4\omega^2 \lambda^2)} \quad (2.8-39)$$

$$\theta''(\omega) = \frac{\eta_o \lambda}{Z(\alpha)} \sum_{p=1}^{\infty} \frac{3 \omega \lambda p^\alpha}{(p^{2\alpha} + \omega^2 \lambda^2)(p^{2\alpha} + 4\omega^2 \lambda^2)} \quad (2.8-40)$$

From Equations (2.8-16), (2.8-34), and (2.8-35)

$$d_1^p - d_2^p = - \frac{\eta_p \lambda_p (1 - i\omega\lambda_p) |\dot{\gamma}^o|^2}{1 + \omega^2 \lambda^2} \quad (2.8-41)$$

Hence, from Equations (2.8-5), (2.8-6), and (2.8-41) the primary normal stress displacement function  $\theta^d(\omega)$  is given as:

$$\begin{aligned}\theta^d(\omega) &\equiv \text{Re}\{d_1 - d_2\}/(-|\dot{\gamma}^o|^2) \\ &= \frac{\eta_o \lambda}{Z(\alpha)} \sum_{p=1}^{\infty} \frac{1}{p^{2\alpha} + \omega^2 \lambda^2}\end{aligned}\quad (2.8-42)$$

Similarly, from Equations (2.8-5), (2.8-6), (2.8-16), (2.8-32), (2.8-33), (2.8-35), and (2.8-36) one can obtain the secondary complex normal stress coefficient  $\beta^*(\omega)$  and the secondary normal displacement function  $\beta^d(\omega)$  as:

$$\tau_{22}^{po} - \tau_{33}^{po} = - \left(\frac{\epsilon}{2}\right) \frac{\lambda_p \eta_p (\dot{\gamma}^o)^2}{(1 + i\omega\lambda_p)(1 + i2\omega\lambda_p)} \quad (2.8-43)$$

$$\beta^*(\omega) = \frac{\epsilon}{2} \frac{\lambda \eta_o}{Z(\alpha)} \sum_{p=1}^{\infty} \frac{p^{2\alpha} - 2\omega^2 \lambda^2 - i3\omega\lambda p^\alpha}{(p^{2\alpha} + \omega^2 \lambda^2)(p^{2\alpha} + 4\omega^2 \lambda^2)} \quad (2.8-44)$$

$$\beta'(\omega) = \frac{\epsilon}{2} \frac{\lambda \eta_o}{Z(\alpha)} \sum_{p=1}^{\infty} \frac{p^{2\alpha} - 2\omega^2 \lambda^2}{(p^{2\alpha} + \omega^2 \lambda^2)(p^{2\alpha} + 4\omega^2 \lambda^2)} \quad (2.8-45)$$

$$\beta''(\omega) = \frac{\epsilon}{2} \frac{\lambda \eta_o}{Z(\alpha)} \sum_{p=1}^{\infty} \frac{3\omega\lambda p^\alpha}{(p^{2\alpha} + \omega^2 \lambda^2)(p^{2\alpha} + 4\omega^2 \lambda^2)} \quad (2.8-46)$$

$$\beta^d(\omega) = \frac{\epsilon}{2} \frac{\lambda \eta_o}{Z(\alpha)} \sum_{p=1}^{\infty} \frac{1}{p^{2\alpha} + \omega^2 \lambda^2} \quad (2.8-47)$$

### C. Stress Relaxation

The transient stresses of a viscoelastic fluid can be studied under simple unsteady flows: stress relaxation after cessation of steady simple shear which has the following velocity distributions:

$$V_1(x_2, t) = \dot{\gamma}_0 x_2 [1 - h(t)]$$

$$V_2 = V_3 = 0 \quad (2.8-48)$$

where  $h(t)$  is the unit step function. For stress relaxation, the following material functions are given by model as:

$$\begin{aligned} \frac{\tilde{\eta}(\dot{\gamma}_0, t)}{\eta_0} &\equiv \frac{-1}{\eta_0} \left( \frac{\tau_{12}(t)}{\dot{\gamma}_0} \right) = \frac{1}{\eta_0} \sum_{p=1}^{\infty} \frac{\eta_p \exp[-t/\lambda_p]}{1 + (c\lambda_p \dot{\gamma}_0)^2} \\ &= \frac{1}{Z(\alpha)} \sum_{p=1}^{\infty} \frac{p^\alpha \exp[-p^\alpha t/\lambda]}{p^{2\alpha} + (c\lambda \dot{\gamma}_0)^2} \end{aligned} \quad (2.8-49)$$

$$\begin{aligned} \frac{\theta(\dot{\gamma}_0, t)}{\eta_0} &\equiv \frac{1}{\eta_0} \left( \frac{\tau_{11}(t) - \tau_{22}(t)}{\dot{\gamma}_0^2} \right) = \frac{1}{\eta_0} \sum_{p=1}^{\infty} \frac{2\lambda_p \eta_p \exp[-t/\lambda_p]}{1 + (c\lambda_p \dot{\gamma}_0)^2} \\ &= \frac{2\lambda}{Z(\alpha)} \sum_{p=1}^{\infty} \frac{\exp[-p^\alpha t/\lambda]}{p^{2\alpha} + (c\lambda \dot{\gamma}_0)^2} \end{aligned} \quad (2.8-50)$$

## §2.8.1.2 Computation of Material Functions

For general  $\alpha$ , simple rearrangement leads to the rapidly converging series. From Eq. (2.8-18)

$$\begin{aligned}
 \frac{\eta(\dot{\gamma})}{\eta_0} &= \frac{1}{Z(\alpha)} \sum_{p=1}^{\infty} \frac{p^\alpha}{p^{2\alpha} + c^2 \lambda^2 \dot{\gamma}^2} \\
 &= \frac{1}{Z(\alpha)} \left[ \sum_{p=1}^{\infty} \frac{1}{p^\alpha} - \sum_{p=1}^{\infty} \frac{c^2 \lambda^2 \dot{\gamma}^2}{p^\alpha (p^{2\alpha} + c^2 \lambda^2 \dot{\gamma}^2)} \right] \\
 &= 1 - \frac{c^2 \lambda^2 \dot{\gamma}^2}{Z(\alpha)} \sum_{p=1}^{\infty} \frac{1}{p^\alpha (p^{2\alpha} + c^2 \lambda^2 \dot{\gamma}^2)} \quad (2.8-51)
 \end{aligned}$$

Similarly,

$$\begin{aligned}
 \frac{\theta(\dot{\gamma})}{2\eta_0 \lambda} &= \frac{1}{Z(\alpha)} \sum_{p=1}^{\infty} \frac{1}{p^{2\alpha} + c^2 \lambda^2 \dot{\gamma}^2} \\
 &= \frac{Z(2\alpha)}{Z(\alpha)} - \frac{c^2 \lambda^2 \dot{\gamma}^2}{Z(\alpha)} \sum_{p=1}^{\infty} \frac{1}{p^{2\alpha} (p^{2\alpha} + c^2 \lambda^2 \dot{\gamma}^2)} \quad (2.8-52)
 \end{aligned}$$

$$\begin{aligned}
 \frac{\beta(\dot{\gamma})}{\epsilon \eta_0 \lambda} &= \frac{1}{Z(\alpha)} \sum_{p=1}^{\infty} \frac{1}{p^{2\alpha} + c^2 \lambda^2 \dot{\gamma}^2} \\
 &= \frac{Z(2\alpha)}{Z(\alpha)} - \frac{c^2 \lambda^2 \dot{\gamma}^2}{Z(\alpha)} \sum_{p=1}^{\infty} \frac{1}{p^{2\alpha} (p^{2\alpha} + c^2 \lambda^2 \dot{\gamma}^2)} \quad (2.8-53)
 \end{aligned}$$

$$\begin{aligned} \frac{\eta'(\omega)}{\eta_0} &= \frac{1}{Z(\alpha)} \sum_{p=1}^{\infty} \frac{p^\alpha}{p^{2\alpha} + \lambda^2 \omega^2} \\ &= 1 - \frac{\lambda^2 \omega^2}{Z(\alpha)} \sum_{p=1}^{\infty} \frac{1}{p^\alpha (p^{2\alpha} + \lambda^2 \omega^2)} \end{aligned} \quad (2.8-54)$$

$$\begin{aligned} \frac{\eta''(\omega)}{\omega \eta_0 \lambda} &= \frac{1}{Z(\alpha)} \sum_{p=1}^{\infty} \frac{1}{p^{2\alpha} + \lambda^2 \omega^2} \\ &= \frac{Z(2\alpha)}{Z(\alpha)} - \frac{\lambda^2 \omega^2}{Z(\alpha)} \sum_{p=1}^{\infty} \frac{1}{p^{2\alpha} (p^{2\alpha} + \lambda^2 \omega^2)} \end{aligned} \quad (2.8-55)$$

For  $c\lambda\dot{\gamma} \gg 1$  Gregory's formula in the form [62]

$$\int_0^{\infty} f(x) dx = \sum_{p=1}^{\infty} f(p) + \frac{f(0)}{2} + \text{error terms} \quad (2.8-56)$$

can be used to give asymptotic expressions for  $\eta(\dot{\gamma})$ ,  $\theta(\dot{\gamma})$ ,  $\beta(\dot{\gamma})$ ,  $\eta'(\omega)$ , and  $\eta''(\omega)$ . From Eq. (2.8-18)

$$\frac{\eta(\dot{\gamma})}{\eta_0} = \frac{1}{Z(\alpha)} \sum_{p=1}^{\infty} \frac{p^\alpha}{p^{2\alpha} + c^2 \lambda^2 \dot{\gamma}^2}$$

Hence,

$$f(p) = \frac{p^\alpha}{p^{2\alpha} + c^2 \lambda^2 \dot{\gamma}^2}, \quad \frac{f(0)}{2} = 0, \text{ and}$$

$$\begin{aligned} \int_0^{\infty} f(x) dx &= \int_0^{\infty} \frac{x^{\alpha}}{x^{2\alpha} + c^2 \lambda^2 \dot{\gamma}^2} dx \\ &= \frac{\pi (c\lambda\dot{\gamma})^{\frac{1}{\alpha}-1}}{2\alpha \cos \frac{\pi}{2\alpha}} \end{aligned}$$

Therefore,

$$\frac{\eta(\dot{\gamma})}{\eta_0} = \frac{\pi}{2\alpha \cos \frac{\pi}{2\alpha}} \frac{(c\lambda\dot{\gamma})^{\frac{1}{\alpha}-1}}{Z(\alpha)} \quad (2.8-57)$$

Similarly,

$$\frac{\eta'(\omega)}{\eta_0} = \frac{\pi}{2\alpha \cos \frac{\pi}{2\alpha}} \frac{(\lambda\omega)^{\frac{1}{\alpha}-1}}{Z(\alpha)} \quad (2.8-58)$$

$$\frac{\eta''(\omega)}{\omega\lambda\eta_0} = \frac{1}{Z(\alpha)} \left[ \frac{\pi}{\sin \frac{\pi}{2\alpha}} \frac{(\lambda\omega)^{\frac{1}{\alpha}-2}}{2\alpha} - \frac{(\lambda\omega)^{-2}}{2} \right] \quad (2.8-59)$$

$$\frac{\theta(\dot{\gamma})}{2\lambda\eta_0} = \frac{1}{Z(\alpha)} \left[ \frac{\pi}{\sin \frac{\pi}{2\alpha}} \frac{(c\lambda\dot{\gamma})^{\frac{1}{\alpha}-2}}{2\alpha} - \frac{(c\lambda\dot{\gamma})^{-2}}{2} \right] \quad (2.8-60)$$

$$\frac{\beta(\dot{\gamma})}{\varepsilon\lambda\eta_0} = \frac{1}{Z(\alpha)} \left[ \frac{\pi}{\sin \frac{\pi}{2\alpha}} \frac{(c\lambda\dot{\gamma})^{\frac{1}{\alpha}-2}}{2\alpha} - \frac{(c\lambda\dot{\gamma})^{-2}}{2} \right] \quad (2.8-61)$$

From Equations (2.8-18) and (2.8-57) the limiting slope  $s$  of a plot  $\log \eta$  vs.  $\log \dot{\gamma}$  is given by

$$s = \frac{1}{\alpha} - 1 \quad (2.8-62)$$

Hence, for high shear rate  $\dot{\gamma}$ , the viscosity function given by Equations (2.8-18) and (2.8-57) exhibits power-law behavior with  $n = \frac{1}{\alpha}$ .

### §2.8.2 Bird-Carreau Model

Bird and Carreau [63, 64, 65] proposed a non-linear extension of the generalized Maxwell model for polymeric fluids as a constitutive equation which is given by:

$$\tau^{ij} = - \int_{-\infty}^t \sum_{p=1}^{\infty} \frac{\eta_p e^{-(t-t')/\lambda_{2p}}}{\lambda_{2p}^2 [1 + \frac{1}{2} I_1(t') \lambda_{1p}^2]} \bar{\Gamma}^{ij} dt' \quad (2.8-63)$$

where  $\lambda_{1p}$  and  $\lambda_{2p}$  are two sets of time constants;  $\lambda_{1p}$  is associated with the rate of creation of network junctions, whereas the second set  $\lambda_{2p}$  is associated with the rate of loss of junctions. The term  $1 + \frac{1}{2} I_1(t') \lambda_{1p}^2$  accounts for the structural changes of the material when undergoing strain. The finite strain tensor  $\bar{\Gamma}^{ij}$  is defined by [66]

$$\bar{\Gamma}^{ij} = \left[ \left[ 1 + \frac{E}{2} \right] \left( \hat{g}^{ij}(t') - \hat{g}^{ij}(t) \right) + \frac{E}{2} \hat{g}^{ir}(t) \hat{g}^{js}(t) \times \right. \\ \left. \left[ \hat{g}_{rs}(t') - \hat{g}_{rs}(t) \right] \right] \quad (2.8-64)$$

If one lets

$$\eta_p = \eta_0 \lambda_{1p} / \sum_{p=1}^{\infty} \lambda_{1p} \quad ; \quad (2.8-65)$$

$$\lambda_{1p} = \lambda_1 \left(\frac{2}{p+1}\right)^{\alpha_1} \quad ; \quad (2.8-66)$$

and

$$\lambda_{2p} = \lambda_2 \left(\frac{2}{p+1}\right)^{\alpha_2} \quad (2.8-67)$$

then, expressions for the material functions  $\eta^*$ ,  $\theta^*$ ,  $\theta^d$ ,  $\beta^*$ ,  $\beta^d$ ,  $\eta$ ,  $\theta$ , and  $\beta$  can be derived in terms of six parameters: (1) a zero-shear viscosity  $\eta_0$ , (2) two sets of the characteristic time constants  $\lambda_1$  and  $\lambda_2$ , (3) two sets of dimensionless parameters  $\alpha_1$  and  $\alpha_2$  which describe the slopes of  $\log \eta$  vs.  $\log \dot{\gamma}$  and  $\log \theta$  vs.  $\log \dot{\gamma}$  plots, respectively, and (4) a dimensionless parameter  $\epsilon$  which accounts for deviations from the Weissenberg hypothesis that  $\tau_{22} - \tau_{33} = 0$ .

The Bird-Carreau model is an improvement over Sprigg's four-parameter model which has several weak points: (1) the curve of the  $\log \eta$  vs.  $\log \dot{\gamma}$  incorrectly has the same slope in the power-law region as  $\log \eta'$  vs.  $\log \omega$ , (2) in the power-law region the slope of normal stress curve is too rigidly related to the slope of the viscosity curve, and (3) the ratio of the normal stress difference is required to be constant.

### §2.8.2.1 Derivation of Material Functions

For a steady simple shearing motion for which the velocity profile is given by  $V_1 = \dot{\gamma}x_2$  and then  $II_e(t') = \dot{\gamma}^2$ . The finite strain tensor  $\bar{\Gamma}^{ij}$  is given by:

$$\bar{\Gamma}^{ij} = \begin{bmatrix} \gamma\theta^2 & \gamma\theta & 0 \\ \gamma\theta & \gamma\theta^2 & 0 \\ 0 & 0 & 0 \end{bmatrix} \quad (2.8-68)$$

where  $\theta$  is the time elapsed ( $t-t'$ ) since a given interaction was formed.

Substitution of Eq. (2.8-68) into Eq. (2.8-63) and integrating yields the following equations for the shear and normal stresses:

$$\tau_{12} = - \sum_{p=1}^{\infty} \frac{\eta_p \dot{\gamma}}{1 + (\lambda_{1p} \dot{\gamma})^2} \quad (2.8-69)$$

$$\tau_{11} - \tau_{22} = -2 \sum_{p=1}^{\infty} \frac{\eta_p \lambda_{2p} \dot{\gamma}^2}{1 + (\lambda_{1p} \dot{\gamma})^2} \quad (2.8-70)$$

$$\tau_{22} - \tau_{33} = -E \sum_{p=1}^{\infty} \frac{\eta_p \lambda_{2p} \dot{\gamma}^2}{1 + (\lambda_{1p} \dot{\gamma})^2} \quad (2.8-71)$$

Hence, the material functions  $\eta$ ,  $\theta$ ,  $\beta$  are given as:

$$\begin{aligned}\eta(\dot{\gamma}) &\equiv \frac{\tau_{12}}{-\dot{\gamma}} = \sum_{p=1}^{\infty} \frac{\eta_p}{1 + (\lambda_{1p}\dot{\gamma})^2} \\ &= \frac{\eta_0}{Z(\alpha_1) - 1} \sum_{p=2}^{\infty} \frac{p^{\alpha_1}}{2\alpha_1 + (2^{\alpha_1}\lambda_1\dot{\gamma})^2} \quad (2.8-72)\end{aligned}$$

$$\begin{aligned}\theta(\dot{\gamma}) &\equiv \frac{\tau_{11} - \tau_{22}}{-\dot{\gamma}^2} = 2 \sum_{p=1}^{\infty} \frac{\eta_p \lambda_{2p}}{1 + (\lambda_{1p}\dot{\gamma})^2} \\ &= \frac{2^{\alpha_2+1} \lambda_2 \eta_0}{Z(\alpha_1) - 1} \sum_{p=2}^{\infty} \frac{p^{\alpha_1 - \alpha_2}}{2\alpha_1 + (2^{\alpha_1}\lambda_1\dot{\gamma})^2} \quad (2.8-73)\end{aligned}$$

$$\begin{aligned}\beta(\dot{\gamma}) &\equiv \frac{\tau_{22} - \tau_{33}}{-\dot{\gamma}^2} = E \sum_{p=1}^{\infty} \frac{\eta_p \lambda_{2p}}{1 + (\lambda_{1p}\dot{\gamma})^2} \\ &= \frac{E 2^{\alpha_2} \lambda_2 \eta_0}{Z(\alpha_1) - 1} \sum_{p=2}^{\infty} \frac{p^{\alpha_1 - \alpha_2}}{2\alpha_1 + (2^{\alpha_1}\lambda_1\dot{\gamma})^2} \quad (2.8-74)\end{aligned}$$

Note that  $\beta(\dot{\gamma})$  is proportional to  $\theta(\dot{\gamma})$  only if  $E$  is taken to be a constant,  $\epsilon$ . Note further that, whereas  $\eta$  contains only the  $\lambda_1$ , the functions  $\theta$  and  $\beta$  contain both  $\lambda_1$  and  $\lambda_2$ . Hence one would expect that, in the power-law region, the slopes of  $\eta$  and  $\theta$  would not be connected in the same way for all fluids.

For oscillatory, small-amplitude motion, the components of the complex viscosity  $\eta^*(\omega)$  are:

$$\eta^*(\omega) \equiv \eta' - i\eta''$$

$$= \sum_{p=1}^{\infty} \frac{\eta_p}{1 + (\lambda_{2p}\omega)^2} - i \sum_{p=1}^{\infty} \frac{\omega \eta_p \lambda_{2p}}{1 + (\lambda_{2p}\omega)^2} \quad (2.8-75)$$

$$\begin{aligned} \eta'(\omega) &= \sum_{p=1}^{\infty} \frac{\eta_p}{1 + (\lambda_{2p}\omega)^2} \\ &= \frac{\eta_0}{Z(\alpha_1) - 1} \sum_{p=2}^{\infty} \frac{p^{-\alpha_1+2\alpha_2}}{p^{2\alpha_2} + (2^{\alpha_2} \lambda_2 \omega)^2} \end{aligned} \quad (2.8-76)$$

$$\begin{aligned} \eta''(\omega) &= \sum_{p=1}^{\infty} \frac{\omega \eta_p \lambda_{2p}}{1 + (\lambda_{2p}\omega)^2} \\ &= \frac{2^{\alpha_2} \omega \lambda_2 \eta_0}{Z(\alpha_1) - 1} \sum_{p=2}^{\infty} \frac{p^{-\alpha_1+\alpha_2}}{p^{2\alpha_2} + (2^{\alpha_2} \lambda_2 \omega)^2} \end{aligned} \quad (2.8-77)$$

The transient stresses of a viscoelastic fluid can be studied under simple unsteady flows; stress relaxation after cessation of steady simple shear which has the following velocity distributions:

$$V_1(x_2, t) = \dot{\gamma}_0 x_2 [1 - h(t)]$$

$$V_2 = V_3 = 0 \quad (2.8-78)$$

where  $h(t)$  is the unit step function.

For stress relaxation, the following material functions are given by the model as:

$$\begin{aligned} \frac{\tilde{\eta}(\dot{\gamma}_o, t)}{\eta_o} &\equiv \frac{-1}{\eta_o} \left[ \frac{\tau_{12}(t)}{\dot{\gamma}_o} \right] = \frac{1}{\eta_o} \sum_{p=1}^{\infty} \frac{\eta_p \exp(-t/\lambda_{2p})}{1 + (\lambda_{1p} \dot{\gamma}_o)^2} \\ &= \frac{1}{Z(\alpha_1) - 1} \sum_{p=2}^{\infty} \frac{p^{\alpha_1} \exp[-(p^{\alpha_2}/2^{\alpha_2} \lambda_2) t]}{p^{2\alpha_1} + (2^{\alpha_1} \lambda_1 \dot{\gamma}_o)^2} \end{aligned} \quad (2.8-79)$$

$$\begin{aligned} \frac{\tilde{\theta}(\dot{\gamma}_o, t)}{\eta_o} &\equiv \frac{-1}{\eta_o} \left[ \frac{\tau_{11} - \tau_{22}}{\dot{\gamma}_o^2} \right] = \frac{2}{\eta_o} \sum_{p=1}^{\infty} \frac{\eta_p \lambda_{2p} \exp(-t/\lambda_{2p})}{1 + (\lambda_{1p} \dot{\gamma}_o)^2} \\ &= \frac{2^{\alpha_2+1} \lambda_2}{Z(\alpha_1) - 1} \sum_{p=2}^{\infty} \frac{p^{\alpha_1 - \alpha_2} \exp[-(p^{\alpha_2}/2^{\alpha_2} \lambda_2) t]}{p^{2\alpha_1} + (2^{\alpha_1} \lambda_1 \dot{\gamma}_o)^2} \end{aligned} \quad (2.8-80)$$

### §2.8.2.2 Computation of Material Functions

As discussed in section 2.8.1.2, for low shear rate of frequency, the series for the material functions given above can be rearranged into rapidly convergent series, in which usually only the first few terms are needed. Hence,

$$\frac{\eta(\dot{\gamma})}{\eta_o} = 1 - \frac{(2^{\alpha_1} \lambda_1 \dot{\gamma})^2}{Z(\alpha_1) - 1} \sum_{p=2}^{\infty} \frac{1}{p^{\alpha_1} (p^{2\alpha_1} + (2^{\alpha_1} \lambda_1 \dot{\gamma})^2)} \quad (2.8-81)$$

10

11

12

13

14

15

16

$$\frac{\theta(\dot{\gamma})}{\eta_0} = \frac{2^{\alpha_2+1} \lambda_2}{Z(\alpha_1) - 1} \left[ Z(\alpha_1 + \alpha_2) - 1 - (2^{\alpha_1} \lambda_1 \dot{\gamma})^2 \sum_{p=2}^{\infty} \frac{p^{-(\alpha_1 + \alpha_2)}}{p^{2\alpha_1} + (2^{\alpha_1} \lambda_1 \dot{\gamma})^2} \right] \quad (2.8-82)$$

$$\frac{\eta'(\omega)}{\eta_0} = 1 - \frac{(2^{\alpha_2} \lambda_2 \omega)^2}{Z(\alpha_1) - 1} \sum_{p=2}^{\infty} \frac{1}{p^{\alpha_1} (p^{2\alpha_2} + (2^{\alpha_2} \lambda_2 \omega)^2)} \quad (2.8-83)$$

$$\frac{\eta''(\omega)}{\eta_0} = \frac{2^{\alpha_2} \lambda_2 \omega}{Z(\alpha_1) - 1} \left[ Z(\alpha_1 + \alpha_2) - 1 - (2^{\alpha_2} \lambda_2 \omega)^2 \sum_{p=2}^{\infty} \frac{p^{-(\alpha_1 + \alpha_2)}}{p^{2\alpha_2} + (2^{\alpha_2} \lambda_2 \omega)^2} \right] \quad (2.8-84)$$

For  $\lambda_1 p^{\dot{\gamma}} \gg 1$  and  $\lambda_2 p^{\omega} \gg 1$  Gregory's formula in the form [62]

$$\int_0^{\infty} f(x) dx = \sum_{p=1}^{\infty} f(p) + \frac{f(0)}{2} + \text{error terms} \quad (2.8-85)$$

can be used to give asymptotic expressions for  $\eta(\dot{\gamma})$ ,  $\theta(\dot{\gamma})$ ,  $\eta'(\omega)$ , and  $\eta''(\omega)$ .

$$\frac{\eta(\dot{\gamma})}{\eta_0} = \frac{1}{Z(\alpha_1) - 1} \left[ \frac{\pi (2^{\alpha_1} \lambda_1 \dot{\gamma})^{\frac{1-\alpha_1}{\alpha_1}}}{2\alpha_1 \sin(\frac{1+\alpha_1}{2\alpha_1}\pi)} - \frac{1}{(\alpha_1+1) (2^{\alpha_1} \lambda_1 \dot{\gamma})^2} - \frac{1 + \frac{1}{6} \alpha_1}{2(1 + (2^{\alpha_1} \lambda_1 \dot{\gamma})^2)} \right] \quad (2.8-86)$$

$$\frac{\theta(\dot{\gamma})}{\eta_0} = \frac{2^{\alpha_2+1} \lambda_2}{Z(\alpha_1) - 1} \left[ \frac{\pi (2^{\alpha_1} \lambda_1 \dot{\gamma})^{\frac{1-\alpha_1-\alpha_2}{\alpha_1}}}{2\alpha_1 \sin\left(\frac{1+\alpha_1-\alpha_2}{2\alpha_1}\pi\right)} - \frac{1}{(\alpha_1-\alpha_2) (2^{\alpha_1} \lambda_1 \dot{\gamma})^2} - \frac{1 + \frac{1}{6}(\alpha_1 - \alpha_2)}{2(1 + (2^{\alpha_1} \lambda_1 \dot{\gamma})^2)} \right] \quad (2.8-87)$$

$$\frac{\eta'(\omega)}{\eta_0} = \frac{1}{Z(\alpha_1) - 1} \left[ \frac{\pi (2^{\alpha_2} \lambda_2 \omega)^{\frac{1-\alpha_1}{\alpha_2}}}{2\alpha_2 \sin\left(\frac{1+2\alpha_2-\alpha_1}{2\alpha_2}\pi\right)} - \frac{1}{(2\alpha_2 - \alpha_1 + 1) (2^{\alpha_2} \lambda_2 \omega)^2} - \frac{1 + \frac{1}{6}(2\alpha_2 - \alpha_1)}{2(1 + (2^{\alpha_2} \lambda_2 \omega)^2)} \right] \quad (2.8-88)$$

$$\frac{\eta''(\omega)}{\eta_0} = \frac{2^{\alpha_2} \lambda_2 \omega}{Z(\alpha_1) - 1} \left[ \frac{\pi (2^{\alpha_2} \lambda_2 \omega)^{\frac{1-\alpha_1-\alpha_2}{\alpha_2}}}{2\alpha_2 \sin\left(\frac{1+\alpha_2-\alpha_1}{2\alpha_2}\pi\right)} - \frac{1}{(\alpha_2 - \alpha_1 + 1) (2^{\alpha_2} \lambda_2 \omega)^2} - \frac{1 + \frac{1}{6}(\alpha_2 - \alpha_1)}{2(1 + (2^{\alpha_2} \lambda_2 \omega)^2)} \right] \quad (2.8-89)$$

## CHAPTER 3

### POROUS MEDIA PARAMETERS FOR VARIOUS CONSTITUTIVE EQUATIONS

When a fluid flows through a porous medium, the velocity of its elements changes rapidly from point to point along its tortuous flow path. The forces which produce these changes in velocity vary rapidly from point to point. It is reasonable to suppose that the random variations in flow path for any particular fluid element are uniformly distributed. Also the variations in magnitude of velocity can be expected to be distributed uniformly with mean zero. Thus, for steady laminar flow the lateral forces associated with the microscopic random variations in velocity can be expected to average to zero over any macroscopic volume. The only non-zero macroscopic force exerted on the fluid by the solid is that associated with the viscous resistance to flow. For steady laminar flow this force must be in equilibrium with the external and body forces on the fluid.

The literature on this subject is voluminous and experimental investigations have been done by many

workers [67, 68, 69, 70, 71, 72, 73, 74] to determine the correlation between the pressure drop and the flow rate of fluids through packed beds. An excellent reference is the monograph of Scheidegger [75], which contains a particularly good discussion of permeability concept. Other general references are those of Collins [76], Carman [77], Muskat [78], Leva [79], and Richardson [80].

Some effort has been extended toward establishing methods for predicting non-Newtonian flow behavior in porous media and for correlating pressure drop versus flow rate data with viscometric data for porous media experiments. At the present time there is no universally acceptable scale-up method for flow of rheologically complex fluids in porous media. The various methods currently employed or suggested, can be arbitrarily divided into at least three major categories. The method which seems to have received the most attention is based on the coupling of a particular model for a porous medium--i.e., the so-called hydraulic radius model, with an assumed functional relationship between shear rate and shear stress to describe the rheological behavior of a non-Newtonian fluid. This method involves correlations of experimental data from one-dimensional flow experiments in unconsolidated porous media--i.e., mostly bead packs, with the appropriate rheological parameters derived from viscometric experiments on the fluid of interest. The

power-law and Ellis models have been used to describe the purely viscous behavior of the non-Newtonian fluids. Another category involves generalized scale-up methods which adapt Darcy's law to non-Newtonian fluids without invoking a particular rheological model of purely viscous behavior. The appropriate rheological description can, in principle, be derived from viscometric and porous media flow experiments. A third approach, based on the concept of the simple fluid, involves the application of dimensional analysis to the scale-up of porous media flow data for an arbitrary viscoelastic fluid.

This work was mainly directed at developing a generalized scale-up method based on the capillary model. Wall effects were accounted for using the hydraulic radius concept. Various empirical and derived models for non-Newtonian fluids were applied to the problem of flow through porous media. Development of packed bed equations for various constitutive equations are contained in Appendix A and the results of the modified Ergun friction factor versus appropriate modified Reynolds number correlation for each rheological model are listed in Table 3-1.

It has been indicated that Darcy's law is fundamental within the assumptions made. Two significant aspects of this law are the analysis of capillary flow and the assumption of fluid homogeneity. It is the

TABLE 1-1 Porous Media Parameters

Model	Constitutive Equation	Model Parameters	Solution and Concentration	Friction Factor and Modified Reynolds Number	Porous Media Parameters
Newtonian	$\tau_{13} = -2\mu e_{13}$	$\mu$	Distilled Water	$N_{Re} = \frac{D_p G_o}{\mu(\Gamma - c)}$ , $f_{\text{expt}} = \frac{\Delta P D_p c^3}{M G_o^2 \Gamma^2} \cdot f_{\text{calc}} = \frac{150}{N_{Re}}$ , $f_{\text{calc}} = \frac{150}{N_{Re}}$	$\frac{M D_p G_o}{\mu(\Gamma - c)}$
Power-Law	$\tau_{13} = -\left(k \left(\frac{\partial u}{\partial x}\right)^n\right)^{1/n}$	$k$ $n$	Polyacrylamide in Distilled Water, 0.05, 0.10, 0.25, and 0.50 weight percent	$N_{Re, \text{eff}} = \frac{D_p G_o}{M(\Gamma - c)} \left[ \frac{4n}{3n+1} \left(\frac{v_w}{\mu}\right)^{n-1} \right]$ $f_{\text{expt}} = \frac{\Delta P D_p c^3}{M G_o^2 \Gamma^2} \cdot f_{\text{calc}} = \frac{150}{N_{Re, \text{eff}}}$	$\frac{\lambda^{n-1} D_p G_o}{M(\Gamma - c)}$ $\frac{\lambda^{n-1}}{\mu}$ $n$
Bilge	$\tau_{13} = -\frac{1}{n_0} \left[ 1 + \left( \frac{\sqrt{2} \tau_{13}}{\mu} \right)^{2n} \right]^{1/2}$	$n_0$ $a$ $\tau_h$	Polyacrylamide in Distilled Water, 0.05, 0.10, 0.25, and 0.50 weight percent	$N_{Re, \text{eff}} = \frac{D_p G_o}{M(\Gamma - c)n_0} \left[ 1 + \frac{4}{3n} \left(\frac{v_w}{\mu}\right)^{2n} \right]$ $f_{\text{expt}} = \frac{\Delta P D_p c^3}{M G_o^2 \Gamma^2} \cdot f_{\text{calc}} = \frac{150}{N_{Re, \text{eff}}}$	$\frac{D_p G_o}{M(\Gamma - c)n_0}$ $\frac{1}{\mu}$ $a$
Spriggs	$\tau^p + \lambda_p \tau^q = -2\eta_0 e^p$ $\tau = \frac{\mu}{\rho} \tau^p$	$n_0$ $a$ $\lambda$ $c$	Polyacrylamide in Distilled Water, 0.05, 0.10, 0.25, and 0.50 weight percent	$N_{Re, \text{eff}} = \frac{D_p G_o}{M(\Gamma - c)n_0} \left[ 1 + \frac{4}{3n} \left( \frac{2.3005 \sqrt{2} \tau(c)}{\mu} \right)^{2n} \left( \frac{c^2 v_w}{\mu} \right)^{a-1} \right]$ $f_{\text{expt}} = \frac{\Delta P D_p c^3}{M G_o^2 \Gamma^2} \cdot f_{\text{calc}} = \frac{150}{N_{Re, \text{eff}}}$	$\frac{D_p G_o}{M(\Gamma - c)n_0}$ $\frac{c^2 v_w}{\mu}$ $a$
Mezer	$\tau_{13} = -\left\{ \frac{\tau_0 - n_0}{1 + \left[ \frac{\sqrt{2} \tau_{13}}{\mu} \right]^{2n}} \right\}^{1/2}$	$n_0$ $n$ $a$ $\tau_m$	Polyvinylpyrrolidone in Distilled Water, 0.50, 1.0, 3.0, and 4.0 weight percent	$N_{Re, \text{eff}} = \frac{D_p G_o}{M(\Gamma - c)n_0} \left[ 1 + \frac{4}{3n} \left(\frac{v_w}{\mu}\right)^{2n-1} \left( \frac{c^2 v_w}{\mu} \right)^{a-1} \right]$ $f_{\text{expt}} = \frac{\Delta P D_p c^3}{M G_o^2 \Gamma^2} \cdot f_{\text{calc}} = \frac{150}{N_{Re, \text{eff}}}$	$\frac{D_p G_o}{M(\Gamma - c)n_0}$ $\frac{v_w}{\mu}$ $\frac{c^2 v_w}{\mu}$ $a$
Herschel-Bulkley	$\tau_{13} = -\tau_0 - \left[ \frac{\mu}{\rho} \left( \frac{\partial u}{\partial x} \right)^n \right]^{1/n}$	$n_0$ $m$ $\gamma$	Polyethylcellulose in Distilled Water, 0.3 and 0.5 weight percent, different H.M.	$N_{Re, \text{eff}} = \frac{4 D_p G_o \tau_0^{m+1}}{M(\Gamma - c) \mu \gamma} \left[ \frac{m+1}{m} \left( \frac{v_w}{\mu} \right)^{m-1} \left( \frac{c^2 v_w}{\mu} \right)^{a-1} \right]$ $f_{\text{expt}} = \frac{\Delta P D_p c^3}{M G_o^2 \Gamma^2} \cdot f_{\text{calc}} = \frac{150}{N_{Re, \text{eff}}}$	$\frac{D_p G_o \tau_0^{m+1}}{M(\Gamma - c) \mu \gamma}$ $\frac{c^2 v_w}{\mu}$ $\frac{v_w}{\mu}$ $a$

failure of these very same aspects which lead to the more obvious deviations of Darcy's law. By analogy to flow through tubes, at high flow rates, deviations from Darcy's law are expected due to the inertial effects. By the same analogy, we would expect deviations to occur in systems where the pore diameters become comparable with, or less than, the molecular mean free paths of the flowing gas, i.e., the so-called "slip" flow region and the region of "molecular streaming" or Knudsen flow. Other anomalies (based on Darcy's law) are adsorption, capillary condensation, and molecular diffusion. These latter effects may be referred to as surface flow effects, i.e., the behavior of non-homogeneous flows. Finally, there are deviations due to chemical reactions and ionic effects as they are not included in Darcy's law. Scheidegger [75] has given an extensive discussion of general equations which account both for high flow rates and for molecular effects. Carman [77] has presented a thorough summary of surface flow effects.

## CHAPTER 4

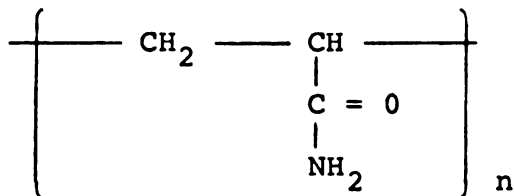
### POLYACRYLAMIDE SYSTEM

Polyacrylamide is a common industrial flocculant used for clarification, thickening, and filtration. A host of factors influence the efficiency of these operations, and in most systems, it has been found that flocculation of the solid results in greatly improved separations. Flocculation by definition is the agglomeration of particles into larger units called flocs, which normally settle and filter better due to their increased size.

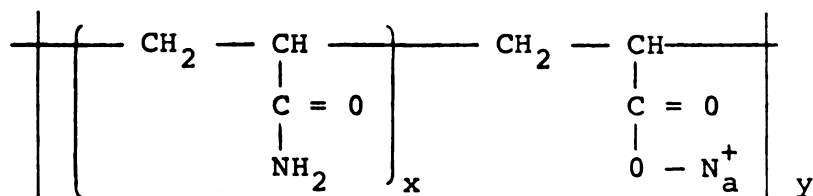
#### §4.1 Chemistry

Separan is Dow Chemical Company's (Midland, Michigan) trademark for a group of synthetic, organic, high-molecular weight materials of the polyacrylamide type with normal molecular weight distribution. Dow Chemical Company provided the Separan AP 30 for this research project with a molecular weight range of 860,000 to 1,000,000. Separan polymers are very high-molecular weight synthetic water soluble polymers formed from the

polymerization of acrylamide. The family of Separan polymers is comprised of varied molecular weight products ranging from essentially nonionic nature to varying degrees of anionic character. They are all composed of the illustrated unit structure



Because of the preponderance of amide groups, polyacrylamide is essentially nonionic in solution, although a small portion of the amide groups are usually hydrolyzed to anionic carboxyl groups. The nonionic character of acrylamide may be altered by further replacement of amide groups with carboxyl groups thereby increasing the ionic nature of the polymer. Such polymers may be classified as anionic polyelectrolytes in neutral and alkaline solutions. Under acidic conditions the ionization is repressed and the polyelectrolyte assumes a nonionic character. Such polymers may be represented by the following structure.



The exact mechanism by which Separan polymers agglomerate suspended inorganic solids is not known. It is strongly suspected, however, that these long linear-chain polymers are adsorbed by suspended solids, forming strong bonds between the polymer and the solid at one end while the other end of the long molecule is still free in the suspension to be adsorbed on other particles. With many polymer molecules in solution, this action quickly results in the quick and irreversible agglomeration and flocculation of the particles in suspension.

#### §4.2 Physical Properties

##### A. Appearance

Separan polymers are produced as white, free flowing, amorphous solids with a bulk density of 0.55 grams per cubic centimeter. Ninety-five percent of the particles have a diameter of less than one millimeter. Particle size can be reduced to less than 40 microns by various grinding techniques similar to those used with other thermoplastic materials.

##### B. Thermal Stability

The solids soften at 220-230°C. and decomposition becomes evident at 270°C. The Separan flocculants do not become fluid upon heating.

### C. Solution Concentrations

Separan polymers are rapidly wetted by water and can be dissolved in all proportions. In practice, however, solutions of higher than 1.0% concentration by weight are rarely used, due to their high viscosity.

### D. Solubility in Organic Solvents

Organic solvents such as ether, benzene, hexane, methanol, and chloroform will not dissolve the Separan polymers. Some liquids having a high oxygen to carbon ratio, as in glycerine and ethylene glycol, will, however, dissolve or swell the Separan polymers.

### E. Storage Life

Under usual conditions of storage, the Separan polymers show excellent stability. To avoid even slight degradation, however, prolonged periods of storage, such as a year or more, should be avoided, especially where storage temperatures are likely to be high.

## §4.3 Solution Preparation

The schematic diagram of the stock solution preparation is shown in Figure 4.3-1.

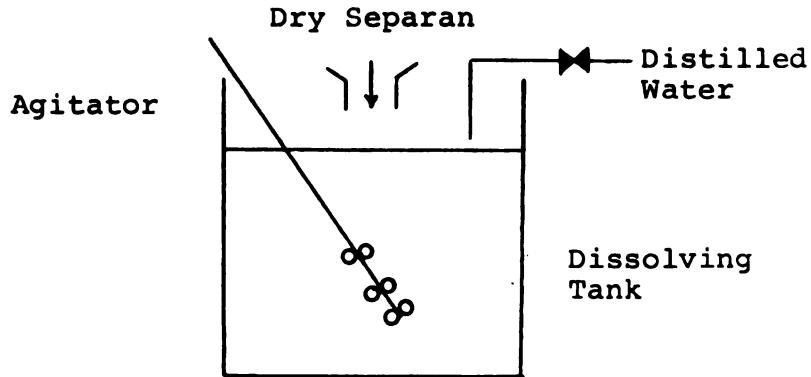


Figure 4.3-1 Schematic Diagram of the Stock Solution Preparation

1. Calculate and weigh out the amount of Separan necessary for the batch. (For example, 200 grams will prepare 20 liters of 1.0% stock solution in a 30 liter vessel.)
2. Fill the vessel one-fourth full or more of distilled water.
3. Turn on the agitator and distilled water.
4. Add the Separan polymer to the funnel and watch it feed to make sure there is no interruption. If an interruption occurs, the distilled water should be turned off immediately, the Separan polymers removed from the funnel, and the cause of the stoppage removed. The distilled water flow may then be started again, and the balance of the Separan polymers placed in the funnel.

5. After all the powder is dispersed, leave the distilled water on until it reaches desired amount (20 liters in example).
6. Continue the gentle agitation until no translucent particles can be seen in the solution (1 to 2 hours). The stock solution is now ready to use. While increased temperatures will increase the rate of solution, those higher than 150°F. should be avoided.

#### §4.4 Rheology

The non-Newtonian viscosity of bulk polymers and their concentrated solutions has been studied extensively during the past several years [94, 95, 96, 97]. For most systems of steady shearing flow the viscosity coefficient depends on the shear rate in a rather characteristic manner. At sufficiently low shear rates the viscosity is independent of the shear rate (the Newtonian region); however, within some critical range of shear rates the viscosity begins to decrease as the shear rate is increased to still higher values. The Newtonian viscosity (zero-shear viscosity,  $\eta_0$ ) and the critical shear rate region may change by many orders of magnitude from one system to another depending on the nature of the polymer, its molecular weight, the solvent, and the concentration.

Several proposed models and material functions were fully discussed in Chapter 2.

#### §4.4.1 Experiment

The fluids investigated were solutions of monodisperse polyacrylamide in distilled water. The polyacrylamide was manufactured and provided for this study by Dow Chemical Company, Midland, Michigan.

Concentrations were converted to units of gram/100 cc by assuming additivity of volumes. Solutions were prepared in the range 0.05-0.5 gram/100 cc of polyacrylamide.

Viscosity and primary normal stress difference measurements of the four series of polyacrylamide solutions were made for the shear rate range of 0.00675 to 851.0  $\text{sec}^{-1}$  with a Weissenberg rheogoniometer, a commercial cone-and-plate viscometer manufactured by Farol Research Engineers Ltd., Manchester, England. Although a range of sizes are available with the instruments, a platen diameter of 10 cm and a cone of angle  $2.0083^\circ$  were used with a 1/16" torsion bar and a 1/16" normal force spring. The operation of this Weissenberg rheogoniometer is fully discussed in Appendix B, and several problems arising with the use of this instrument are discussed elsewhere [98, 99].

Room temperature was carefully adjusted to 21°C prior to taking measurements so as to maintain the temperatures of samples and reservoir platen arrangement which is shown in Figure 4.4-1 constant at  $21 \pm 0.5^\circ\text{C}$ .

In the start-up experiment, the material was initially at rest. All stresses due to earlier experiments or loading the sample were allowed to relax. When this instrument was started, the stresses increased with time, quite often overshooting, then approaching a steady state value from the high side as shown in Figure 4.4-2.

The maximum chart speed was used in this experiment during high shear rates in order to get the most accurate curves of shear stress versus time. Using these data, the relaxation spectrum,  $H(\tau)$ , was constructed from the following equation

$$H(\tau) = - \frac{N}{\dot{\gamma}t} \frac{d\tau_{12}(t)}{d\ln t} \quad (4.4-1)$$

where

$$N = \frac{1}{\Gamma(m)} .$$

Ordinarily, a series of points equally spaced on the logarithmic time scale is chosen, each providing a value of  $H$  at  $\tau = t$ . Then from a tentative logarithmic plot of  $H$  vs.  $\tau$ , the slope  $m$  is measured at each point; the corresponding value of  $N$  is obtained and multiplied by the provisional value of  $H$  (see Ferry, 45, p. 90).

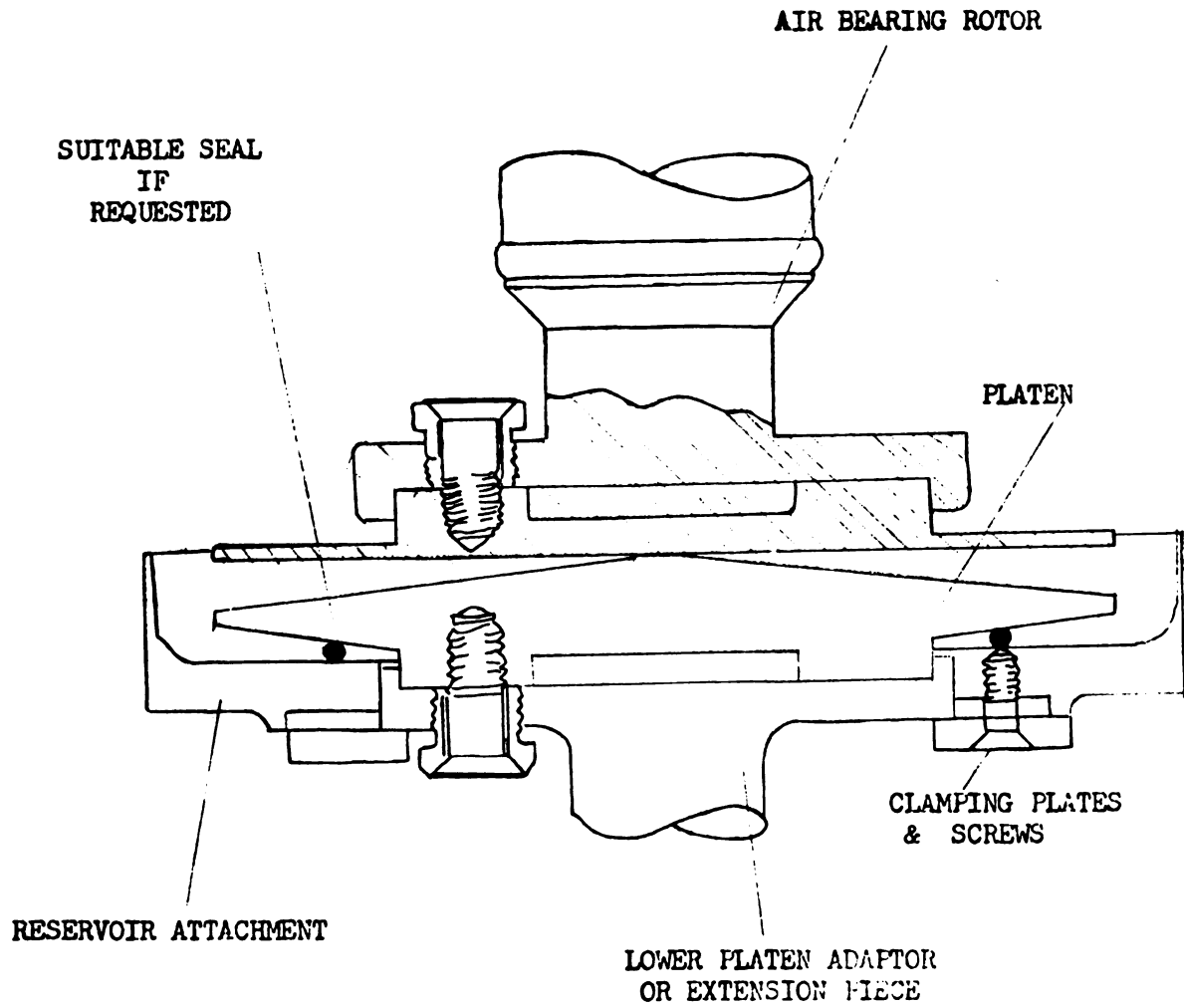


Figure 4.4-1 Reservoir Platen Arrangement

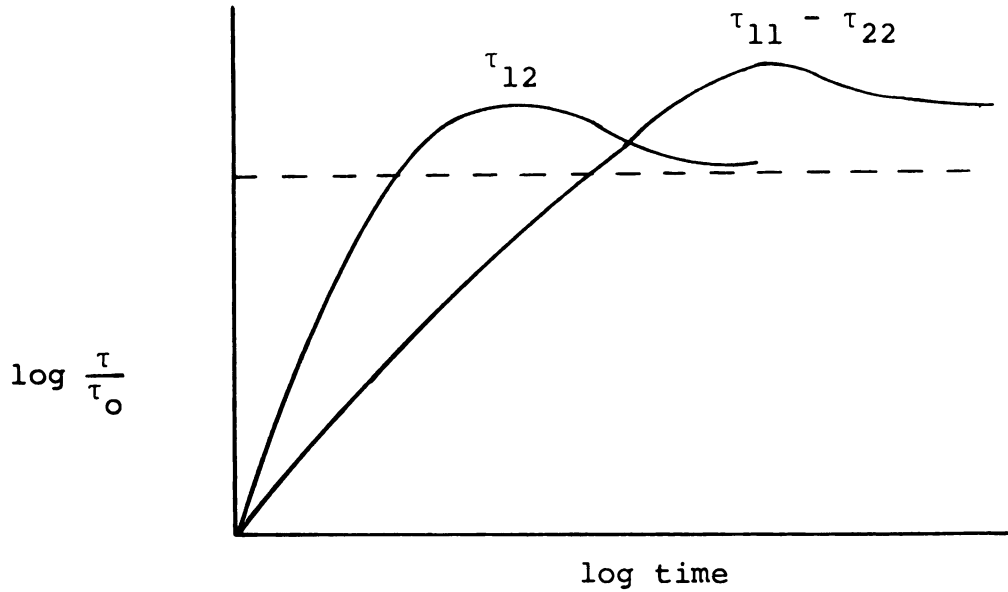


Figure 4.4-2 Start-up Experiment

Data reduction and discussion of experimental errors follow.

#### Viscosity Measurement

The equation to determine the viscosity from the rheogoniometer is

$$\eta(\dot{\gamma}) \equiv \tau_{12}/(-\dot{\gamma}) = k_T \Delta_T / \dot{\gamma} \quad (4.4-2)$$

where  $\Delta_T$  is the measurement made on the torque meter (0.001 in.),  $k_T$  is the machine constant (see Appendix A), and  $\dot{\gamma}$  is the shear rate. For the shear stress greater than 80 dyne/cm<sup>2</sup>, the error in the torque meter reading,  $\Delta_T$ , is not greater than 3%. This error appears as fluctuations in the reading. The errors in  $\dot{\gamma}$  and  $k_T$  (~0.1%) are negligible compared to the error in  $\Delta_T$ .

### Normal Stress Measurement

The primary normal stress difference from a rheo-  
goniometer measurement is given by

$$-(\tau_{11} - \tau_{22}) = k_N \Delta_N \quad (4.4-3)$$

where  $\Delta_N$  is the measurement made on the normal force meter (0.001 in.) and  $k_N$  is a machine constant. For values of  $-(\tau_{11} - \tau_{22}) < 500 \text{ dyne/cm}^2$  there is a fluctuation of the meter reading of 15% and for values of  $-(\tau_{11} - \tau_{22}) > 1000 \text{ dyne/cm}^2$  this fluctuation is 5%. The error in  $k_N$  is negligible. Thus, primary normal stress difference data are accurate to within 15% for low values ( $< 500 \text{ dyne/cm}^2$ ) and 5% for high values ( $> 1000 \text{ dyne/cm}^2$ ). For values of  $-(\tau_{11} - \tau_{22}) < 100 \text{ dyne/cm}^2$  the errors are too great to consider the values reliable.

#### §4.4.2 Results

The basic rheological data for Separan AP30 are summarized in:

Appendix D: Steady Shear Stress, as  $\eta(\dot{\gamma})$   
vs.  $\dot{\gamma}$

Appendix E: Steady Normal Stress, as  
 $-(\tau_{11} - \tau_{22})$  vs.  $\dot{\gamma}$

Appendix F: Stress Relaxation Spectrum, as  
 $H(\tau)$  vs.  $t$

As discussed earlier, the viscometric curves should have a precision of about 3%. Some typical data

are plotted in Figures 4.4-3,4,5, and 6 as  $\tau_{12}$  vs.  $\dot{\gamma}$ ,  $\eta(\dot{\gamma})$  vs.  $\dot{\gamma}$ ,  $\theta(\dot{\gamma})$  vs.  $\dot{\gamma}$ , and  $H(\tau)$  vs.  $t$ , respectively.

There are two important effects which may influence the viscometric data; these are viscous heating and aging of the fluid. Viscous heating is a problem at high cone speed. Readings are not valid when the heat resulting from viscous dissipation produces significant temperature gradients within the fluid. Turian and Bird [100] have derived a formula for the threshold shear rate at which viscous heating would influence the steady state torque readings. They did not provide a method by which the observed readings may be corrected. There was no tendency for the torque reading to decrease with time for a fixed cone speed because of heating effects.

Viscous heating was not a problem and shear degradation over the time of testing was not usually measurable on this instrument. No attempt was made to measure shear degradation rigorously but the viscosity curve was essentially retraced from low speed to high. It is possible that shearing during preparation of the solution had already reduced the polymer average molecular weight to the point where the solution was no longer sensitive to the levels of shear encountered viscometrically. The high-shear behavior is determined by the coordinated motion of closely-neighboring segments of the molecular chain. This response is not greatly

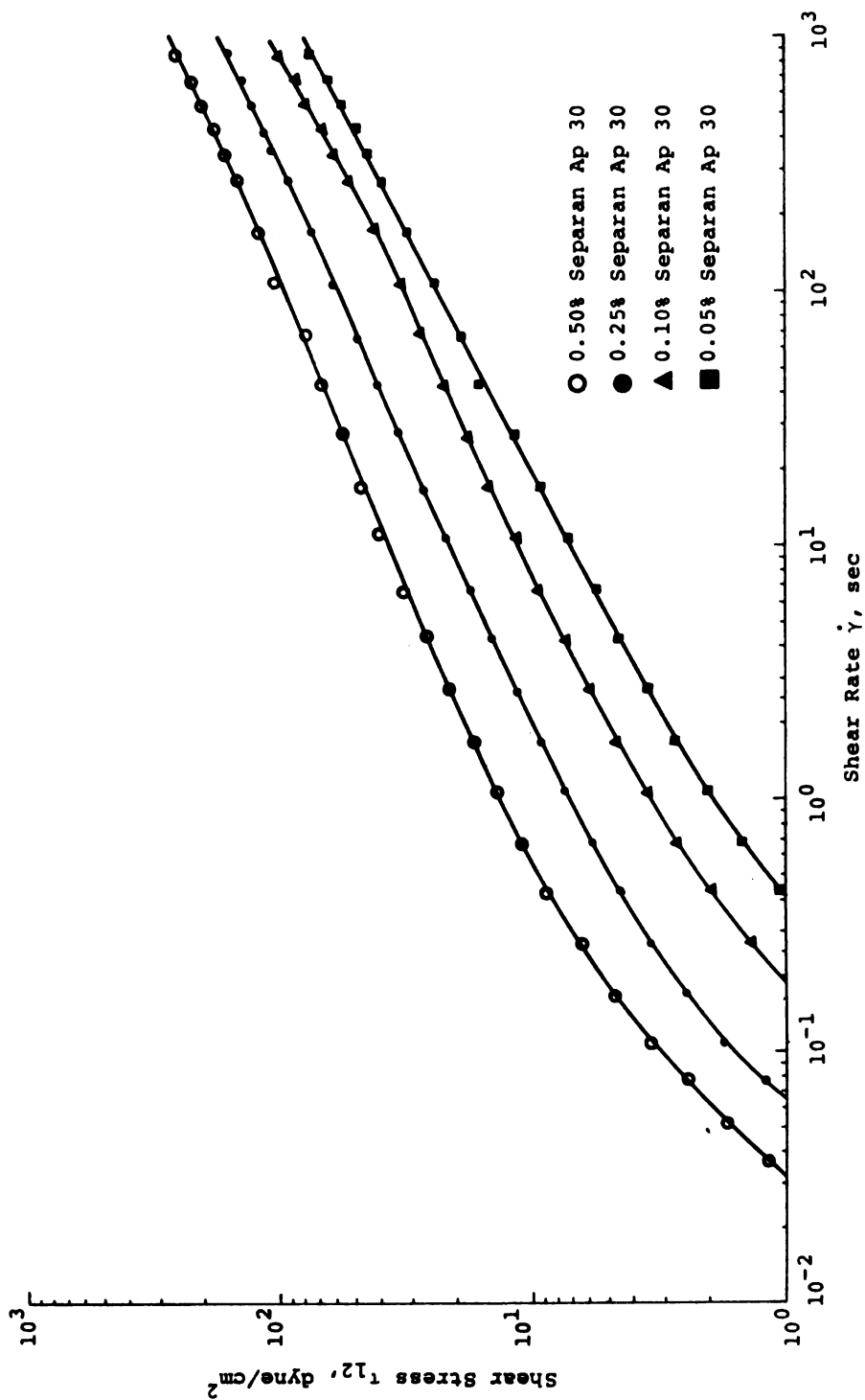


Figure 4.4-3 Shear Stress-Shear Rate Data for Aqueous Separan Ap 30 Solutions

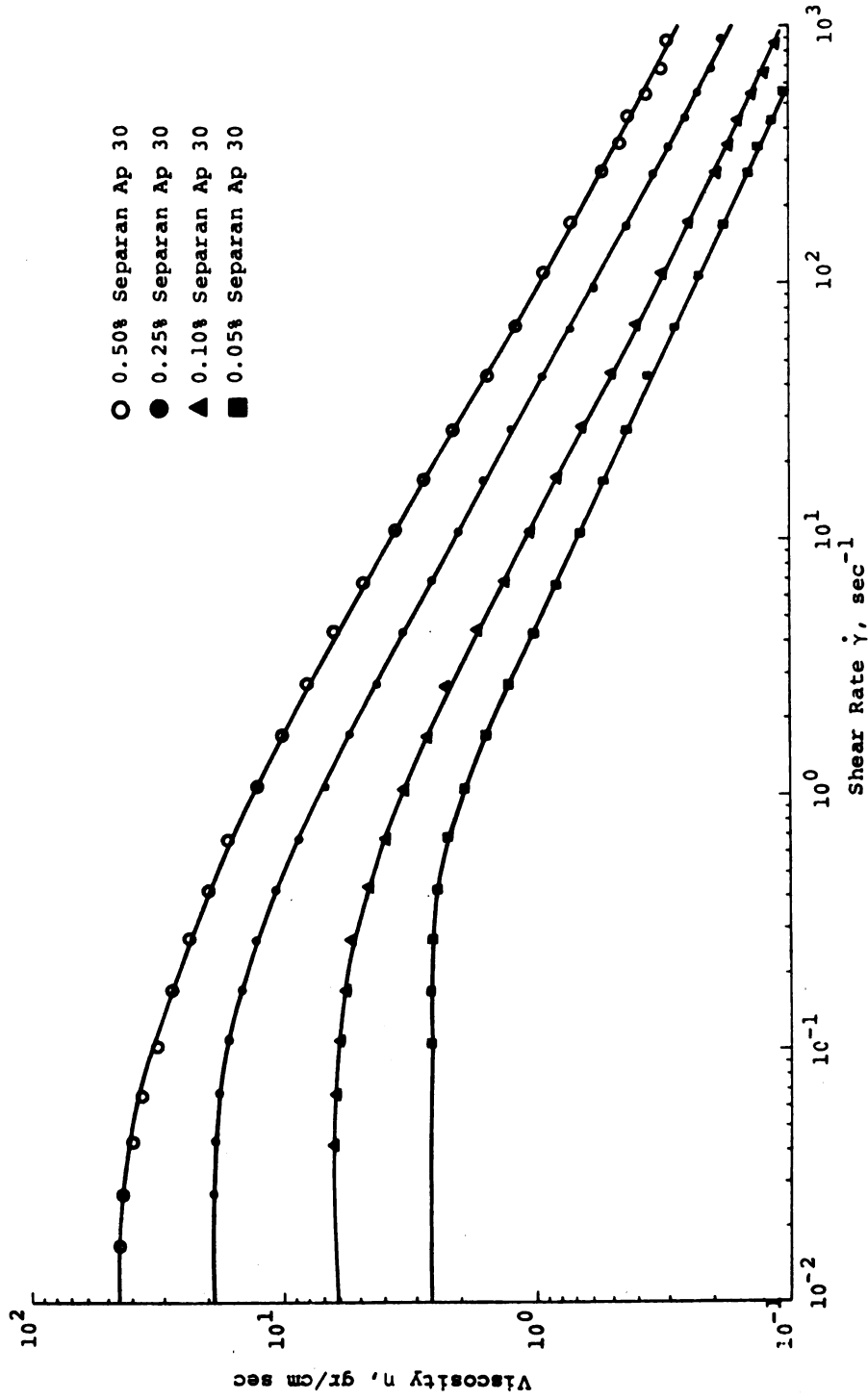


Figure 4.4-4 Non-Newtonian Viscosity of Separan Ap 30 Solutions

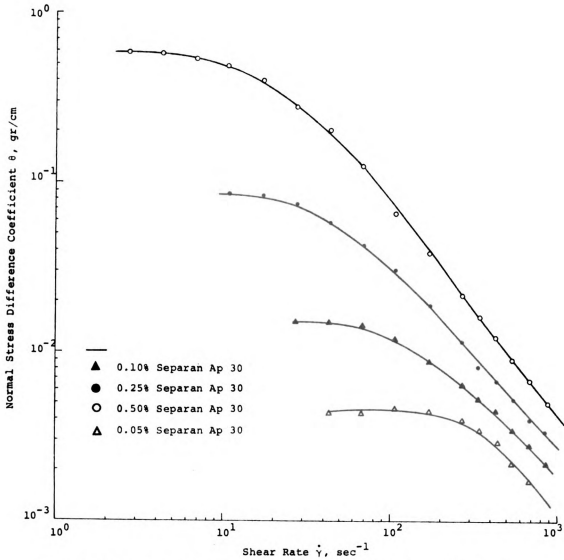


Figure 4.4-5 Primary Normal Stress Difference Coefficient of Separan Ap 30 Solutions

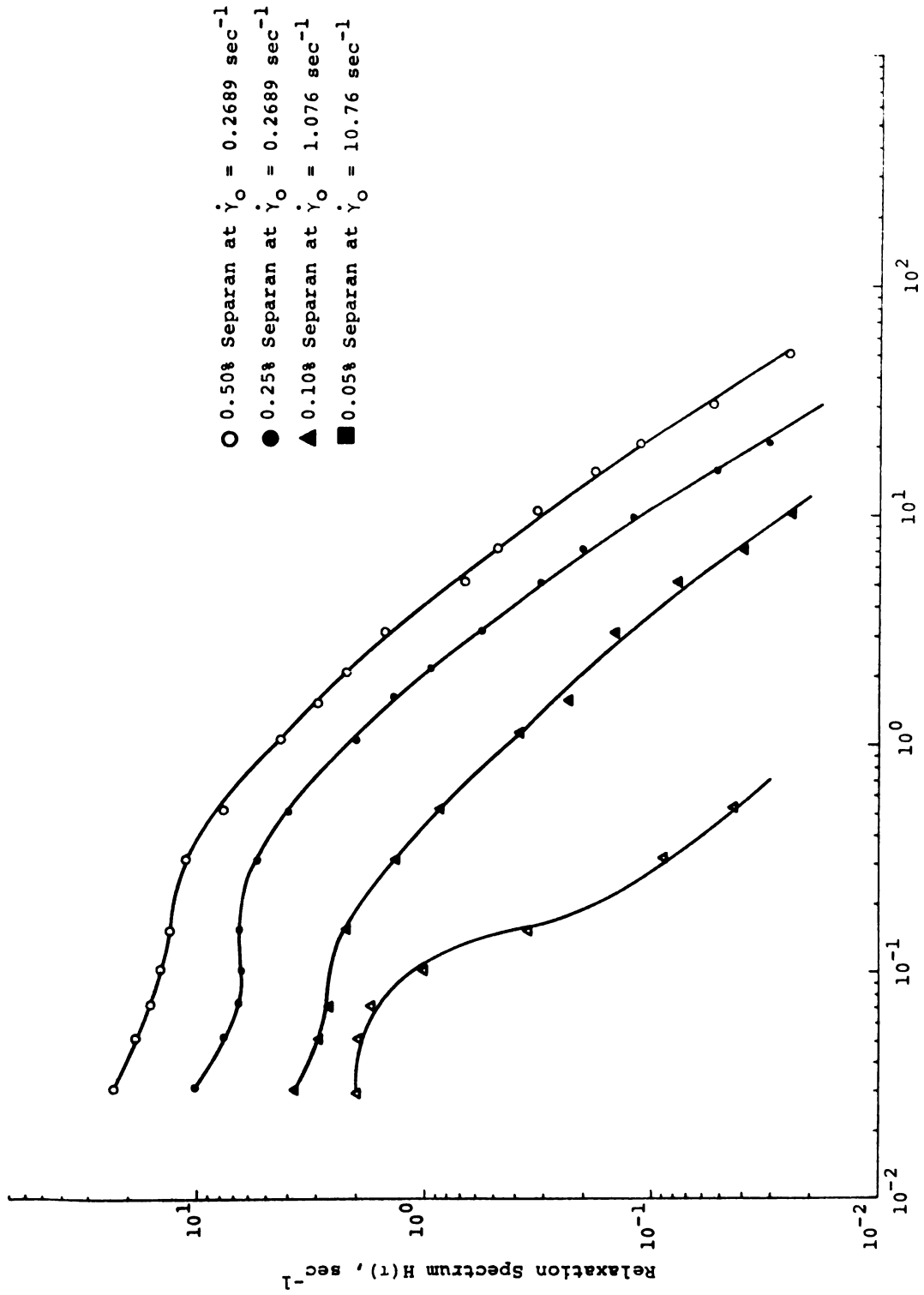


Figure 4.4-6 Relaxation Spectrum of Separan Ap 30 Solutions

affe

best

poli

rand

l'ed

app

poli

den

pla

par

com

ins

fin

com

pac

den

vic

che

ter

com

par

poli

vic

fin

affected by the long-chain entanglements which are destroyed by degradation processes. For most of the polyacrylamide solutions tested here, the entire shear range of the viscometer would have to be classed as "low"; limiting values of  $\eta$  for each solution were approached.

One difficulty was noted with measurements on the polyacrylamide solutions: an apparent flow instability developed at the higher shear rates, which effectively placed an upper limit on shear rates attainable with a given sample and geometry. This problem is apparently a common one for viscoelastic fluids in cone-and-plate instruments [101, 102]. In the instability region the fluid somewhat erratically exuded from the gap between cone and plate at some locations on the rim and pulled back from the rim at others. For any sample the condition developed near or somewhat beyond the range of shear rates where the viscosity begins to decrease with shear rate. The instability could be deferred and measurements extended by using the sample reservoir and filling it deep enough to cover the gap. Eventually, however, the same problem again developed and the run had to be terminated.

The location of the instability depended on the polymer molecular weight and concentration of the solution. As a general rule it was possible to penetrate further into the non-Newtonian region for higher molecular

weights of the polymer and for higher polymer concentrations. All experimental tests indicated that viscosities measured in this work were outside of the instability region.

One measure of the reliability of the data was the consistency of the points in Figures 4.4-3 through 6, which were highly reproducible. The data which might be suspect are for the measurements of the primary normal stress difference of 0.05% solutions of Separan AP30. The primary normal stress data for 0.05% solution was furnished by Meister [117].

A more general warning of fundamental errors in normal stress measurement should be noted, however. It seems that the presence of time-dependent normal stress fluctuations--not seen before because of the damping and averaging action of manometers--could greatly influence results.

#### §4.4.3 Discussions and Evaluations of Data

##### 1. Zero-shear Viscosity

The zero-shear viscosity exhibits a functional dependence on temperature, on solute concentration, and molecular weight which is smooth and roughly similar to the behavior predicted from molecular theory.

For example, it is well known that  $\eta_0$  of many fluids--Newtonian or polymeric--can be characterized by

21. 1

18. 0

When

18. 8

18. 7

18. 6

18. 5

18. 4

18. 3

18. 2

18. 1

18. 0

18. 0

18. 0

18. 0

18. 0

18. 0

an inverse-exponential dependence on temperature. This is often expressed as

$$\eta_0 = \bar{\eta} \exp \left( - \frac{Q_0}{RT} \right) \quad (4.4-4)$$

where  $Q_0$  is an activation energy (kcal/gr. mole) and  $\bar{\eta}$  is a frequency factor; both are nearly independent of temperature.

An important study of the temperature-dependent properties of polymers is the work of Williams, Landel, and Ferry [103]. They showed the temperature dependence of the relaxation time associated with viscoelastic response, and measured a coefficient  $a_T$  defined by

$$a_T = \eta_{r,T} \rho_r / \eta_r T \rho \quad (4.4-5)$$

where the subscript r means that the quantity to which it is appended is measured at the temperature  $T_r$ .  $a_T$  is essentially the shift factor defined in Eq. (4.4-6)

$$a_T = (\eta_0 - \eta_s)_{T_0} / (\eta_0 - \eta_s)_T \quad (4.4-6)$$

where  $T_0$  would be some arbitrary reference temperature. In this testing the zero-shear limiting viscosity,  $\eta_0$ , is obtained by extrapolating viscosity-shear rate curve as follows:

$$\eta_0 = \lim_{\dot{\gamma} \rightarrow 0} \eta \quad (4.4-7)$$

Experimental evidence [104, 105] indicates that this viscosity-molecular weight relationship exhibits two distinct regions. In the low molecular weight region, the viscosity increases with a low power of  $M$ , generally in the neighborhood of unity. In the high molecular weight region, the viscosity shows a very strong molecular weight dependence,  $\eta_0$  being proportional to  $M^{3.4}$ . The transition between these two regions occurs over such a narrow range of molecular weight that one is led to define a "critical" molecular weight  $M_c$  as the intersection of the lines representing the high and low molecular regions.

Such a sharp change in the molecular weight dependence must be associated with a corresponding change in the mechanism, on a molecular level, responsible for viscosity. Bueche [106, 107] has offered a theory which is in general agreement with observed behavior. The essential idea of his theory is that, above a certain chain length, molecules are sufficiently long to become entangled at various points along their lengths with neighboring molecules. The force required to move an entangled molecule is much greater than that for a shorter, unentangled molecule, because the entangled molecule drags other molecules with it, each of which may itself drag other molecules. The number of primary, secondary, etc., entanglements increases sharply with chain length, and thus the viscosity shows a strong dependence on molecular weight.

The influence of solute content on  $\eta_0$  is depicted by the solid line in Figure 4.4-7 for polyacrylamide. The slope of this line, as well as its elevation, is dependent on shear rate to a great extent [94].

Porter and Johnson [94] have remarked that in many concentrated solutions of linear polymers,  $\eta(\dot{\gamma})$  is proportional to the "s" power of concentration, with s dependent upon shear rate. A zero-shear rate, values of s between 3 and 14--often near 5--have been measured. With the data taken by Meister [117] zero-shear limiting viscosity,  $\eta_0$ , is extended up to concentrations of 2.0%. An insufficient range of concentration was studied here to check this, but the data of polyacrylamide appeared to violate such a relationship.

Most of the commonly used non-Newtonian models incorporate  $\eta_0$ . It is thus vital that a reliable means be developed to estimate  $\eta_0$ .

## 2. Cone-and-Plate Viscosities

Since the viscometer is characterized by constant-strain conditions everywhere under the cone, interpretation of the data is usually unambiguous. Even though shear degradation is possible in polyacrylamide, it was not noticeable during the short time of viscometric testing. As is indicated in several instances in Appendix D, viscosity curves for all fluids could be retraced as cone speed was decreased after high-speed shearing.

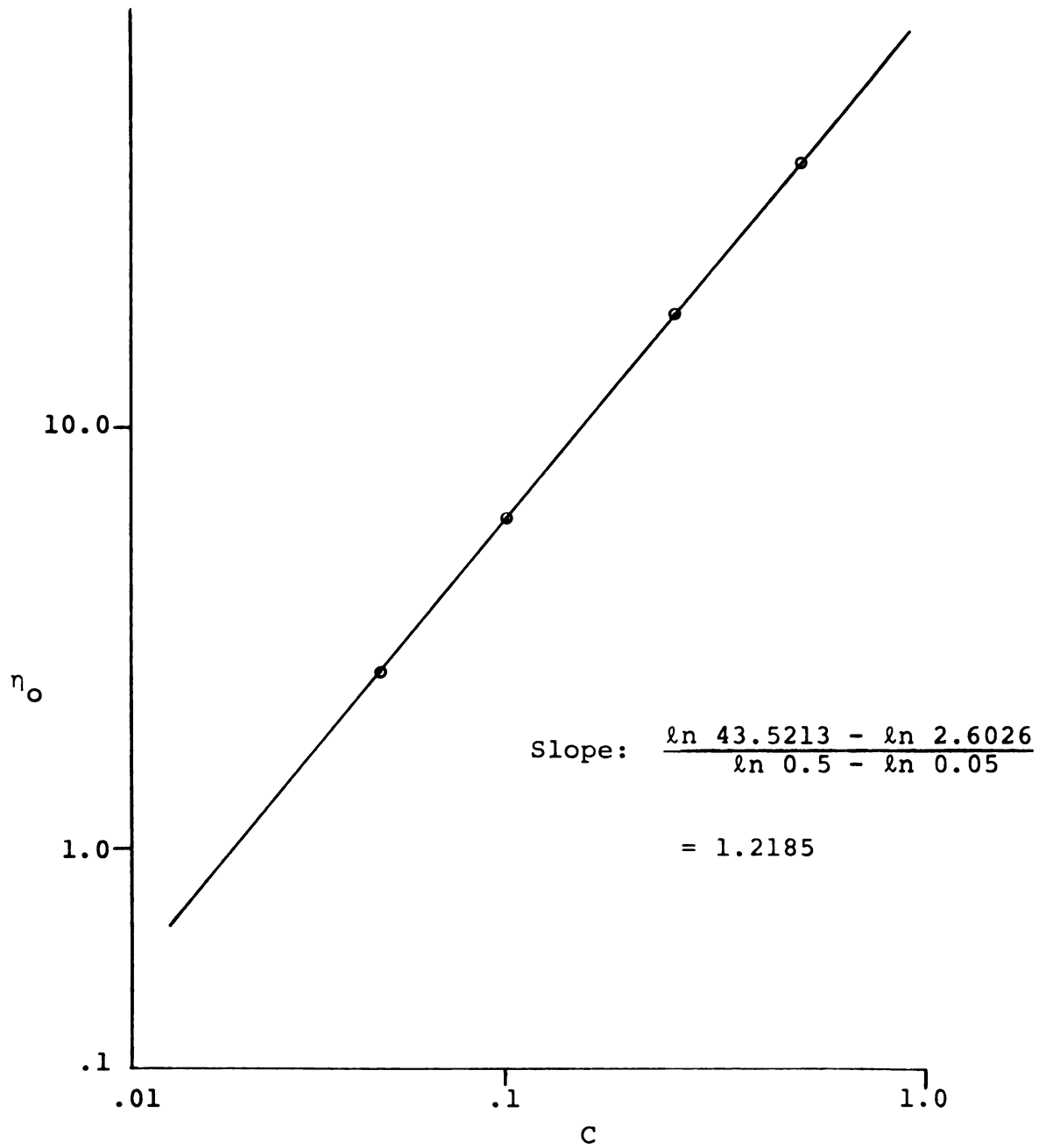


Figure 4.4-7  $\eta_0$ , Zero-shear Viscosity, vs.  $C$ , Concentration

### 3. Normal Stress Coefficients

Analogous to the viscosity for describing shear stress are the normal stress coefficients for describing normal stress. One set of coefficients, used by Williams and Bird [16, 17] is

$$\theta(\dot{\gamma}) \equiv - \frac{\tau_{11} - \tau_{22}}{\dot{\gamma}^2} = - \frac{(\tau_{\phi\phi} - \tau_{\theta\theta})}{4e_{\phi\theta}^2} \quad (4.4-8)$$

$$\beta(\dot{\gamma}) \equiv - \frac{\tau_{22} - \tau_{33}}{\dot{\gamma}^2} = - \frac{(\tau_{\theta\theta} - \tau_{rr})}{4e_{\phi\theta}^2} \quad (4.4-9)$$

where  $\theta(\dot{\gamma})$  and  $\beta(\dot{\gamma})$  are allowed to vary with shear rate. This is the approximation employed in presenting the normal stress data from Section 4.4.2 as  $\theta(\dot{\gamma})$  vs.  $\dot{\gamma}$  in Figure 4.4-7.

The vast change in the magnitude of  $\theta(\dot{\gamma})$  makes it difficult for one to appreciate the physical influence of the parameter. A more convenient variable might be the product  $\dot{\gamma}\theta(\dot{\gamma})$ , which increases from a very small number (0.05% polyacrylamide) to a maximum, then decreases to a plateau and seems to increase again as  $\dot{\gamma}$  becomes very large (0.1% polyacrylamide). It has the advantage of relatively small changes in magnitude and the familiar unit of  $\text{gr. cm.}^{-1} \text{ sec}^{-1}$ ; however, it loses significance as a purely material parameter.

#### 4. Combination of $\theta(\dot{\gamma})$ and $\eta(\dot{\gamma})$

A feel for the magnitude of viscosity is acquired from values of  $\theta(\dot{\gamma})$  and  $\eta(\dot{\gamma})$ . Therefore, it is often preferable to express normal stress phenomena in terms of comparisons with the magnitude of shear stress in the same fluid. Many such comparisons are possible. Weissenberg [42], in extending theories of rubber-like continua to liquids, initiated for introduction of the recoverable shear (strain)  $S_w$  and the shear modulus  $G_w$ :

$$S_w \equiv \frac{\tau_{11} - \tau_{22}}{\tau_{12}} \quad (4.4-10)$$

$$G_w \equiv \frac{\tau_{12}}{S_w} \quad (4.4-11)$$

Physically,  $S_w$  is conceived as the amount of deformation experienced by a flowing elastic element in dynamic equilibrium with the imposed shear stress. As such it is a measure of stored elastic energy. Mooney [54] has independently evolved a continuum theory employing strain and two shear moduli; in the limit of  $\tau_{22} - \tau_{33} = 0$  which is identical to the Weissenberg hypothesis.

Using the definitions of  $\theta(\dot{\gamma})$  and  $\eta(\dot{\gamma})$  leads to:

$$S_w = \frac{\theta \dot{\gamma}^2}{\tau_{12}} = \frac{\theta \dot{\gamma}}{\eta} \quad (4.4-12)$$

$$G_w = \frac{\eta^2}{\theta^2} \quad (4.4-13)$$

It is interesting to note that  $G_w$  is the same quantity which was predicted by molecular theory [61, 108]. From the steady state viscometric data presented in section 4.4.2  $S_w$  and  $G_w$  were calculated and tabulated in Appendix H. Values of  $S_w$  versus shear rate were plotted in Figure 4.4-8. For the aqueous solutions of polyacrylamide studied here,  $S_w$  is a steadily increasing function of  $\dot{\gamma}$  over almost the entire range of shear rate. Solutions of low concentration exhibit low elasticity as seen by the concentration dependence of  $S_w$  in Figure 4.4-8. The implication of a single curve which is almost independent of concentration is that very similar recoverable-shear behavior is exhibited at all concentrations and molecular weights of the same type of molecular chain, as long as the solutions are "sufficiently" concentrated and long-range of entanglement couplings between molecules are the dominant feature in resisting stress. From this explanation, all four sets of the aqueous solutions of polyacrylamide are concluded to be effectively dilute solutions.

So far, the discussion has considered only recoverable shear; the earlier-mentioned concept of the modulus  $G_w$  will now be examined. Values of modulus  $G_w$  and reduced modulus  $\bar{G}_{wr}$  are defined as follows:

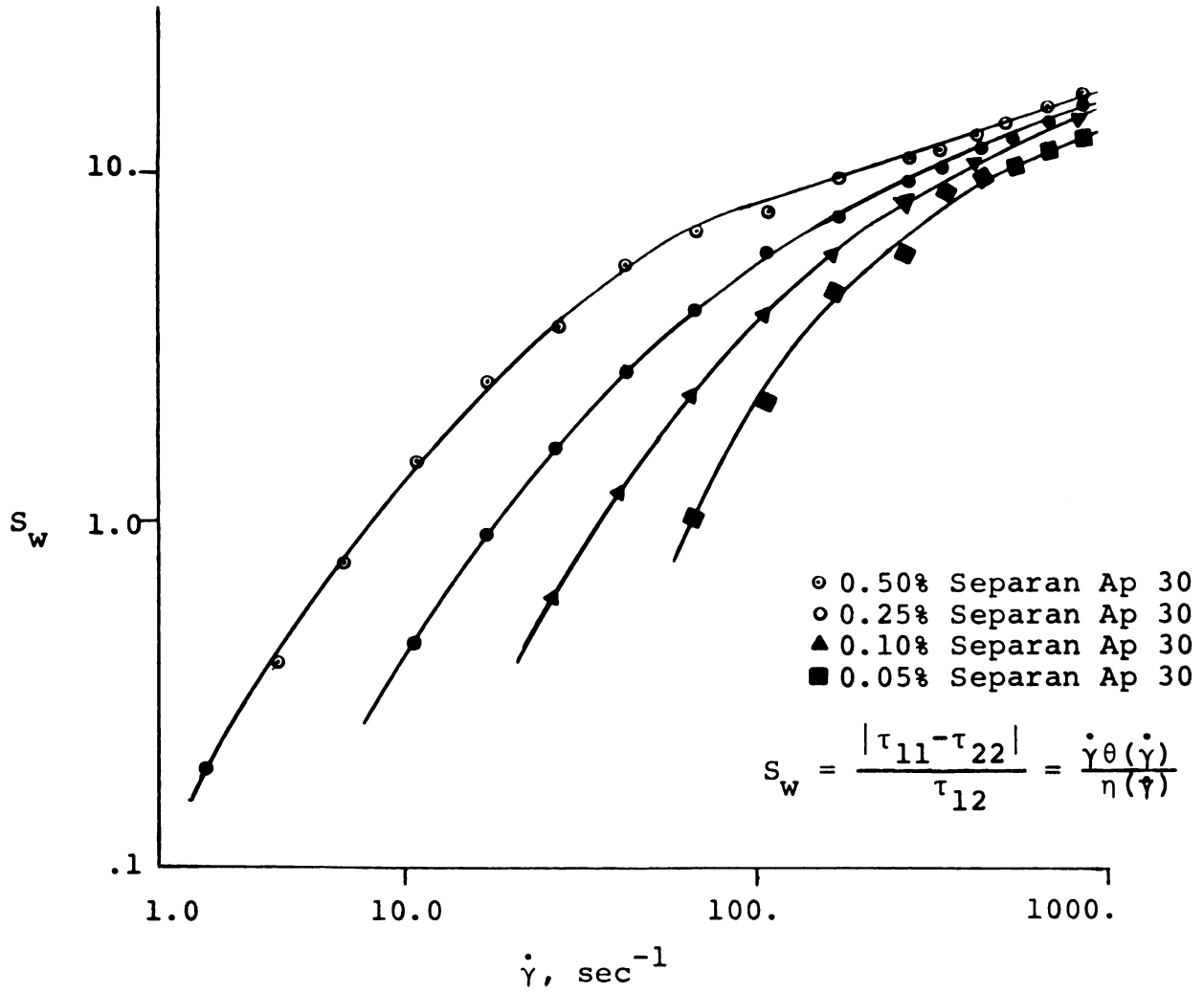


Figure 4.4-8  $S_w$ , Recoverable Shear Strain, vs.  $\dot{\gamma}$ , Shear Rate

$$\bar{G}_{wr} = G_w \left(\frac{1.0}{c}\right)^2 \quad (4.4-14)$$

In the above equation  $c$  represents polymer concentration. Figure 4.4-9 is a plot of  $\log G_w$  vs.  $\log \dot{\gamma}$ , and the modulus is seen to be a slightly-increasing function of shear rate which attains an asymptotic value at high rates. This plateau or constant value is reached experimentally at lower shear rates for higher concentration solutions. Since  $G_w$  is nearly constant it can be seen from the following relationship that  $\sqrt{\theta}$  is nearly proportional to  $\eta$ .

$$\sqrt{\theta} \equiv \sqrt{\frac{\eta^2}{G_w}} = \eta \sqrt{\frac{1}{G_w}} = \eta \times \text{const.} \quad (4.4-15)$$

Further, it can be shown that  $\tau_{12}$  is proportional to  $\dot{\gamma}^n$  and that  $\tau_{11} - \tau_{22}$  is proportional to  $\dot{\gamma}^{2n}$ :

$$S_w \equiv \frac{\tau_{11} - \tau_{22}}{\tau_{12}} = \frac{\tau_{12}}{G_w}$$

Therefore,

$$\tau_{11} - \tau_{22} = \frac{\tau_{12}^2}{G_w} = \frac{(k\dot{\gamma}^n)^2}{G_w} = \dot{\gamma}^{2n} \times \text{const} \quad (4.4-16)$$

The ratio  $\theta(\dot{\gamma})/\eta(\dot{\gamma})$ , with units of time, may be considered as an effective time-constant characteristic of the modes of molecular motion which are on the verge of being

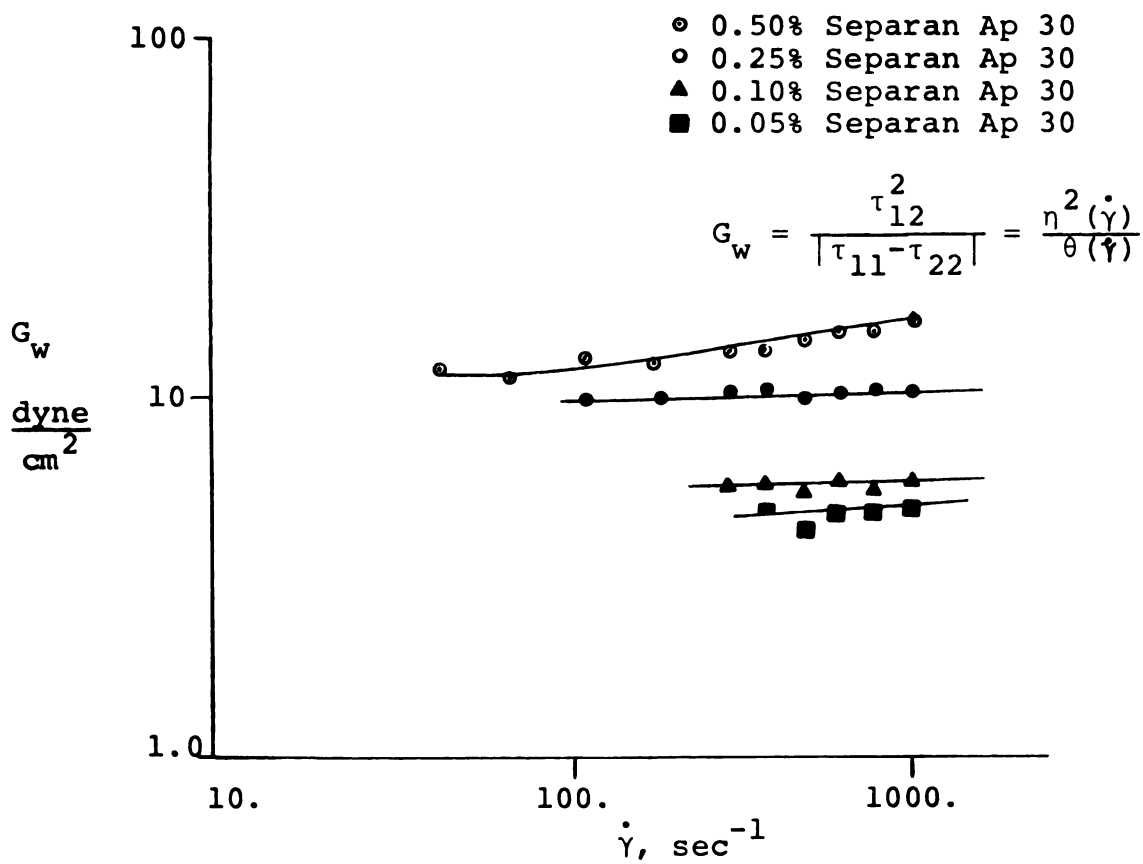


Figure 4.4-9  $G_w$ , Shear Modulus, vs.  $\dot{\gamma}$ , Shear Rate

extended in shear. Values of  $\theta(\dot{\gamma})/\eta(\dot{\gamma})$  are tabulated in Appendix G and plotted in Figure 4.4-10 for the four sets of aqueous solutions of polyacrylamide. This concept of a time-constant is entirely independent of the specific rheological model.

## 5. Evaluations of Material Parameters

Various material parameters of several rheological models were determined using the data as previously described.

### A. Power-law Model (n,K)

The value of  $n$  was obtained from the slope of the plot  $\log \eta$  vs.  $\log \dot{\gamma}$  and  $K$  was chosen based on best fit for data. The material parameters for the power-law model are summarized in Table 4.4-1 and percent deviations of values calculated from data and model are tabulated in Appendix J.

The power-law model provided a good fit to the viscometric data at high shear rate. At low shear rate deviations are large because the model does not predict a limiting viscosity at zero-shear. The power-law model does not describe normal stress difference. The deviation of viscosity calculated from this model with the data at sufficiently large values of  $\dot{\gamma}$  ( $\dot{\gamma} > 10.76 \text{ sec}^{-1}$ ) was 6.36 percent.

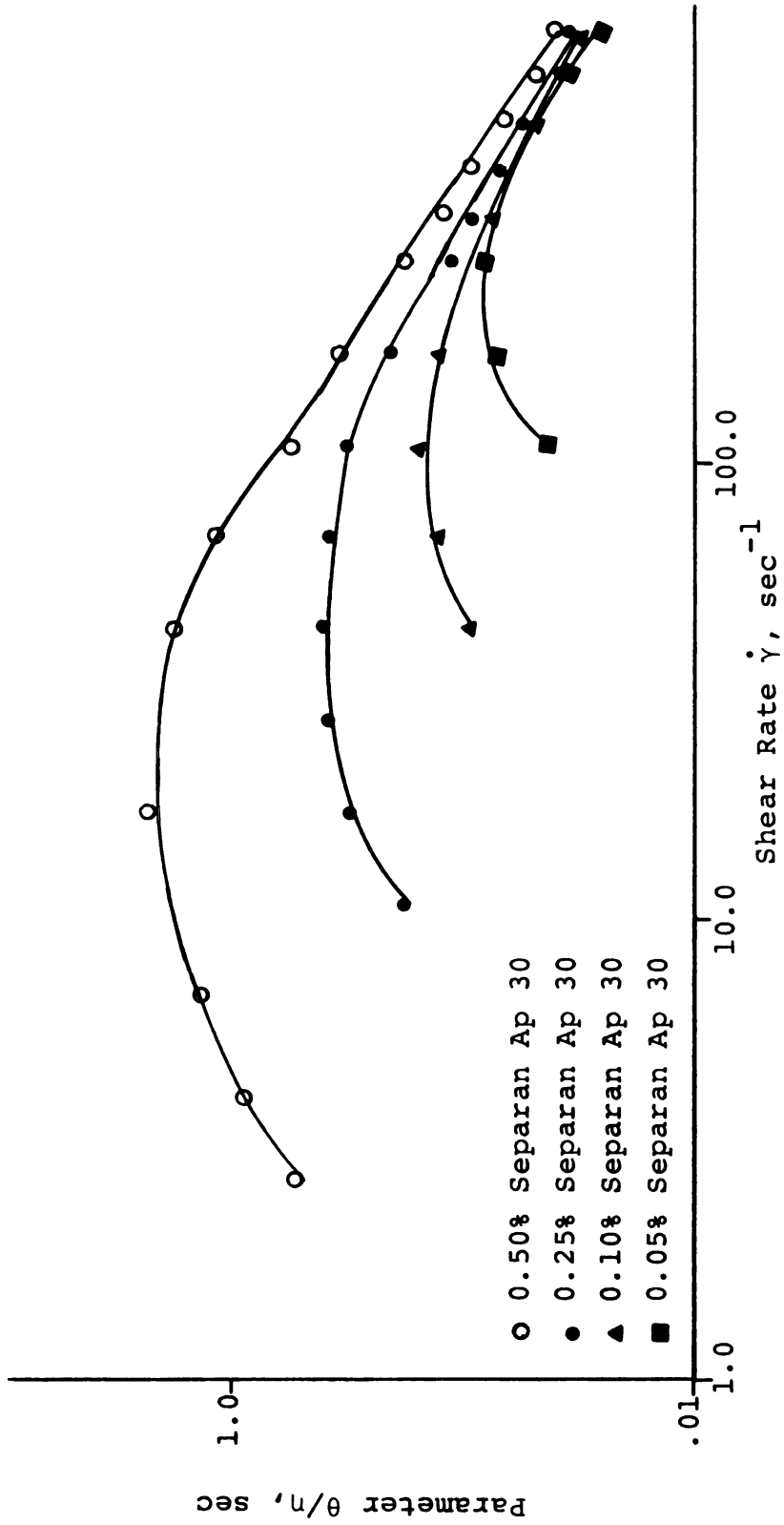


Figure 4.4-10 Model Independent Parameter  $\theta/\eta$  vs.  $\dot{\gamma}$

TABLE 4.4-1 Power-law Parameters for Polyacrylamide Solutions as Obtained from a Weissenberg Rheogoniometer at 21°C

Solution Concentration (weight %)	Fluid Density $\rho$ (gr./cc)	$n$ (dimensionless)	$k$ (gr./cm. sec <sup>2-n</sup> )	Experimental Range of Shear Rate (sec <sup>-1</sup> )	Avg. % Error in $\eta_{calc}$ for the Large Values of $\dot{\gamma}$
0.50	0.9999	0.4047	14.8919	0.675-851.	4.02
0.25	0.9982	0.4104	8.9187	1.076-851.	6.51
0.10	0.9978	0.4259	4.7281	2.689-851.	8.55
0.05	0.9975	0.4566	3.0046	16.97-851.	6.96

<sup>a</sup> Average of the absolute values of error tabulated in Appendix J.

<sup>b</sup> Average % error in  $\eta_{calc}$  was calculated as:

$$\frac{\eta_{calc} - \eta_{expt}}{\eta_{calc}} \times 100$$

B. Ellis Model ( $\eta_0$ ,  $\alpha$ ,  $\tau_{1/2}$ )

From the viscosity data the zero-shear limiting viscosity,  $\eta_0$ , was determined as

$$\eta_0 = \lim_{\dot{\gamma}_0 \rightarrow 0} \eta \quad (4.4-17)$$

Then, the value of  $\tau_{1/2}$  was obtained immediately as:

$$\tau_{1/2} = |\tau_{12}| \quad \text{at } \eta = \frac{1}{2} \eta_0 \quad (4.4-18)$$

Next,  $\log |\eta_0/\eta - 1|$  vs.  $\log |\tau_{12}/\tau_{1/2}|$  was plotted. The slope is equal to  $(\alpha - 1)$ . A summary of Ellis parameters for polyacrylamide solutions is contained in Table 4.4-2. Calculated viscosities for each polyacrylamide solution with corresponding material parameters are tabulated in Appendix I. As discussed in the previous chapter the Ellis model does not describe normal stress differences. The agreement of the model with the data was characterized by an average deviation of 7.16%.

C. Sprigg's Four-parameter Model ( $\eta_0$ ,  $\alpha$ ,  $\lambda$ ,  $\epsilon$ )

The Sprigg's model parameters for polyacrylamide solutions are summarized in Table 4.4-3. The value of  $\epsilon$  was set to be zero according to the Weissenberg hypothesis. Considerable controversy exists regarding the relative magnitudes of the primary and secondary normal stress differences. No attempt was made to measure secondary

TABLE 4.4-2 Ellis Parameters for Polyacrylamide Solutions as Obtained from a Weissenberg Rheogoniometer at 21°C

Solution Concentration (weight %)	Fluid Density, (gr./cc)	$\eta_0$ (gr./cm. sec)	$\alpha$ (dimensionless)	$\tau_{1/2}$ (dynes/cm <sup>2</sup> )	Experimental Range of Shear Rate (sec <sup>-1</sup> )	Avg. % Error in $\eta_{calc}$
0.50	0.9999	43.5213	2.4712	7.185	.00675-851	4.70
0.25	0.9982	18.7862	2.4367	5.310	.02689-851	6.49
0.10	0.9978	6.0870	2.3481	3.920	.04272-851	6.88
0.05	0.9975	2.6026	2.1902	3.390	.1076-851	9.39

<sup>a</sup>Average of the absolute values of error are tabulated in Appendix I.

TABLE 4.4-3 Spriggs 4-Constant Model Parameters for Polyacrylamide Solutions  
as Obtained from a Weissenberg Rheogoniometer at 21°C

Solution Concen- tration (weight %)	Fluid Density $\rho$ (gr./cc)	$\eta_0$ (gr./cm. sec)	$\alpha$ (dimensionless)	$\lambda$ (sec)	Average % Error in $\eta_{cal}$
0.50	0.9999	43.5213	2.3770	3.6273	5.10
0.25	0.9982	18.7862	2.2701	2.6084	3.76
0.10	0.9978	7.0870	2.0812	1.4798	3.03
0.05	0.9975	2.6026	1.8900	0.9933	1.87

<sup>a</sup>The value of  $\epsilon$  was taken as being of 0.

<sup>b</sup>The value of  $c$  was calculated to be 0.8165.

<sup>c</sup>The relaxation time constant,  $\lambda$ , was evaluated based on above values, i.e.,  
 $c$  is 0.8165 and  $\epsilon$  is 0.

normal stress difference in this study, but there is evidence that secondary normal stress,  $(\tau_{22} - \tau_{33})$ , is considerably smaller than the primary normal stress difference. Both positive and negative values for the coefficient of the secondary normal stress difference have been reported [44, 49, 50, 51, 52, 53].

The Sprigg's four-parameter model provided an excellent fit to the viscometric data at both low and high shear rates. At intermediate shear rates where viscosity starts to decrease as shear rate increases the fit is somewhat poorer. Calculated viscosities and normal stresses for each of the polyacrylamide solutions are tabulated in Appendix K. The deviation of viscosity calculated from this model with the data was 3.43 percent.

Comparisons of model predictions with the data for shear stress relaxation are given in Figure 4.4-11. The agreement is fair because all the parameters were determined from the data on steady shear flow only. This model adequately predicts how the ratio  $\tau_{12}(t)/\tau_{12}(0)$  relaxes rapidly as the initial shear rate  $\dot{\gamma}_0$  is increased.

#### D. Bird-Carreau Model ( $\eta_0, \alpha_1, \alpha_2, \lambda_1, \lambda_2, \epsilon$ )

The material parameters for the Bird-Carreau model are summarized in Table 4.4-4. The value of  $\epsilon$  was assumed to be zero according to the Weissenberg hypothesis.

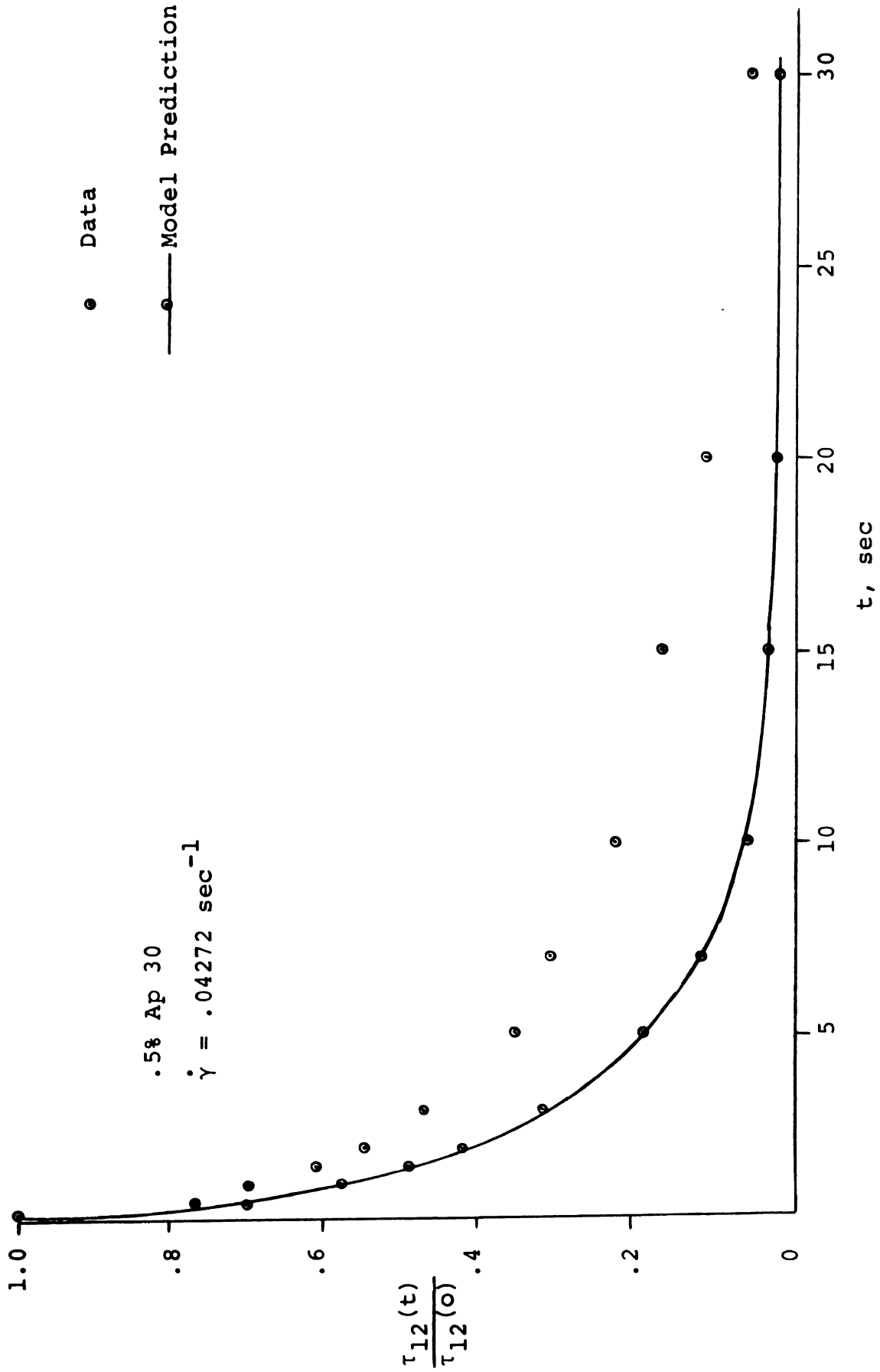
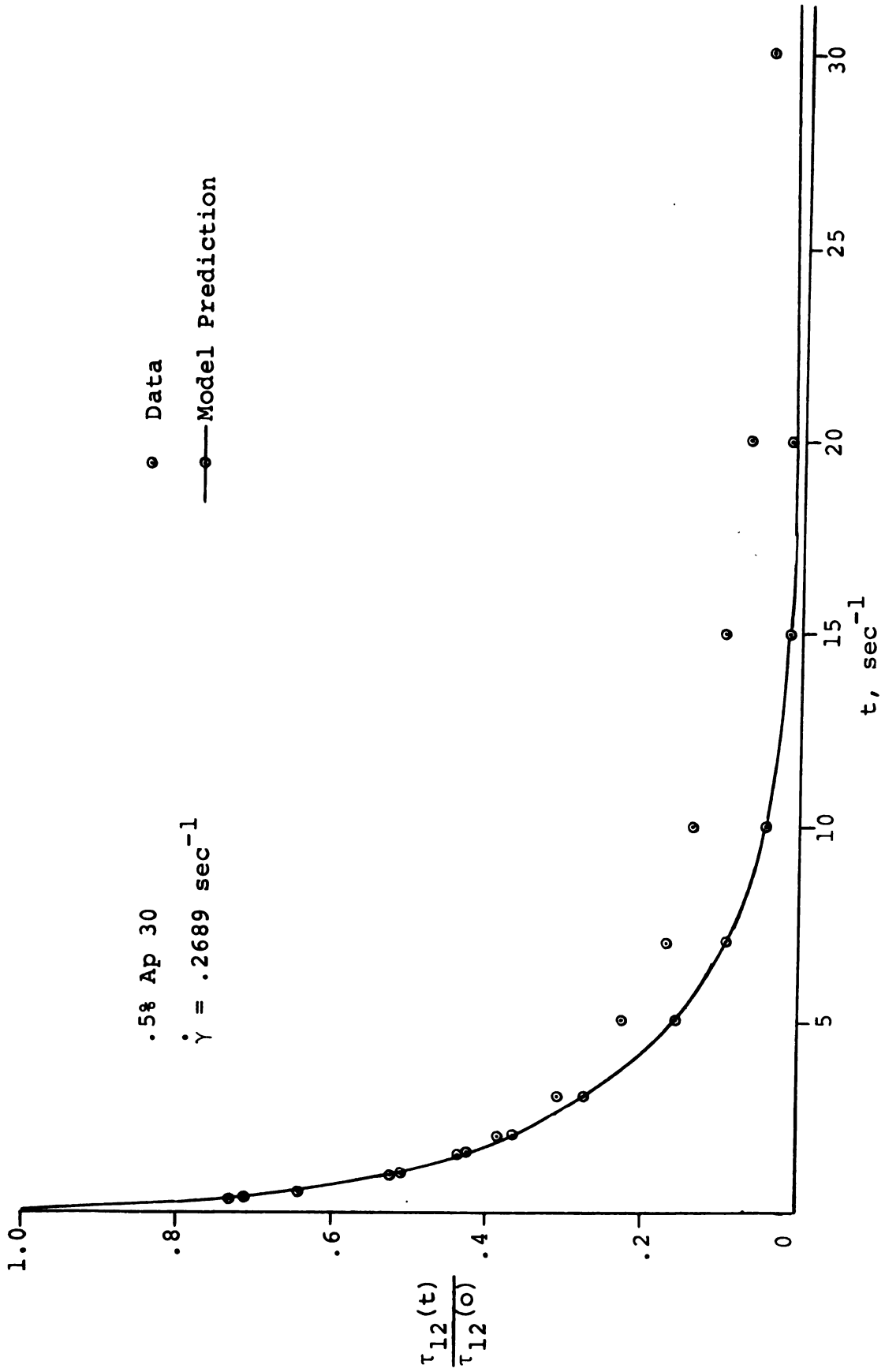
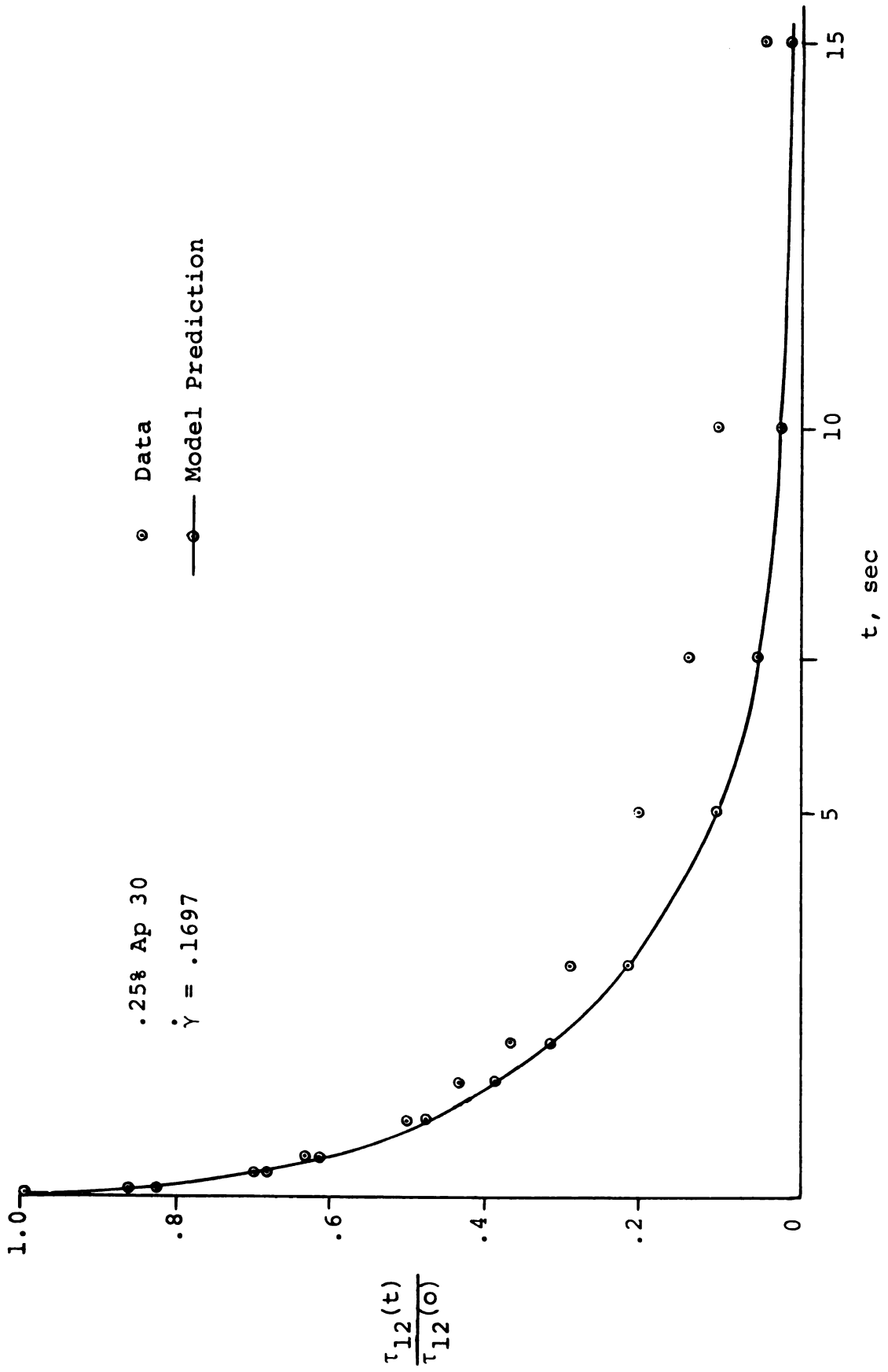
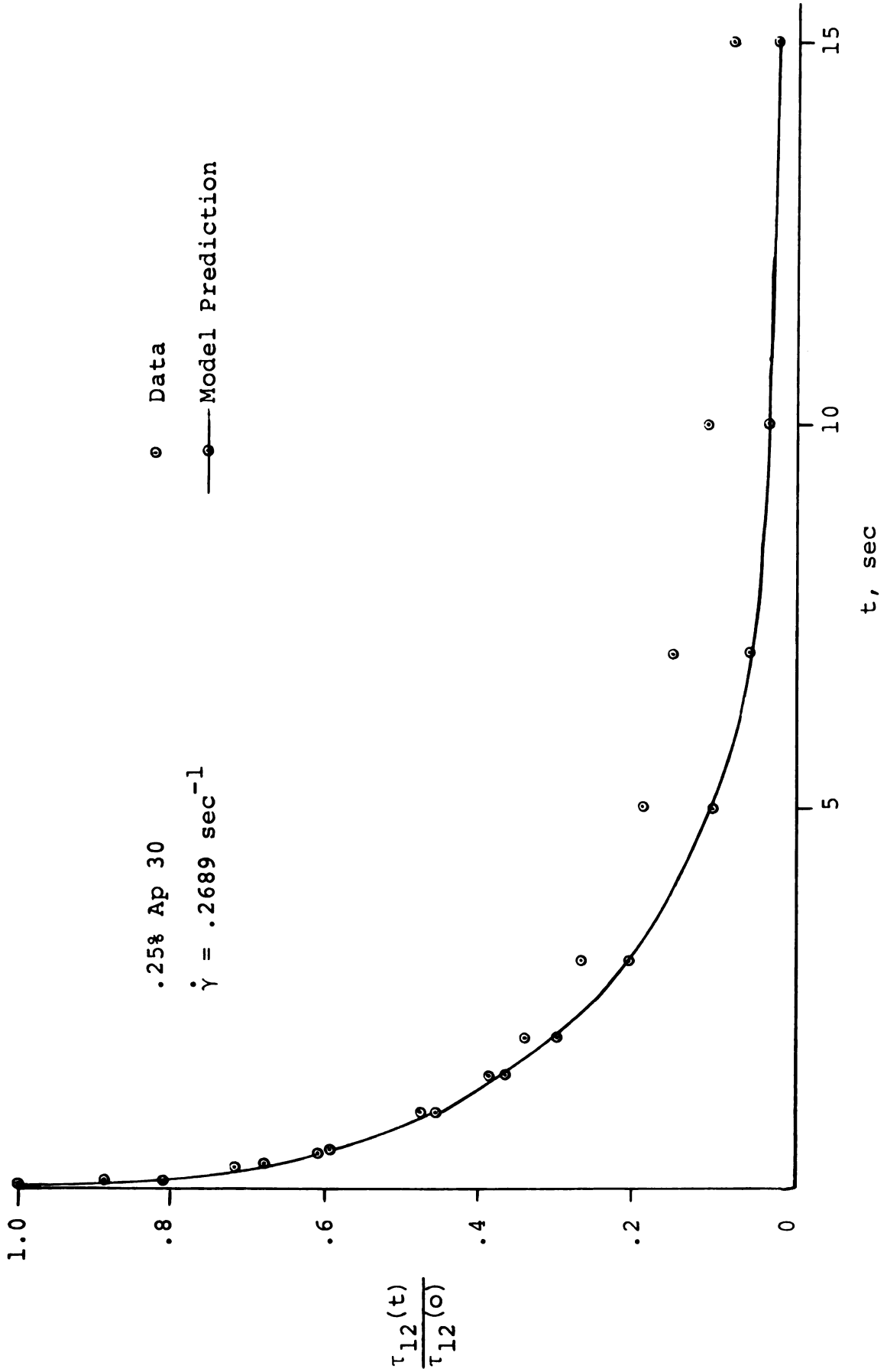
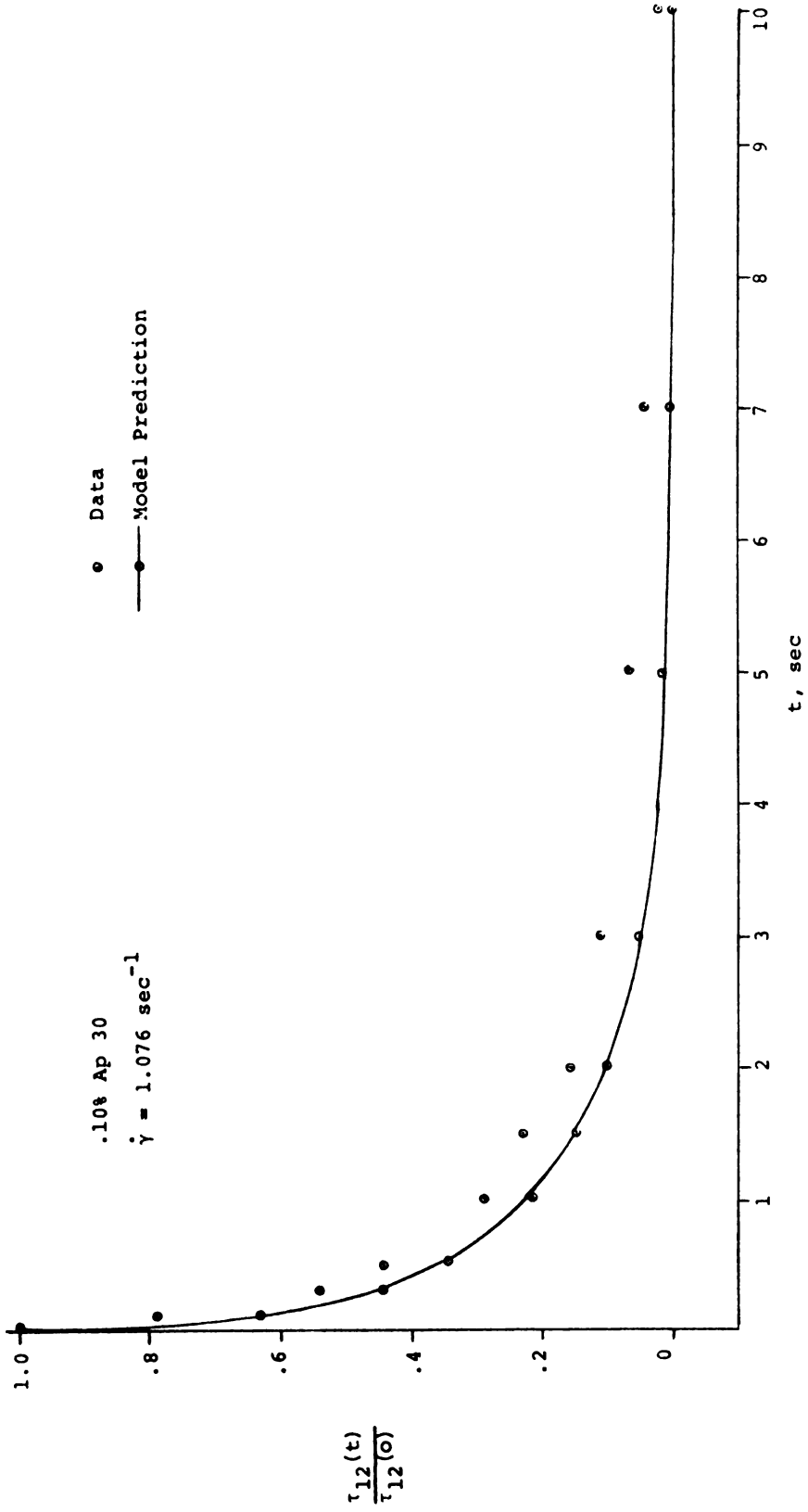


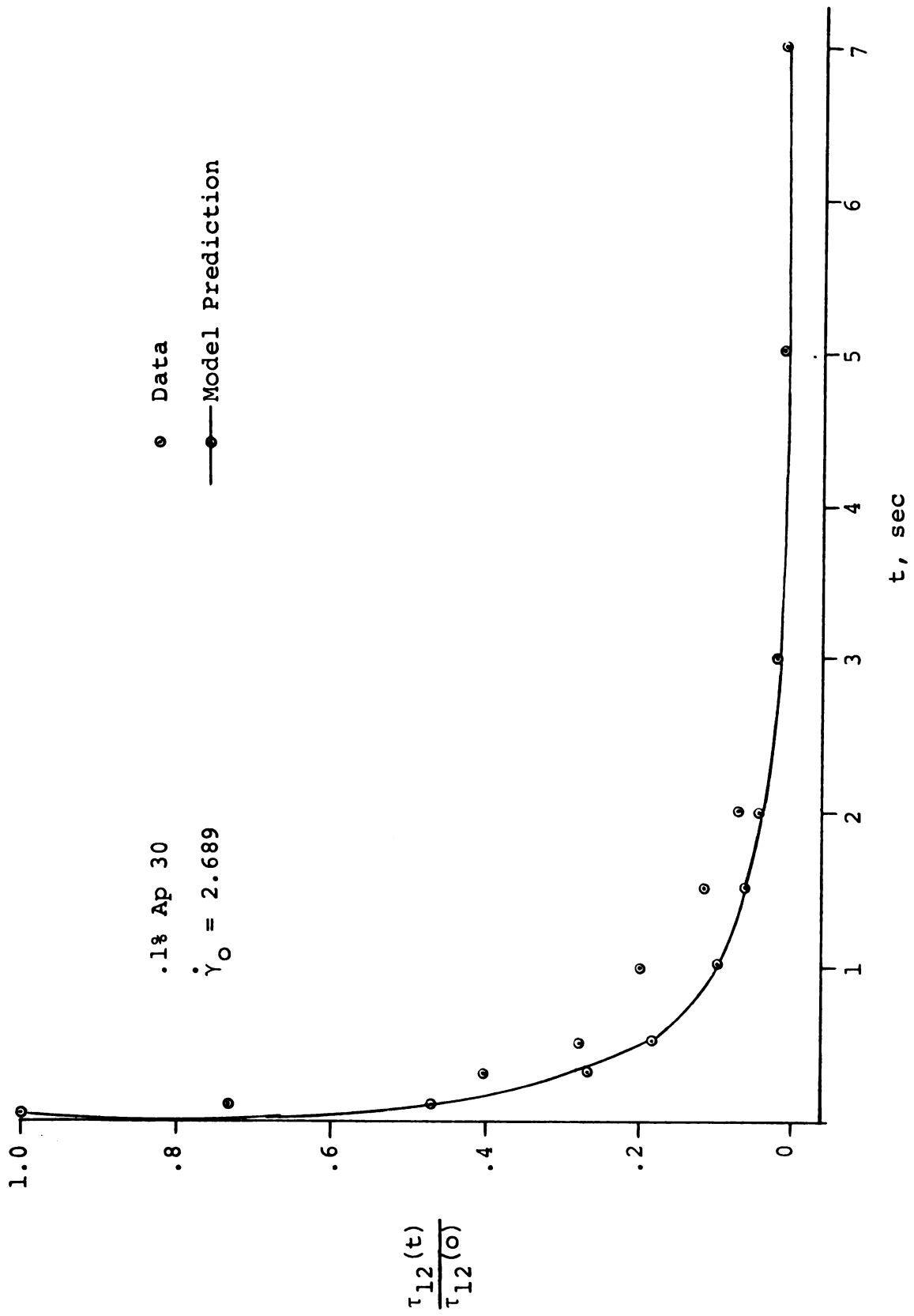
Figure 4.4-11  $\frac{\tau_{12}(t)}{\tau_{12}(0)}$ , Unsteady State Shear Stress, vs. t, Real time for Polyacrylamide Solutions

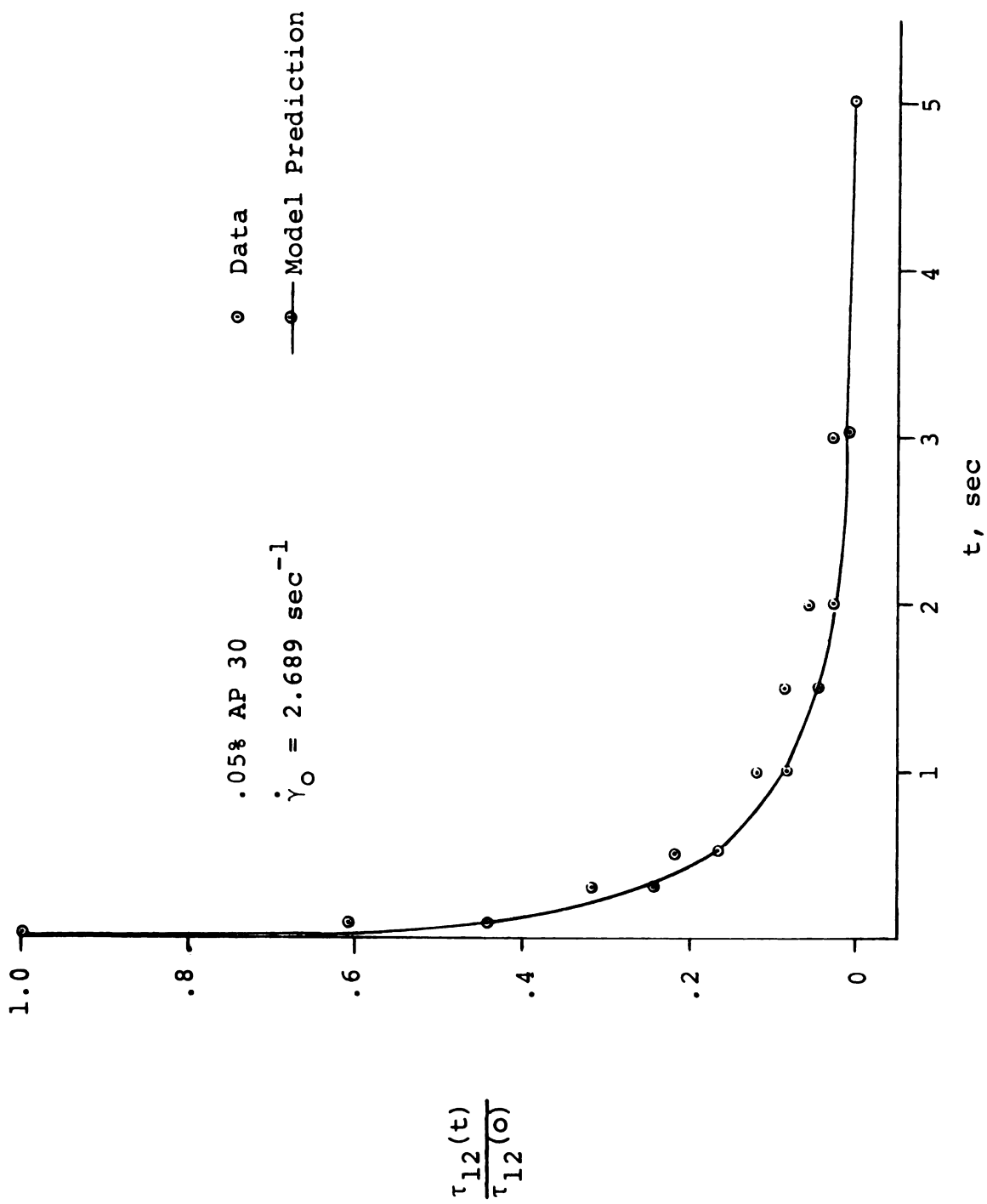












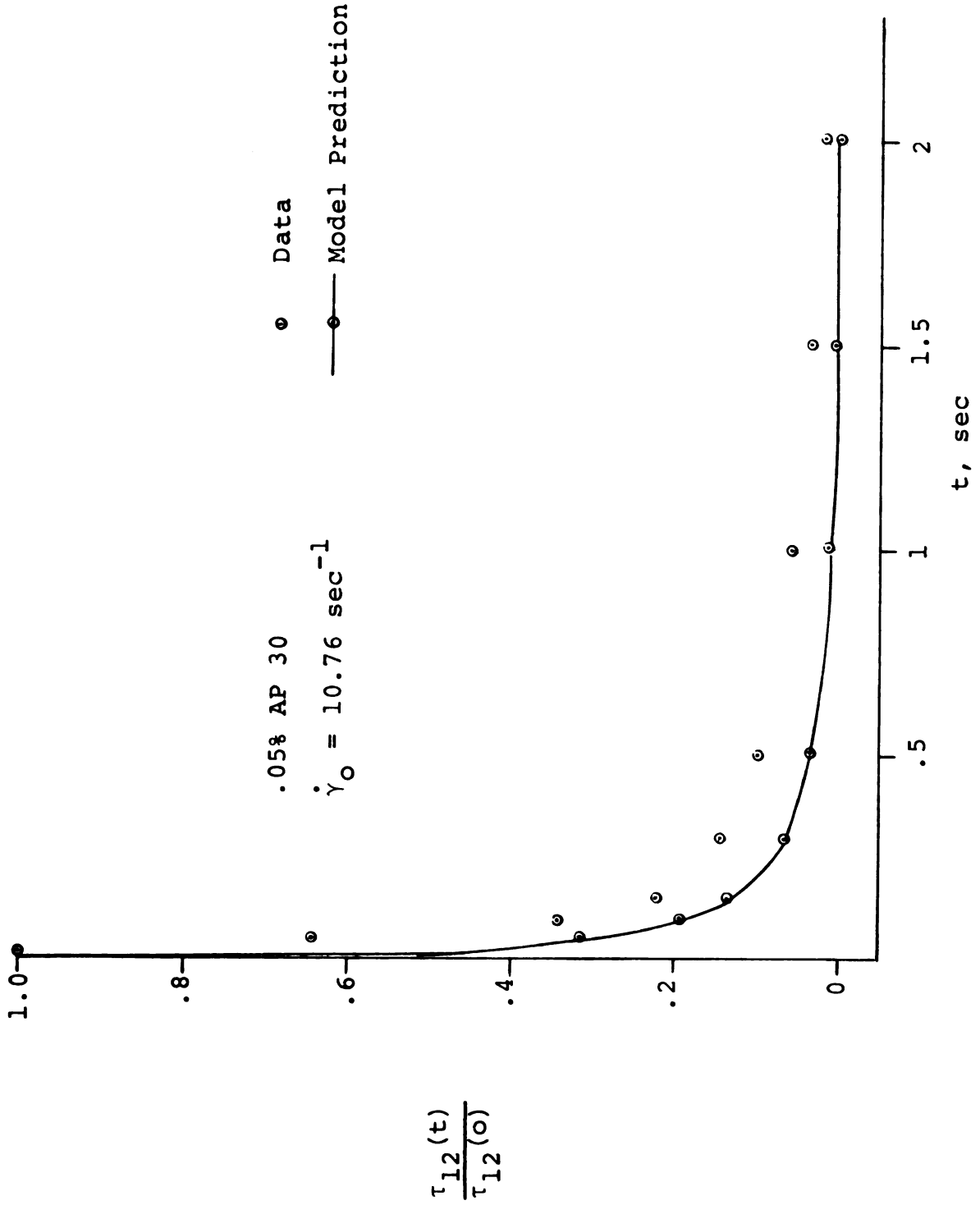


TABLE 4.4-4 Bird-Carreau Model Parameters for Polyacrylamide Solutions as Obtained from a Weissenberg Rheogoniometer at 21°C

Solution Concentration (weight %)	Fluid Density $\rho$ (gr./cc)	$\eta_0$ (gr./cm. sec)	$\alpha_1$ (dimensionless)	$\alpha_2$ (dimensionless)	$\lambda_1$ (sec)	$\lambda_2$ (sec)
0.50	0.9999	43.5213	2.3770	1.6228	5.0816	3.2735
0.25	0.9982	18.7862	2.2701	1.2131	3.5921	0.9093
0.10	0.9978	6.0870	2.0812	0.9218	1.9976	0.3753
0.05	0.9975	2.6026	1.8900	0.8118	1.2905	0.2742

<sup>a</sup>All Model parameters were obtained by eyeball fitting.

Viscosity and primary normal stress difference were calculated for each polyacrylamide solution. As indicated previously, the Bird-Carreau model is supposed to be an improvement over the Sprigg's model. The predictions of viscosity with the Bird-Carreau model were similar to those of the Sprigg's model; however, the Bird-Carreau model correlated primary normal stress differences much better than the Sprigg's model.

Viscosity data were weighted three times as heavily as normal stress data for evaluation of material parameters using a least squares criterion for best fit. Details of the least squares procedure and computer program used for data analysis are reported elsewhere [109, 110]. The material parameters for the Bird-Carreau model are contained in Table 4.4-5. Calculated viscosities and normal stresses for each polyacrylamide solution with the corresponding material parameters are tabulated in Appendix L. The deviation of viscosity calculated from this model with the data was 2.77 percent.

#### §4.5 The Flow of Non-Newtonian Fluids Through Porous Media

Equations for the modified Reynolds number based on the result of a hydrodynamic analysis of the capillary model of the packed bed for the power-law, Ellis, and Sprigg's model were developed in Appendix A

TABLE 4.4-5 Bird-Carreau Model Parameters for Polyacrylamide Solutions as Obtained from a Weissenberg Rheogoniometer at 21°C

Solution Concen- tration (weight %)	Fluid Density $\rho$ (gr./cc.)	$\eta_0$ (gr./cm. sec)	$\alpha_1$ (dimension- less)	$\alpha_2$ (dimension- less)	$\lambda_1$ (sec)	$\lambda_2$ (sec)
0.50	0.9999	43.5213	2.2777	1.5872	4.4578	4.6395
0.25	0.9982	18.7862	2.2071	1.2401	5.0023	1.2335
0.10	0.9978	6.0870	2.1133	0.7179	2.3172	0.1874
0.05	0.9975	2.6026	1.9112	0.6179	1.2323	0.1166

<sup>a</sup>All parameters were obtained by computer analysis for the least square errors.

with results listed in Table 3-1. The modified Ergun friction factor for these models is:

$$f_{\text{calc}}^* = \frac{150}{N_{\text{Re,eff}}} + 1.75 \quad (4.5-1)$$

Data from flow experiments for aqueous solutions of polyacrylamide in packed beds were correlated with the Ergun friction factor.

#### §4.5.1 Experiments

Polyacrylamide solutions of four different concentrations (0.05, 0.10, 0.25, and 0.50 weight percent) were made up and filtered to avoid gel formation, and then poured into the jacketed storage tank maintained at 21°C. Gentle stirring was maintained for about one day preceding the flow experiments.

All electrical circuits were switched on for about 5 minutes before runs were made. The schematic diagram of the jacketed flow system which maintained constant temperature  $21 \pm 0.5^\circ\text{C}$  is shown in Figure 4.5-1. Nitrogen tank A was used to cause the flow of polymer solution from the storage tank to the packed bed, whereas nitrogen tank B was used as a controlling device to maintain a constant flow rate through the bed. The pressure transducer was connected into two taps of the column which were 1.5 ft. apart. Various flow rates were obtained

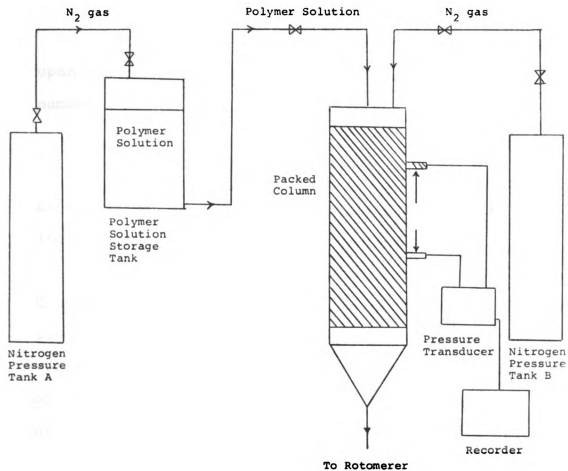


Figure 4.5-1 Schematic Diagram of the Equipment

by adjusting valves at the top and bottom of the column and measured with the appropriate rotometer. Pressure drop for each flow rate was recorded. Details of experimental procedures are contained in Appendix C.

#### §4.5.2 Results and Discussion

The analysis of the flow experiments was based upon the packed bed friction factor and modified Reynolds number

$$f^* = f^*(N_{Re,eff}) \quad (4.5-2)$$

as summarized in the previous chapter for various rheological models of fluids in porous media.

Ergun [83] and Carman [69] reported the value of  $C$  in the permeability equation for Newtonian fluid to be 150 and 180, respectively. Sadowski [2, 3] used the value of 180 for  $C$  for non-Newtonian fluids. Christopher and Middleman [4], Gregory and Griskey [6] used the value of 150 for  $C$  for non-Newtonian fluids. The form of data with Newtonian fluid (distilled water) exhibited good agreement with Ergun's correlation, i.e.,  $C = 150$  for values of  $N_{Re} < 1.0$ . The average percent deviation for the friction factor, based on this value, was 4.6% for 33 experimental points. Henceforth, the value of  $C$  used for this study was 150.

The result of friction factor versus Reynolds number for the Newtonian fluid (distilled water) is plotted in Figure 4.5-2 and tabulated in Appendix M. Results for non-Newtonian fluids are plotted in Figures 4.5-3,4,5, and 6 and are tabulated in Appendices N, O, and P for the power-law, Ellis, and Sprigg's model modifications, respectively. The modified Reynolds numbers ranged between  $10^{-5}$  and 1.0. Wall effects correction was introduced in each calculation with M defined in Eq. (A.3-32). This is shown in Figure 4.5-7.

#### Power-law Model

The data for all concentrations showed larger deviations from the theoretical line as seen in Figures 4.5-3,4,5, and 6. The average percent deviation is listed in Table 4.5-1. The friction factor,  $f^*$ , was consistently too low for the entire range of Reynolds numbers. No trends were observed with respect to Reynolds numbers or fluid concentrations. The departure from the relation

$$f^* = \frac{150}{N_{Re,eff}} + 1.75 \quad (4.5-3)$$

was so great as to suggest that it was a result of a failure in the development of theory rather than a result of experimental error. That is,  $N_{Re,eff}$  decreased faster with an increasing shear rate than the power-law model predicted.

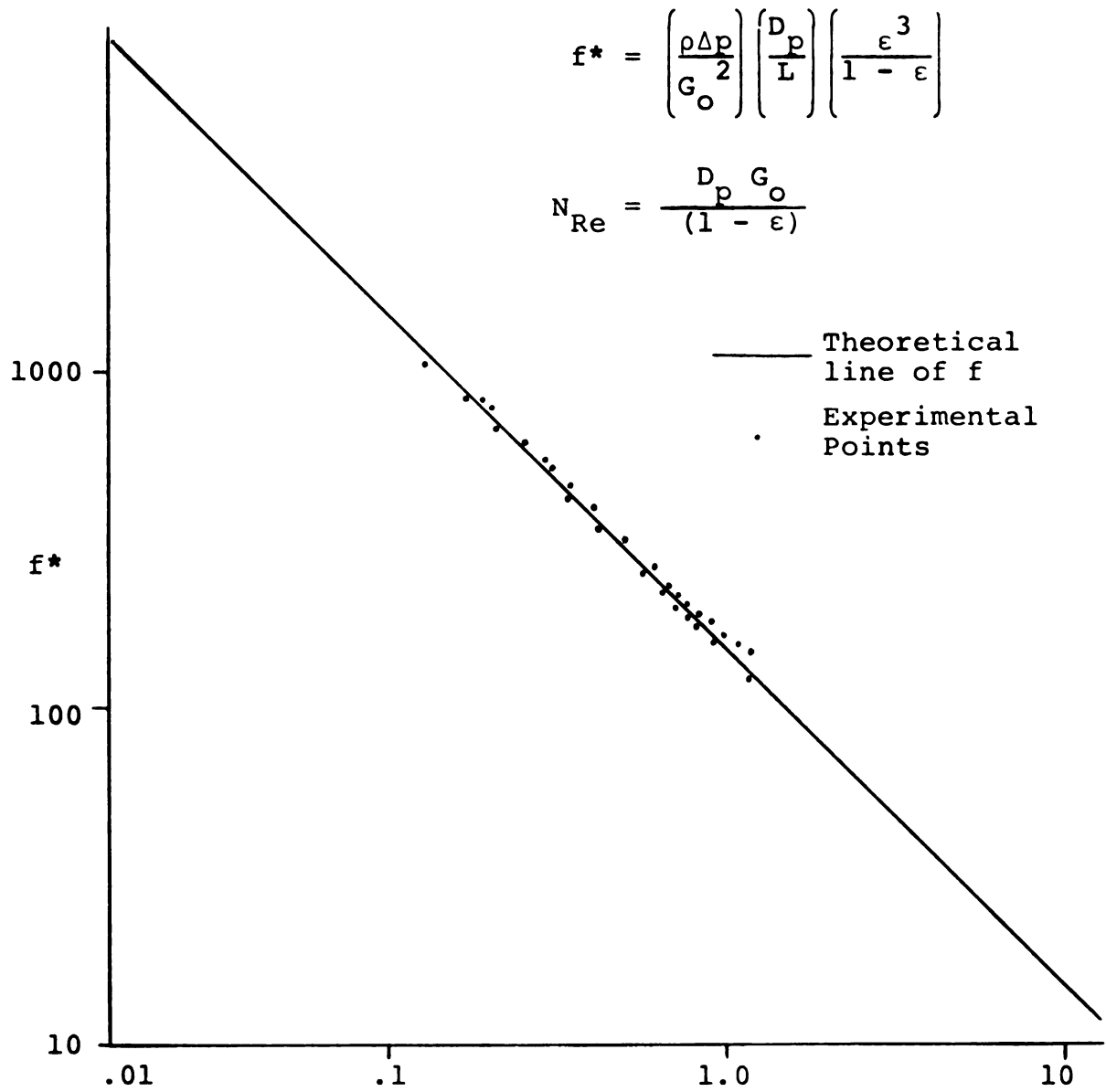


Figure 4.5-2  $f^*$ , Friction Factor vs.  $N_{Re}$ , Reynolds Number for Newtonian Fluid

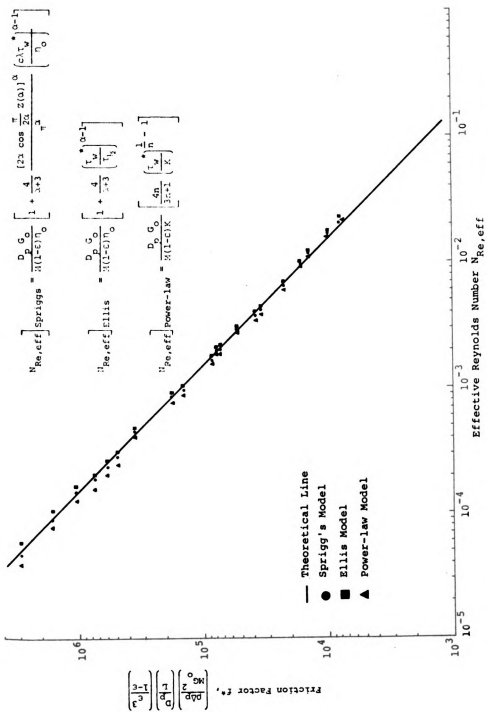


Figure 4.5-3 Pressure Drop-Flow Rate Correlation for Flow of 0.50% Aqueous Solutions of Separan Ap 30 Through Packed Beds

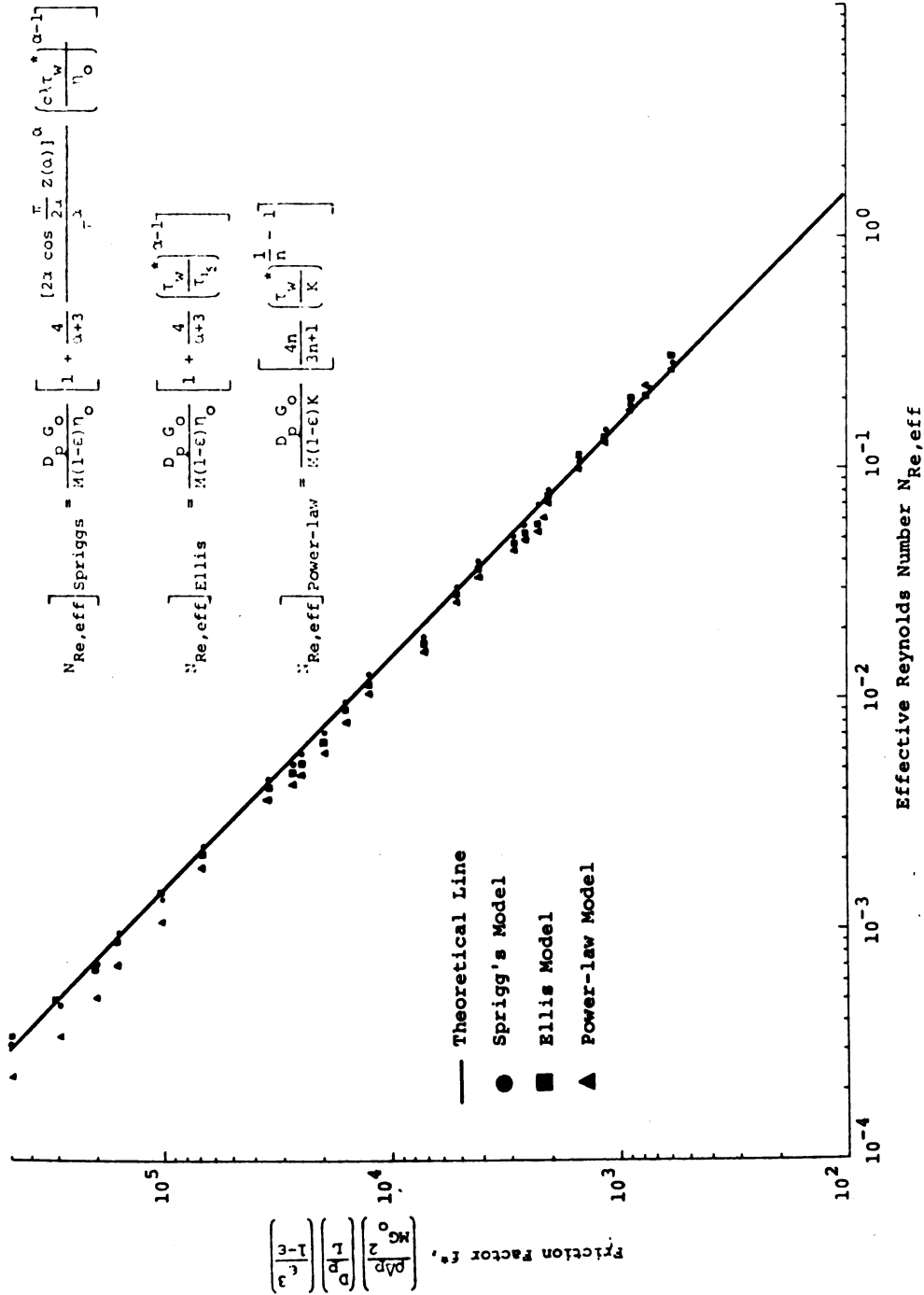


Figure 4.5-4 Pressure Drop-Flow Rate Correlation for Flow of 0.25% Aqueous Solutions of Separan Ap 30 Through Packed Beds

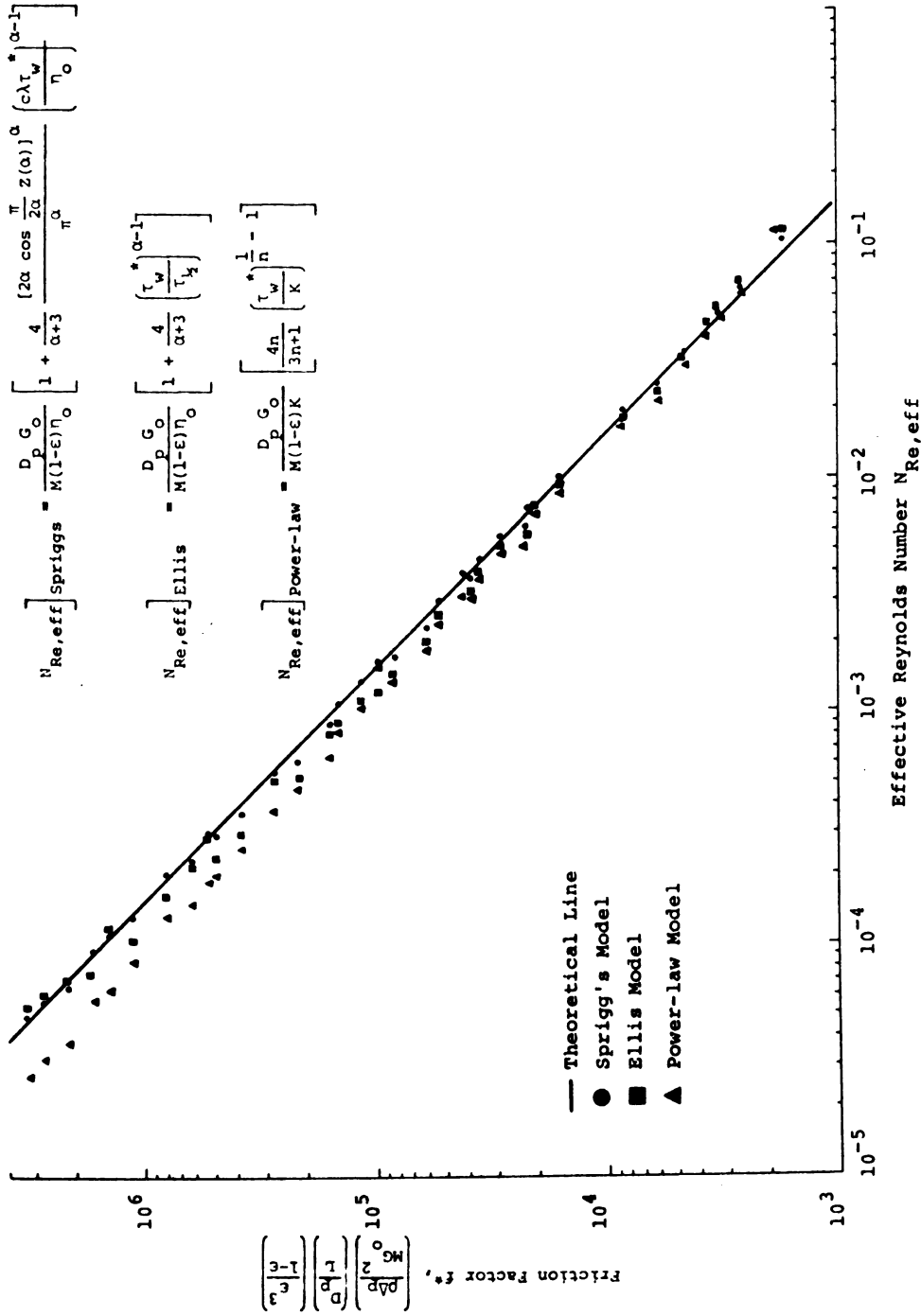


Figure 4.5-5 Pressure Drop-Flow Rate Correlation for Flow of 0.10% Aqueous Solutions of Separan Ap 30 Through Packed Beds

$$N_{Re,eff} \text{ [Spriggs]} = \frac{D_p G_o}{M(1-\epsilon)\eta_o} \left[ 1 + \frac{4}{\alpha+3} \frac{[2\alpha \cos \frac{\pi}{2\alpha} z(\alpha)]^\alpha}{\pi} \left( \frac{c\lambda \tau_w^*}{\eta_o} \right)^{\alpha-1} \right]$$

$$N_{Re,eff} \text{ [Ellis]} = \frac{D_p G_o}{M(1-\epsilon)\eta_o} \left[ 1 + \frac{4}{\alpha+3} \left( \frac{\tau_w^*}{\tau_k} \right)^{\alpha-1} \right]$$

$$N_{Re,eff} \text{ [Power-law]} = \frac{D_p G_o}{M(1-\epsilon)K} \left[ \frac{4n}{3n+1} \left( \frac{\tau_w^*}{K} \right)^{\frac{1}{n}-1} \right]$$

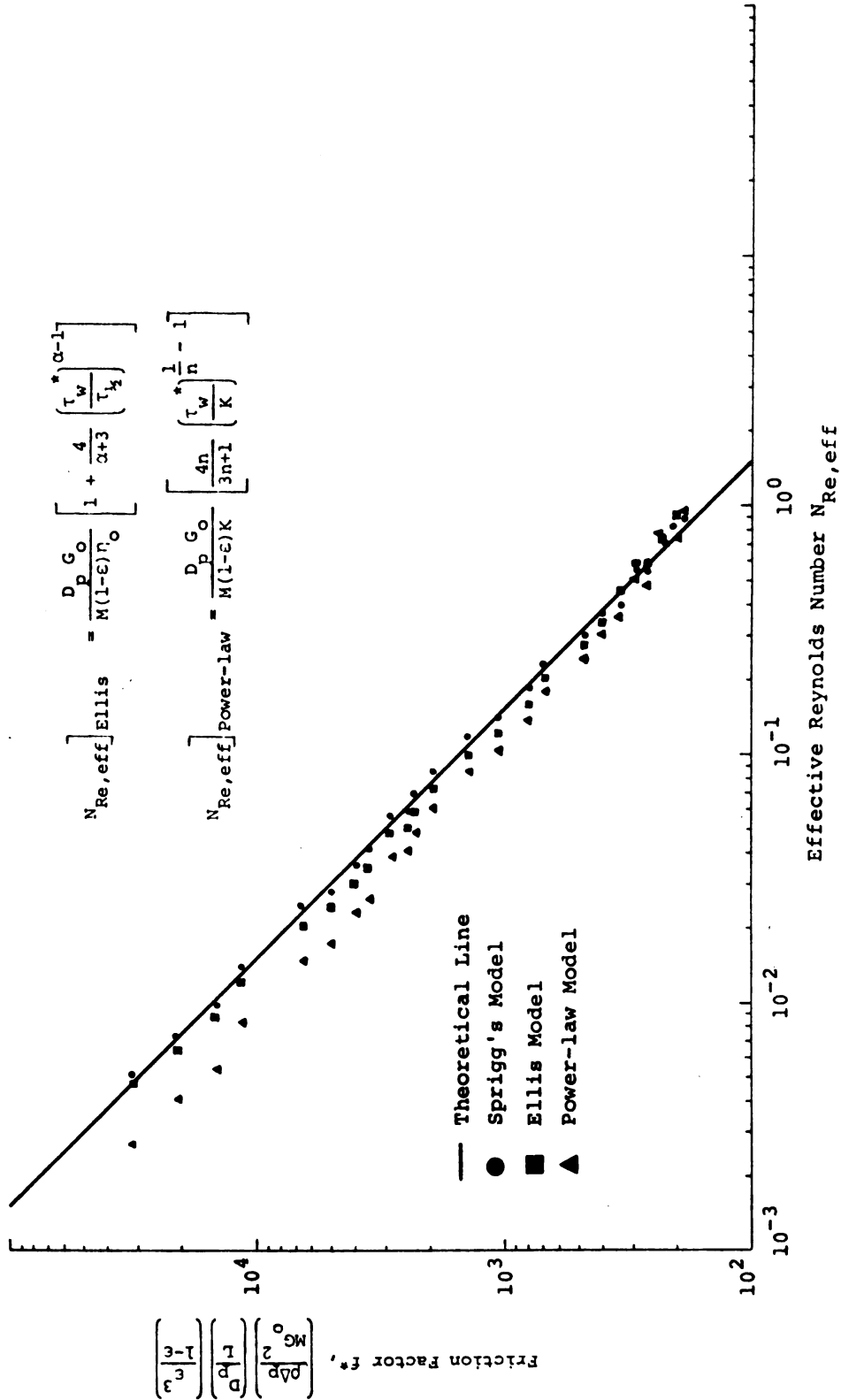
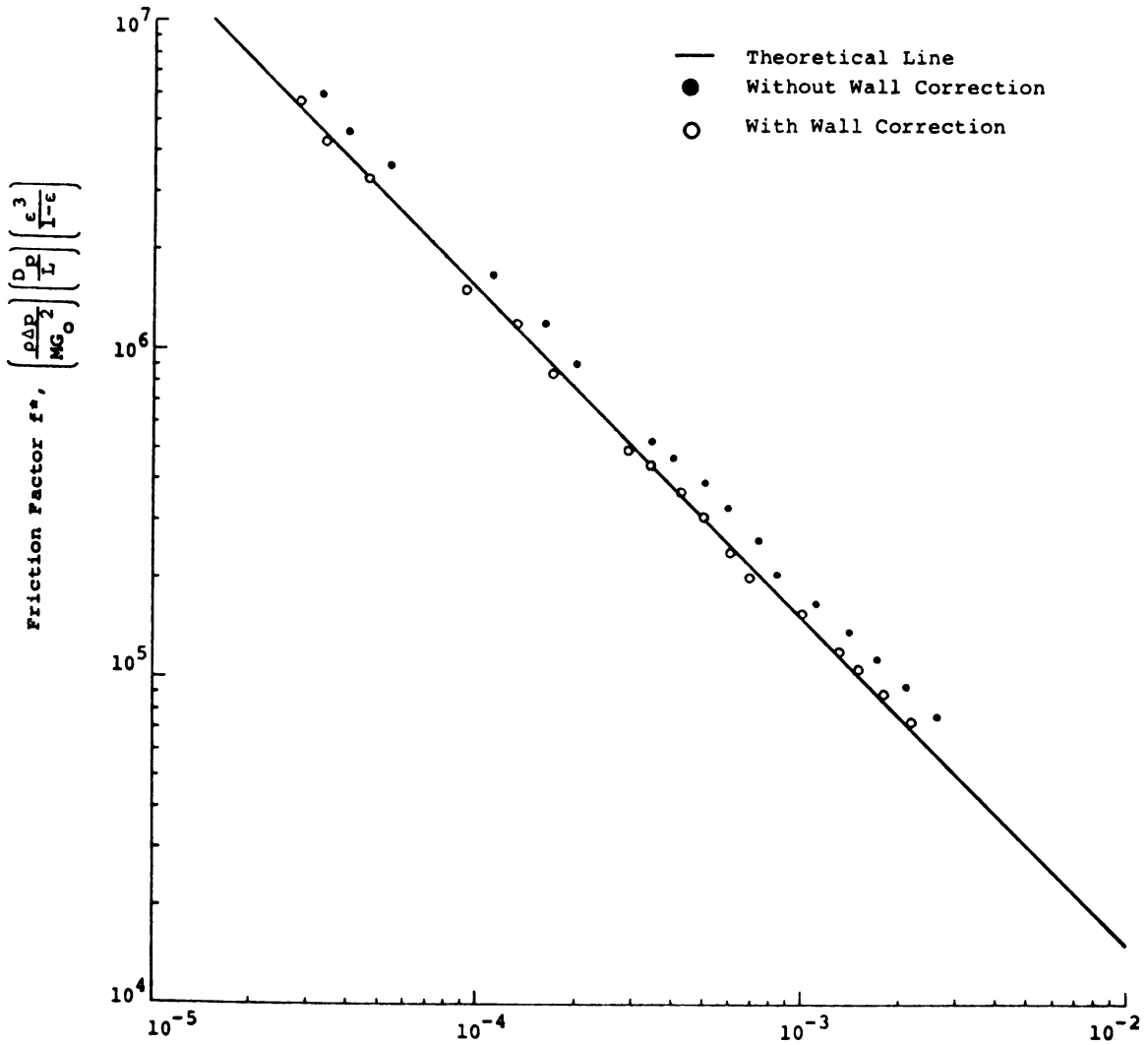


Figure 4.5-6 Pressure Drop-Flow Rate Correlation for Flow of 0.05% Aqueous Solutions of Separan Ap 30 Through Packed Beds





$$\text{Effective Reynolds Number } N_{Re,eff} = \frac{D_p G_0}{M(1-\epsilon)\eta_0} \left[ 1 + \frac{4}{\alpha+3} \frac{[2\alpha \cos \frac{\pi}{2\alpha} Z(\alpha)]^\alpha}{\pi^\alpha} \left(\frac{c\lambda r_w}{\eta_0}\right)^{\alpha-1} \right]$$

Figure 4.5-7 The Effects of the Wall Correction Factor in Friction Factor-Reynolds Number Correlation for .50% Separan Ap 30 Solution

TABLE 4.5-1 Summary of Experimental Data for Power-law Modification

Solution Concentration (weight %)	Average % Error <sup>a</sup> in f* calculated from Eq. (4.5-38)	Number of Experimental Points	Maximum Range of % Error
0.50	10.07	20.0	-8.07 to +22.04
0.25	14.32	25.0	-10.39 to +31.14
0.10	22.52	39.0	-25.01 to +45.89
0.05	23.77	33.0	-7.97 to +47.09
All Solutions	19.08	117.0	-25.01 to +47.09

<sup>a</sup>Average % error was calculated as

$$\frac{f^*_{\text{calc}} - f^*_{\text{expt}}}{f^*_{\text{calc}}} \times 100$$

Arithmetic average of absolute values are given in Appendix N.

Inertial effects are not apparent for Newtonian fluids until the Reynolds number exceeds a value of one. As seen in Table 4.5-1, the percent deviation of experimental and calculated friction factors was quite large, but uniform over the Reynolds number range of  $10^{-5}$  to 1.0 using the power-law model. Since the Reynolds number is less than 1.0, these deviations are not due to inertial effects.

#### Ellis Model

Some improvement over the power-law model on the friction factor correlation was obtained with the Ellis model. The average percent deviation for the Ellis model correlation is listed in Table 4.5-2.

#### Sprigg's Model

The Sprigg's model modification of the Ergun equation (see Appendix A for the development) yielded the best results. As shown in Figures 4.5-3 through 6, the data scatter about the theoretical line with an average error of 5.7%. No trends were observed with respect to Reynolds numbers or fluid concentrations. These results appear to confirm the utility of the correlation developed in this study. Sprigg's model predicts the Newtonian behavior at very low shear rates as is characteristic of most real polymer solutions. The average percent deviation for the Sprigg's model correlation is listed in Table 4.5-3.

TABLE 4.5-2 Summary of Experimental Data for Ellis Model Modification

Solution Concentration (weight %)	Average % Error <sup>a</sup> in f* Calculation from Eq. (4.5-25)	Number of Experimental Points	Maximum Range of % Error
0.50	7.96	20.0	-16.9 to + 4.4
0.25	6.57	25.0	-13.7 to +14.4
0.10	11.06	39.0	-29.3 to +24.0
0.05	9.98	33.0	-16.3 to +19.3
All Solutions	9.30	117.0	-29.3 to +24.0

<sup>a</sup>Average % error was calculated as

$$\frac{f^*_{\text{calc}} - f^*_{\text{expt}}}{f^*_{\text{calc}}} \times 100$$

Arithmetic average of absolute values are given in Appendix O.

TABLE 4.5-3 Summary of Experimental Data for Spriggs Model Modification

Solution Concentration (weight %)	Average % Error <sup>a</sup> in f* Calculation from Eq. (4.5-50)	Number of Experimental Points	Maximum Range of % Error
0.50	5.11	20.0	-11.2 to +6.7
0.25	6.06	25.0	-13.5 to +8.2
0.10	5.61	39.0	-16.1 to +7.4
0.05	5.82	33.0	-15.5 to +7.93
All Solutions	5.72	117.0	-16.1 to +8.2

<sup>a</sup>Average % error was calculated as

$$\frac{f^*_{\text{calc}} - f^*_{\text{expt}}}{f^*_{\text{calc}}} \times 100$$

Arithmetic average of absolute values are given in Appendix P.

### Comparison of Models

A complete error analysis was performed at this point to check out the deviations stated above. For each concentration and model the low and high values of shear rate at the wall in the bed were calculated. On the basis of these values error in  $\eta_{\text{calc}}$  and  $f^*_{\text{calc}}$  for each model was calculated. As expected, the Sprigg's model gave the best results followed by the Ellis model. The deviation in  $f^*_{\text{calc}}$  for the Ellis model may be due to the imperfect curve fitting process. Comparison of the Ellis model with the power-law model gave an interesting fact. The error in  $\eta_{\text{calc}}$  is the same order of magnitude for both models but the power-law model has an error in  $f^*_{\text{calc}}$  twice as large as the error in the Ellis model. This shows clearly that there is something wrong with the power-law model. A comparison of the error for each model is listed in Table 4.5-4.

Some objections to the use of the power-law model should be pointed out now. Most real polymer solutions approach Newtonian behavior at very low flow rates. The power-law does not predict this behavior. As shown in Appendix J, the power-law predicts an infinite viscosity in the limit of vanishing shear rate. This is a fundamental failure, and provides for a valid objection to the general applicability of the power-law model. By using Eq. (A.3-32), the bed shear rate at the wall,  $\dot{\gamma}_w$ , for

TABLE 4.5-4 Summary of Error Analysis

Solution Concentration (weight %)	Ranges of Experimental (sec <sup>-1</sup> ) Shear Rates in the Beds	% Error in $\eta_{calc}$	% Error in $f^*_{cal}$
<b>A. Sprigg's Model</b>			
0.50	1.13- 51.22	1.95	5.11
0.25	2.43-188.0	1.36	6.06
0.10	1.92-297.2	1.69	5.61
0.05	6.16-221.97	2.23	5.83
<b>B. Ellis Model</b>			
0.50	1.36- 61.64	3.65	7.96
0.25	2.96-229.88	6.10	6.57
0.10	2.39-371.26	8.36	11.06
0.05	7.80-280.99	8.30	9.98
<b>C. Power-law Model</b>			
0.50	1.15- 52.12	3.70	10.07
0.25	2.51-194.16	5.99	14.32
0.10	2.02-312.78	7.52	22.87
.05	6.54-253.59	10.29	23.57

each experimental point was calculated and compared with viscometric data. Shear rate at the wall of the hypothetical capillary is in the power-law region; but the shear rate at the center of the capillary is zero. The power-law model would be expected to characterize the fluid close to the wall rather well, but not toward the center because of the existence of a limiting viscosity at low shear rate which is not predicted by the power-law model. A more serious problem is that it is an inelastic model. Polyacrylamide does exhibit viscoelastic behavior which is predicted by the Sprigg's model but not by the power-law or Ellis model. An elemental volume of fluid actually experiences continual acceleration and deceleration as the fluid moves through irregular interstices between particles. Hence, for flow of non-Newtonian fluids in porous media, we might expect to observe viscoelastic effects which do not show up in the steady state spatially homogeneous flows usually used to establish the rheological parameters.

#### §4.6 Conclusions

Results of the present investigation may be summarized as follows:

1. Material parameters for the power-law, Ellis, Sprigg's, and Bird-Carreau model for aqueous solutions of polyacrylamide were evaluated.

The Ellis model adequately represented the fluid. The power-law model represented the fluid well only in the power-law region. Both the power-law and the Ellis models do not account for normal stress differences. The Sprigg's model correlated the steady shear experimental data very well, but did not correlate the normal stress difference data well. The Bird-Carreau model correlated the normal stress difference data considerably better than the Sprigg's model and described the steady shear data very well.

2. When the flow rate of the 0.50 percent solution passing through the packed bed was less than 1 cc./min., the flow rate continuously decreased. Adsorption of large polymer molecules on the surface of beads and consequent gel formation was observed at very low flow rate and long test run. Polymer adsorption and gel formation reduced the bed permeability which automatically lowered the flow rate.
3. The Sprigg's model gave the most successful results for values of effective Reynolds numbers less than one. These results appear to confirm the utility of the correlation developed in this study. The error analysis confirmed that there is some objection in the use of the power-law model for flow problems.

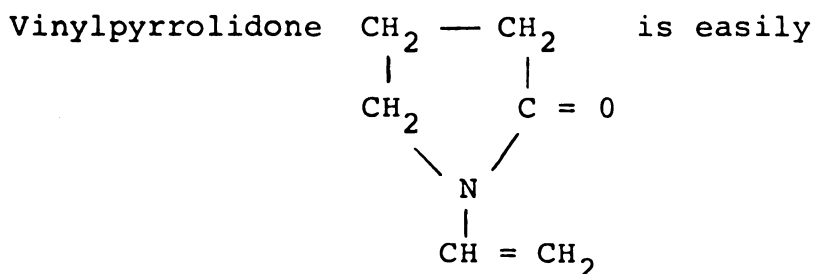
## CHAPTER 5

### POLYVINYLPIRROLIDONE SYSTEM

Polyvinylpyrrolidone (PVP) is an essentially linear polymerization product of vinylpyrrolidone. The polymerization is usually carried out in aqueous solution at somewhat elevated temperatures. Hydrogen peroxide is used as catalyst and ammonia or an amine as activator. Of various parameters determining the chain length, the concentration of hydrogen peroxide has the greatest effect [92].

The polymer, when prepared in a certain range of molecular weight, is a valuable blood plasma extender. A plasma extender is a compound which, when infused into the blood stream, keeps a normal volume of liquid in circulation by its osmotic effect.

#### §5.1 Chemistry



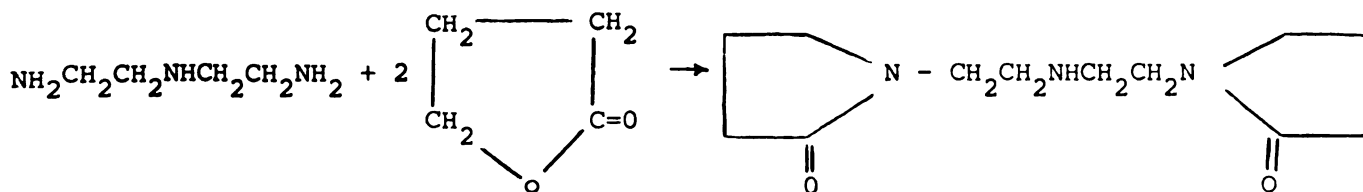


block-polymerized in a simple manner with hydrogen peroxide as catalyst. Thirty-five Kg of vinylpyrrolidone are added to 150 cc of hydrogen peroxide (30%) and heated to 110°C. The polymerization is exothermic and the temperature rises to 180 to 190°C. The molten polymer is poured from the kettle, cooled on a plate and milled on a ball mill to a fine, white, somewhat hygroscopic powder.

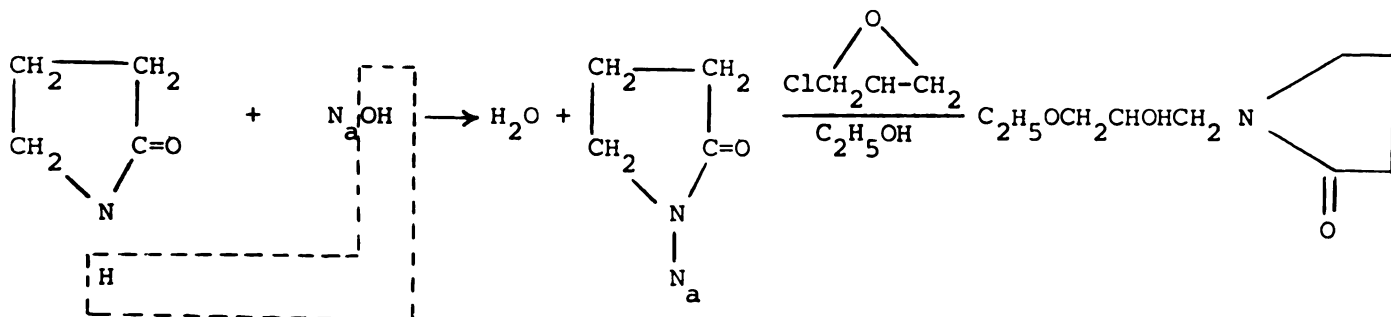
This process gives a more or less strongly discolored product due to the high temperature; the product also has an unpleasant odor attributable to decomposition products caused by the rapid initiation of polymerization. Furthermore, the polymer contains up to 10% of monomeric vinylpyrrolidone, which is probably responsible for the hygroscopicity of the material.

### Chemical Reactions of Pyrrolidones

The introduction of a pyrrolidone ring into a molecule imparts a hydrophilic character which in some cases may even extend as far as causing solubility in water. By using two moles of butyrolactone per mole of diamine, two pyrrolidone residues can be introduced. For example with diethylenetriamine,



With these compounds, the presence of the amino group offers a possibility of further reaction. Pyrrolidone reacts with concentrated sodium hydroxide solution in acetone to give N-sodium pyrrolidone which reacts with alkyl halides, i.e., epichlorohydrine in alcohol.



## §5.2 Physical Properties

Commercial N-vinyl pyrrolidone may contain up to 2 percent oily impurities which are insoluble in water. In small quantities these impurities often cause turbidity when diluted with water during the subsequent polymerization. In accordance with the preceding investigation, the commercial production of the Polyvinylpyrrolidone ("Kollidone") is polymerized in a 30 percent solution because the product can still be dried in this concentration. In order to dry the high viscosity solutions of the higher polymeric Polyvinylpyrrolidone, or the more concentrated solutions, drum drying is contemplated.

Pure polyvinylpyrrolidones, polymerized by using light as a catalyst, are glass-clear masses. Exposed to air, they gradually absorb water and form highly viscous

solutions in water. The softening point is over 100°C. In contrast to the high polymer produced by light polymerization, the block polymer is discolored yellow to brown and is of low viscosity.

### Solubility

Polyvinylpyrrolidone forms clear solutions with water. Highly concentrated warm solutions of alkalies and sodium chloride will cause salting out, but precipitation will not occur in strong acids. The aqueous solutions are completely neutral and very resistant to saponifying agents; however, when boiled with concentrated alkali, they form an insoluble product.

Polyvinylpyrrolidones (hereafter called PVP) are soluble and compatible with water and organic solvents. They dissolve easily in alcohols, ketones, tetrahydrofuran, chlorinated hydrocarbons, pyridine, and lactones. They swell in esters and aromatic hydrocarbons and are insoluble in ether and aliphatic hydrocarbons. The addition of ligroin to monomeric vinylpyrrolidone gives a turbidity or precipitate if the monomer has started to polymerize in storage. The monomeric vinylpyrrolidone is miscible with all organic solvents.

### Applications of Polyvinylpyrrolidone

Polyvinylpyrrolidones (PVP) may be used for various purposes depending in large part upon the degree of

polymerization. They are of interest as gums and glues, raw materials for adhesives, substitutes for animal glues, bonding agents in the film, reproduction, and coating industries, and as thickeners for emulsions, solutions, and for soaps and cosmetic preparations. They may be used as sizing agents for papers, fibers, and fabrics; and are reported to bring out a deeper color tone, particularly in combination with basic dyes. PVP films can be rendered water-insoluble by reaction with diisocyanates.

A unique and important application for the low viscosity PVP (molecular weight approximately 40,000) was as a blood plasma substitute, where it was called "Periston." To prepare the Periston solution, PVP was dissolved in water to give a 20 percent solution, filtered and sterilized at 120°C. The manufacturing formula is as follows [119]:

NaCl	: 800 gr.	Hcl (1710 cc)	: 1728.8 gr.
Kcl	: 42 gr.	NaHCO <sub>3</sub>	: 168.0 gr.
Cacl <sub>2</sub> ·6H <sub>2</sub> O	: 50 gr.	PVP (20% solution)	: 12,500 cc.
Mgcl <sub>2</sub> ·6H <sub>2</sub> O	: 0.5 gr.	Water (distilled)	: 101.3 Kg.

The solution prepared from the above recipe is filtered and sterilized in 100, 250, and 500 cc. ampoules at 105°C for one hour. The ampoules are stored at 30 to 35°C for three weeks to permit detection of any separation of material from solution.

"Periston" is used as a blood plasma substitute to replace loss of blood in the following cases:

1. Acute loss of blood (lesions, operations, child birth, etc.).
2. Shock due to trauma, operations of narcosis.
3. Thickening of the blood resulting from increased loss of liquid due to diarrhea, vomiting, or protoplasmic collapse.

"Periston," which can only be used intravenously, has no toxic effects, and may be used simultaneously with other water-soluble pharmaceuticals.

### §5.3 Rheology

For most systems in steady shearing flow the viscosity depends on the shear rate in a rather characteristic manner. At sufficiently low shear rates the viscosity is independent of the shear rate (the Newtonian region); however, within the same critical range of shear rates the viscosity begins to decrease as the shear rate is increased to still higher values, and apparently if the shear rate can be increased sufficiently the viscosity becomes constant, a limiting viscosity at infinite-shear rate. The limiting viscosities both at zero- and infinite-shear rate and the critical shear rate region may change by many orders of magnitude from one system to

another depending on the nature of polymer, its molecular weight, the solvent, and the concentration.

Meter's four-parameter model was selected to characterize the rheological properties of aqueous solutions of polyvinylpyrrolidone because these solutions were purely viscous and have both upper and lower limiting viscosities. Meter's model and material functions were fully discussed in Chapter 2.

### §5.3.1 Experiment

Fluids investigated were aqueous solutions of PVP of four different concentrations, 0.5, 1.0, 3.0, and 4.0 weight percent. PVP was manufactured by Badische Anilin und Soda Fabrik, Ludwigshafen, Germany. Concentrations were converted to the units of gr./100 cc. of solution by assuming additivity of volumes.

Viscosity and primary normal stress difference measurements of the four PVP solutions were made over the shear rate range of 0.02689 to 1076.0  $\text{sec}^{-1}$  with a Weissenberg rheogoniometer, a commercial type cone-and-plate viscometer manufactured by Farol Research Engineers Ltd., England. A platen diameter of 10 cm. and a cone of angle  $2.0083^\circ$  was used with a 1/16" torsion bar and a 1/16" normal force spring. Room temperature was carefully adjusted to  $21^\circ\text{C}$  prior to taking measurements so as to maintain temperatures of samples and reservoir

platen arrangement which is shown in Figure 4.4-1 constant at  $21 \pm 0.5^\circ\text{C}$ .

The operation and run procedure of the Weissenberg rheogoniometer is contained in Appendix B.

### §5.3.2 Results and Discussion

Four material parameters of Meter's model ( $\eta_0$ ,  $\eta_\infty$ ,  $\alpha$ ,  $\tau_m$ ) were determined from shear stress versus shear rate data for PVP. Shear stress versus shear rate values for PVP solutions are tabulated in Appendix R and typical results are plotted in Figures 5.3-1 and 5.3-2 as  $\tau_{12}$  vs.  $\dot{\gamma}$ ,  $\eta$  vs.  $\dot{\gamma}$ , respectively.

The zero-shear limiting viscosity  $\eta_0$  and infinite-shear limiting viscosity  $\eta_\infty$  were obtained directly from Figure 5.3-2 and listed in Table 5.3-1. The value of  $\tau_m$  was obtained as the value of the shear stress at  $\eta = \frac{1}{2}(\eta_0 + \eta_\infty)$ .

It should be emphasized that  $\eta_0$ ,  $\eta_\infty$ , and  $\tau_m$  are measurable properties, independent of any assumed model of the fluid. It is therefore reasonable to try to introduce these quantities into any proposed empirical model; however, it may be that the procedure used to determine model parameters is such that the quantities  $\eta_0$ ,  $\eta_\infty$ , and  $\tau_m$  are merely values which give the best fit over the range of available data, and that they may not quite have their intended physical significance. Such

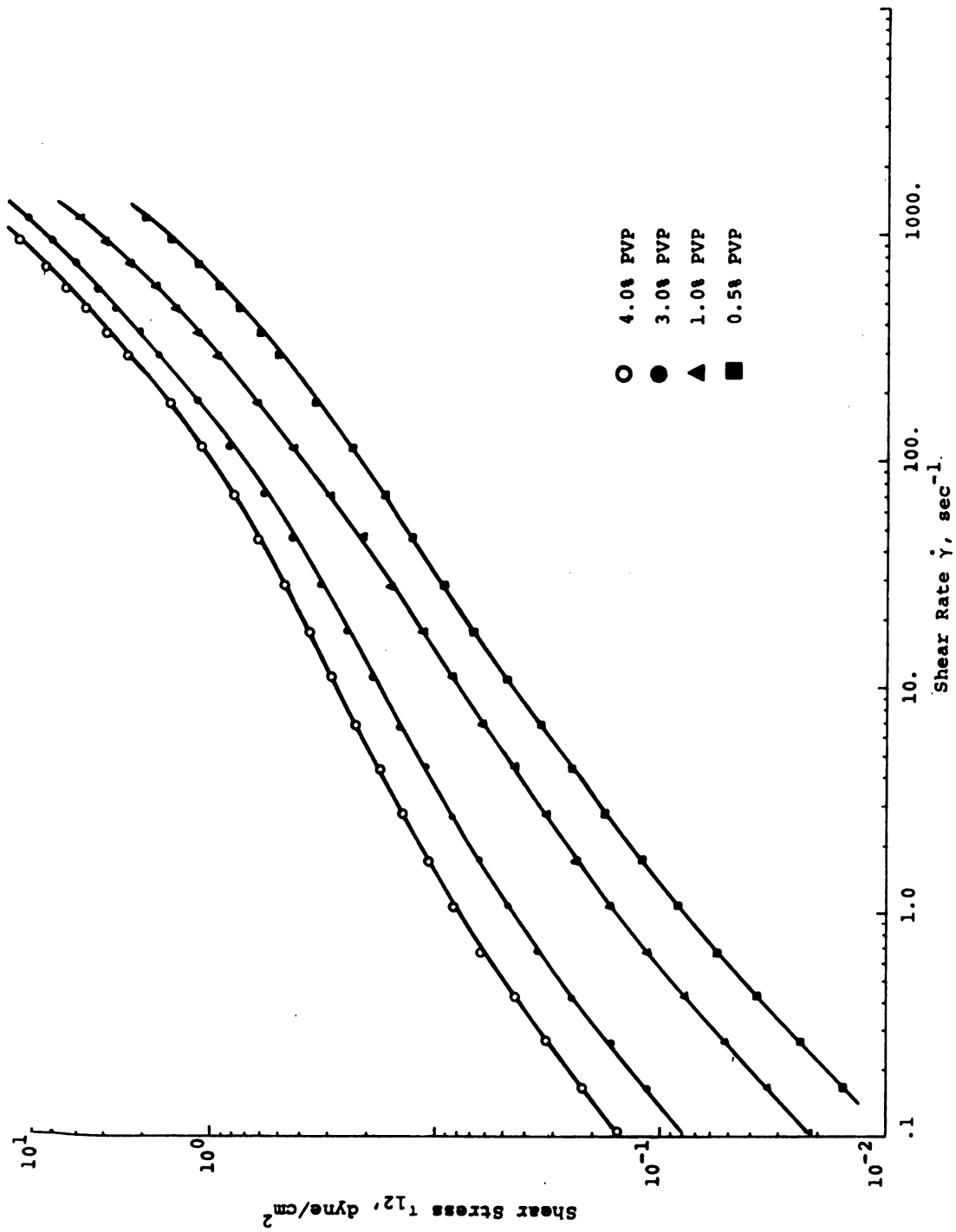


Figure 5.3-1 Shear Stress-Shear Rate Behavior for Four Aqueous Solutions of PVP

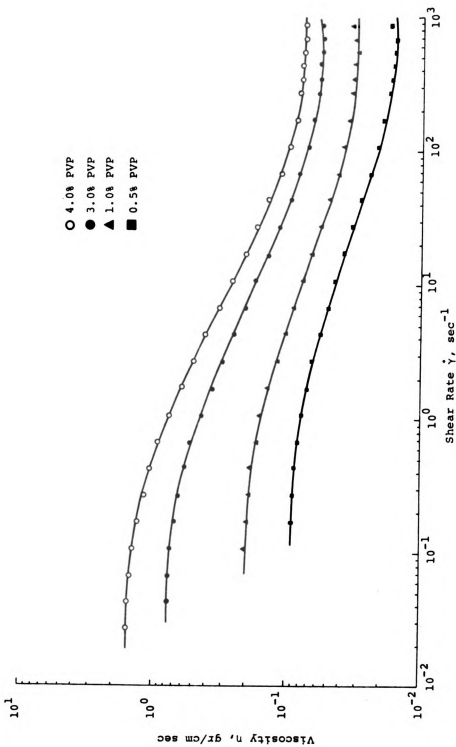


Figure 5.3-2 Non-Newtonian Viscosity for Four Aqueous Solutions of PVP

would certainly be true in the case of a fluid which forms a gel structure when not in motion; then there is no zero-shear limiting viscosity and a  $\tau_m$  would be impossible to determine.

In this study  $\alpha$  and  $\tau_m$  were obtained by using a computer program for determining the best fit of the shear stress versus shear rate data for aqueous solutions of PVP. Values of the material parameters for Meter's model for PVP solutions are listed in Table 5.3-1.

Meter's model provided an excellent fit to the viscometric data as can be seen in Figure 5.3-3 containing calculated viscosities as point for each PVP solution with the determined material parameters. The solid line represents the best line through the data. The main deviation between the data and correlation is in the instability region where viscosity starts to decrease with increasing shear rate and in the high shear rate region. The average absolute percentage deviation between values predicted from the model and experiment for the 98 data points was 2.10 percent.

The parameters listed in Table 5.3-1 show that both  $\eta_0$  and  $\eta_\infty$  decrease with decreasing polymer concentration, tending to the Newtonian viscosity of the solvent at infinite dilution. The parameter  $\alpha$  also decreases with decreasing concentration, whereas  $\tau_m$  appears to approach a definite value, characteristic of the polymer, as infinite dilution is approached.

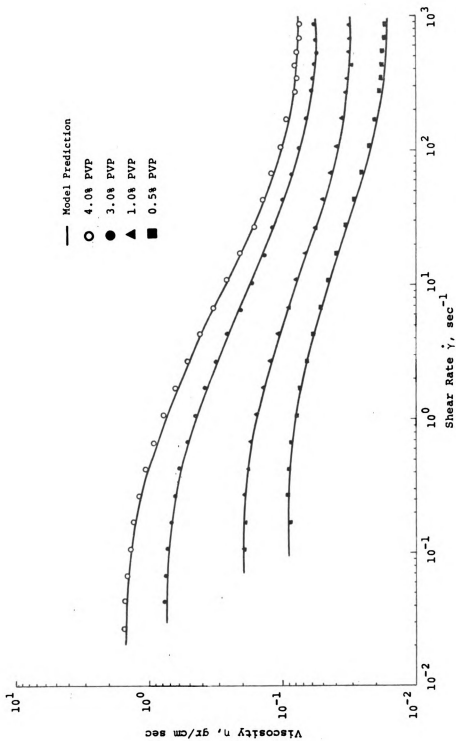


Figure 5.3-3 Comparison of Experimental and Calculated Values of the Apparent Viscosity for Aqueous Solutions of PVP

TABLE 5.3-1 Meter Model Parameters for PVP Solutions as Obtained from a Weissenberg Rheogoniometer at 21°C

Solution Concen- tration (wt. %)	$\eta_0$ (gr./cm sec)	$\eta_\infty$ (gr./cm sec)	$\alpha$ (Dimension- less)	$\tau_m$ (gr./cm sec)	Experimental Range of Shear Rate (sec <sup>-1</sup> )	% Error in $\eta_{cal}$	
4.0	1.0047	1.5736	0.0724	2.4712	0.7434	0.0268-1076	2.75
3.0	1.0027	0.7824	0.0526	2.3132	0.5124	0.0427-1076	1.78
1.0	0.9986	0.2053	0.0288	2.1653	0.3342	0.1076-1076	1.88
0.5	0.9976	0.0942	0.0138	2.0714	0.2728	0.1697-1076	2.28

<sup>a</sup>Average of absolute values of error tabulated in Appendix Q.

#### §5.4 The Flow of Non-Newtonian Fluids Through Porous Media

The equation for the modified Reynolds number based on the result of a hydrodynamic analysis of the capillary model of the packed bed for Meter's model was developed in Appendix A with the following result:

$$N_{Re,eff} = \frac{D_p G_o}{M(1-\epsilon)\eta_o} \left[ 1 + \frac{4}{\alpha+3} \left( \frac{\tau_{\omega^*}}{\tau_m} \right)^{\alpha-1} - \frac{\eta_{\infty}}{\eta_o} \left( \frac{\tau_{\omega^*}}{\tau_m} \right)^{\alpha-1} \left( \frac{4}{\alpha+3} + \frac{2}{\alpha+1} \left( \frac{\tau_{\omega^*}}{\tau_m} \right)^{\alpha-1} \right) + \left( \frac{\eta_{\infty}}{\eta_o} \right)^2 \left( \frac{\tau_{\omega^*}}{\tau_m} \right)^{2\alpha-2} \left( \frac{2}{\alpha+1} + \frac{4}{3\alpha+1} \left( \frac{\tau_{\omega^*}}{\tau_m} \right)^{\alpha-1} \right) \right]$$

$$f^*_{expt} = \left( \frac{\rho \Delta p}{MG_o} \right) \left( \frac{D_p}{L} \right) \left( \frac{G_o^3}{1-\epsilon} \right) \quad (5.4-1)$$

The modified Ergun friction factor for Meter's model is:

$$f^*_{calc} = \frac{150}{N_{Re,eff}} + 1.75 \quad (5.4-2)$$

The pressure drop-flow rate data for PVP solutions in packed beds were correlated with the Ergun friction factor.

#### §5.4.1 Experiment

Polyvinylpyrrolidone solutions of four different concentrations (0.50, 1.0, 3.0, and 4.0 weight percent) were made up and filtered to avoid gel formation, and then poured into the jacketed storage tank maintained at 21°C. Gentle stirring was maintained for about one day preceding the flow experiments.

All electrical circuits were switched on for about 5 minutes before runs were made. The schematic diagram of the jacketed flow system which maintained constant temperature  $21 \pm 0.5^\circ\text{C}$  is shown in Figure 4.5-1. Nitrogen tank A was used to cause the flow of polymer solution from the storage tank to the packed beds, whereas nitrogen tank B was used as a controlling device to maintain a constant flow rate through the bed. The pressure transducer was connected into two taps of the column which were 1.5 ft. apart. Various flow rates were obtained by adjusting the valves at the top and bottom of the column and measured with the appropriate rotometer. Pressure drop for each flow rate was recorded. Details of experimental procedure are contained in Appendix C.

#### §5.4.2 Results and Discussion

The analysis of the flow experiment is based upon the friction factor-Reynolds number analysis as developed in the previous section. The flow data are presented in terms of

$$f^* = f^*(N_{Re,eff}) \quad (5.4-1)$$

where  $f^*$  is the friction factor for flow through a packed bed and  $N_{Re,eff}$  is an effective Reynolds number for the flow of non-Newtonian fluid through a packed bed.

The modified friction factor versus modified Reynolds number for aqueous solutions of PVP are plotted in Figures 5.4-1,2,3,4 and are tabulated in Appendix R. The Reynolds number ranged  $10^{-2}$  to  $10^2$ . Wall effect correction was introduced in each calculation with  $M$  defined in Eq. (A.3-32).

The data for all concentrations agreed with the Ergun equation at the value of effective Reynolds numbers less than one. But the friction factor,  $f^*$ , was consistently too high for  $N_{Re,eff} > 1.0$ . The departure from the relation

$$f^* = \frac{150}{N_{Re,eff}} + 1.75 \quad (5.4-2)$$

was so great as to suggest that it was a result of a failure in the theoretical development rather than a result of experimental error. That is, either the effective coefficient of viscosity  $\eta_{eff}$ , did not decrease with an increasing rate of shear as rapidly as Meter's model would predict or there is a possibility that the inertial terms have not been properly accounted for.

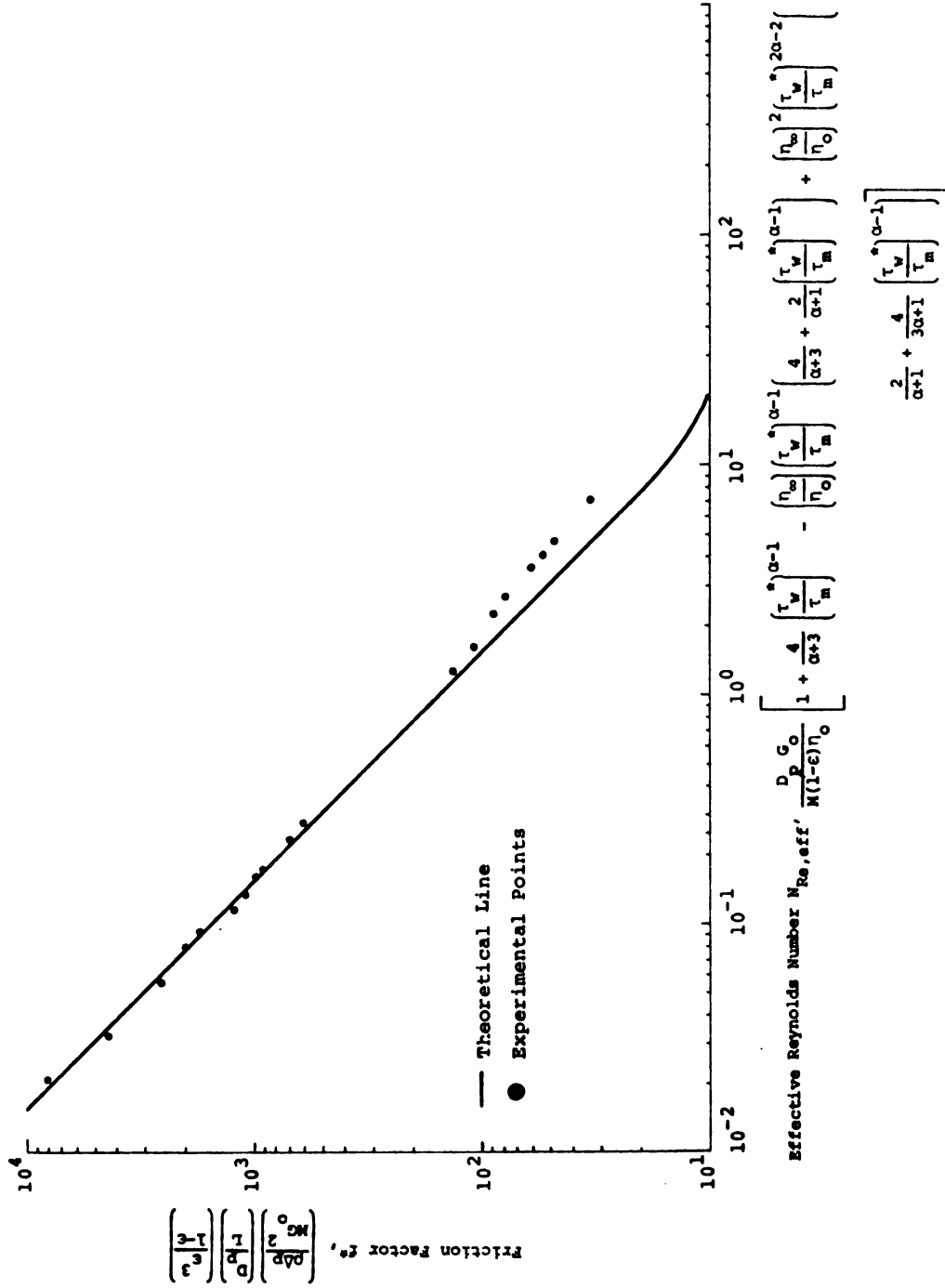


Figure 5.4-1 Pressure Drop-Flow Rate Correlation for Flow of 4.0% PVP Solutions Through Packed Beds

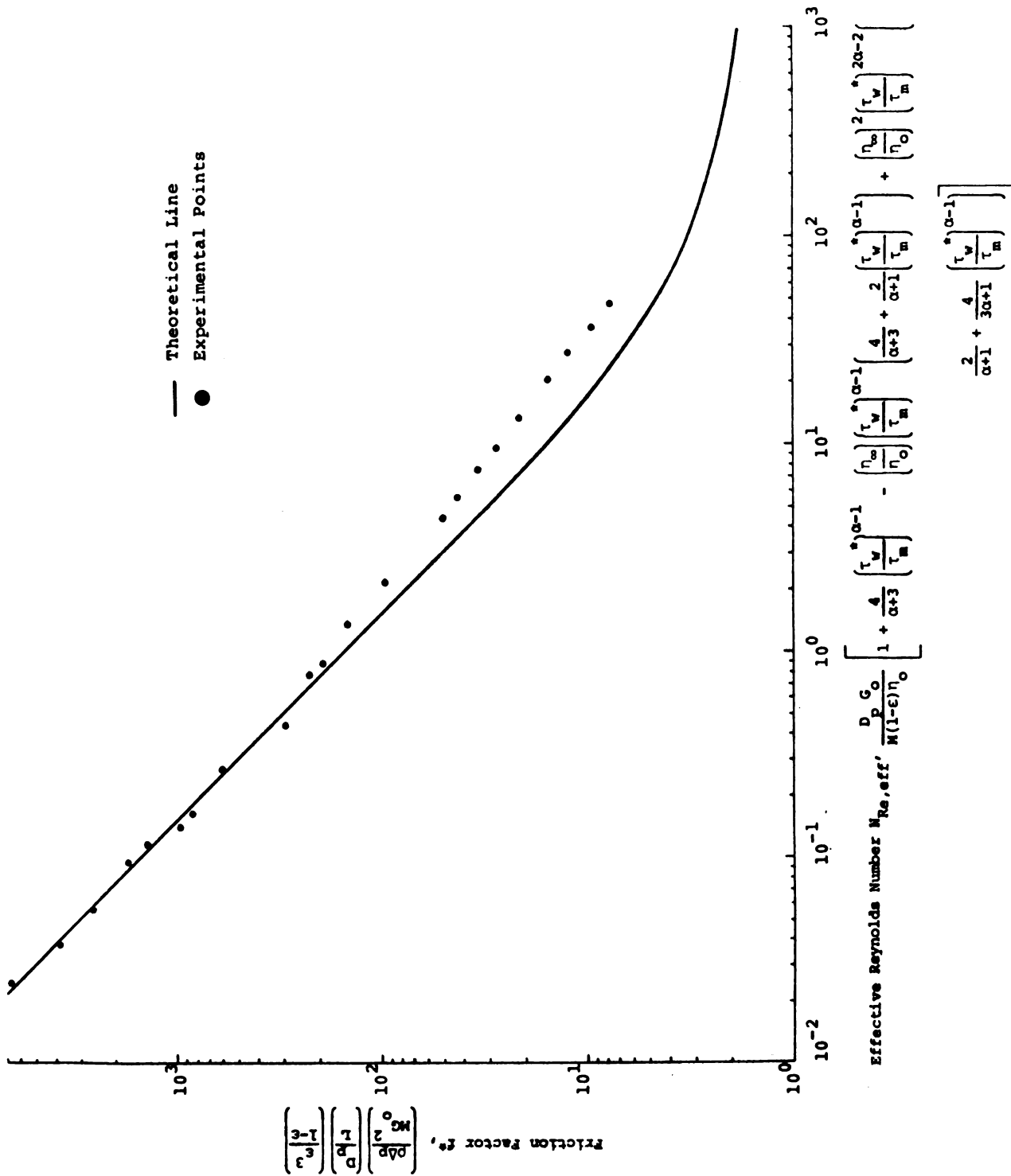


Figure 5.4-2 Pressure Drop-Flow Rate Correlation for Flow of 3.0% PVP Solutions Through Packed Beds

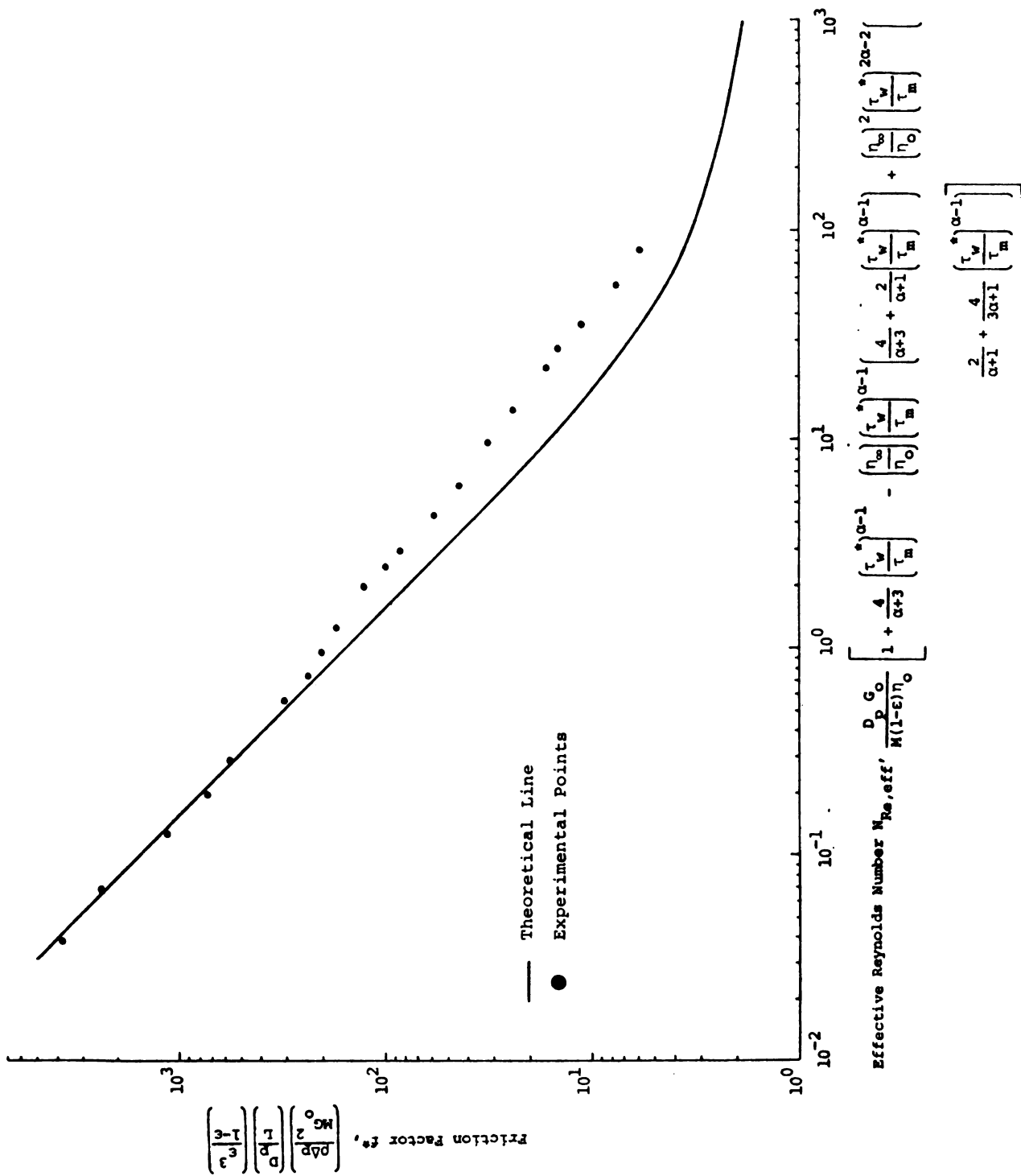


Figure 5.4-3 Pressure Drop-Flow Rate Correlation for Flow of 1.0% PVP Solutions Through Packed Beds

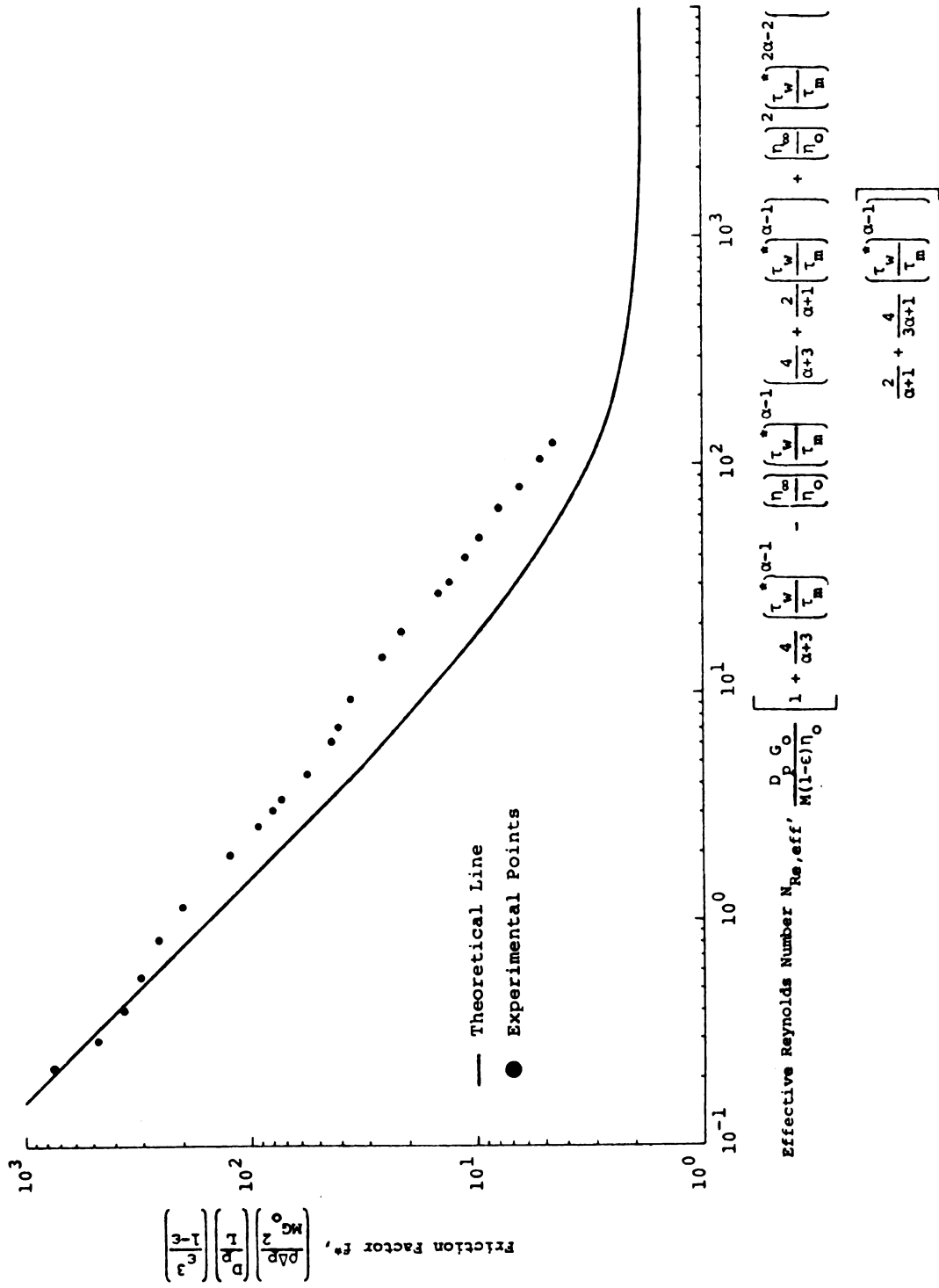


Figure 5.4-4 Pressure Drop-Flow Rate Correlation for Flow of 0.5% PVP Solutions Through Packed Beds

The flow behavior of PVP solutions in packed beds depends upon the bed geometry since it is this geometry which conditions the flow patterns of the solution. A porous medium may be visualized as made up of innumerable flow constrictions and expansions with interconnecting curved pore channels. An elemental volume of solution actually involves continual accelerations and decelerations as it proceeds through irregular interstices between particles in the bed. This alternating, or oscillating, behavior becomes more manifest as the average solution velocity increases. It is this locally unsteady-state phenomenon which leads to the observed deviation. Hence, for flow of non-Newtonian fluids in porous media, we might expect to observe inertial effects and surface effects which do not show up in the steady-state spatially homogeneous flows usually used to establish rheological parameters. The experiment would indicate that an additional parameter may be necessary to correlate packed bed flow data. By method of dimensional analysis, a new dimensionless group, for flow in tubes, arises, viz., [116]

$$\left(\frac{DV\rho}{\eta}\right) \left(\frac{V\lambda}{D}\right)$$

Similarly, the new dimensionless group, for packed bed, would be

$$\left(\frac{D_p G_o}{M(1-\epsilon)\eta_o}\right) \left(\frac{G_o \lambda}{\rho D_p}\right)$$

As pointed out by Meter [39], the relaxation time constant  $\lambda$  can be obtained from model parameters as  $\lambda = \eta_o / \tau_m$  with unit of time. Since the observed modified Reynolds number for a given friction factor is too large, the modified Reynolds number (Eq. 5.4-1) may be expressed as:

$$\begin{aligned}
 N_{Re,eff} = & \frac{D_p G_o}{M(1-\epsilon)\eta_o} \left[ 1 + \frac{4}{\alpha+3} \left( \frac{\tau_{\omega}^*}{\tau_m} \right)^{\alpha-1} \right. \\
 & - \left( \frac{\eta_{\infty}}{\eta_o} \right) \left( \frac{\tau_{\omega}^*}{\tau_m} \right)^{\alpha-1} \left[ \frac{4}{\alpha+3} + \frac{2}{\alpha+1} \left( \frac{\tau_{\omega}^*}{\tau_m} \right)^{\alpha-1} \right] \\
 & + \left. \left( \frac{\eta_{\infty}}{\eta_o} \right)^2 \left( \frac{\tau_{\omega}^*}{\tau_m} \right)^{2\alpha-2} \left( \frac{2}{\alpha+1} + \frac{4}{3\alpha+1} \left( \frac{\tau_{\omega}^*}{\tau_m} \right)^{\alpha-1} \right) \right] \\
 & - c_1 \left( \frac{D_p G_o}{M(1-\epsilon)\eta_o} \cdot \frac{G_o \eta_o}{\rho D_p \tau_m} \right)^{c_2} \tag{5.4-3}
 \end{aligned}$$

where  $c_1$  and  $c_2$  are constants to be determined from the packed bed experimental data. For each PVP solution,  $c_2$  was 1.36, whereas  $c_1$  was 0.43 for 4.0% solution, 1.3 for 3.0% solution, 3.5 for 1.0% solution; and 4.0 for 0.5% solution. The agreement was excellent. The average absolute percent deviation between the calculated value of the friction factor (Eq. 5.4-2) and experimental value (Eq. 5.4-1) was 10.8% for 87 experimental points representing four fluids of different concentration. This was in contrast to the average percent deviation of 60.4% for those same data points without the correction.

This is shown in Figure 5.4-5 and the average percent deviation is listed in Table 5.4-1.

### §5.5 Conclusions

Results of the present investigation may be summarized as follows:

1. Material parameters for Meter's model for aqueous solutions of PVP were evaluated. Aqueous solutions of PVP did not exhibit viscoelastic behavior. Meter's model correlated the steady shear experimental data very well over the entire range of shear rate.
2. The application of the Meter's model to the capillary model of a porous media led to a generalized Darcy's law. This development led to a successful correlation of the flow rate data for polymer solutions of low and medium molecular weights for the value of effective Reynolds numbers less than one.
3. For the high flow rates where the inertial effects become significant, the modified Ergun equation correlated the friction factor versus the modified Reynolds number well. Extensive experimental works are desired for the generalization of this correlation thereby

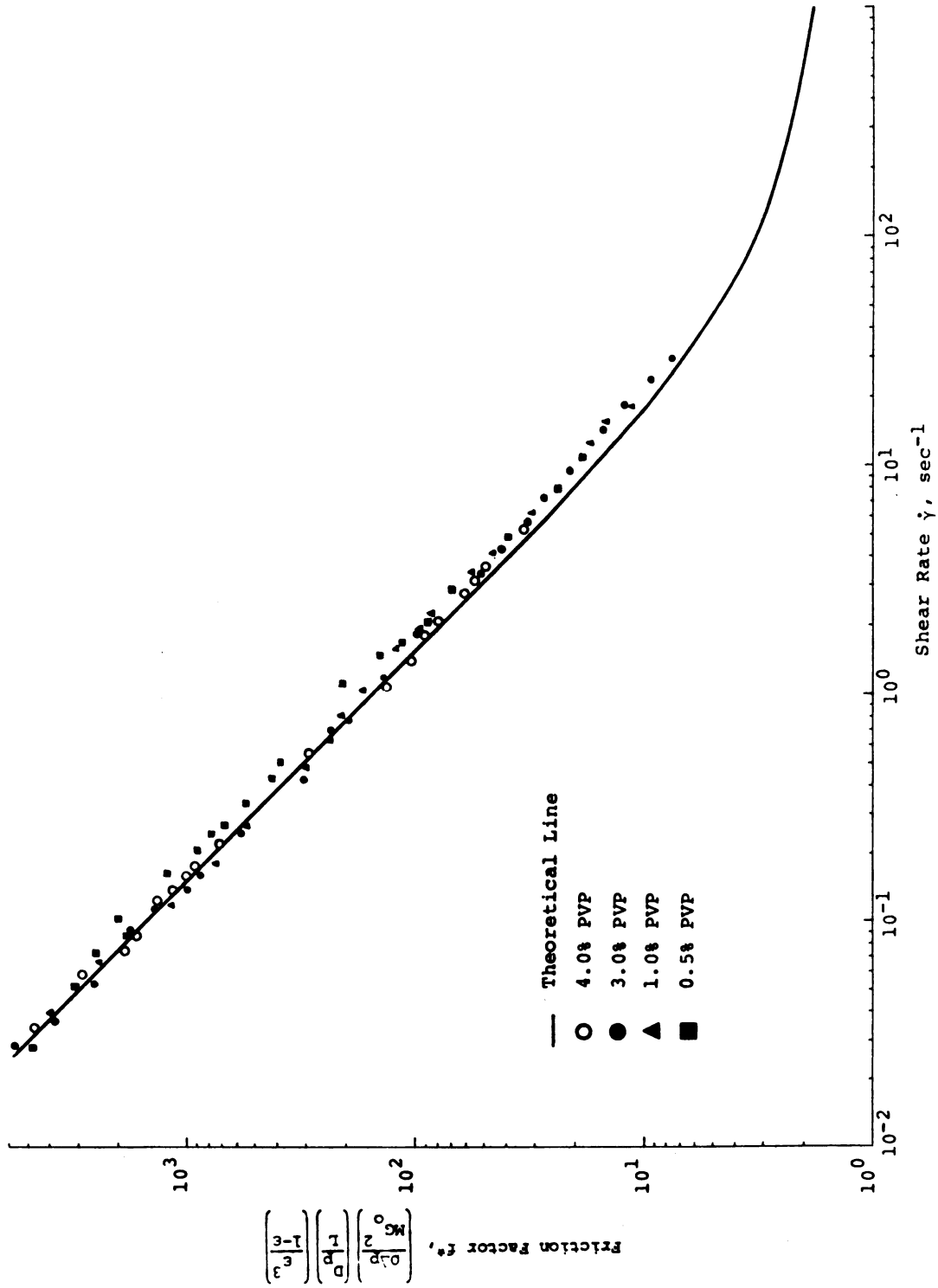


Figure 5.4-5 Pressure Drop-Flow Rate Correlation for Flow of PVP Solutions Through Packed Beds

TABLE 5.4-1 Summary of Experimental Data for PVP Solutions

Solution Concentration (weight %)	Average % Deviation in f* Calculations	Number of Experimental Points	Maximum Range of % Deviation
4.0	5.31	23	-7.84 to +12.42
3.0	8.39	23	-18.31 to +18.97
1.0	11.51	19	-27.35 to +12.83
0.5	18.32	22	-36.11 to +21.43
All Solutions	10.77	87	-36.11 to +21.43

<sup>a</sup>Average % deviation was calculated based on

$$\frac{f^*_{\text{calc}} - f^*_{\text{expt}}}{f^*_{\text{calc}}} \times 100$$

Arithmetic average of absolute values are tabulated in Appendix R.

setting up the procedure for use of this correlation to confirm the utility of the correlation developed in this study.

## CHAPTER 6

### POLYMETHYLCELLULOSE SYSTEM

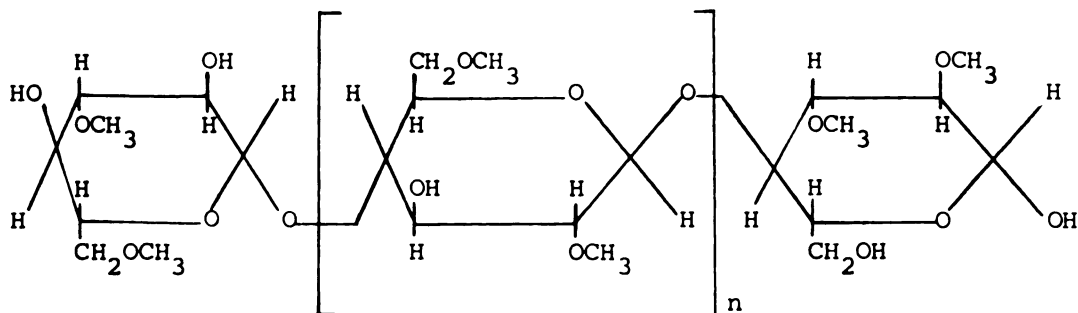
The use of natural products to thicken fluids is an ancient art. These products from nature, however, can often be limited in their properties and capabilities. Nature has also given man cellulose, a substance existing abundantly in cotton and trees, that can be modified in many ways to provide new areas of utility based on unique and unusual combinations of properties.

The chemist has discovered that the reaction of cellulose materials with caustic soda and appropriate organic chemical produces substances that not only thicken but do more. They bind, suspend, emulsify, stabilize. They act as nonionic surfactants, and in water solutions they gel on the application of heat and liquefy on cooling.

#### §6.1 Chemistry

Polymethylcellulose is manufactured and provided under trademark Methocel by the Dow Chemical Company

(Midland, Michigan). Methocel products are derived from and have the polymeric backbone of cellulose, a natural carbohydrate that contains a basic repeating structure of anhydroglucose units. The basic structure for Methocel (methylcellulose) is as follows:



Cellulose fibers, obtained from cotton linters or wood pulp, are swelled by a caustic soda solution to produce alkali cellulose which is treated with methyl chloride, yielding the methyl ether of cellulose. The fibrous reaction product is purified and ground to a fine, uniform powder or granule, a Methocel MC product.

The number of substituent groups on the ring determines the properties of the various Methocel products. Methocel contains 27.5 to 31.5% methoxyl or a methoxyl D.S.<sup>1</sup> of 1.64 to 1.92, this range yielding maximum water solubility. A lower degree of substitution gives products soluble only in alkali while higher degrees of substitution produce methylcellulose products soluble only in organic solvents.

---

<sup>1</sup>D.S. means degree of substitution.

## §6.2 Physical Properties

### Appearance

Methocel products are produced as white, odorless, tasteless powders or granules. It is available in several viscosity designations, specified as the viscosity of 2% aqueous solution of a particular molecular weight material at 20°C (see Figure 6.2-1 and Table 6.2-1). The apparent density is in the range of 0.4-0.6 gr./cc., the ignition temperature is 360°C (680°F) and the relative flammability in a furnace at 700°C is 90+.

### Moisture Absorption

Methocel sealed in its original shipping container absorbs scarcely any atmospheric moisture; once the container is opened, however, Methocel picks up moisture from the air. Allowance must be made when exposed Methocel is weighed since a portion of the total weight may be water; this weight must be correlated for moisture content to assure using the proper weight of Methocel to give the viscosity desired. For this reason, opened bags should be tightly resealed. Typical moisture absorption is shown in Figure 6.2-2.

### Physical Characteristics of Aqueous Solutions

Methocel products are water-soluble polymers which form aqueous dispersions by swelling and by

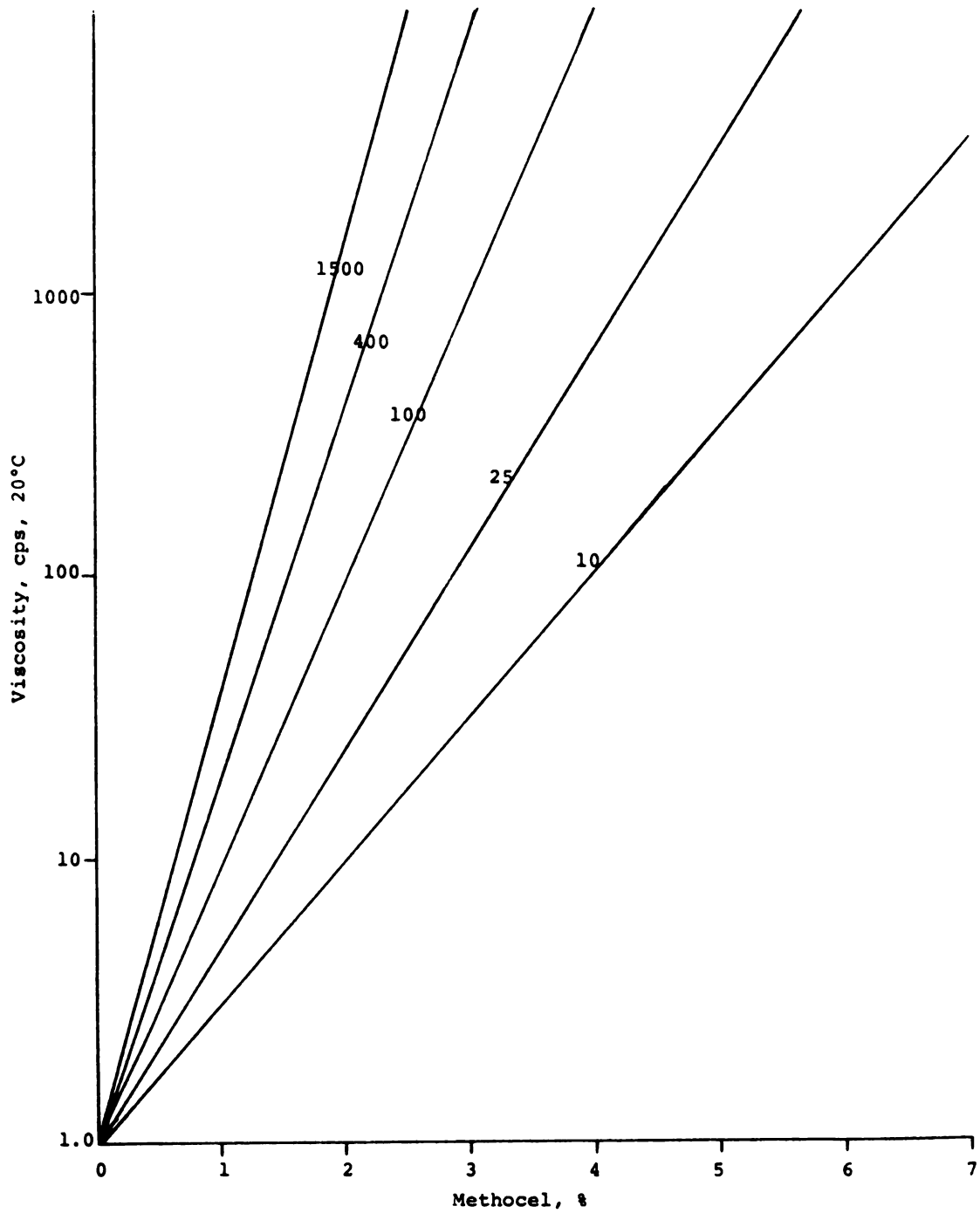


Figure 6.2-1 Viscosity of Polymethylcellulose of Various Molecular Weights

TABLE 6.2-1 Viscosities of Methylcellulose of Various Molecular Weights

Viscosity Grade, 2% 20C (cps)	Intrinsic Viscosity (dl/g.)	Number Average DP <sub>n</sub>	Number Average Molecular Weight M <sub>n</sub>
10.	1.40	70.	13,000.
40.	2.05	110.	20,000.
100.	2.65	140.	26,000.
400.	3.90	220.	41,000.
1,500.	5.70	340.	63,000.
4,000.	7.50	460.	86,000.
8,000.	9.30	580.	110,000.
15,000.	11.00	650.	120,000.
19,000.	12.00	750.	140,000.

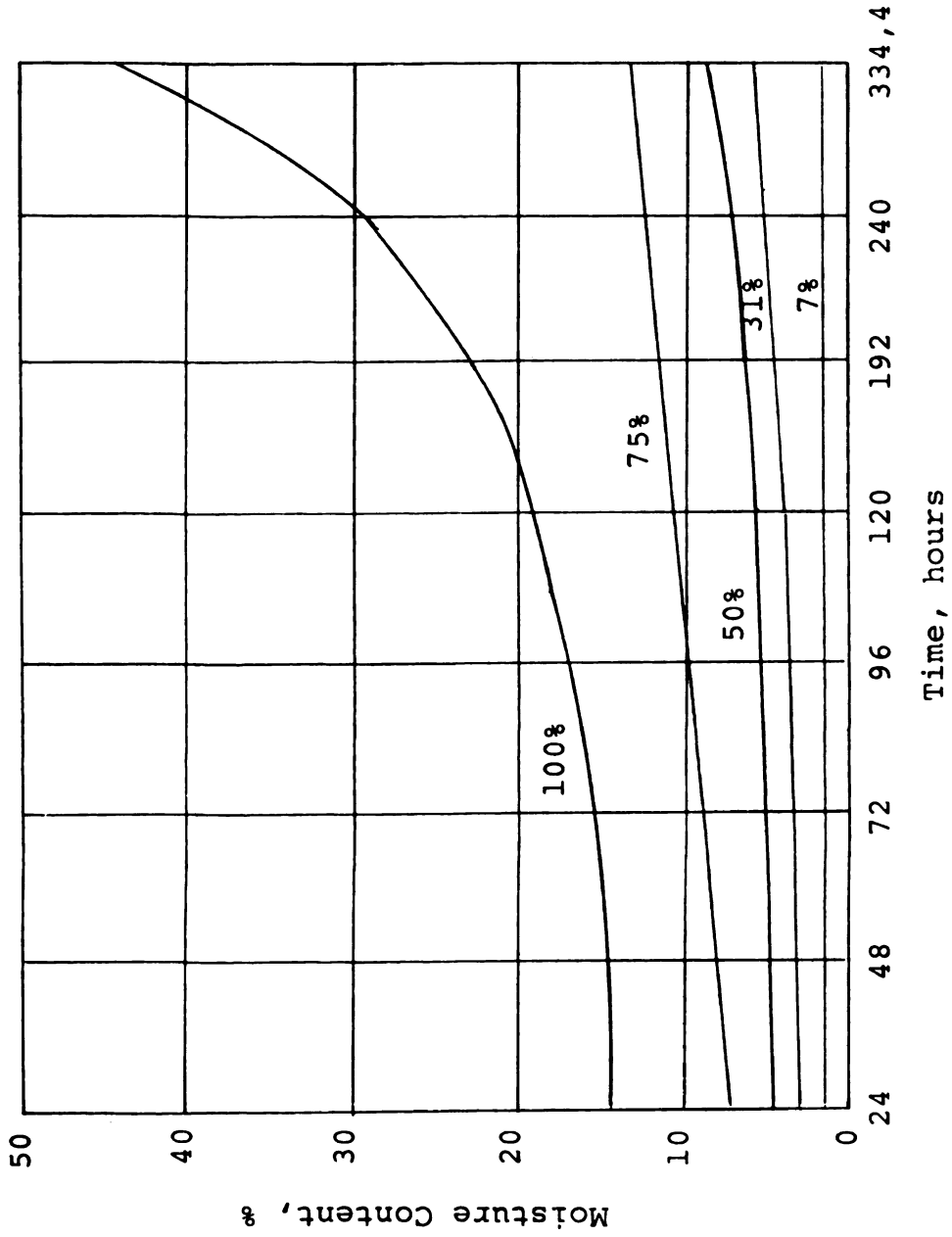


Figure 6.2-2 Typical Moisture Absorption of Methocel Products at Relative Humidity Shown at 20°C

successive hydration of their structural layers. Because of the swelling mechanism, there is no sharp solubility limit.

Methocel products have the unique and valuable property of cold-water solubility but they are insoluble in hot water. The water solubility of all Methocel products in cold water is limited only by the range of viscosity a manufacturer is mechanically equipped to handle.

#### (1) Properties of Aqueous Solutions of Methocel Products

Specific gravity, 20°C/4°C (all types):

1%: 1.0012

5%: 1.0117

10%: 1.0245

Refractive Index (2%, all types): 1.336

Partial Specific Volume (Methocel MC 4000 cps):

0.725 cc./gr.

PH (all types): Neutral

Freezing Point (2%, all types): 0.0°C

Surface Tension (below 500 cps at 25°C):

47-53 dynes/cm.

#### §6.3 Solution Preparation

The principle underlying the methods of solubilization of Methocel is to disperse it in water before

attempting to dissolve it. Such dispersion prevents lumping caused by the formation of a gelatinous membrane on the particle.

Methocel in powder form is blended into water by first mixing it thoroughly with 1/5 to 1/3 the required amount of water as hot water (80-90°C). Mixing should continue to assure that all particles are thoroughly wetted. The remainder of the water should then be added as cold water or even ice, if desired. Stir the mixture until smooth. For maximum clarity and reproducible viscosities the solution of Methocel should be cooled to a range from 0 to 5°C, for 20 to 40 minutes.

Since Methocel products disperse well in water above 80°C, the preliminary use of hot water assures wetting all portions of the particle prior to solution in cold water. If cold water is mixed directly with the powder, it creates a gelatinous membrane on the outside of the particles which causes lumping and slow diffusion of water into the interior of the particles. It is very important, however, to have adequate cooling after wetting with hot water to insure complete dissolution of Methocel.

#### §6.4 Rheology

For most systems in steady shearing flow the viscosity depends on shear rate in a rather characteristic manner. Any proposed rheological model should represent

the actual behavior of a fluid with accuracy, convenience, and simplicity. Different models may be necessary to describe different fluids, or even the same fluid under different conditions. The best relationship for a given fluid is not necessarily known until an experiment is made on the fluid to relate  $\tau_{ij}$  and  $e_{ij}$ .

The physical behavior of fluids with a yield stress is usually explained in terms of a three-dimensional internal structure which is capable of preventing movement for values of shear stress less than the yield value. For the shear stress greater than the yield value the internal structure collapses completely, allowing shearing movement to occur. The internal structure is considered to be reformed virtually instantaneously when the shear stress becomes less than the yield value.

The Herschel-Bulkley three-parameter model was selected to characterize the rheological properties of aqueous solutions of polymethylcellulose because these solutions had yield stresses with non-linear flow curves. Herschel-Bulkley model parameters and material functions were fully described in Chapter 2.

$$\tau_{ij} - \tau_y = \left[ \mu_o \left( \frac{e:e}{2} \right)^{\frac{1-m}{2}} \right]^{1/m} e_{ij} \quad (2.6-6)$$

#### §6.4.1 Experiment

Aqueous solutions of polymethylcellulose of molecular weight of 18,000 (25 cps material called PMC 25) of concentrations 0.3 and 0.5 weight percent and molecular weight of 41,000 (400 cps material called PMC 400) of concentrations 0.3 and 0.5 weight percent were investigated. Concentrations were converted to the units of gr./100 cc. of solution by assuming additivity of volumes.

Viscosity and primary normal stress difference measurements of the four PMC solutions were made over the shear rate range of 1.076 to 851.0  $\text{sec}^{-1}$  with a Weissenberg rheogoniometer, a commercial type cone-and-plate viscometer manufactured by Farol Research Engineers Ltd., England. A platen diameter of 10 cm. and a cone of angle  $2.0083^\circ$  was used with a 1/16" torsion bar and a 1/16" normal force spring. Room temperature was carefully adjusted to  $21^\circ\text{C}$  prior to taking measurements so as to maintain the temperatures of  $21 \pm 0.3^\circ\text{C}$  of samples and reservoir platen arrangement which was shown in Figure 4.4-1.

The operation and run procedure of the Weissenberg rheogoniometer is contained in Appendix B.

#### §6.4.2 Results and Discussion

Three material parameters of the Herschel-Bulkley model ( $\mu_0$ ,  $m$ ,  $\tau_y$ ) were determined from shear stress versus

shear rate data for aqueous solutions of PMC. Shear stress versus shear rate values for PMC solutions are tabulated in Appendix S and typical results are plotted in Figures 6.4-1 and 6.4-2 as  $\tau_{12}$  vs.  $\dot{\gamma}$ ,  $\eta$  vs.  $\dot{\gamma}$ , respectively.

The yield stress,  $\tau_y$ , of each solution was obtained from the intercept of Figure 6.4-2. Parameters  $m$  and  $\mu_0$  characterize the slope and intercept of a logarithmic plot of  $\dot{\gamma}$  vs.  $\tau_{12} - \tau_y$ . In this study parameters  $m$  and  $\mu_0$  were obtained by trial-and-error until the best fit of the experimental curve was obtained. The values of the parameters thus obtained are presented in Table 6.4-1.

The Herschel-Bulkley model provided an excellent fit to the viscometric data. Calculated viscosities for each PMC solution with these material parameters are shown in Figure 6.4-3. The solid line represents the best line through the data. The average absolute percentage deviation between the values predicted from the model and experiment for the 72 data points was 1.71 percent. All the parameters listed in Table 6.4-1 decreased with decreasing polymer concentration and molecular weight.

Values of primary normal stress differences were small and on the order of  $150 \text{ dyne/cm}^2$ . The error of measurements of the normal stress difference determined with a Weissenberg rheogoniometer is about 20% or greater for normal stress differences of  $500 \text{ dyne/cm}^2$  or less.

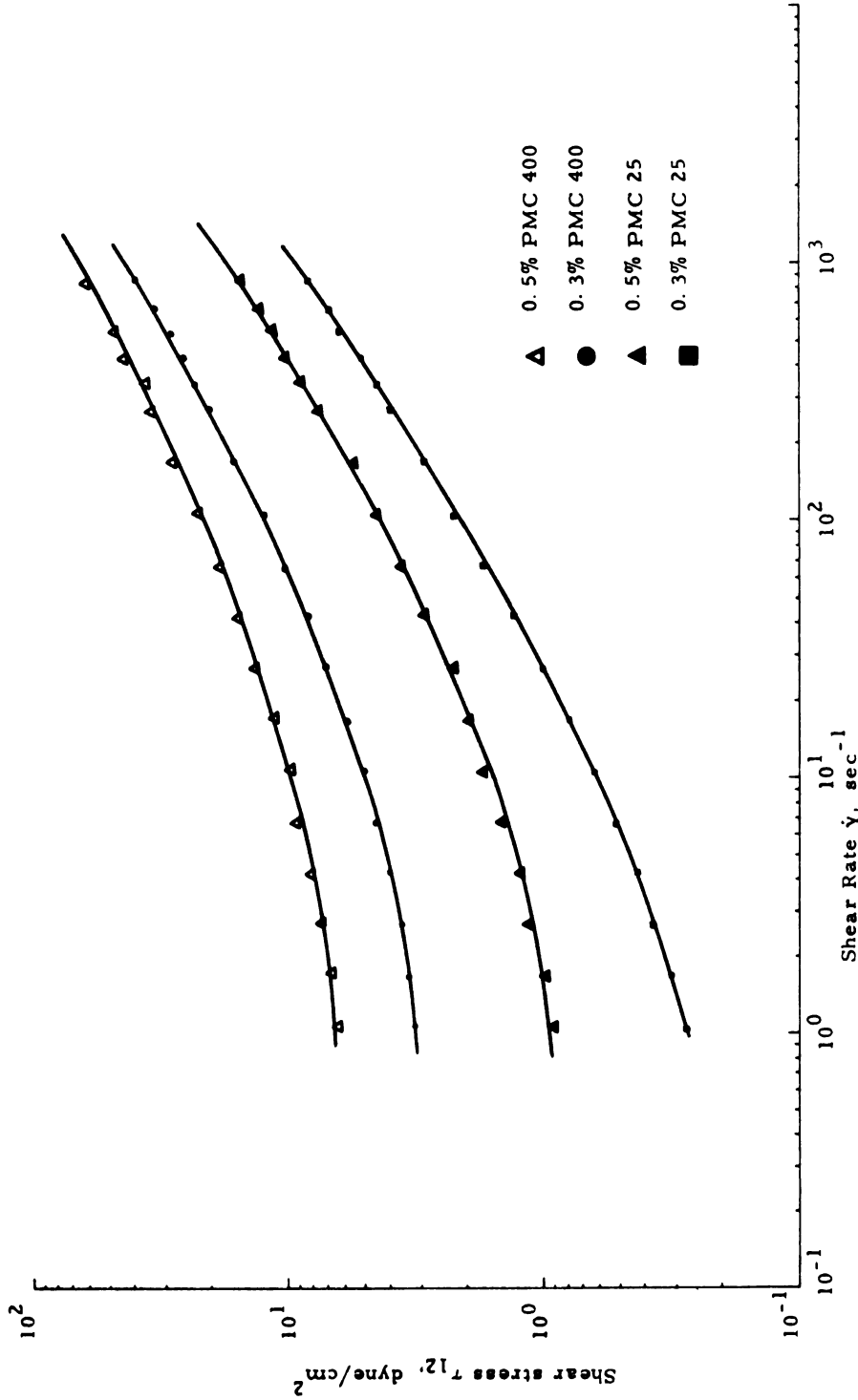


Figure 6.4-1 Shear Stress-Shear Rate Behavior for Four Aqueous Solutions of Polymethylcellulose

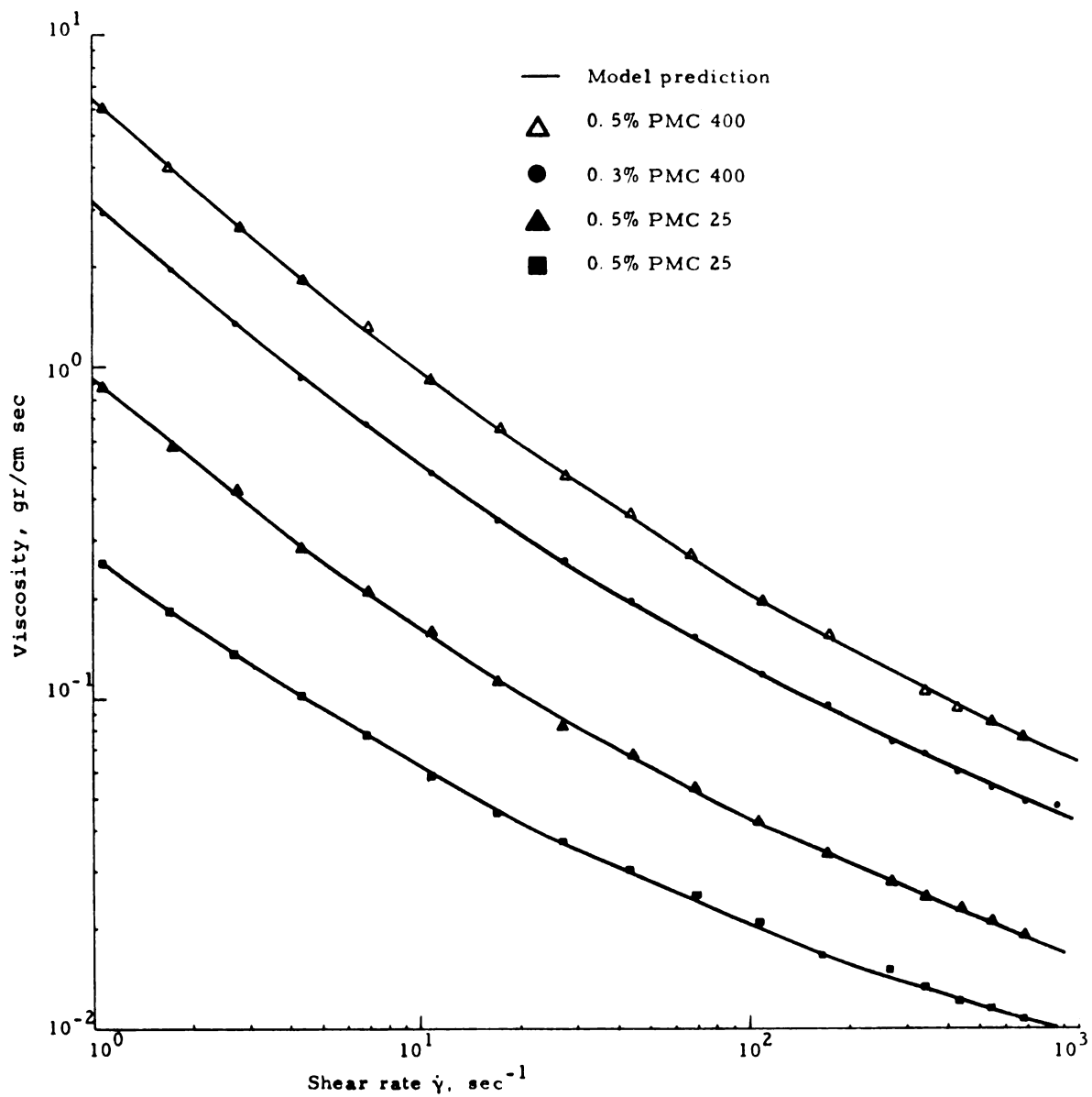


Figure 6.4-2 Non-Newtonian Viscosity for Aqueous Solutions of Polymethylcellulose

TABLE 6.4-1 Herschel-Bulkley Model Parameters for PMC Solutions as Obtained from a Weissenberg Rheogoniometer at 21°C

Solution Concentration (wt. %)	Fluid Density (gr./cc)	$\mu_0$ ( $\text{gr}^m/\text{cm}^m \text{sec}^{2m-1}$ )	$m$ (Dimensionless)	$\tau_y$ (gr/cm sec <sup>2</sup> )	Experimental Range of Shear Rate $\dot{\gamma}$ (sec <sup>-1</sup> )	% Error in $\eta_{\text{calc}}$
PMC 400						
0.5	0.9980	1.30	1.7525	5.35	1.076-851	1.4
0.3	0.9974	0.42	1.6332	2.50	1.076-851	1.5
PMC 25						
0.5	0.9979	0.082	1.5876	0.72	1.076-851	2.2
0.3	0.9974	0.028	1.5094	0.18	1.076-851	1.6

<sup>a</sup>Average of absolute values of error tabulated in Appendix S.

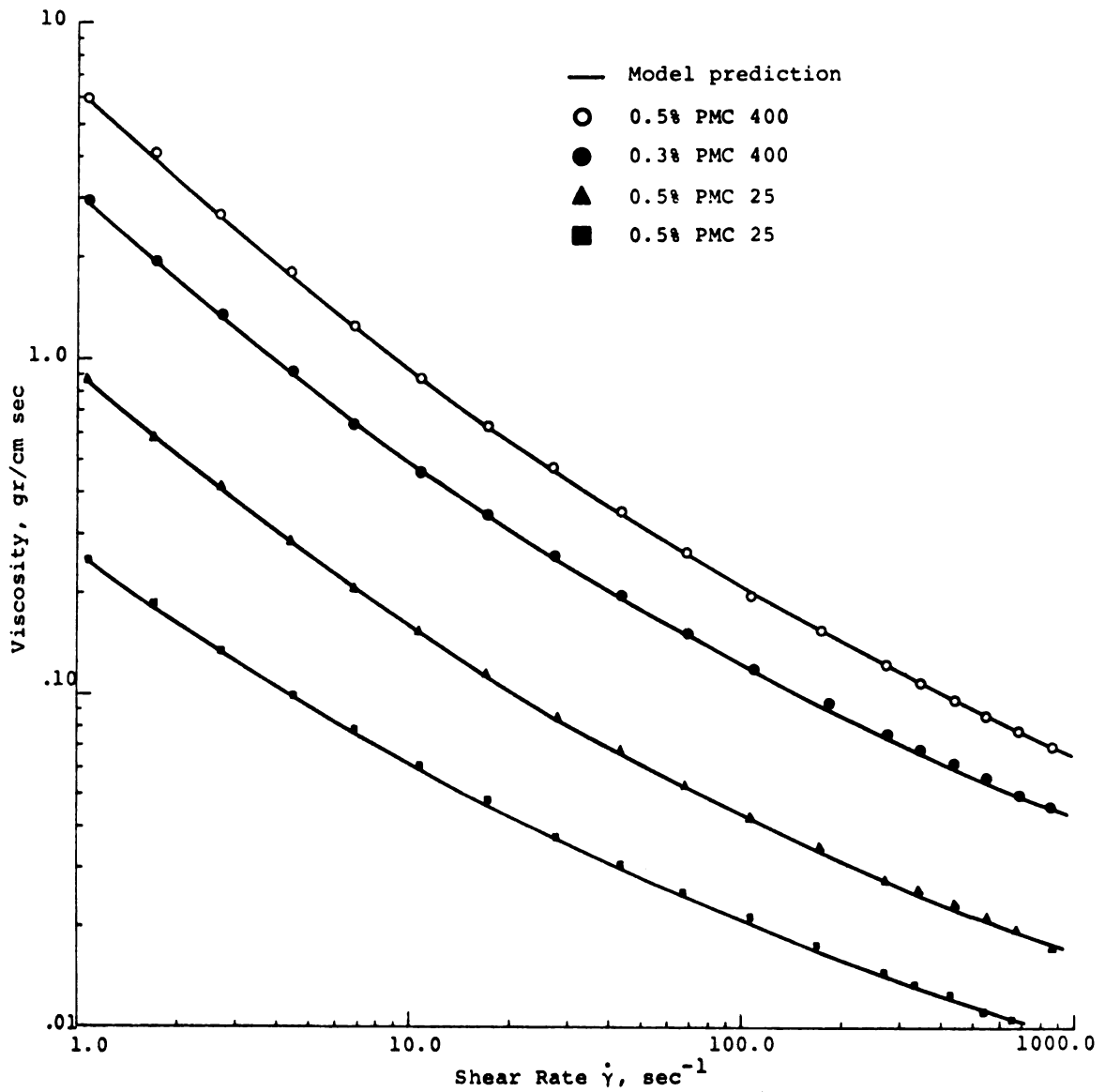


Figure 6.4-3 Comparison of Experimental and Calculated Values of the Apparent Viscosity for Aqueous Solutions of Poly-methylcellulose.

The normal stress difference data for PMC solutions were not analyzed further because of inaccuracy in the measurements. The stress relaxed instantaneously up to the point where yield stresses were prevailing; therefore, a relaxation time spectrum could not be obtained.

Shear rates less than  $1.076 \text{ sec}^{-1}$  were not reproducible. An explanation for this nonreproducible was postulated by Meister [117] as follows. Two chains of polymer are tightly linked around each other by bending back on themselves in a short-range contour. This means polymer molecules are entangled. When shear is applied the entanglements start to disentangle and shift to another preferred state. After shear is removed the material will revert to the entangled state, only after a long time.

#### §6.5 The Flow of Non-Newtonian Fluids Through Porous Media

The equation for the modified Reynolds number based on the capillary model of the packed bed for the Herschel-Bulkley fluid model was developed in Appendix A with the following result:

$$N_{Re,eff} = \frac{4D_p G_o \tau_y^{m+3}}{M(1-\epsilon) \mu_o (\tau_\omega^*)^4} \left( \frac{\tau_\omega^*}{\tau_y} - 1 \right)^{m+1} \left[ \frac{\left( \frac{\tau_\omega^*}{\tau_y} - 1 \right)^2}{m+3} + \frac{2 \left( \frac{\tau_\omega^*}{\tau_y} - 1 \right)}{m+2} + \frac{1}{m+1} \right]$$

$$f^*_{expt} = \frac{\Delta p \rho}{M G_o^2} \frac{D_p}{L} \frac{\epsilon^3}{1-\epsilon} \quad (6.5-1)$$

The modified Ergun friction factor for the Herschel-Bulkley model is:

$$f^*_{calc} = \frac{150}{N_{Re,eff}} + 1.75 \quad (6.5-2)$$

Data from flow experiments for PMC solutions in packed beds were correlated with the Ergun friction factor.

### §6.5.1 Experiment

Polymethylcellulose solutions of 0.3 and 0.5 weight percent for each molecular weight of 18,000 and 41,000 were made up and filtered to avoid gel formation. Gentle stirring was maintained in the constant temperature (21°C) storage tank for about one day preceding the flow experiments.

All electrical circuits were switched on for about 5 minutes before runs were made. The schematic diagram of the jacketed flow system was shown in Figure 4.5-1. Nitrogen tank A was used to cause the

flow of polymer solution from the storage tank to the packed beds, whereas nitrogen tank B was used as a controlling device to maintain a constant flow rate through the bed. The pressure transducer was connected into two taps of the column which were 1.5 ft. apart. Various flow rates were obtained by adjusting the valves at the top and the bottom of the column and measured with the appropriate rotometer. Pressure drop for each flow rate was recorded. Details of experimental procedure are contained in Appendix C.

#### §6.5.2 Results and Discussion

The data of the flow experiments were correlated with the previously developed friction factor-Reynolds number relationship for the Herschel-Bulkley model, Eq. 6.5-2.

The modified friction factor versus modified Reynolds number for aqueous solutions of PMC was plotted in Figures 6.5-1,2,3,4,5 and tabulated in Appendix T. The Reynolds numbers ranged from  $10^{-3}$  to  $10^0$ . Wall effect correction was introduced in each calculation with M defined in Eq. A.3-32.

As shown in Figures 6.5-1,2,3,4, and 5, the data scattered about the expected line with an average deviation of 8.53 percent. This is excellent. No effects were observed on the correlation due to various

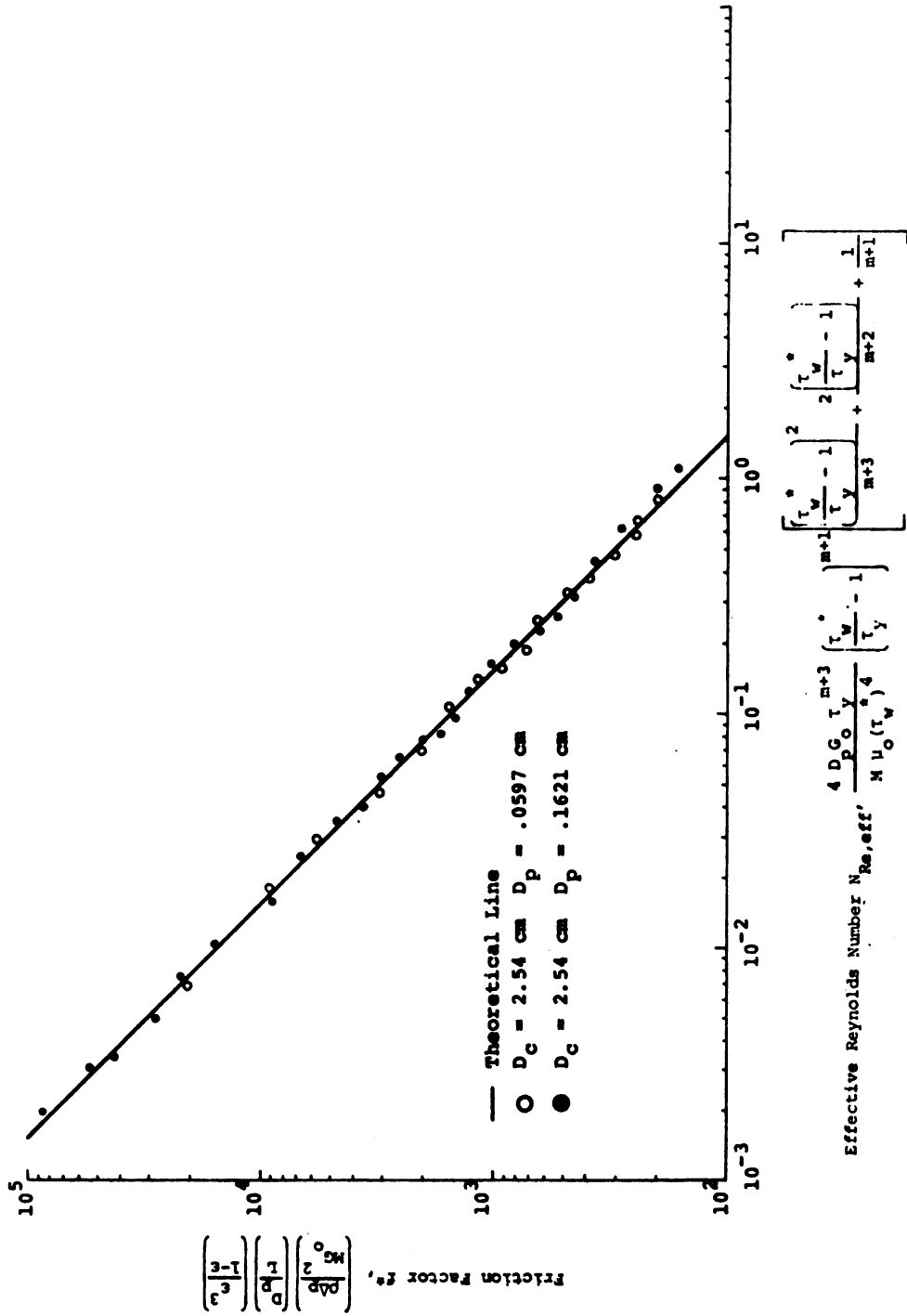


Figure 6.5-1 Pressure Drop-Flow Rate Correlation for Flow of 0.5% PMC 400 Solutions Through Packed Beds

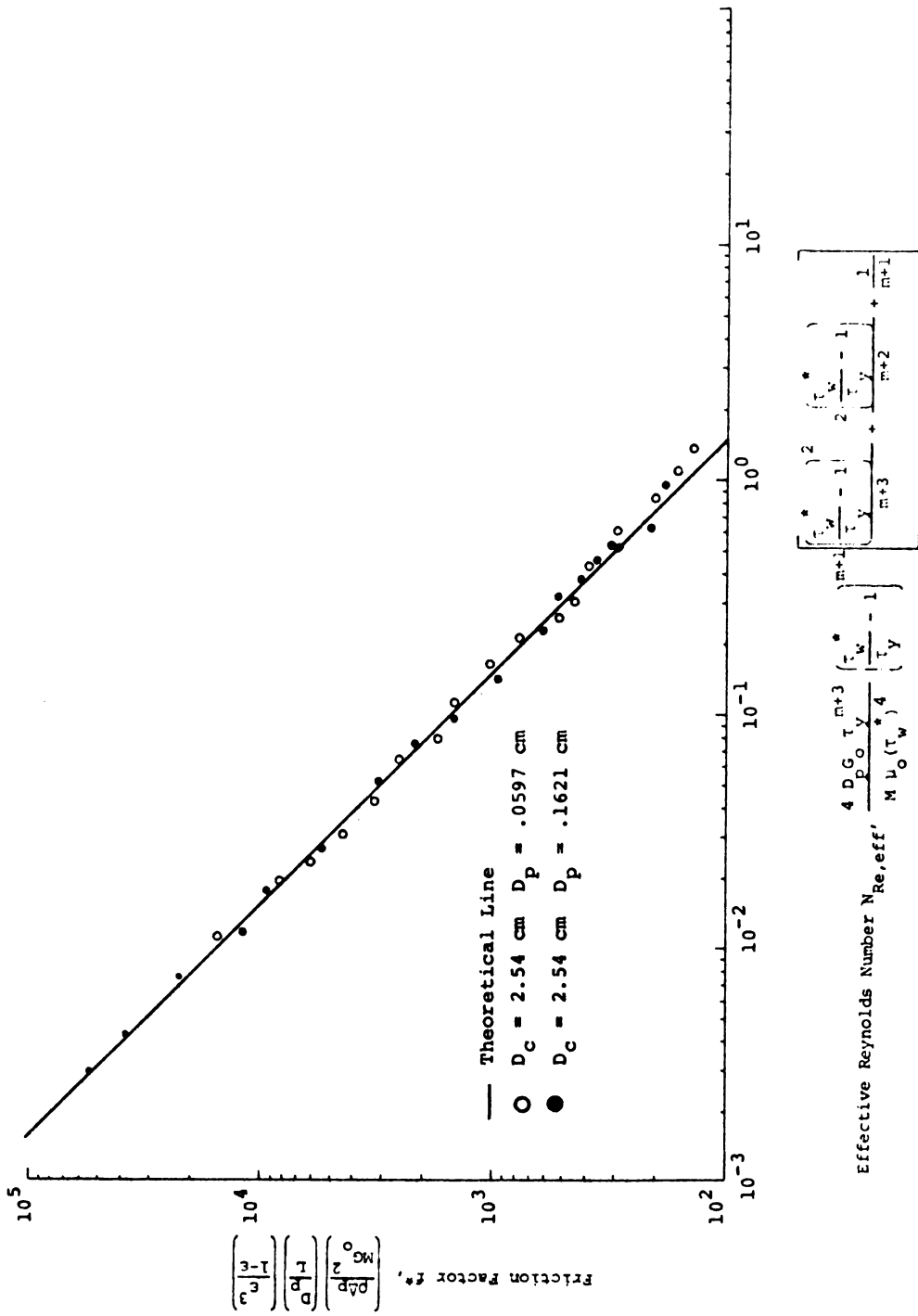


Figure 6.5-2 Pressure Drop-Flow Rate Correlation for Flow of .3% PMC 400 Solutions Through Packed Beds

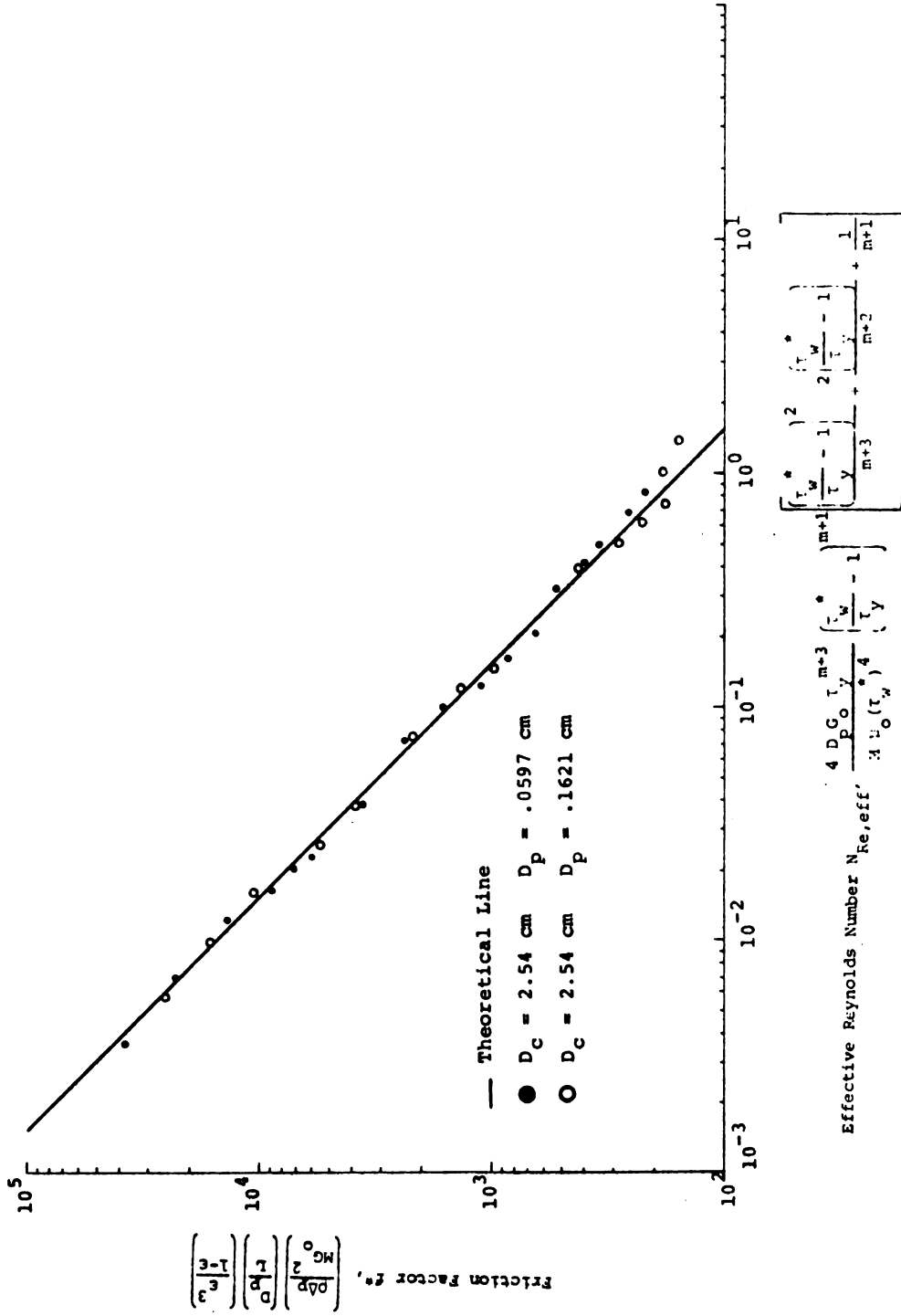


Figure 6.5-3 Pressure Drop-Flow Rate Correlation for Flow of 0.5% PMC 25 Solutions Through Packed Beds

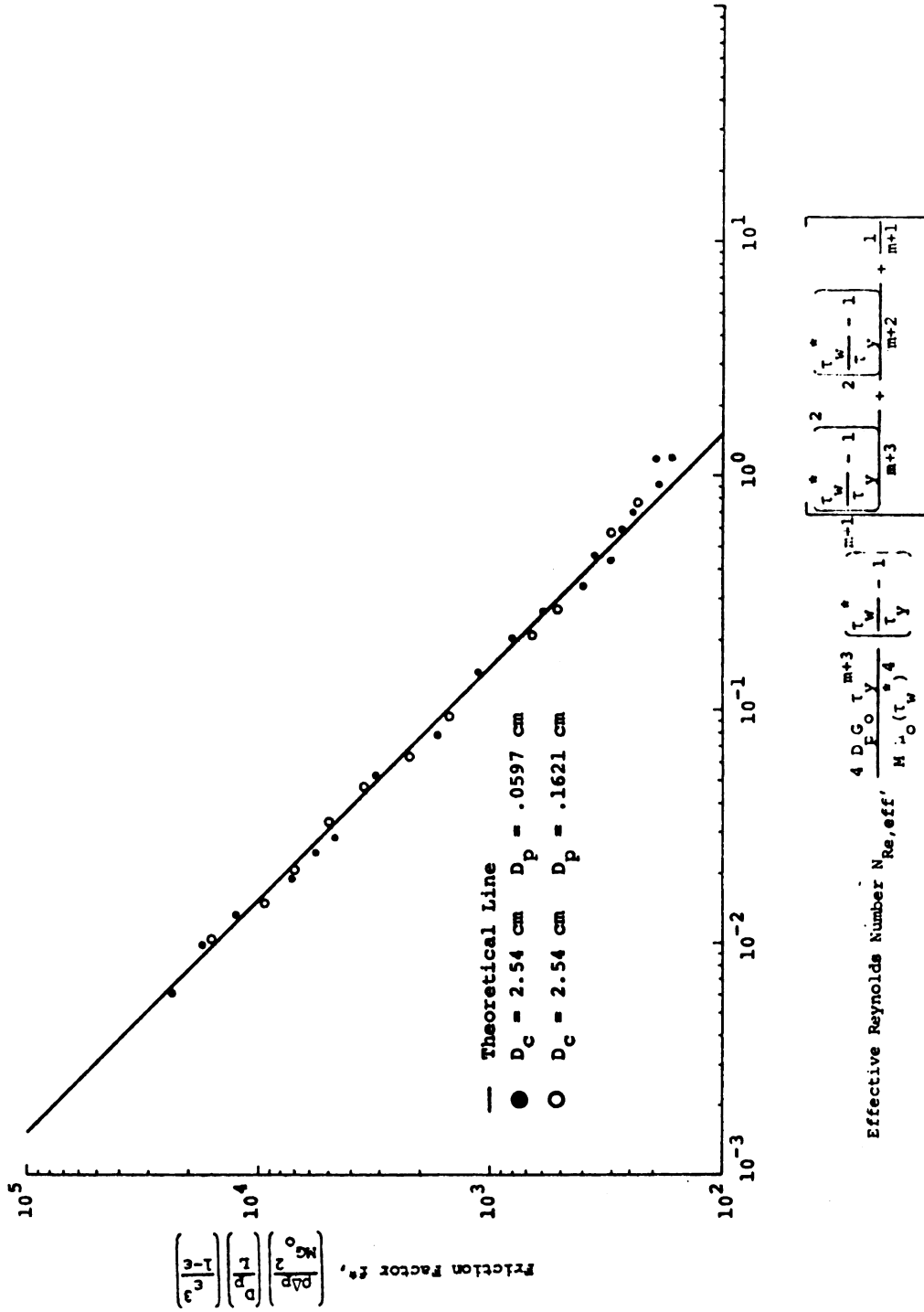


Figure 6.5-4 Pressure Drop-Flow Rate Correlation for Flow of 0.38 PMC 25 Solutions Through Packed Beds

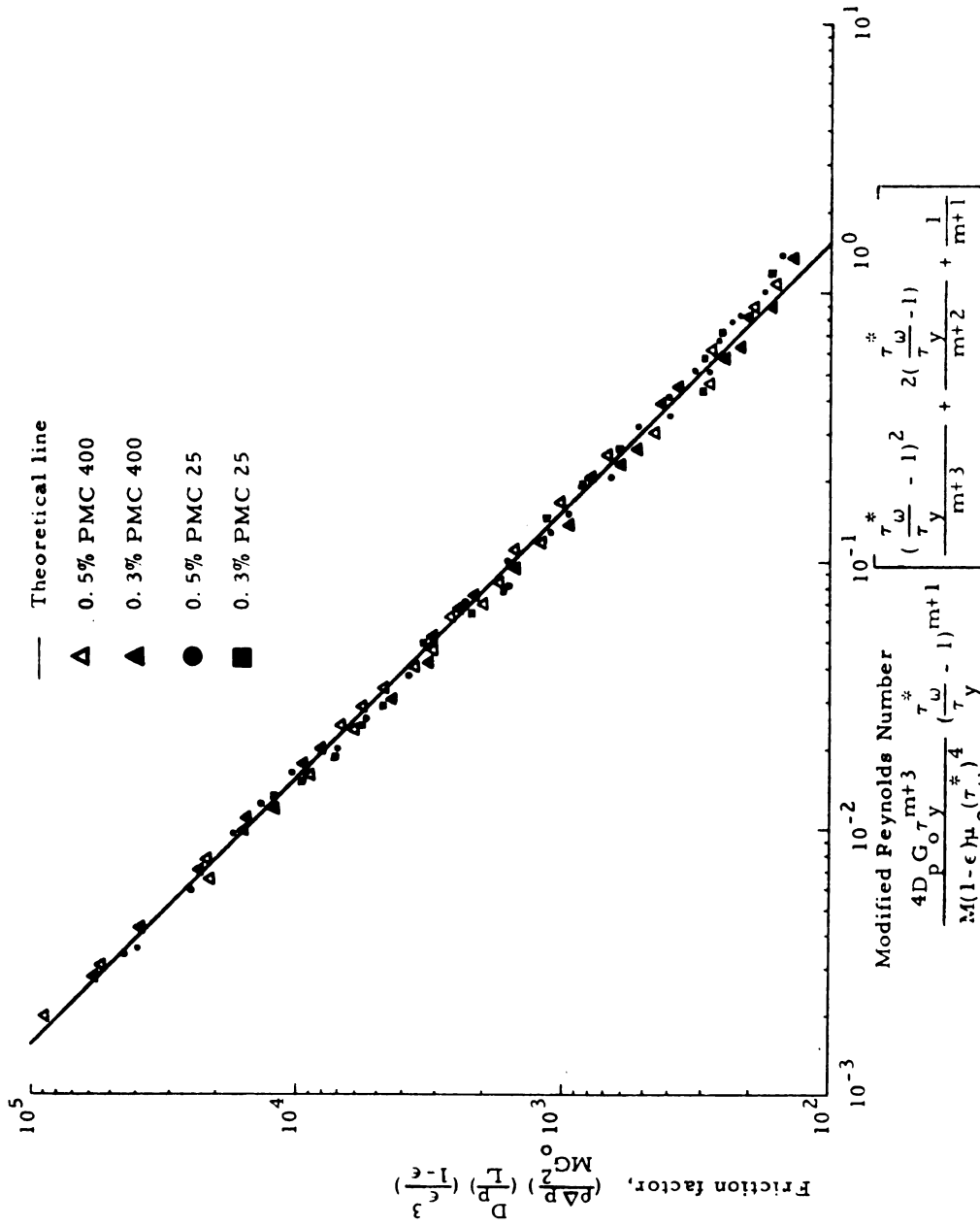


Figure 6.5-5 Pressure Drop-flow Rate Correlation for Flow of Aqueous Solutions of Polymethylcellulose Through Packed Beds

concentrations. The average percent deviation for each concentration are listed in Table 6.5-1.

## §6.6 Conclusions

The results of the present investigation may be summarized as follows:

1. The material parameters for the Herschel-Bulkley model for aqueous solutions of PMC were evaluated. The Herschel-Bulkley model correlated the steady shear experimental data very well over the entire range of shear rate. The data of primary normal stress difference of aqueous solutions of PMC were not reliable because of experimental error. The presence of a yield stress prevented measurement of the relaxation time spectrum.
2. The modified friction factor-modified Reynolds number correlation was developed for the Herschel-Bulkley rheological model. Packed bed flow data for aqueous solutions of PMC were well correlated for effective Reynolds numbers less than one. This result appears to confirm the utility of the correlation developed in this study.
3. It appears that an improvement could be made on the capillary model for the packed bed. There seems to be an upward deviation from the Ergun

TABLE 6.5-1 Summary of Experimental Data for Herschel-Bulkley Modification

Solution Concentration (weight %)	Average % Error <sup>a</sup> in f* Calculated from Table 3-1	Number of Experimental Points	Maximum Range of % Error f* calc
PMC 400			
0.5	6.75	41	-20.15 to +10.30
0.3	8.65	35	-26.42 to +10.70
PMC 25			
0.5	9.26	33	-36.55 to +13.94
0.3	10.03	30	-29.48 to +11.59
All Solutions	8.53	139	-36.55 to +13.94

<sup>a</sup>Average % error was calculated as

$$\frac{f^*_{\text{calc}} - f^*_{\text{expt}}}{f^*_{\text{calc}}} \times 100$$

Arithmetic average of absolute values are given in Appendix T.

correlation in the effective Reynolds number region of one (see Figure 6.5-5).

## CHAPTER 7

### CONCLUSIONS AND RECOMMENDATIONS

#### §7.1 Conclusions

The Ergun equation,

$$\left( \frac{\rho \Delta p}{G_o^2} \right) \left( \frac{D_p}{L} \right) \left( \frac{\epsilon^3}{1 - \epsilon} \right) = 150 \frac{(1 - \epsilon)}{D_p G_o / \mu} + 1.75$$

is widely used to relate pressure drop to flow rate of Newtonian fluids in packed beds. In this study the Ergun equation was extended to non-Newtonian fluids by using an effective viscosity in place of the Newtonian viscosity, i.e.,

$$\left( \frac{\rho \Delta p}{MG_o^2} \right) \left( \frac{D_p}{L} \right) \left( \frac{\epsilon^3}{1 - \epsilon} \right) = 150 \frac{(1 - \epsilon)}{D_p G_o / \eta_{eff}} + 1.75$$

The effective viscosity was calculated based on the result of a hydrodynamic analysis of the capillary model of the packed bed using the appropriate constitutive equation for each non-Newtonian fluid. Therefore, the effective viscosity is not only a function of the material parameters but also a function of the porous medium.

Measurements of pressure drops and corresponding flow rates were made for several concentrations of aqueous solutions of three different polymers (polyacrylamide, polyvinylpyrrolidone, and polymethylcellulose) flowing through packed beds, and the rheological properties of these polymer fluids were determined.

The following conclusions were based on the analysis of these experiments and comparisons with the literature:

1. The Ergun equation can be used to correlate pressure drop-flow rate data for non-Newtonian fluids flowing through packed beds by using the appropriate effective viscosity.
2. The rheological model which characterizes the shear stress-shear rate relationship with minimum error should be used to calculate the effective viscosity for use in the Ergun equation. Previous investigators [1, 2, 3, 4, 5] have calculated the effective viscosity based on either the power-law or the Ellis model.

### 3. Polyacrylamide

The Sprigg's model,

$$\tau^p + \lambda_p F_e \tau^p = -2\eta_p e$$

$$\tau = \sum_{p=1}^{\infty} \tau^p$$

where material parameters  $\eta_0$ ,  $\alpha$ ,  $\lambda$ , and  $\epsilon$  were listed in Table 4.4-3, correlated the shear stress-shear rate data with the least square error between predicted and experimental values of apparent viscosities when compared to the power-law and the Ellis model. Correspondingly, the least square error between experimental and calculated values of the friction factor was obtained using the effective viscosity calculated from the Sprigg's model when compared with the use of the effective viscosity from the power-law and the Ellis model. The effective Reynolds number for packed beds ranged from  $10^{-5}$  to  $10^{-1}$  in our experiments with aqueous solutions of polyacrylamide.

#### 4. Polyvinylpyrrolidone

Meter's model,

$$\tau_{ij} = -\left\{ \eta_{\infty} + \frac{\eta_0 - \eta_{\infty}}{1 + \left[ \frac{\sqrt{\frac{1}{2}(\tau:\tau)}}{\tau_m} \right]^{\alpha-1}} \right\} e_{ij}$$

where material functions  $\eta_0$ ,  $\eta_{\infty}$ ,  $\alpha$ , and  $\tau_m$  were listed in Table 5.3-1, was used to correlate the shear stress-shear rate data. The average percent deviation between values predicted from the model and experimental values of the apparent

viscosity was 2.1 percent. Aqueous solutions of polyvinylpyrrolidone were purely viscous having both upper and lower limiting viscosities. The pressure drop-flow rate data for aqueous solutions of polyvinylpyrrolidone were correlated well (error less than 6.1%) by the Ergun equation with the use of the effective viscosity calculated from Meter's model for effective Reynolds numbers less than one. The effective Reynolds number for packed beds ranged from  $10^{-2}$  to  $10^2$  in our experiments for aqueous solutions of polyvinylpyrrolidone.

#### 5. Polymethylcellulose

The Herschel-Bulkley model,

$$\tau_{ij} - \tau_y = \left[ \mu_0 \left( \frac{e_{ij}}{2} \right)^{\frac{1-m}{2}} \right]^{\frac{1}{m}} e_{ij}$$

where material parameters  $\mu_0$ ,  $m$ , and  $\tau_y$  were listed in Table 6.4-1, was used to correlate the shear stress-shear rate data for aqueous solutions of polymethylcellulose because these solutions exhibited yield stresses with non-linear flow curves. The average percent deviation between values predicted from the model and experimental values of the apparent viscosity was 1.7 percent. The Ergun equation with the use of the effective

viscosity calculated from the Herschel-Bulkley model correlated pressure drop-flow rate data within an error of 8.2 percent. The effective Reynolds number for packed beds ranged from  $10^{-3}$  to 1.0 in our experiments with aqueous solutions of polymethylcellulose.

6. Neither the power-law nor the Ellis model will predict the proper shapes of the apparent viscosity versus shear rate for aqueous solutions of polyvinylpyrrolidone and polymethylcellulose; and therefore, neither model would be very useful for predicting the effective viscosities for calculations of friction factors in packed beds.
7. Basic rheological data on polyvinylpyrrolidone and polymethylcellulose were obtained; this information has not been reported in literature previously.
8. The wall effect correction factor as defined in Eq. A.3-32 and reported in the literature [90] was determined to be applicable for non-Newtonian fluids as well as Newtonian fluids.
9. An improvement in the model for packed beds is required in order to account for the inertial and surface effects for polymer solutions. This conclusion is based on the friction factor-Reynolds

number data for polyvinylpyrrolidone solutions for effective Reynolds numbers greater than one (see Figure 5.4-7). An attempt was made to improve the correlation of the friction factor data for effective Reynolds numbers greater than one. A correction parameter  $(D_p G_o) / (M(1-\epsilon)\eta_o) \cdot (G_o \lambda / \rho D_p)$  was used to account for the deviations. However, this correction should not be considered general at this time because of limited information.

## §7.2 Recommendations

1. Of greater potential value would be an investigation of time-dependent normal stress. For such a measurement one needs the response of the pressure-sensing system. If an appreciable time lag was introduced, a calibration of the system response characteristics might still permit meaningful data analysis. In that way, the secondary normal stress difference,  $(\tau_{22} - \tau_{33})$ , can also be measured.
2. Continued attention to the quantity  $\bar{G}_{wr}$  and its utility for data-correlation purposes, is recommended. The implications of its behavior with temperature should be explored in an effort to clarify its fundamental significance.

3. It is of paramount importance that the polymer fluids chosen for study remain stable in storage and in shear. Months, if necessary, should be taken to determine these stability characteristics for every fluid to be tested. Special attention to chemical preservations and their subsidiary effects will be a great help.
4. Many water-soluble polymers are frequently poorly characterized with regard to molecular weight, thereby confusing the interpretation of measurements. Behavior in a polar solvent may be anomalous, with ionic and association effects implying structures not characteristic of the polymer chain. Future experimental work should definitely move into the area of non-aqueous solutions.
5. Appropriately designed apparatus is desired for extensive work of the quantitative correlation of the data in regards to the polymer adsorption, gel formation, shear degradation, and surface effects. Multiple flow loop system is recommended for these purposes.

## NOMENCLATURE

## NOMENCLATURE

A	cross-sectional area of a packed bed, $\text{cm}^2$
C	constant in permeability expression, dimensionless
$D_c, D_p$	diameter of tube, diameter of particle, cm
$\frac{\partial}{\partial t}$	partial time derivative, $\text{sec}^{-1}$
D/Dt	Jaumann time derivative, $\text{sec}^{-1}$
$e_{ij}$	shear-rate tensor, $\text{sec}^{-1}$
$e_{12}^o$	complex amplitude of shear rate in oscillation
f	friction factor for flow in a tube, dimensionless
f*	friction factor for flow in packed beds, dimensionless
$G_o$	mass velocity, $\text{g}_r/\text{cm}^2 \text{ sec}$
g	gravitational acceleration, $\text{cm}/\text{sec}^2$
K	fluid consistency index (power-law parameter), $\text{dyne sec}^n/\text{cm}^2$
K	proportionality constant in Darcy's law, $\text{cm}^3 \text{ sec}/\text{gr}$
$K_T, K_N$	machine constants for Weissenberg rheogoniometer
k	packed bed permeability, $\text{cm}^2$
H( $\tau$ )	relaxation time spectrum, $\text{sec}^{-1}$

L	length of tube, cm
m	Herschel-Bulkley model constant, dimensionless
M	wall effect correction factor, dimensionless
n, n'	parameters in various non-Newtonian model
$N_{Re}$	Reynolds number (Newtonian), dimensionless
$N_{Re,eff}$	non-Newtonian effective Reynolds number, dimensionless
p	fluid pressure, gr/cm sec <sup>2</sup>
P,Q	linear differential operators (Eq. 2.7-1)
Q	volumetric flow rate, cm <sup>3</sup> /sec
R	gas constant, gr cm <sup>2</sup> /sec <sup>2</sup> °C mole
R	radius of tube, cm
$R_h$	hydraulic radius of porous medium, cm
$S_o$	specific surface, $S(1 - \epsilon)$ , cm <sup>-1</sup>
$S_w$	recoverable shear, dimensionless
T	temperature, °C or °F
V	velocity, cm/sec
$V_o$	superficial velocity, Q/A, cm/sec
$\langle V_z \rangle$ , $\langle V \rangle$	average tube velocity, average pore velocity, cm/sec
$\alpha$	parameters in various non-Newtonian model
$\beta$	secondary normal stress difference coefficient, gr/cm
$\dot{\gamma}$	magnitude of shear rate, sec <sup>-1</sup>
$\dot{\gamma}^\circ$	complex amplitude of shear rate in oscillation
$\Delta P/L$	pressure gradient, gr/cm <sup>2</sup> sec <sup>2</sup>

$\delta_{ik}$	Kronecker delta
$\epsilon$	bed porosity, dimensionless
$\theta$	primary normal stress difference coefficient, gr/cm
$\eta_0$	lower-limiting viscosity, gr/cm sec
$\eta_c$	cross viscosity, gr/cm
$\eta$	non-Newtonian viscosity, gr/cm sec
$\eta(s)$	solvent viscosity, gr/cm sec
$\eta', \eta'', \eta^*$	oscillatory-shear viscosity parameters, gr/cm sec
$\eta_r$	reduced viscosity, dimensionless
$\eta_{eff}$	non-Newtonian effective viscosity, gr/cm sec
$\eta_\infty$	upper-limiting viscosity, gr/cm sec
$\bar{\eta}$	frequency factor, gr/cm sec
$\lambda$	relaxation time, sec
$\lambda_1, \lambda_2$	relaxation time, retardation time, sec
$\lambda_p$	relaxation time in p-th mode, sec
$\lambda_R$	longest relaxation time of Rouse theory, sec
$\mu$	Newtonian viscosity, gr/cm sec
$\mu_a$	apparent viscosity for non-Newtonian models, gr/cm sec
$\mu_0$	constant in Herschel-Bulkley model, gr <sup>m</sup> /cm <sup>m</sup> sec <sup>2m-1</sup>
$\rho$	fluid density, gr/cm <sup>3</sup>
$\tau_{ij}$	shear stress tensor, gr/cm sec <sup>2</sup>
$\tau_{L2}^0$	complex amplitude of shear stress in oscillation

$\tau_{12}$	constant in Ellis model, $\text{gr/cm sec}^2$
$\tau_m$	constant in Meter model, $\text{gr/cm sec}^2$
$\tau_w$	wall shear stress, $\text{gr/cm sec}^2$
$\tau_w^*$	wall shear stress of the packed bed, $\frac{12}{25} \frac{D_p}{6M} \frac{\epsilon}{1-\epsilon} \frac{\rho_p}{L}$ , $\text{gr/cm sec}^2$
$\phi$	force potential, $\text{cm}^2/\text{sec}^2$
$\psi$	velocity potential, $\text{cm}^2/\text{sec}$
$\Psi$	relaxation function appearing in integral formulations of viscoelasticity
$\omega$	radian frequency, $\text{sec}^{-1}$
$\omega_{ik}$	vorticity tensor, $\text{sec}^{-1}$
$G_w$	shear modulus for fluids, $\text{gr/cm sec}^2$
$\bar{G}_{wr}$	reduced shear modulus, $\text{gr/cm sec}^2$

## BIBLIOGRAPHY

## BIBLIOGRAPHY

1. Bird, R. B. and T. J. Sadowski, *Trans. Soc. Rheol.*, 9, 243 (1965).
2. Sadowski, T. J., *Trans. Soc. Rheol.*, 9, 251 (1965).
3. Sadowski, T. J., Ph.D. Thesis, Univ. of Wisconsin, Madison, Wis. (1963).
4. Christopher, R. H. and S. Middleman, *Ind. Eng. Chem.*, 57, 93 (1965).
5. Marshall, R. J. and A. B. Metzner, *Ind. Eng. Chem. Fund.*, 6, 393 (1967).
6. Gregory, D. R. and R. G. Griskey, *A. I. Ch. E. Jour.*, 13, 122 (1967).
7. Mooney, M., *J. Rheol.*, 2, 210 (1931).
8. Metzner, A. B., Advance in Chem. Eng., vol. 1, Acad. Press, N. Y. (1958).
9. Metzner, A. B., *Ind. Eng. Chem.*, 49, 1429 (1957).
10. Oldroyd, J. G., *Proc. Roy. Soc.*, A 218, 122 (1953).
11. Oldroyd, J. G., *Proc. Roy. Soc.*, A 245, 278 (1958).
12. Bird, R. B., W. E. Stewart, and E. N. Lightfoot, *Transport Phenomena*, Wiley, New York (1960).
13. Landau, L. D. and E. M. Lifshitz, Theory of Elasticity, Addison Wesley, Reading, Mass. (1959).
14. Coleman, B., *Ann. N. Y. Acad. Sci.*, 89, 672 (1961).
15. Coleman, B. and W. Noll, *Rev. Mod. Phys.*, 33, 239 (1961).

16. Williams, M. C., *Phys. of Fluids*, 5, 1126 (1962).
17. Williams, M. C., *Ind. Eng. Chem. Fund.*, 3, 42 (1964).
18. Reiner, M., *Twelve Lectures on Theoretical Rheology*, North-Holland, Amsterdam (1949).
19. Reiner, M., *Deformation, Strain, and Flow*, Interscience, New York (1960).
20. Pragger, W., *Introduction to Mechanics of Continua*, Ginn, New York (1960).
21. Foster, R. D., M. S. Thesis, Northwestern Univ., Evanston, Ill. (1961).
22. Rathna, S. L., *Quart. J. Mech. and Appl. Math.*, 15, 427 (1962).
23. Leigh, D. C., *Phys. of Fluids*, 5, 501 (1962).
24. Lyche, B. C. and R. B. Bird, *Chem. Eng. Sci.*, 6, 35 (1956).
25. Fredrickson, A. G. and R. B. Bird, *Ind. Eng. Chem.*, 50, 347 (1958).
26. Tomita, Y., *Bulletin of the Japanese Soc. of Mech. Eng.*, 2, 469 (1959).
27. Slattery, J. C., *A. I. Ch. E. Jour.*, 8, 663 (1962).
28. Bird, R. B., *Phys. of Fluids*, 3, 539 (1960).
29. Schechter, R. S., *A. I. Ch. E. Jour.*, 7, 445 (1961).
30. Hanks, R. W. and E. B. Christiansen, *A. I. Ch. E. Jour.*, 7, 519 (1961).
31. Gee, R. E. and J. B. Lyon, *Ind. Eng. Chem.*, 49, 956 (1957).
32. Slattery, J. C. and R. B. Bird, *Chem. Eng. Sci.*, 16, 231 (1961).
33. Ree, T. and H. Eyring, "The Relaxation Theory of Transport Phenomena," Chapter 3 in *Rheology: Theory and Applications*, Eirich (Ed.), Academic, New York (1958).
34. McEachern, D. W., Ph.D. Thesis, Univ. of Wisconsin, Madison, Wis. (1963).

35. Ziegenhagen, J. A., Ph.D. Thesis, Univ. of Wisconsin, Madison, Wis. (1962).
36. Meter, D. M., Ph.D. Thesis, Univ. of Wis., Madison, Wis. (1963).
37. Peek, R. L. and S. Mclean, J. Rheol., 2, 377 (1931).
38. Phillippoff, W., Viscosität der Kolloide, Edward Brothers, Ann Arbor, Mich. (1944).
39. Meter, D. M., A. I. Ch. E. Jour., 10, 878 (1964).
40. Herschel, W. H. and R. Bulkley, Proc. Am. Soc. Test. Mat., XXVI, 621 (1926).
41. Herschel, W. H. and R. Bulkley, Kolloid Z., XXXIX, 291 (1926).
42. Weissenberg, K., Proc. Intern. Congr. Rheol., II-142 (1948).
43. Greensmith, H. W. and R. S. Rivlin, Phil. Trans. Roy. Soc., London, A245, 399 (1953).
44. Markovitz, H. and R. B. Williams, Trans. Soc. Rheol., 1, 25 (1957).
45. Ferry, J. D., Viscoelastic Properties of Polymers, Wiley, New York (1961).
46. Zimm, B. H., J. Chem. Phys., 24, 269 (1956).
47. Rouse, P., J. Chem. Phys., 21, 1272 (1953).
48. Bueche, R., J. Chem. Phys., 22, 603, 1570 (1954).
49. Bougue, D. C., Ind. Eng. Chem., 5, 253 (1966).
50. White, J. L. and A. B. Metzner, J. Appl. Poly. Sci., 1, 1867 (1963).
51. Spriggs, T. W., J. D. Huppler, and R. B. Bird, Trans. Soc. Rheol., 10(1), 191 (1966).
52. Bougue, D. C. and J. O. Doughty, Ind. Eng. Chem. Fund., 5, 243 (1966).
53. Metzner, A. B., J. L. White, and M. M. Denn, Chem. Eng. Progr., 62(12), 81 (1966).
54. Mooney, J., J. Poly. Sci., 34, 599 (1959).

55. Lodge, A. S., Trans. Fard Soc., 52, 120 (1956).
56. Yamamoto, M., J. Phys. Soc. Jap., 11, 413 (1956).
57. Rivlin, R. S. and J. L. Ericksen, J. Rat. Mech. Anal., 4, 323 (1955).
58. Spriggs, T. W., Chem. Eng. Sci., 20, 931-940 (1965).
59. Brodnyan, J. G., F. H. Gaskins, and W. Philippoff, Trans. Soc. Rheol., 1, 109 (1957).
60. Dwight, H. B., Mathematical Tables of Elementary and Some Higher Mathematical Functions, 212-213, Dover, New York (1961).
61. Markovitz, H. and D. R. Brown, Trans. Soc. Rheol., 7, 137-154 (1963).
62. Hamming, R. W., Numerical Methods for Scientist and Engineers, 158-162, McGraw-Hill, New York (1962).
63. Bird, R. B. and P. J. Carreau, Chem. Eng. Sci., 23, 427-434 (1968).
64. Carreau, P. J., I. F. MacDonald, and R. R. Bird, Chem. Eng. Sci., 23, 901 (1968).
65. Ashare, E., Trans. Soc. Rheol., 12(4), 535-557 (1968).
66. Oldroyd, J. G., Proc. Roy. Soc., A200, 523 (1950).
67. Blake, S. P., Trans. in A. I. Ch. Engineers, 14, 415 (1922).
68. Burke, S. P., and W. B. Plummer, I & EC, 20, 1196 (1928).
69. Carman, P. C., Trans. in A. I. Ch. Engineers (London), 15, 150 (1937).
70. Ergun, S. and A. A. Orning, I & EC, 41, 1179 (1949).
71. Lea, F. M. and R. W. Nurse, Trans. in A. I. Ch. Engineers (London), 25, 47 (1947).
72. Leva, M. and M. Grummer, Chem. Eng. Progress, 33, 549, 633, 713 (1947).
73. Morcom, A. R., Trans. A. I. Ch. Engineers (London), 24, 30 (1946).

74. Morse, R. D., I & EC, 41, 1117 (1949).
75. Scheidegger, A. E., The Physics of Flow Through Porous Media, MacMillan, New York (1960).
76. Collins, R. W., Flow of Fluids Through Porous Media, Reinhold, New York (1961).
77. Carman, P. C., Flow of Gases Through Porous Media, Butterworth, London (1956).
78. Muskat, M., The Flow of Homogeneous Fluids Through Porous Media, Edwards, Ann Arbor (1937).
79. Leva, M., Fluidization, McGraw-Hill, New York (1959).
80. Richardson, J. G., "Flow Through Porous Media" in Handbook of Fluid Dynamics, V. L. Streeter (Ed.), McGraw-Hill, New York (1961).
81. Darcy, H. P. G., Les Fontaines Publiques de la ville de Dijon, Victor Dalmont, Paris (1856).
82. Kozeny, J., S-Ber. Wiener Akad., Abt. II a, 136, 271 (1927).
83. Ergun, S., Chem. Eng. Progr., 48, 89 (1952).
84. Fahien, R. W. and C. B. Schriver, "The Effect of Porosity and Transition Flow on Pressure Drop in Packed Beds," Presented at the Denver Meeting of the A. I. Ch. E., August 26-29 (1962).
85. Iberall, A. S., J. Res. Nat. Bur. Stand., 45, 398 (1950).
86. Brinkman, H. C., Appl. Sci. Res., A1, 27 (1947).
87. Ranz, W. E., Chem. Eng. Progr., 48, 247 (1952).
88. Happel, J. and N. Epstein, Ind. Eng. Chem., 46, 1187 (1954).
89. Rose, H. E. and A. Rizk, Proc. Inst. Mech. Engineers, 160, 493 (1949).
90. Metha, D. and M. C. Hawley, I & EC Process Design and Development, 8, 280 (1969).
91. Forchheimer, P., Z. Ver. Deuts. Ing., 45, 1782 (1901).
92. Klinkenberg, L. J., A. P. I. Drill. Prod. Pract., 200 (1941).

93. Debye, P. and R. L. Cleveland, J. Appl. Phys., 30, 843 (1959).
94. Porter, R. S. and J. F. Johnson, Trans. Soc. Rheol., 7, 241 (1963).
95. Bueche, J. and S. W. Harding, J. Polymer Sci., 32, 177 (1958).
96. Collins, E. A. and W. H. Bauer, Trans. Soc. Rheol., 9, 1 (1965).
97. Dunleavy, J. E. and S. Middleman, Trans. Soc. Rheol., 10, 157 (1966).
98. Huppler, J. D., E. Ashare, and L. A. Holmes, Trans. Soc. Rheol., 11(2), 1959 (1967).
99. Hullper, J. D., I. F. MacDonald, E. Ashare, T. W. Spriggs, R. B. Bird and L. A. Holmes, Trans. Soc. Rheol., 11(2), 181 (1967).
100. Turian, R. M. and R. B. Bird, Chem. Eng. Sci., 18, 689 (1963).
101. Hutlon, J. F., Nature, 200, 646 (1963).
102. King, R. G., Rheol. Acta, 5, 35 (1966).
103. Williams, M. L., R. Landel, and J. D. Ferry, J. Am. Chem. Soc., 77, 3701 (1955).
104. Fox, T. G. and V. R. Allen, J. Chem. Phys., 41, 344 (1964).
105. Fox, T. G., J. Polymer Sci., 9, 35 (1965).
106. Bueche, F., Physical Properties of Polymers, Interscience, New York (1962).
107. Bueche, F., J. Chem. Phys., 20, 1959 (1952); 25, 599 (1956).
108. Arai, T. and H. Aoyama, Trans. Soc. Rheol., 7, 333 (1963).
109. Dye, J. L., Private Communications.
110. Blanks, R. F., D. Patel, H. C. Park, to be published.
111. Hermas, J. J., Flow Properties of Disperse Systems, North-Holland, Amsterdam (1953).

112. Bird, R. B., Canadian J. Chem. Eng., 43(4), 161 (1965).
113. Dauben, D. L. and P. E. Menzie, Trans. Soc. Petrol. Eng., 240(I), 1065 (1967).
114. Burcik, P., Earth Mineral Sci., 37(7), 57 (1968).
115. Encyclopedia of Polymer Science and Technology, 3, 504, Wiley, New York (1965).
116. Bird, R. B., Private communications.
117. Meister, B. J., Private communications.
118. Landel, R. F., J. W. Berge and J. D. Ferry, J. Colloid Sci., 12, 400 (1957).
119. Copenhaver, J. W. and M. H. Bigelow, Acetylene and Carbon Monoxide Chemistry, Reinhold, New York (1949).
120. Skelland, A. H. P., Non-Newtonian Flow and Heat Transfer, Wiley, New York (1967).

## APPENDICES

APPENDIX A

DEVELOPMENT OF PACKED BED EQUATIONS

## APPENDIX A

### DEVELOPMENT OF PACKED BED EQUATIONS

When a fluid flows through a porous medium, the velocity of its elements changes rapidly from point to point along its tortuous flow path. The forces which produce these changes in velocity vary rapidly from point to point. It is reasonable to suppose that the random variations in flow path for any particular fluid element are uniformly distributed. Also the variations in magnitude of velocity can be expected to be distributed uniformly with mean zero. Thus, for steady laminar flow the lateral forces associated with the microscopic random variations in velocity can be expected to average to zero over any macroscopic volume. The only non-zero macroscopic force exerted on the fluid by the solid is that associated with the viscous resistance to flow. For steady laminar flow this force must be in equilibrium with the external and body forces on the fluid.

The basic equation which governs the study of the flow of homogeneous fluids through porous media is the law of Darcy. In this chapter Darcy's experiment and the

appropriate differential forms of Darcy's law will first be discussed. Next, the salient features of those theories which enable one to evaluate the coefficient which appears in Darcy's law, viz., the permeability coefficient will be considered. With these concepts and flow characteristics the friction factor and Reynolds number will be developed and correlated.

The literature on this subject is voluminous and experimental investigations have been done by many workers [67, 68, 69, 70, 71, 72, 73, 74] to determine the correlation between the pressure drop and the flow rate of a fluid through a packed column. An excellent source of literature reference is the monograph of Scheidegger [75], which contains a particularly good discussion of permeability concept. Other general references are those of Collins [76], Carman [77], Muskat [78], Leva [79], and Richardson [80].

#### §A.1 Darcy's Law

The theory of the viscous flow of a Newtonian fluid through an isotropic, homogeneous, porous medium is based upon the classic experiment of Darcy [81]. This experiment, the study of linear flow of water through a bed of sand, led to the law, to which we give Darcy's name, which states that the volumetric flow rate,  $Q$ , through a porous medium is directly proportional to the

cross-sectional area of the bed,  $A$ , and to the pressure gradient,  $\Delta p/L$ , causing flow, i.e.,

$$Q = K A \Delta p/L \quad (\text{A.1-1})$$

And the proportionality constant  $K$  is:

$$K = k/\mu \quad (\text{A.1-2})$$

where  $k$  is the permeability of the porous medium and  $\mu$  is the viscosity of the fluid.

Second, it is desirable to express the law in the differential form. There are two possible expressions which reduces to the same basic law, viz.,

$$V_o = - (k\rho/\mu) \nabla\phi \quad (\text{A.1-3})$$

and

$$V_o = - \nabla\psi \quad (\text{A.1-4})$$

where  $V_o (=Q/A)$  is the "filter velocity." The first expression, Eq. A.1-3, introduces a force potential

$$\phi = \int_{P_o}^P \frac{dP}{\rho} + gz \quad (\text{A.1-5})$$

The permeability,  $k$ , and the viscosity,  $\mu$ , are considered to be constants. The second expression, Eq. A.1-4, introduces a velocity potential

$$\psi = k\rho/\mu + \int_{z_0}^z \frac{k\rho g}{\mu} dz \quad (\text{A.1-6})$$

where  $k$  and  $\mu$  are intrinsic variables of the system.

#### §A.1.1 Darcy's Law for Anisotropic Porous Media

Many porous materials exhibit a distinct anisotropic character, particularly fibrous materials, such as wood as well as some sedimentary rocks. For isotropic porous media Darcy's law predicts the simple proportionality between the components of the volumetric flux and the corresponding components of the gradient of flow potential. Thus,

$$V_i = -(k\rho/\mu) \frac{\partial \phi}{\partial x_i}, \quad i = 1, 2, 3 \quad (\text{A.1-7})$$

The most general linear relationship between the  $V_i$  and the components of  $\partial\phi/\partial x_i$  that can be postulated takes the form:

$$V_i = -\left(\frac{\rho}{\mu}\right) \left[ k_{i1} \frac{\partial \phi}{\partial x_1} + k_{i2} \frac{\partial \phi}{\partial x_2} + k_{i3} \frac{\partial \phi}{\partial x_3} \right], \quad i = 1, 2, 3 \quad (\text{A.1-8})$$

Here the nine quantities,  $k_{ij}$ , ( $i, j=1, 2, 3$ ) form the elements of a tensor. The Eq. A.1-8 can be written as the single matrix equation

F

P

Si

pa

the

$$\begin{pmatrix} v_1 \\ v_2 \\ v_3 \end{pmatrix} = - \frac{\rho}{\mu} \begin{bmatrix} k_{11} & k_{12} & k_{13} \\ k_{21} & k_{22} & k_{23} \\ k_{31} & k_{32} & k_{33} \end{bmatrix} \begin{bmatrix} \partial\phi/\partial x_1 \\ \partial\phi/\partial x_2 \\ \partial\phi/\partial x_3 \end{bmatrix} \quad (\text{A.1-9})$$

If  $k$ -matrix is symmetric, then rotation of the axes to a particular orientation produces a diagonal  $k$ -matrix.

Thus, if

$$k_{ij} = k_{ji} \quad ; \quad i, j = 1, 2, 3 \quad (\text{A.1-10})$$

then for a particular set of rectangular axis,  $x_i'$  :  $i=1, 2, 3$ , the  $k$ -matrix takes the form (denoted as  $k'$ -matrix):

$$k'\text{-matrix} = \begin{pmatrix} k_1 & 0 & 0 \\ 0 & k_2 & 0 \\ 0 & 0 & k_3 \end{pmatrix} \quad (\text{A.1-11})$$

For the coordinate axes oriented parallel to the principal axes of the porous medium having orthogonal principal axes, the postulated form of Darcy's law becomes

$$v_i = - k_i (\rho/\mu) \frac{\partial\phi}{\partial x_i} \quad , \quad i=1, 2, 3 \quad (\text{A.1-12})$$

Since, in general, not one of the prime coordinates is parallel to the vertical axis which is the direction of the gravitational force, it must be written as:

$$\phi = g \sum_{i=1}^3 x_i' \cos \alpha_i + \int_{p_0}^p \frac{dp}{\rho(p)} \quad (\text{A.1-13})$$

## §A.2 Permeability Relations

Darcy's law permits a description of flow through porous media in certain flow regions. It provides no understanding of the property of "permeability." This understanding is possible only if the concept of permeability is reduced to more fundamental physical principles. Many attempts, theoretical and empirical, have been made to connect permeability to the properties of the porous medium. Such properties are porosity, pore structure, and grain size distribution. Despite innumerable investigations, there is no universally accepted correlation.

There are three theoretical approaches for studying flow through porous media. Common to each approach is the assumption that the flow may be analyzed on the basis of microscopic flow within pores. Theoretical models which describe the microscopic structure of pores are proposed and the microscopic flow properties are derived. By extension, macroscopic flow behavior is deduced. In the first method, the hydraulic radius theory, the porous medium is assumed to be equivalent to an assemblage of channels. The Navier-Stokes equations are solved for a single channel and the results are applied to the collection. The second method, the drag theory, considers

the particles to be obstacles to an otherwise straight flow of the fluid. The drag on each particle is calculated from the Navier-Stokes equations and the sum of the resistances of all the particles is thought to equal the total resistance of the bed to the flow of the fluid. The third method, the statistical theory, suggests that the porous medium should be considered intrinsically disordered. This is the opposite view of the other methods which consider the porous medium to be intrinsically ordered. The Navier-Stokes equations may not be used for such disordered media; a statistical mechanics method has to be applied instead. In practice, the hydraulic radius theory has been most successful in correlating flow experiments for Newtonian fluids flowing through dense beds.

The basic concept of the hydraulic radius theory is a consequence of dimensional considerations. It is observed that the permeability,  $k$ , in absolute units, has the dimension of length squared. It is reasonable that there exists a characteristic length which describes the permeability of the porous medium. This length is termed the "hydraulic radius" of the porous medium. A possible measure of this length,  $R_h$ , would be the ratio of volume to surface of the pore space, Presumably, the permeability will depend upon dimensionless quantities, e.g., some function of porosity,  $\epsilon$ .

Therefore an expression for permeability may have the form

$$k = C \frac{(R_h)^2}{f(\epsilon)} \quad (\text{A.2-1})$$

Blake [67] introduced the hydraulic radius concept and was led to the permeability expression

$$k = \frac{1}{C} \frac{\epsilon^3}{s} \quad (\text{A.2-2})$$

where  $s$  is the surface area per unit volume. Blake's approach does not indicate what the value of  $C$  should be. Kozeny [82] assumed the pore space to be equivalent to a bundle of capillaries of varying cross-section but of a definite length. This approach gave a specific meaning to the constant  $C$ . For example, for a circular cross-section  $C=2.00$  while  $C=3.00$  for a parallel slit. Carman [69] further modified the expression to include the effect of tortuosity,  $T$ , which accounted for the fact that the actual length of a pore is greater than the length of the bed. Carman obtained

$$k = \frac{1}{C} \frac{\epsilon^3}{s T^2} \quad (\text{A.2-3})$$

or adopting the value of  $\sqrt{2}$  for the tortuosity and the value 2.5 for  $C$ ,

$$k = \frac{1}{5} \frac{\epsilon^3}{s_o^2 (1 - \epsilon)^2} \quad (\text{A.2-4})$$

where  $s_o$  is the "specific surface," i.e., the surface area per unit volume of solid (not porous) material. Eq. 3.2-4 is the Balke-Kozeny-Carman equation. Further modifications have been proposed by Ergun [83], but they differ only in the value of the constant. Fahien and Schriver [84] have a modified equation to account for the effects of large porosities and of flow in the transition region.

There have been two approaches to the drag theory of permeability. Iberal [85] proposed the model of a random distribution of widely separated (high porosity), long, circular cylindrical fibers. Brinkman [86] and Ranz [87] assumed that the particles in the fluid are spheres held in position by external contact forces.

Iberall arrives at:

$$k = \frac{3}{16} \left( \frac{\epsilon D_p^2}{1 - \epsilon} \right) \left[ \frac{2 - \ln(D_p V_o \rho / \mu \epsilon)}{4 - \ln(D_p V_o \rho / \mu \epsilon)} \right] \quad (\text{A.2-5})$$

whereas Brinkman gives:

$$k = \frac{D_p^2}{72} \left[ 3 + \frac{4}{1 - \epsilon} - 3 \sqrt{\frac{8}{1 - \epsilon} - 3} \right] \quad (\text{A.2-6})$$

One observes that the drag theories lead to different accounts of permeability than do the hydraulic

radius theories. Happel and Epstein [88] have shown that Brinkman's approach has been the most successful in describing experimental results for flow through expanded, cubical assemblage of uniform spheres. These correlations have proved most useful for the study of the sedimentation of particle aggregates.

### §A.3 The Flow of Newtonian Fluids Through Porous Media

Consider the flow of an incompressible fluid with density  $\rho$  through a pipe as shown in Figure A.3-1.

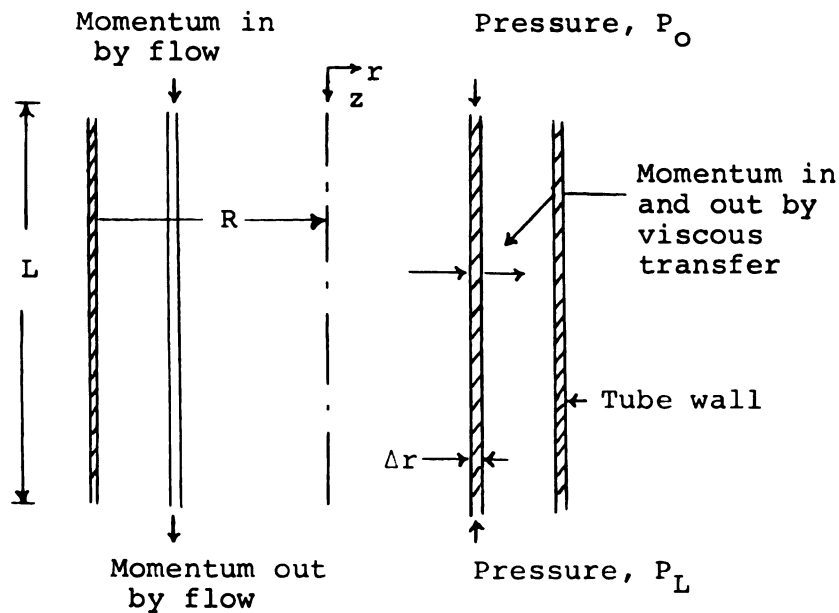


Figure A.3-1 Cylindrical Shell of Fluid Over Which Momentum Balance is Made to Get the Velocity Profile

Setting up a momentum balance on a shell of thickness  $\Delta r$ .

$$2\pi r L \tau_{rz} \Big|_r - 2\pi r L \tau_{rz} \Big|_{r+\Delta r} + 2\pi r \Delta r \rho V_z^2 \Big|_{z=0} - 2\pi r \Delta r \rho V_z^2 \Big|_{z=L} + 2\pi r \Delta r L \rho g + 2\pi r \Delta r (P_0 - P_L) = 0 \quad (\text{A.3-1})$$

Dividing Eq. A.3-1 by  $2\pi L \Delta r$  and taking the limit as  $\Delta r$  goes to zero; this gives

$$\frac{d}{dr} (r \tau_{rz}) = \left( \frac{P_0 - P_L}{L} \right) r \quad (\text{A.3-2})$$

where  $P = P - \rho g z$ ,  $\Delta p = P_0 - P_L$ . Equation 4.3-2 may be integrated to give:

$$\tau_{rz} = \left( \frac{\Delta p}{2L} \right) r + \frac{c_1}{r} \quad (\text{A.3-3})$$

Since the momentum flux is finite at  $r=0$ ,  $c_1$  must be zero.

$$\tau_{rz} = \frac{\Delta p}{2L} r \quad (\text{A.3-4})$$

Newton's law of viscosity for this situation is

$$\tau_{rz} = -\mu \frac{dv_z}{dr} \quad (\text{A.3-5})$$

Hence, from Equations A.3-4 and A.3-5

$$\frac{dv_z}{dr} = - \left( \frac{\Delta p}{2\mu L} \right) r \quad (\text{A.3-6})$$

$$v_z = - \left( \frac{\Delta p}{4\mu L} \right) r^2 + c_2 \quad (\text{A.3-7})$$

From boundary condition  $v_z = 0$  at  $r = R$

$$c_2 = \frac{\Delta p}{4\mu L} R^2$$

Hence,

$$v_z = \left( \frac{\Delta p}{4\mu L} \right) R^2 \left[ 1 - \left( \frac{r}{R} \right)^2 \right] \quad (\text{A.3-8})$$

The average velocity  $\langle v_z \rangle$  is calculated by summing up all velocities over the cross-section and then dividing by the cross-sectional area:

$$\begin{aligned} \langle v_z \rangle &= \frac{\int_0^{2\pi} \int_0^R v_z r \, dr \, d\theta}{\int_0^{2\pi} \int_0^R r \, dr \, d\theta} \\ &= \frac{\Delta p R^2}{8\mu L} \quad (\text{A.3-9}) \end{aligned}$$

Momentum flux and velocity distributions in flow in cylindrical tube were shown in Figure A.3-2.

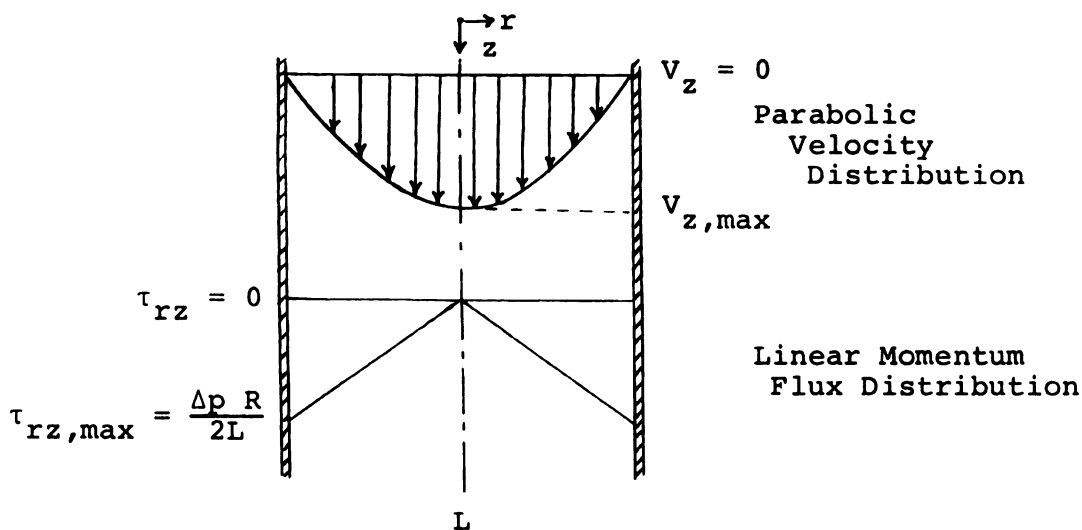


Figure A.3-2 Momentum Flux and Velocity Distributions in Flow in Cylindrical Tubes

As suggested before, the results for flow through a tube will be applied to that for flow through a porous medium by means of hydraulic radius concept. Hydraulic radius,  $R_h$ , is defined as:

$$D = 4R_h \quad \text{or} \quad R = 2R_h \quad (\text{A.3-10})$$

where

$$\begin{aligned} R_h &= \frac{\text{Cross-section available for flow}}{\text{Wetted perimeter}} \\ &= \frac{\text{Volume available for flow}}{\text{Total wetted perimeter}} \\ &= \frac{(\text{volume of voids})/(\text{volume of medium})}{(\text{wetted surface})/(\text{volume of medium})} \\ &= \epsilon/S \end{aligned} \quad (\text{A.3-11})$$

Since the "specific" surface area,  $S_o$ , is defined by

$$S = S_o(1 - \epsilon) \quad (\text{A.3-12})$$

and a mean particle diameter

$$D_p = 6/S_o \quad (\text{A.3-13})$$

Hence, from Equations A.3-11, A.3-12, and A.3-13

$$R_h = \frac{1}{2} R = \frac{\epsilon}{S} = \frac{\epsilon}{S_o(1 - \epsilon)} = \frac{D_p \epsilon}{6(1 - \epsilon)} \quad (\text{A.3-14})$$

Substituting Equation A.3-14 into Equation A.3-9)

$$\begin{aligned} \langle V_z \rangle &= \frac{\Delta p R^2}{8\mu L} \\ &= \frac{4\Delta p R_h^2}{8\mu L} = \frac{\Delta p D_p^2 \epsilon^2}{72\mu L(1 - \epsilon)^2} \end{aligned} \quad (\text{A.3-15})$$

The commonly accepted Dupuit-Forchheimer assumption [69].

is:

$$\begin{aligned} V_o &= \epsilon \langle V_z \rangle \\ &= \frac{\Delta p D_p^2 \epsilon^3}{72\mu L(1 - \epsilon)^2} \end{aligned} \quad (\text{A.3-16})$$

Therefore the permeability expression is:

$$k = \frac{D_p^2}{C} \frac{\epsilon^3}{(1 - \epsilon)^2} \quad (\text{A.3-17})$$

where the constant C is left to be determined from experiments for the flow of Newtonian fluids in packed beds.

The effect of tortuosity results in an actual pore length greater than the length of the bed. The experimental measurements indicate that the number 72 in the denominator in Equation A.3-16 be replaced by 150 [83]. Hence, Equation A.3-16 becomes:

$$v_o = \frac{\Delta p D_p^2 \epsilon^3}{150\mu L(1 - \epsilon)^2} \quad (\text{A.3-18})$$

This equation is known as the Blake-Kozeny [12, 69, 83] equation and valid for low flow rates.

For highly turbulent flow, the friction factor is only a function of roughness when the Reynolds number is high. The friction factor  $f$ , a dimensionless quantity is also called a drag coefficient. It is approximately a constant at higher Reynolds numbers. For the flow of a fluid through a bed of spheres, the pressure drop,  $\Delta p$ , is given as follows:

$$\Delta p = F/A \quad (\text{A.3-19})$$

where  $F$  is the force exerted on the solid surfaces and  $A$  is the cross-sectional area.

Consider the fluid flowing through a cylindrical tube. The fluid will exert force  $F$  on the solid surfaces which is equal to:

$$F = A' K f \quad (\text{A.3-20})$$

where  $A'$  is the surface area of the column or wetted surface,  $K$  is the kinetic energy per unit volume, and  $f$  is the friction factor; therefore,

$$K = \frac{1}{2} \rho \langle V \rangle^2$$

and

$$A' = 2\pi R L \quad (\text{A.3-21})$$

$$F = (2\pi R L) \left( \frac{1}{2} \rho \langle V \rangle^2 \right) f \quad (\text{A.3-22})$$

From Equations A.3-19 and A.3-22

$$f = \frac{R \Delta p}{2L \left( \frac{1}{2} \rho \langle V \rangle^2 \right)} \quad (\text{A.3-23})$$

Since the hydraulic radius,  $R_h$ , is:

$$R_h = \frac{\epsilon}{S} = \frac{\epsilon}{S_o (1 - \epsilon)} = \frac{D_p \epsilon}{6(1 - \epsilon)} \quad (\text{A.3-14})$$

$$f = \frac{R_h}{L} \left( \frac{\Delta p}{\frac{1}{2} \rho \langle V \rangle^2} \right) \quad (\text{A.3-24})$$

Therefore,

$$\frac{\Delta p}{L} = \frac{1}{R_h} \frac{1}{2} \rho \langle V \rangle^2 f \quad (\text{A.3-25})$$

From Equations A.3-14, A.3-16, and A.3-25

$$\frac{\Delta p}{L} = \frac{3(1 - \epsilon)\rho V_o^2 f}{D_p \epsilon^3} \quad (\text{A.3-26})$$

Experimental data [12, 83] indicate that:

$$6 f = 3.5$$

Hence,

$$\frac{\Delta p}{L} = \frac{1.75 \rho (1 - \epsilon) V_o^2}{\epsilon^3 D_p} \quad (\text{A.3-27})$$

Equation A.3-27 is known as the Burke-Plummer equation [12, 68, 83]. When Equations A.3-18 and A.3-27 are combined, the following equation results:

$$\frac{\Delta p}{L} = \frac{150 \mu V_o}{D_p^2} \frac{(1 - \epsilon)^2}{\epsilon^3} + \frac{1.75 V_o^2}{D_p} \frac{1 - \epsilon}{\epsilon^3} \quad (\text{A.3-28})$$

This is known as Ergun equation [12, 83]. This can be also written in terms of  $G$ , the mass flow rate, and in the dimensionless group:

$$\left( \frac{\Delta p}{G^2} \right) \left( \frac{D_p}{L} \right) \left( \frac{\epsilon^3}{1 - \epsilon} \right) = \frac{150 \mu (1 - \epsilon)}{D_p G} + 1.75 \quad (\text{A.3-29})$$

It can be seen that in the low flow regions where most of the experiments are performed, the plot of

$\log \left( \frac{\Delta p \rho D_p \epsilon^3}{G^2 L (1 - \epsilon)} \right)$  vs.  $\log \left( \frac{D_p G}{\mu (1 - \epsilon)} \right)$  will be a straight line with the slope of -1.

At very low flow rates or in laminar flow, the  $\frac{(1 - \epsilon)\mu}{D_p G}$  factor is dominant in the right-hand side of the Equation A.3-29. At very high flow rates or in turbulent flow rates,  $\frac{(1 - \epsilon)}{D_p G}$  becomes comparatively negligible to 1.75. So,  $\left( \frac{\Delta p \rho D_p \epsilon^3}{G^2 L (1 - \epsilon)} \right)$  remains constant at 1.75.

The above derived relationship does not include the wall effects. If the diameter of the column is very large compared to that of packing particles, the pressure drop and the flow rates are unaffected by the friction factor due to the wall.

Carman [69] and Rose and Rizk [89] indicated that a practical minimum of a column diameter to particle diameter ratio,  $D_c/D_p$ , for which tube wall effects are negligible should be about 20. Metha and Hawley [90] modified the Ergun equation by correcting the hydraulic radius relation as follows:

$$\frac{\text{Wetted surface of spheres} + \text{Wetted surface of wall}}{\text{Volume of bed}} = \frac{\text{Wetted surface}}{\text{Volume of bed}} = \frac{6(1 - \epsilon)}{D_p} + \frac{4}{D_c}$$

Thus,

$$R_h = \frac{\epsilon}{\frac{6(1-\epsilon)}{D_p} + \frac{4}{D_c}} \quad (\text{A.3-30})$$

Hence, the Ergun equation becomes:

$$\frac{\rho \Delta p}{MG_o} \frac{D_p}{L} \frac{\epsilon^3}{1-\epsilon} = \frac{150 \mu (1-\epsilon) M}{D_p G_o} + 1.75 \quad (\text{A.3-31})$$

where

$$M = \frac{4 D_p}{6 D_c (1-\epsilon)} + 1$$

$$M = 1 \quad \text{when} \quad D_c \gg D_p \quad (\text{A.3-32})$$

#### §A.4 The Flow of Non-Newtonian Fluids Through Porous Media

Some effort has been extended toward establishing methods for predicting non-Newtonian flow behavior in porous media and for correlating pressure drop versus flow rate data with viscometric data for porous media experiments. At the present time there is no universally acceptable scale-up method for flow of rheologically complex fluids in porous media. The various methods currently employed can be arbitrarily divided into at least three major categories. The method which seems to have received the most attention is based on the coupling of a particular model for a porous medium--i.e., the so-called hydraulic radius model, with an assumed functional

relationship between shear rate and shear stress to describe the rheological behavior of a non-Newtonian fluid. This method involves correlations of experimental data from one-dimensional flow experiments in unconsolidated porous media, i.e., mostly bead packs, with the appropriate rheological parameters derived from viscometric experiments on the fluid of interest. The power-law and Ellis models have been used to describe the purely viscous behavior of the non-Newtonian fluids. Another category involves generalized scale-up methods which adapt Darcy's law to non-Newtonian fluids without invoking a particular rheological model of purely viscous behavior. The appropriate rheological description can, in principle, be derived from viscometric and porous media flow experiments. A third approach, based on the concept of the simple fluid, involves the application of dimensional analysis to the scale-up of porous media flow data for an arbitrary viscoelastic fluid.

This work was mainly directed at developing a generalized scale-up method based on the capillary model. Wall effects were accounted for by using the hydraulic concept. Various empirical and derived models for non-Newtonian fluids were applied to the problem of flow through porous media. In this section application of Sprigg's model will be developed. Several other models applied in this study will be similar to that of Sprigg's

model application. The results are listed in Table 3-1.

For steady upward cylindrical tube flow as shown in Figure A.4-1 the sum of all forces acting on the fluid between section 1 and 2 must be zero. The forces involved are those due to static pressure, gravity, and shear, so that

$$\pi R^2 P_1 - \pi R^2 P_2 - \pi R^2 L \rho g - 2\pi R L \tau_w = 0 \quad (\text{A.4-1})$$

then:

$$2\pi R L \tau_w = \pi R^2 (P_1 - P_2 - L \rho g) = \pi R^2 \Delta P$$

$$(\tau_{rz})_{r=R} = \tau_w = \frac{R \Delta P}{2L} \quad (\text{A.4-2})$$

Similarly, if the shear stress at any  $r$  is  $\tau_{rz}$ , where  $r \leq R$ , then:

$$\tau_{rz} = \frac{r \Delta P}{2L} \quad (\text{A.4-3})$$

Combining Equations A.4-2 and A.4-3,

$$\tau_{rz} = \tau_w \frac{r}{R} \quad (\text{A.4-4})$$

Equation A.4-4 indicates a linear distribution of shear stress in the fluid, from zero at the centerline to  $\tau_w$  at the tube wall, regardless of flow regime.

It is assumed that: (1) the fluid is in steady laminar flow, (2) the fluid is time-independent under the prevailing conditions, and (3) there is no slip between the fluid and the tube wall.

The volumetric flow rate through the differential annulus between  $r$  and  $r + dr$  is

$$dQ = V_z 2\pi r dr \quad (\text{A.4-5})$$

where  $V_z$  is the local velocity at  $r$ .

$$Q = \int_0^Q dQ = \pi \int_0^R V_z^2 r dr = \pi \int_0^R V_z^2 d(r^2)$$

Integrating by parts

$$Q = \pi [V_z r^2 - \int_0^R r^2 dV_z] \quad (\text{A.4-6})$$

The term  $V_z r^2$  is eliminated by assumption (3), and from assumptions (1) and (2),

$$\frac{dV_z}{dr} = -f(\tau_{rz}) \quad (\text{A.4-7})$$

From Equation A.4-4)

$$r^2 = \frac{R^2 \tau_{rz}^2}{\tau_w^2} \quad ; \quad dr = \frac{R}{\tau_w} d\tau_{rz}$$

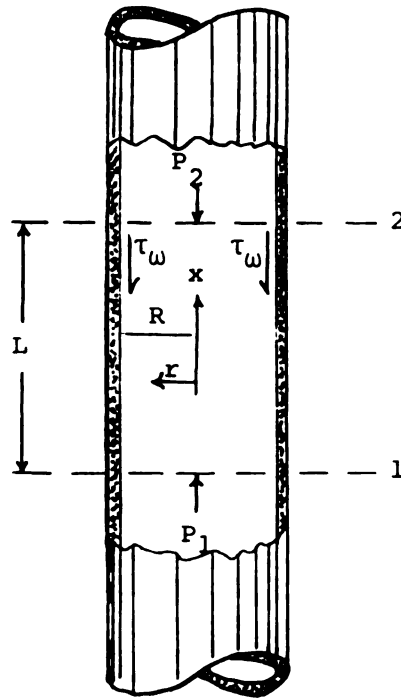


Figure A.4-1 Stress Acting on a Cylindrical Element of Fluid of Radius  $R$  in Steady Flow

Substituting these into Equation A.4-6,

$$Q = \pi \int_0^{\tau_w} \frac{R^2 \tau_{rz}^2}{\tau_w^2} f(\tau_{rz}) \frac{R}{\tau_w} d\tau_{rz}$$

or

$$\frac{Q}{\pi R^3} = \frac{1}{\tau_w^3} \int_0^{\tau_w} \tau_{rz}^2 f(\tau_{rz}) d\tau_{rz} \quad (\text{A.4-8})$$

Since  $Q = \langle V_z \rangle \pi R^2$ , therefore,

$$\langle V_z \rangle = \frac{R}{\tau_w} \int_0^{\tau_w} \tau_{rz}^2 f(\tau_{rz}) d\tau_{rz} \quad (\text{A.4-9})$$

## Sprigg's 4-Constant Model

Sprigg's model gives

$$\frac{\eta}{\eta_0} = \frac{1}{Z(\alpha)} \sum_{p=1}^{\infty} \frac{1}{p^\alpha + c \frac{2}{\lambda} \dot{\gamma}^{2.2}} \quad \text{for low } \dot{\gamma}$$

$$\frac{\eta}{\eta_0} = \frac{\pi}{2\alpha \cos \frac{\pi}{2\alpha}} \frac{(c\lambda\dot{\gamma})^{\frac{1}{\alpha}-1}}{Z(\alpha)} \quad \text{for high } \dot{\gamma}$$

Therefore, at Newtonian range the relationship of friction factor  $f^*$ , and effective Reynolds number  $N_{Re,eff}$ , is the same as the Newtonian case except for the viscosity:

$$f^* = \frac{\Delta p}{MG_0} \frac{D_p}{L} \frac{\epsilon^3}{1-\epsilon} \rho \quad (\text{A.4-10})$$

$$N_{Re,eff} = \frac{M D_p G_0}{(1-\epsilon)\eta_0} ; \quad \frac{1}{\eta_{eff}} = \frac{1}{M^2 \eta_0} \quad (\text{A.4-11})$$

For the high shear rate:

$$\eta = \frac{\eta_0 \pi}{2\alpha \cos \frac{\pi}{2\alpha}} \frac{(c\lambda)^{\frac{1}{\alpha}-1} \dot{\gamma}^{\frac{1}{\alpha}-1}}{Z(\alpha)} \quad (2.8-57)$$

Then,

$$\begin{aligned}\tau_{rz} &= -\eta \dot{\gamma} \\ &= -\frac{\eta_0 \pi}{2\alpha \cos \frac{\pi}{2\alpha}} \frac{(c\lambda)^{\frac{1}{\alpha}-1}}{Z(\alpha)} \dot{\gamma}^{\frac{1}{\alpha}} = -A \frac{dv_z}{dr}^{\frac{1}{\alpha}}\end{aligned}$$

In this case, for high shear rate

$$\frac{dv_z}{dr} = -\left(\frac{\tau_{rz}}{A}\right)^\alpha = -f(\tau_{rz}) \quad (\text{A.4-12})$$

Substituting for  $f(\tau_{rz})$  into Equation 4.5-9

$$\begin{aligned}\langle v_z \rangle &= \frac{R}{\tau_w^3} \int_0^{\tau_w} \tau_{rz}^2 \left(\frac{\tau_{rz}}{A}\right)^\alpha d\tau_{rz} \\ &= \frac{R}{\tau_w^3} \left[ \left(\frac{1}{A}\right)^\alpha \frac{\tau_{rz}^{\alpha+3}}{\alpha+3} \right]_0^{\tau_w} = \frac{R}{A^\alpha} \frac{\tau_w^\alpha}{\alpha+3}\end{aligned}$$

$$\langle v_z \rangle = \frac{1}{\alpha+3} \left(\frac{\Delta p}{2AL}\right)^\alpha R^{\alpha+1} \quad (\text{A.4-13})$$

Introducing the hydraulic radius and increasing  $L$  by a factor of  $25/12$ , Equation A.4-13 becomes:

$$\langle v_z \rangle = \frac{1}{\alpha+3} \left(\frac{6\Delta p}{25AL}\right)^\alpha \left(\frac{\epsilon D_p}{3(1-\epsilon)M}\right)^{\alpha+1} \quad (\text{A.4-14})$$

Since

$$\begin{aligned}V_o &= \epsilon \langle v_z \rangle \\ &= \frac{\epsilon}{\alpha+3} \left(\frac{6\Delta p}{25AL}\right)^\alpha \left[\frac{\epsilon D_p}{3(1-\epsilon)M}\right]^{\alpha+1}\end{aligned} \quad (\text{A.4-15})$$

where  $\langle V_z \rangle$  is average pore velocity.

The permeability expression is:

$$k = \frac{D_p^2}{C} \frac{\epsilon^3}{(1 - \epsilon)^2} \quad (\text{A.4-16})$$

where the constant  $C$  is left to be determined from experiments for the flow of Newtonian fluids in packed beds.

Rearranging Equation A.4-15, gives

$$\begin{aligned} v_o &= \frac{\epsilon}{\alpha+3} \left( \frac{6\Delta p}{25AL} \right)^\alpha \left( \frac{\epsilon D_p}{3(1-\epsilon)M} \right)^{\alpha+1} \\ &= \frac{c}{\alpha+3} \left( \frac{6\Delta p}{25AL} \right)^\alpha \left( \frac{\epsilon D_p}{1-\epsilon} \right)^{\alpha-1} \left( \frac{1}{3M} \right)^{\alpha+1} k \\ &= \left( \frac{12}{25} \right)^{\alpha-1} \left( \frac{1}{A} \right)^\alpha \left( \frac{1}{M} \right)^{\alpha+1} \frac{72}{2^\alpha (\alpha+3) 3^{\alpha+1}} \left( \frac{\epsilon D_p}{1-\epsilon} \right)^{\alpha-1} \left( \frac{\Delta p}{L} \right)^{\alpha-1} k \frac{\Delta p}{L} \end{aligned} \quad (\text{A.4-17})$$

From Equation A.4-17 we may obtain the Sprigg's model analog of Darcy's law, i.e.,

$$v_o = \frac{k}{\eta_{\text{eff}}} \frac{\Delta p}{L} \quad (\text{A.4-18})$$

where  $k$  is the same permeability defined previously for Newtonian fluids, and  $\eta_{\text{eff}}$  is an effective viscosity obtained from Equation A.4-18.

$$\frac{1}{\eta_{\text{eff}}} = \left(\frac{12}{25}\right)^{\alpha-1} \frac{1}{A^\alpha} \frac{1}{M^{\alpha+1}} \frac{72}{2^\alpha (\alpha+3) 3^{\alpha+1}} \left(\frac{\epsilon D_p}{1-\epsilon}\right)^{\alpha-1} \left(\frac{\Delta p}{L}\right)^{\alpha-1}$$

(A.4-19)

If we combine Equation A.4-11 and A.4-19, the effective viscosity for the entire range of shear becomes:

$$\frac{1}{\eta_{\text{eff}}} = \frac{1}{M^2 \eta_0} \left[ 1 + \left(\frac{12}{25}\right)^{\alpha-1} \frac{4}{\alpha+3} \left(\frac{c\lambda}{\eta_0}\right)^{\alpha-1} \frac{1}{3^{\alpha-1} M^{\alpha-1}} \frac{\left[\alpha \cos \frac{\pi}{2\alpha} Z(\alpha)\right]}{\pi^\alpha} \cdot \left(\frac{\epsilon D_p}{1-\epsilon}\right)^{\alpha-1} \left(\frac{D_p}{L}\right)^{\alpha-1} \right]$$

(A.4-20)

Equations A.4-18 and A.4-20 show that for non-Newtonian fluids the superficial velocity is not directly proportional to the pressure gradient. Equation A.4-20 shows that the effective viscosity is not only a function of fluid parameters but a function of the porous medium too.

The bed friction factor  $f^*$ , proposed by Ergun [83], is given:

$$f^* = \frac{\Delta p}{M G_0} \frac{D_p}{L} \frac{\epsilon^3}{1-\epsilon} \rho = C \left\{ \frac{(1-\epsilon) \eta_{\text{eff}}}{M D_p G_0} \right\} \quad (\text{A.4-21})$$

where  $G_0 = \rho V_0$ . For laminar flow:

$$f^* = C/N_{Re,eff} \quad (A.4-22)$$

where:

$$\begin{aligned} N_{Re,eff} &= \frac{M D_p G_o}{(1 - \epsilon) \eta_{eff}} \\ &= \frac{D_p G_o}{M(1 - \epsilon) \eta_o} \left[ 1 + \left( \frac{12}{25} \right)^{\alpha-1} \frac{4}{\alpha+3} \left( \frac{c\lambda}{\eta_o} \right)^{\alpha-1} \right. \\ &\quad \left. \frac{1}{6^{\alpha-1} M^{\alpha-1}} \frac{\left( 2\alpha \cos \frac{\pi}{2\alpha} Z(\alpha) \right)^\alpha}{\pi^\alpha} \left( \frac{\epsilon D_p}{1 - \epsilon} \right)^{\alpha-1} \right. \\ &\quad \left. \left( \frac{D_p}{L} \right)^{\alpha-1} \right] \end{aligned} \quad (A.4-23)$$

The bed structure parameters may be combined with the pressure gradient as

$$\tau_w^* = \frac{12}{25} \frac{D_p}{6M} \frac{\epsilon}{1 - \epsilon} \frac{\Delta p}{L} \quad (A.4-24)$$

Substituting Equation A.4-24 into Equation A.4-23 gives:

$$\begin{aligned} N_{Re,eff} &= \frac{D_p G_o}{M(1 - \epsilon)} \left[ 1 + \frac{4}{\alpha+3} \frac{\left[ \frac{2\alpha \cos \frac{\pi}{2\alpha} Z(\alpha)}{\eta_o \pi (c\lambda)^{\frac{1}{\alpha} - 1}} \right]^\alpha}{\left( \tau_w^* \right)^{\alpha-1}} \right] \\ &= \frac{D_p G_o}{M(1 - \epsilon) \eta_o} \left[ 1 + \frac{4}{\alpha+3} \frac{\left[ 2\alpha \cos \frac{\pi}{2\alpha} Z(\alpha) \right]^\alpha}{\pi^\alpha} \left( \frac{c\lambda \tau_w^*}{\eta_o} \right)^{\alpha-1} \right] \end{aligned} \quad (A.4-25)$$

Therefore, the friction factor  $f^*$ , for laminar flow, depends upon three dimensionless quantities

$$\frac{D_p G_o}{M(1 - \epsilon)\eta_o}, \quad \frac{c\lambda\tau_w^*}{\eta_o}, \quad \text{and } \alpha.$$

The frictional characteristics of non-Newtonian fluids flowing through packed beds depends upon the irregular geometry of the flow channel since it is this irregularity which causes the inertial terms to be important at Reynolds numbers greater than one. For high flow rates, the friction factor  $f$ , dimensionless quantities which is also called as a drag coefficient, is approximately constant at high Reynolds numbers. For the flow of a fluid through a bed of spheres, the pressure drop,  $\Delta p$ , is given as follows:

$$\Delta p = F/A \quad (\text{A.4-26})$$

where  $F$  is the force exerted on the solid surfaces and  $A$  is the cross-sectional area. For the fluid flowing through a cylindrical tube the force  $F$  on the solid surfaces exerted by the fluid is equal to:

$$F = A' K f \quad (\text{A.4-27})$$

where  $A'$  is the surface area of column or wetted surface,  $K$  is kinetic energy per unit volume, and  $f$  is friction factor. Therefore,

$$F = (2\pi RL) \left(\frac{1}{2} \rho \langle V \rangle^2\right) f \quad (\text{A.4-28})$$

Introducing hydraulic radius  $R_h$  such that:

$$R_h = \frac{R}{2} = \frac{\epsilon}{S} = \frac{\epsilon}{S_o(1 - \epsilon)} = \frac{D_p \epsilon}{6M(1 - \epsilon)} \quad (\text{A.4-29})$$

and rearranging Equation A.4-28) yields:

$$\frac{\Delta p}{L} = \frac{3M(1 - \epsilon)G_o^2 f_o}{\rho D_p \epsilon^3} \quad (\text{A.4-30})$$

Experimental data indicate that  $6f_o = 3.50$  [12, 83].

Hence,

$$\frac{\Delta p}{L} = \frac{1.75(1 - \epsilon)MG_o^2}{\rho D_p \epsilon^3} \quad (\text{A.4-31})$$

Then the Ergun equation becomes:

$$\left( \frac{\rho \Delta p}{MG_o^2} \right) \left( \frac{D_p}{L} \right) \left( \frac{\epsilon^3}{1 - \epsilon} \right) = \frac{150}{N_{Re,eff}} + 1.75 \quad (\text{A.4-32})$$

At very low flow rates,  $150/N_{Re,eff}$  factor is dominant in the right-hand side of Equation A.4-32. At very high flow rates where the inertial terms are significant,  $150/N_{Re,eff}$  becomes very negligible comparing 1.75; therefore, friction factor remains constant at 1.75.

Estimation of Shear Rate in the Bed

From Equation 4.5-9

$$\frac{Q}{\pi R^3} = \frac{8Q}{\pi D^3} = \frac{1}{\tau_w} \int_0^{\tau_w} \tau_{rz}^2 f(\tau_{rz}) d\tau_{rz} \quad (\text{A.4-8})$$

where

$$f(\tau_{rz}) = - \frac{dv_z}{dr}$$

Equation A.4-8 is multiplied through by  $\tau_w^3$  and both sides are then differentiated with respect to  $\tau_w$ , using Leibnitz rule for differentiating integral, i.e.,

$$\frac{d}{dt} \int_{a(t)}^{b(t)} f(x,t) dx = \int_{a(t)}^{b(t)} \frac{\partial f}{\partial t} dx + \left( f(b,t) \frac{db}{dt} - f(a,t) \frac{da}{dt} \right) \quad (\text{A.4-33})$$

$$\frac{8Q}{\pi D^3} = \frac{1}{\tau_w^3} \int_0^{\tau_w} \tau_{rz}^2 f(\tau_{rz}) d\tau_{rz}$$

$$\tau_w \frac{d \left( \frac{8Q}{\pi D^3} \right)}{d \tau_w} + 3 \left( \frac{8Q}{\pi D^3} \right) = f(\tau_w) = \left( - \frac{dv_z}{dr} \right)_w \quad (\text{A.4-34})$$

If  $\tau_w$  is replaced by  $\frac{D\Delta p}{4L}$ , Equation A.4-34 becomes:

$$3 \left( \frac{8Q}{\pi D^3} \right) + \frac{D\Delta p}{4L} \frac{d(8Q/\pi D^3)}{d(D\Delta p/4L)} = f(\tau_w) = - \left( \frac{dv_z}{dr} \right)_w \quad (\text{A.4-35})$$

This is the Rabinowitsch-Mooney equation giving the rate of shear at the wall of a tube when the flow is steady, laminar, and there is no slip at the wall. Rearrangement of Equation A.4-35 gives:

$$\begin{aligned} \left( - \frac{dv_z}{dr} \right)_w &= \frac{3}{4} \left( \frac{8\langle v_z \rangle}{D} \right) + \left( \frac{8\langle v_z \rangle}{D} \right) \frac{d \left[ \frac{1}{4} (8\langle v_z \rangle / D) \right] / (8\langle v_z \rangle / D)}{d[D\Delta p / 4L] / (D\Delta p / 4L)} \\ &= \frac{8\langle v_z \rangle}{D} \left[ \frac{3}{4} + \frac{1}{4} \frac{d \ln(8\langle v_z \rangle / D)}{d \ln(D\Delta p / 4L)} \right] \\ \left( - \frac{dv_z}{dr} \right)_w &= \frac{8\langle v_z \rangle}{D} \left[ \frac{3}{4} + \frac{1}{4n'} \right] = \frac{3n' + 1}{4n'} \frac{8\langle v_z \rangle}{D} \end{aligned} \quad (\text{A.4-36})$$

where

$$n' = \frac{d \ln(D\Delta p / 4L)}{d \ln(8\langle v_z \rangle / D)} \quad (\text{A.4-37})$$

For Newtonian fluid

$$\begin{aligned} Q &= \frac{\pi R^4 \Delta p}{8\mu L} = \pi R^2 \langle v_z \rangle \\ d \ln \frac{D\Delta p}{4L} &= d \ln \left( \frac{8\langle v_z \rangle}{D} \right) + d \ln \overset{\circ}{\mu} \end{aligned}$$

Thus,

$$n' = \frac{d \ln(D\Delta p / 4L)}{d \ln(8\langle v_z \rangle / D)} = 1.0 \quad (\text{A.4-38})$$

$$\left( - \frac{dv_z}{dr} \right)_w = \frac{3 + 1}{4} \frac{8\langle v_z \rangle}{D} = \frac{8\langle v_z \rangle}{D} \quad (\text{A.4-39})$$

For power-law fluid

$$\langle v_z \rangle = \frac{n}{3n+1} D^{\frac{1}{n}+1} \left( \frac{\Delta p}{2KL} \right)^{\frac{1}{n}} \quad (\text{A.4-40})$$

$$\left( \frac{D\Delta p}{4L} \right)^{\frac{1}{n}} = C \frac{8\langle v_z \rangle}{D}$$

C: Constant

$$d \ln \left( \frac{D\Delta p}{4L} \right) + n d \ln C + n d \ln \frac{8\langle v_z \rangle}{D}$$

Thus,

$$n' = \frac{d \ln(D\Delta p/4L)}{d \ln(8\langle v_z \rangle/D)} = n \quad (\text{A.4-41})$$

$$\left( - \frac{dv_z}{dr} \right)_w = \frac{3n+1}{4n} \frac{8\langle v_z \rangle}{D} \quad (\text{A.4-42})$$

For Ellis model fluid

$$\langle v_z \rangle = \frac{R^2 \Delta p}{8\eta_o L} + \frac{\tau_w^{1-\alpha}}{\eta_o^\alpha} \frac{R}{\alpha+3} \left( \frac{R\Delta p}{2L} \right)^\alpha \quad (\text{A.4-43})$$

$$\frac{8\langle v_z \rangle}{D} = \frac{1}{\eta_o} \frac{D\Delta p}{4L} + C \left( \frac{D\Delta p}{4L} \right)^\alpha$$

$$d \ln \frac{8\langle v_z \rangle}{D} = d \ln \frac{1}{\eta_o} + d \ln \left( \frac{D\Delta p}{4L} \right) + d \ln C + \alpha d \ln \left( \frac{D\Delta p}{4L} \right)$$

Thus,

$$n' = \frac{d \ln(D\Delta p/4L)}{d \ln(8\langle v_z \rangle/D)} = \frac{1}{\alpha+1} \quad (\text{A.4-44})$$

$$\left( - \frac{dv_z}{dr} \right)_w = \frac{\alpha+4}{4} \frac{8\langle v_z \rangle}{D} \quad (\text{A.4-45})$$

For Sprigg's model fluid

For low shear rate it will be the same as Newtonian  
and for high shear rate

$$\langle v_z \rangle = \frac{R}{\alpha+3} \left( \frac{R\Delta p}{2AL} \right)^\alpha \quad (\text{A.4-46})$$

$$\alpha d \ln \left( \frac{D\Delta p}{4L} \right) = d \ln \left( \frac{8\langle v_z \rangle}{D} \right)$$

Thus,

$$n' = \frac{d \ln \left( \frac{D\Delta p}{4L} \right)}{d \ln \left( \frac{8\langle v_z \rangle}{D} \right)} = \frac{1}{\alpha} \quad (\text{A.4-47})$$

$$\left( - \frac{dv_z}{dr} \right)_w = \frac{\alpha+3}{4} \frac{8\langle v_z \rangle}{D} \quad (\text{A.4-48})$$

For an estimate of the shear rate in the bed,  $\langle v_z \rangle$  can be replaced by  $G_o/\rho\epsilon$ , and  $D$  by four times the hydraulic radius radius.

$$D = 4R_h = \frac{2\epsilon D_p}{3M(1-\epsilon)}$$

Then

Newtonian:

$$\left( - \frac{dv_z}{dr} \right)_w = \frac{12 M (1 - \epsilon) G_o}{\rho D_p \epsilon^2} \quad (\text{A.4-49})$$

Power-law:

$$\begin{aligned} \left( - \frac{dv_z}{dr} \right)_w &= \frac{3n+1}{4n} \frac{8 \langle V_z \rangle}{D} \\ &= \frac{3n+1}{4n} \frac{12 M (1 - \epsilon) G_o}{\rho D_p \epsilon^2} \end{aligned} \quad (\text{A.4-50})$$

Ellis:

$$\begin{aligned} \left( - \frac{dv_z}{dr} \right)_w &= \frac{\alpha+4}{4} \frac{8 \langle V_z \rangle}{D} \\ &= \frac{\alpha+4}{4} \frac{12 M (1 - \epsilon) G_o}{\rho D_p \epsilon^2} \end{aligned} \quad (\text{A.4-51})$$

Spriggs:

$$\begin{aligned} \left( - \frac{dv_z}{dr} \right)_w &= \frac{\alpha+3}{4} \frac{8 \langle V_z \rangle}{D} \\ &= \frac{\alpha+3}{4} \frac{12 M (1 - \epsilon) G_o}{\rho D_p \epsilon^2} \end{aligned} \quad (\text{A.4-52})$$

### §A.5 Limitations to the Darcy's Law

It has been indicated that Darcy's law is fundamental to the assumptions made. Two significant aspects of this law are the analogies to capillary flow and the assumption of fluid homogeneity. It is the failure of these very same aspects which leads to the more obvious deviations of Darcy's law. By analogy to flow through tubes, at high flow rates, deviations from Darcy's law are expected due to the onset of "turbulent" flow. By the same analogy, we would expect deviations to occur in systems where the pore diameters become comparable with, or less than, the molecular mean free paths of the flowing gas, i.e., the so-called "slip" flow region and the region of "molecular streaming" or Knudsen flow. Other anomalies (based on Darcy's law) are adsorption, capillary condensation, and molecular diffusion. These latter effects may be referred to as surface flow effects, i.e., the behavior of non-homogeneous flows. Finally, there are deviations due to chemical reactions and ionic effects as they are not included in Darcy's law. Scheidegger [75] has given an extensive discussion of general equations which account both for high flow rates and for molecular effects. Carman [77] has presented a thorough summary of surface flow effects.

Both theoretical and empirical equations have been proposed for describing flow at high flow rates.

Forchheimer [91] modified Darcy's law by the addition of a second term, i.e.,

$$\frac{\Delta p}{L} = aV_o + bV_o^2 \quad (\text{A.5-1})$$

where  $a$  and  $b$  are constants depending on the properties of both fluid and porous media. This was derived from a semi-theoretical analogy to turbulent flow in tubes. Many studies have attempted to show that the Forchheimer equation is the correct general flow equation. Most deviations have depended upon a consideration of kinetic energy losses at high flow rates. Rose and Rizk [89] suggested that viscous effects and turbulent effects are not additive as implied by Equation A.5-1. They proposed

$$\frac{\Delta p}{L} = aV_o + bV_o^{1.5} + cV_o^2 \quad (\text{A.5-2})$$

The additional term is an empirical correction for the non-additive nature of the phenomenon. Ergun [83] and Fahien and Schriver [84] indicated that the porosity function is different for each flow region.

The molecular effects of Knudsen flow, slip-flow, adsorption, and capillary condensation are phenomena which primarily occur for the flow of gases in microporous media. As the present study is concerned only with liquid flow, it will suffice to mention that the

necessity of adding a surface-flow term to the Darcy and Knudsen terms in flow through absorbent porous media seems definitely established. That is, introducing Klinkenberg's [92] "superficial" gas permeability

$$k_a = a + b/P_m \quad (\text{A.5-3})$$

where  $a$  and  $b$  are constants and  $P_m$  is the mean gas pressure, and assuming, as does Carman [77], that either adsorbate flow or capillary condensate flow are examples of diffusion along a concentration gradient, one obtains for the total flow:

$$\frac{V_o}{(\Delta p/L)} = D \rho_p (1-\epsilon) \frac{\Delta c}{\Delta p} + \frac{D' \epsilon^2}{(1-\epsilon) S_o \sqrt{MRT}} + \frac{D'' P \epsilon^3}{\mu S_o RT (1-\epsilon)^2} \quad (\text{A.6-4})$$

where the  $D$ 's are diffusion coefficients and  $c$  is the concentration. The two terms on the right-hand side of the equation are the surface flow and slip flow terms, respectively. For each of these effects, the apparent permeability is increased above that for purely viscous flows.

For liquids, the only comparable experiment is that of Debye and Cleveland [93]. They found that in porous Vycor glass the flow of normal paraffins deviated from Darcy's law. The permeability of the glass, rather than being constant, was a function of viscosity.

There is considerable petroleum engineering literature related to adsorption or retention by a porous media of polymeric materials, and to the resultant permeability reduction effects which follows. It is not the intention of this study to consider these investigations in detail. Instead, we will focus attention on some of the frequently cited examples, noting that considerable controversy exists as to how these phenomena relate to flow behavior of non-Newtonian fluids through porous media. Both Marshall and Metzner [5] and Dauben and Menzie [113] considered the role of progressive plugging and adsorption of polymer aggregates in the flow phenomena they observed. They concluded that these aberrations were absent from their experiments. By contrast, Sadowski [3] concluded that polymer adsorption and gel formation was aggravated during constant pressure experiments because, under these conditions, any tendency towards gel formation would lower the permeability and thus automatically lower the flow rate. He reasoned that gel formation would be aggravated because, at lower flow rate, there would be less tendency to remove polymer molecules from the particle surface. Burcik [114] is of the opinion that the shear-thickening behavior observed in flow of dilute polymeric solutions through porous media is related to polymer molecules retained within the pore structure. He suggests that these bound

molecules are uncoiled under the imposed (high) velocity gradient, thereby increasing the resistance to flow. Presumably polymer retention may occur either by adsorption or mechanical entrapment.

At this time, at least qualitatively, the adsorption of polymers from solution by solids is well understood. Polymer molecules are adsorbed on the solid surface at multiple points of attachment, involving only a fraction of the chain segments of the molecules. The remainder of the molecules extended more or less freely into the solvent. A dynamic adsorption-desorption equilibrium may be attained, but in such cases individual segments of the molecule are involved. The extent of adsorption is such as to suggest that the amount of polymer adsorbed is at least one order greater than could be possible if all the chain segments of each molecule occupied the adsorption sites. As might be expected, the amount of polymer adsorbed by a solid surface in "static" experiments increases with (a) increasing molecular weight, (b) decreasing particle size, and (c) decreasing solvent power. Here the solvent power represents the ability of a solvent to dissolve polymer.

In a "dynamic" or flow system it is doubtful if a simple layer of adsorbed polymer affects the permeability of the bed to any extent. First, the amount of adsorbed polymer will be dependent upon the equilibrium

condition for adsorption. There will exist a tendency for the polymer molecule to be adsorbed by the solid surface and a tendency for the polymer molecule to be swept away by the motion of the fluid in the bulk stream. Second, the residence time of a polymer molecule in a packed bed will be extremely short, on the order of seconds. Even in the case of complete coverage of the available surface area in a packed bed by the adsorbed polymer, there would be no apparent effect on the bed permeability. The additional layer of polymer, 1000 to 5000 A in thickness, would have a negligible effect on the effective porosity of the bed and, therefore, the permeability of the bed.

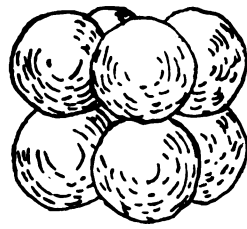
If there is to be an effective change in the bed permeability, another mechanism is responsible. An alternate mechanism may be visualized as follows. The geometry of the bed is extremely complex with much of its surface area in the vicinity of points of particle contact (4 to 12 points of contact per particle). As shown in Figure A.5-1, in such a geometry the magnitude of the distance between two solid surfaces, along any arbitrary line, varies from a maximum value equal to the largest particle diameter to zero on the assumption that there exists no bridging between the particles. In the region in which the distance between two adjacent surfaces converge rapidly to zero (point contacts), it is possible for the adsorption phenomenon to become important. Here, a polymer molecule exists in a velocity field which has

a value slightly greater than zero. Although the rate of shear may be high, the tendency for the polymer molecule to be swept away from the solid surface is markedly lowered. The tendency for adsorption will be favored. The adsorbed polymer molecules, extending into the bulk fluid, may serve as attachment sites for other molecules from the immediately adjacent particle surfaces and from the bulk fluid. In this way, a gel structure may be formed within various parts of the bed.

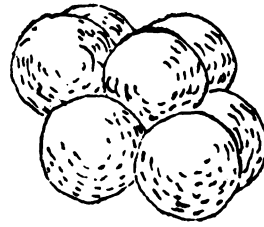
It is generally accepted that a gel owes its character to the fact that one or more of the components forms a coherent structure, or network, throughout the system. The points of coherence may be due to chemical bonds, physical attractive forces (Van der Waals bonds), or regions of crystallinity [111]. An important consequence of the network structure of a gel is that a small amount of the component which makes up the network immobilizes a large amount of the second component. An almost negligible amount of polymer; therefore, may induce significant gel formation which would affect the bed permeability by the plugging of minute pores or the filling of the pendular regions or both. A pendular ring between two spheres is shown in Figure A.5-2. The tendency for gel formation will be enhanced by an increase in the molecular weight of the polymer, by a decrease in the size of the particles, by a decrease in the bulk flow

rate of the fluid, and by an increase in the time during which the fluid flows through the bed.

It is obvious that the occurrence of gel formation invalidates the flow theory as developed in Section 3.1. To test the analysis of that section it is necessary to discover the circumstances under which gel formation will occur and degree of its importance. There are two basic flow experiments: (a) the flow rate of the fluid through the bed may be held constant, and (b) the applied pressure to the fluid in the bed may be held constant. In the absence of the "gelling" effect, each of these experiments is equivalent. In the presence of this effect, each experiment may give different results.

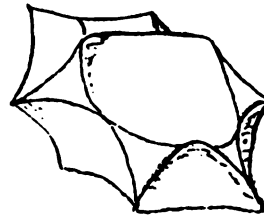
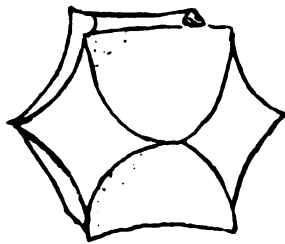
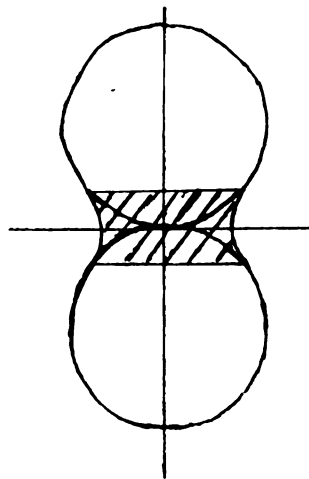


Cubic



Rhombohedral

Figure A.5-1 Packing of Uniform Spheres

Figure A.5-1 Pore Space in Packing of Uniform Spheres  
[After Graton and Fraser, 1935]Figure A.5-2 Pendular Ring Between Two Spheres  
[After Von Engelhardt, 1955]

APPENDIX B

VISCOMETRIC EXPERIMENT: DETAILED DESCRIPTION

WEISSENBERG RHEOGONIOMETER

## APPENDIX B

### VISCOMETRIC EXPERIMENT: DETAILED DESCRIPTION

#### WEISSENBERG RHEOGONIOMETER

##### §B.1 General Description

###### Drive Unit

On the left of the instrument is mounted the motor/gearbox drive unit, as shown in Figure B-1. This consists of an aluminum base standing on anti-vibration mountings and carrying either one or two motors and gearboxes. One motor and gearbox only is necessary if rotation and oscillation are required individually but it may be desirable to have two if frequent changes from rotation to oscillation are to be made, since with a single motor and gearbox the unit has to be mechanically uncoupled and moved each time a change is to be made. The drive between the motor and gearbox is through a flexible coupling and the drive from the gearbox to the rheogoniometer is by a shaft connected by specially chosen universal couplings. These precautions limit the effects of motor and gear vibrations on the instrument when it is being used on the most sensitive ranges.

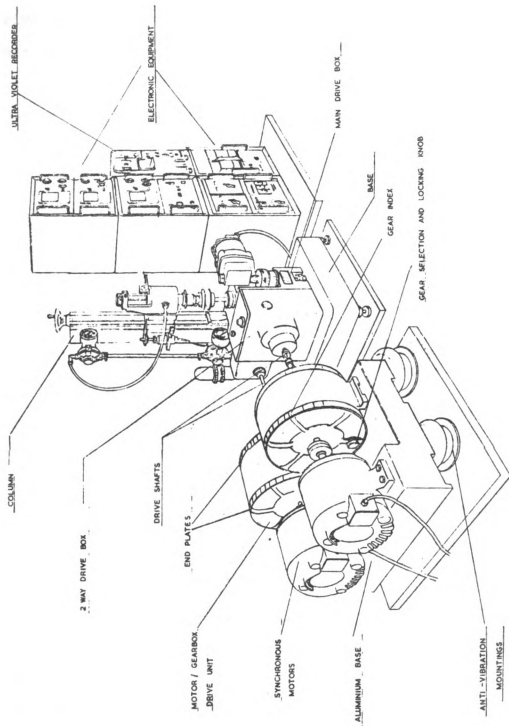


Figure B.1 Typical Arrangement of the Weissensberg Rheogoniometer

### Electric Motor

These are three-phase synchronous motors rated at 1 horse power. This type of motor is used so that the drive speed is rigidly constant through the duration of a test and also has very high consistency even over a longer period of time. The standard motor supplied with the instrument is 220 volt, 1800 r.p.m., 60 c.p.s. The motor is carefully made, the rotors being dynamically balanced to fine limits so as to reduce vibrations to a minimum. The motor is controlled from a three-phase switch mounted on the control panel. In the case of continuous rotation drive, this is a reversing switch which enables the motor to be run in each direction and an average reading taken so as to test the symmetry of the sample.

### Gearbox

Internally this gearbox unit is in two parts, the first five steps of approximately  $1:10^{-0.0}$  (1:1) to  $1:10^{-0.4}$  (1:2.5). The second part has twelve steps of  $1:10^{-0.5}$  from  $1:10^{-0.0}$  (1:1) to  $1:10^{-5.5}$  (1:316,200 reduction) and is driven by the output of the first part. The gear change mechanism associated with each part of the gearbox shows a number indicating the speed reduction to which that side of the gearbox is set as a power of ten. By simply adding these two indexes a figures is obtained which expresses the overall speed reduction

of the gearbox as a power of ten. Anti-friction needle roller bearings are used throughout the gearbox, thus eliminating the tendency towards stop-go motion which is often troublesome where journal bearings are employed at very low speeds.

Gear change may be made in the following way: on each end face of the gearbox there is a gear selection and locking knob, each controlling the associated part of the gearbox. It can be unlocked by rotating it counter-clockwise as far as possible. The knob will be seen to move outwards. The whole end plate of the gearbox can be moved around, so that the selected gear index shows at the top of the box. Selection of the precise position is assisted by using the locking knob in its intermediate position. This can be achieved by rotating the knob clockwise when the end plate is in any position. The knob is not now in its fully locked position but is held in a detent and the locking mechanism is sprung against the inner face of the gearbox. When the end plate is now moved to the precise position required, the locking mechanism will spring into place and the end plate will now be accurately in position and the gears correctly meshed. The locking knob should now be turned once more in a clockwise direction pressing it inwards which will move it to the fully locked position. The end plate is now completely locked and cannot move in use. It is

essential that gear changes are not made while the motor is running, and it is also essential that the locking knob is fully locked before the motor is run.

### Rheogoniometer

#### A. Base

The base of the instrument provides a plane surface and has webs cast in the underside for increased rigidity. There is an adjustable leg at each corner, which enables the base to be adjusted level. This is set by means of the pair of spirit levels mounted at the front. The base also contains the clamps for holding the two transducers associated with normal force measurement and servo operation.

#### B. Main Drive Box

This is mounted roughly at the center of the base and contains the main vertical shaft of the instrument on which the lower platen adaptor and lower platen is carried. This vertical shaft is held in two precision taper roller bearings which are specially selected. They are fitted in opposition and are carefully adjusted to give the smoothest possible operation. This shaft carries a bronze worm wheel, having 48 teeth, which is driven by a four-start steel worm mounted in front of it on a horizontal shaft. This gives a speed reduction of 12:1. The

right-hand bearing is held in a carrier which also serves to clamp a transducer mounted at the end of the shaft and is allowed to pivot a small amount.

#### C. Two-Way Drive Box

This is mounted on the left-hand side of the base, locking at the front of the instrument, and is bolted rigidly to the main drive box. It contains the step-up gear for the rotation drive as well as the brake/drive unit on the extreme left-hand side.

#### D. The Column

This is fitted at the back of the main drive box and is accurately set up so that the working faces are parallel with the axis of the vertical shaft in the main drive box. The column has a high rigidity to minimize any bending under heavy normal forces. It carries the torsion head, the gap setting transducer, and various ancillaries. At the base of the column at the rear there is a slot through which the normal force springs are fitted.

#### Rotation Drive

The drive from the gear box is taken into the electro-magnetic brake/drive unit at the left-hand side of the instrument. This consists of two discs of high permeability metal, each containing a coil winding and

friction pad, mounted on either side of a clutch disc of the same metal. This clutch disc is fixed onto the horizontal drive shaft which carries the rotation drive to the step up spur gears in the two-way drive box. The left-hand or outer coil disc is mounted on a shaft running in sealed ball races and is continuously driven by the motor gearbox unit. The right-hand or inner coil disc is fixed rigidly to the main casting of the two-way drive box. By energizing one or more of the coil windings, the clutch disc is attracted magnetically and forced against the friction pad, so that the instrument is accelerated rapidly up to the chosen speed or rapidly stopped, depending whether "Drive" or "Brake" is chosen on the control switch mounted on the control panel.

### Torsion Head

The torsion head is a complete assembly which is mounted on the column of the Weissenberg Rheogoniometer and carries the top platen. It owes its extreme sensitivity to the air bearing, which is an integral part of the construction, and its very wide range to the variety of torsion bars and platens which can be used.

Air is supplied from the laboratory air supply at about 80 p.s.i. or may be fed from a separate air compressor. The air passes through a filter unit mounted at the back of the instrument at the base of the column. It then passes through one regulator at the base of the

column and another at the top. Two regulators are provided so as to reduce fluctuations of pressure at the bearing to a minimum, which might otherwise cause small variations in the readings of tangential stress when working on the most sensitive ranges. The top regulator is used to select the working pressure (between 20 and 50 p.s.i.) and the bottom one should be preset to a value in excess of the maximum working value (55-65 p.s.i.) to prevent possible interaction between two regulators.

The torsion bar against which the tangential stress is measured has a length of 2.36 in. The top of the torsion bar is held rigidly in a clamp at the top of the air bearing casting and the bottom is clamped on the top of the air bearing rotor. The clamp at the lower end of the torsion bar carries the 10 cm. radius arm, at the other end of which is fitted the armature of the torsion head transducer. The displacement of this transducer noted on the appropriate transducer meter gives, with the calibration constant of the particular torsion bar, a direct reading of torque produced on the top platen, and hence the tangential stress in the specimen. All the calibration constants of the particular torsion bar are tabulated in Table B-1.

TABLE B-1. Torsion Bar Calibration

Torsion Bar	Platen Size (Diameter)			
	2.5 cm	5.0 cm	7.5 cm	10 cm
1/32"	$k_T = 53.8$	$k_T = 6.72$	$k_T = 1.99$	$k_T = 0.84$
1/16"	$k_T = 525$	$k_T = 65.6$	$k_T = 19.54$	$k_T = 8.21$
1/8"	$k_T = 8,800$	$k_T = 1,100$	$k_T = 328$	$k_T = 138$
1/4"	$k_T = 142,500$	$k_T = 17,840$	$k_T = 5,400$	$k_T = 2,230$
3/8"	$k_T = 561,000$	$k_T = 70,240$	$k_T = 20,800$	$k_T = 8,780$

$$\tau_{12} = k_T \Delta_T \quad , \quad \eta = \tau_{12} / \dot{\gamma}$$

### Normal Force Measurement

When normal force measurements are not being made, the platen is mounted directly on the vertical worm wheel shaft by means of the lower platen adaptor. If normal force measurements are to be made, the lower platen adaptor at the top of this vertical shaft is removed and replaced by a special normal force platen assembly which is free to move in a vertical direction, but is located rigidly and driven in rotation through a diaphragm. The general arrangement of normal force measurement and schematic layout of normal force measurement system are shown in Figures B-2 and B-3, respectively. The drive is taken from the top of the vertical shaft by an outer sleeve, which carries at its top a beryllium copper

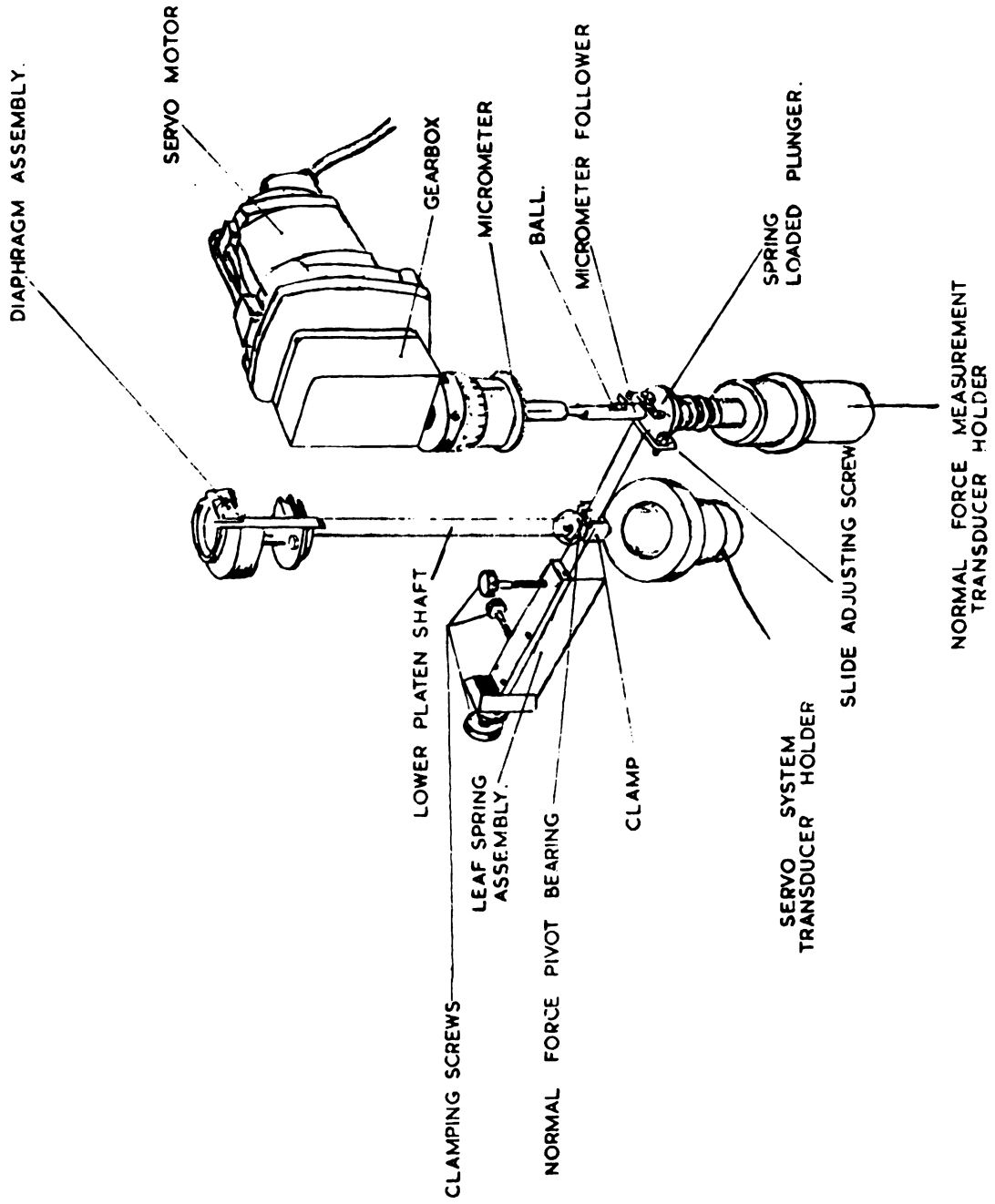


Figure B.2 Arrangement of Normal Force Measurement

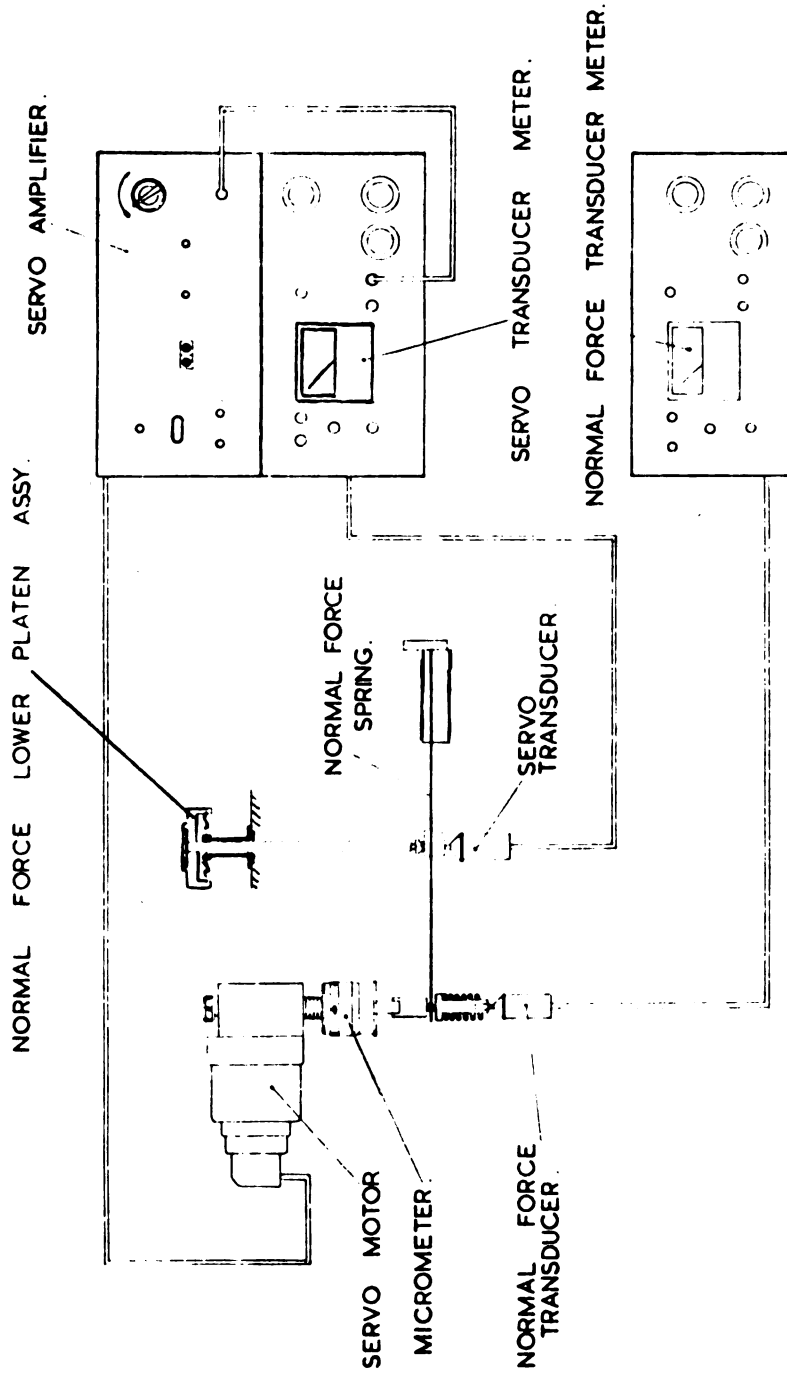


Figure B.3 Schematic Diagram of Normal Force Measurement System

diaphragm and also a locking ring. The diaphragm is free to move in the vertical direction, but it is restrained by the lower platen shaft, without touching, to the normal force pivot bearing. The normal force spring itself is a leaf spring one-half inch in width and of different thickness, depending on the spring rate required.

The cantilever leaf spring has, in its "free" end, a steel ball which provides a low friction pick-up point for the spring plunger and micrometer which position this "free" end. During measurements of normal force it is important to keep the gap between the two platens constant. As the force increases the normal force spring will bend and the lower platen will thus move downwards. This can be detected by the transducer which bears on the under side of the normal force pivot bearing and its deflection seen on the appropriate transducer meter.

Steady state normal forces can be measured by adjusting the micrometer by hand to give zero deflection of the transducer mounted beneath the normal force pivot bearing. The normal force springs have constant spring rates over the full range of deflection used in the instrument. The product of the reading of the micrometer, and the spring rate of the particular normal force spring gives a direct reading of normal force. Normal force spring calibrations are listed in Table B-2.

TABLE B-2. Normal Force Spring Calibration

Normal Forces Spring	Platen Size (Diameter)			
	2.5 cm	5.0 cm	7.5 cm	10 cm
1/8"	$k_N = 56,600$	$k_N = 14,150$	$k_N = 6,300$	$k_N = 3,540$
1/16"	$k_N = 8,330$	$k_N = 2,082$	$k_N = 930$	$k_N = 520$

$$\tau_{11} - \tau_{22} = k_N \Delta_N, \quad \theta = \frac{\tau_{11} - \tau_{22}}{\dot{\gamma}}$$

## §B.2 Experimental Procedure

### Gap Setting

It is important for cone and plate to be precisely positioned, so that there is an accurate known gap. The conical platen is truncated so that the cone and plate are divided at the center by the amount of this truncation. Gap settings according to the platen size and cone angle are listed in Table B-3. The gap can be set as follows:

1. Set the transducer selector switch to "gap setting."
2. Loosen the clamping screw on the right-hand side of the carriage and wind the torsion head down until the platens are seen to be almost touching.
3. Continue lowering the torsion head very slowly watching the servo transducer meter. As soon as

TABLE B-3 Gap Setting

Platens Nominal Diameter (cm.)	Cone Angle (°)	Gap Setting (in.)	Part Number
2.5	4.00	.00713	
2.5	Flat	--	
2.5	Flat	--	
5.0	3.9128	.00685	1153
5.0	Flat	--	947
5.0	Flat	--	955
7.5	1.5333	.00259	554
7.5	0.5502	.00100	993
7.5	Flat	--	427
7.5	Flat	--	584
7.5	Flat	--	1964
10.0	2.0083	.00350	1139
10.0	Flat	--	1167
10.0	Flat	--	

the platens touch this transducer meter will show a small deflection.

4. Adjust the gap setting transducer using the "set zero" on the transducer meter panel for the final operation, so as to give a deflection in a positive direction on the transducer meter equal to the gap required.
5. Raise torsion head slowly until transducer meter reads "zero." The platens are now correctly set and can be reset to this zero position at any time after loading the sample, etc.

#### Loading the Sample

1. Wind the torsion head up until there is about 3 inches gap between the platens.
2. Apply the sample in sufficient amount just to over-fill the gap.
3. Wind the torsion head down slowly until the gap setting transducer meter is at "zero." A short period should be allowed before commencing the test, so that any stress in the sample can subside. The clamping screw on the carriage should be fully tightened--checking that gap setting does not alter when this is done.

4. The surplus material should be removed from around the platens. If the sample is not correctly trimmed it can, especially in the case of more viscous samples, give errors both in tangential and normal force measurements.

#### Steady State Experiment

1. Carry out gap setting procedure.
2. Carry out loading the sample procedure.
3. Set the gearbox from low speed.
4. Lock the gearbox firmly.
5. Turn the rotation motor switch in the main control panel to "FORWARD."
6. Turn the off/brake/drive switch in the main control panel to "DRIVE."
7. Measure  $\Delta_T$  and  $\Delta_N$  for the given gearbox set.
8. Re-set the gearbox and repeat (3) through (7).

Rotation shear rates for various platens are tabulated in Table B-4 and the correction terms for primary normal stress difference are shown in Figure B-4.

TABLE B-4 Rotation Shear Rates for Various Platens

Gearbox Speed	RPM	2.5 cms.		5.0 cms.		7.5 cms.		10.0 cms.	
		4.00° cone	3.9128° cone	0.5502° cone	1.5333° cone	2.0083° cone	7.5 cms.	10.0 cms.	
0.0	0.900	1.350	1.380	9.81	3.522	2.689			
0.1	0.716	1.074	1.099	7.805	2.802	2.139			
0.2	0.568	0.852	0.871	6.193	2.223	1.697			
0.3	0.452	0.678	0.694	4.930	1.769	1.350			
0.4	0.360	0.540	0.552	3.922	1.409	1.076			
0.5	0.284	0.426	0.435	3.098	1.112	0.851			
0.6	0.226	0.339	0.3465	2.462	0.8845	0.675			
0.7	0.1798	0.2697	0.2756	1.960	0.7037	0.5372			
0.8	0.1430	0.2145	0.2194	1.560	0.5597	0.4272			
0.9	0.1136	0.1704	0.1740	1.238	0.4446	0.3394			
0.0	1000								
1.0	100								
2.0	10								
3.0	1.0								
4.0	0.1								
5.0	0.01								
For Instance:		Gearbox Speed	Shear Rate (sec <sup>-1</sup> )						
		0.8	427.2						
		1.8	42.72						
		2.8	4.272						
		3.8	0.4272						
		4.8	0.04272						
		5.8	0.004272						

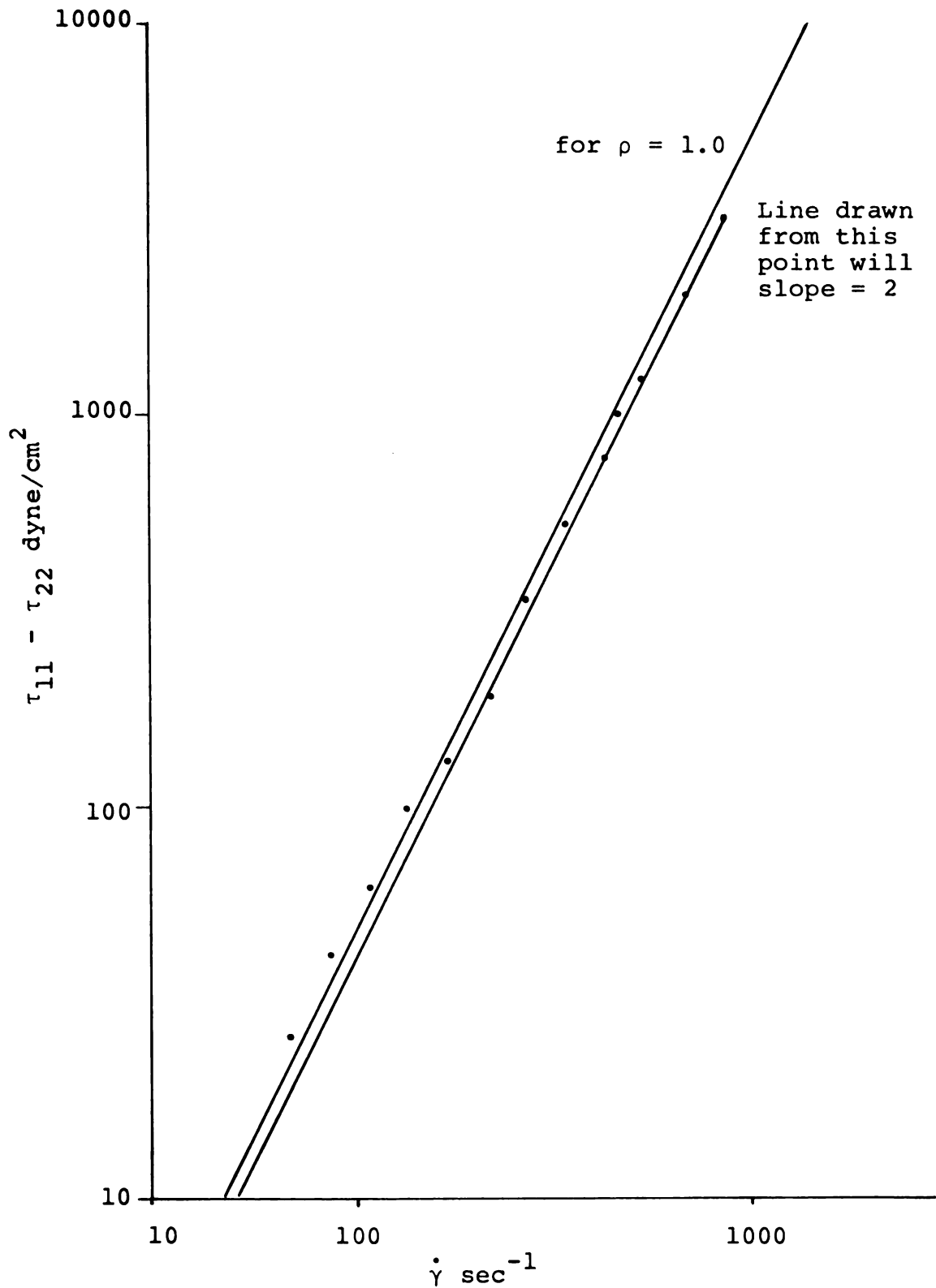


Figure B.4 Correction Terms for Normal Stress Difference

APPENDIX C

FLOW EXPERIMENT: DETAILED DESCRIPTION

## APPENDIX C

### FLOW EXPERIMENT: DETAILED DESCRIPTION

#### §C.1 General Description

The apparatus used for this experiment consisted of a one-half-inch glass column, a one-inch glass column, a pressurized flow system, packing particles (glass beads) for the column, differential pressure transducer (Model KP 15, Pace Engineering Company, North Hollywood, California), a recorder (Linear/Log Varicord 43, Photovolt Company, Broadway, New York), a cathetometer accurate to 0.005 cm. (Gaertner Scientific Company, Chicago, Illinois), and three rotometers (Brooks Instrument Division, Emerson Electric Company, Hatfield, Pennsylvania). The schematic diagram of the jacketed flow system which maintained constant temperature  $21 \pm 0.5^{\circ}\text{C}$  was shown in Figure 4.5-1 previously.

#### Glass Beads

The bed was packed with glass beads which were spherical and uniform in size. Glass beads were sized by "U.S. Standard" sieves. This was done by hand to

minimize damage to the particles. The glass beads used in the experiments were sieve size Nos. 12, 30, and 40. For those particles under 1 mm. in diameter, the particle diameter was measured by means of a microscope, the eyepiece of which had a movable hairline. The movement of the hairline was controlled by a micrometer spindle which was calibrated against an accurately measured 1 mm. line which was etched onto a slide. A random sample, 10 to 15 particles, was placed on a slide having raised sides and one diameter was taken which appeared in the field of the microscope as the hairline was moved from left to right. One hundred diameters were measured in this way. The average diameter of each size of the particles was the arithmetic average of the individual diameters. For particles larger than 1 mm. in diameter, a machinist's micrometer was used to measure directly the diameters. Again, one hundred particles, randomly selected, were measured.

#### Glass Column

There were two glass columns A and B, with 1-inch and 1/2-inch internal diameters, respectively. The jacket around the test section was made of an epoxy glass tube. Epoxy glass was selected for the test section in order to allow the experimenter to observe the flow of fluids within the packed beds. This was particularly useful for checking that air bubbles were not trapped within the

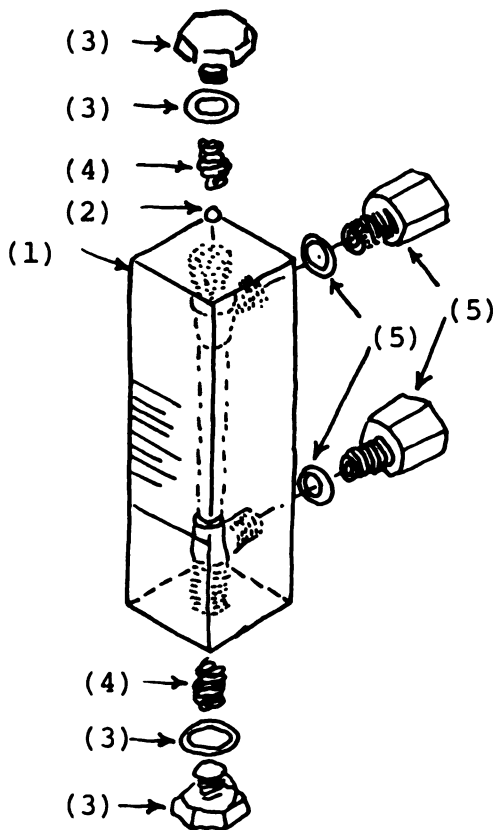
bed. Each glass column was made in several segments. An assembled glass column was made to fit between two aluminum flanges and the entire assembly was bolted together. The pressure tap connections to the top section and to the bottom section were 1/4-inch stainless steel tube which is connected into the pressure transducer. The bed particles were supported by 60-mesh stainless steel screens at both ends of the test section. At the exit end of each glass column was placed a 1/2-inch tee. There was then 1-1/2 inches to 2 inches of packed bed before and after the pressure taps. This arrangement served to eliminate entrance and exit effects for the pressure drop readings.

#### Rotometer

The Brooks-Mite is a small variable area type flow meter. The tapered metering tube is machined directly into a clear acrylic plastic block, and a standard direct reading scale engraved on the meter body. A metering float moves vertically in the tapered tube to indicate rate of flow. Figure C-1 illustrates the assembled rotometer.

#### Pressure Transducer

The transducer circuit is valved to permit either of two variable reluctance differential pressure transducers to be connected to the two taps of the test section or to the calibration system. The transducer signal is



- (1) Meter Body
- (2) Float
- (3) Two End Plugs and O-Rings
- (4) Two Spring Float Stops
- (5) Two Adapters and O-Rings

Figure C-1 Brooks-Mite Rotometer

amplified (Model CD 25, Pace) and recorded. The calibration system consisted of two reservoirs containing distilled water connected to the valving assembly by copper tubing to avoid expansion during calibration, the end of which is connected under the water level. While the down stream reservoir is always open to the atmosphere, the air space over the upstream reservoir can be pressurized by a nitrogen tank. The air space is also connected to one leg of a mercury manometer so that the pressure can be determined. The level of the manometer legs is read with a cathetometer accurate to 0.005 cm. The transducer circuit is also valved to allow any portion to be flushed with distilled water.

#### Measurement of Void Fraction

The void factor was determined by the following procedure. First, the graduated cylinder was filled with water. The height of the water level measured with the cathetometer was X cms. Then, dry glass beads were poured into the cylinder. The cylinder was vibrated until the beads settled down uniformly. The water level in the cylinder rose because the beads were added. The height of the beads in the cylinder was Z cms., whereas the new height of the water level was Y cms. These heights are proportional to the corresponding volumes.

Apparent volume of bed = Z cms.

Volume of beads = (Y-X) cms.

Void fraction =  $(1 - (Y-X)/Z)$

As X, Y, and Z were known,  $\epsilon$  was calculated accordingly.

## §C.2 Experimental Procedure

Packing procedure was important as there was a possibility of air entrapment in the bed during packing. It was absolutely required that there be no air trapped in the column when the experiments were performed. The glass beads were soaked for a day or more in a beaker filled with distilled water.

The test section was first assembled and bolted together. With the glass column filled with the fluid to be tested in a vertical position, particles were dropped into the glass column so as to fill the column to a height of about 2 inches. The partially filled bed was then tamped with a plunger. This was repeated for each 2 inches of bed height until the bed was complete. The bed was just barely overfilled to the level at which the screen support was to be fixed. When the screen was tightened down in place, the compressive force of the screen on the particles served to fix the bed in place. In this way subsequent handling of the column did not disturb the bed structure. About 6 inches of glass tube was connected at both ends of the column so as to avoid end effects.

The column was then inserted into the flow loop. All air bubbles were flushed from the lines and from the bed completely. Upon the completion of the flushing procedure, the test fluid was allowed to flow through the test section at rates greater than would be expected in the experimental run. Any entrapped air bubbles were usually removed by this step. When a visual examination of the bed did not reveal any air bubbles in the system, a run was made.

All electrical circuits were switched on for about 5 minutes before a run was made. Then, the test fluid was forced to flow through the packed column. The constant liquid level above the bed was achieved by applying the gas pressure to the top of the fluid level in the bed. Constant flow rate, constant fluid level at the top of the bed, and the constant reading of the pressure drop were indications of steady flow. The valve on gas tank B was adjusted until the above three observations remained constant. Sometimes, the valve on the connection at the bottom of the bed was also adjusted. The entire system was held at equilibrium for at least five minutes before taking a measurement. The flow rate was measured by a rotometer connected at the bottom of the bed. Pressure drop for the flow rate was transferred into the differential pressure transducer, of which the signal was amplified and recorded. The same procedure was applied for the different flow rates.

For any given flow rate the temperature of the reservoir fluid was adjusted such that the temperature of the fluid leaving the test section was 21°C. The maximum difference in these temperatures was not more than 1°C.

After the experimental run was completed, the test section was removed from the flow loop, dismantled, and washed thoroughly with distilled water. The glass beads were cleaned in a beaker with several rinsings of distilled water. Next, the glass beads were soaked in distilled water and allowed to stand overnight. The next day they were rinsed again and dried with room air in a ventilation hood. A clean particle was distinguished by the lack of white polymer dried onto the surface of the particles. Then, they were soaked again for the following experiment. Finally, the pressure transducer system was flushed with distilled water to remove polymer solutions from the line.

APPENDIX D

SUMMARY OF VISCOMETRIC DATA  
STEADY STATE SHEAR STRESS MEASUREMENT

With

10 cm. platen  
2.0083° cone  
1/16" torsion bar  
 $K_T = 8.21$

TABLE D-1. Results for the Weissenberg Rheogoniometer for  
0.50% Polyacrylamide solution at 21°C

G.B.	$\dot{\gamma}$ ( $\text{sec}^{-1}$ )	$\Delta T$	$\tau_{12}$ ( $\text{dyne/cm.}^2$ )	$\eta$ ( $\text{gr./cm. sec}$ )
5.6	0.00675	0.036	0.2948	43.6745
5.4	0.01076	0.058	0.4748	44.1248
5.2	0.01697	0.090	0.7389	43.5415
5.0	0.02689	0.140	1.1494	42.7445
4.8	0.04272	0.205	1.6831	39.3972
4.6	0.0675	0.295	2.4220	35.8807
4.4	0.1076	0.415	3.4072	31.6650
4.2	0.1697	0.565	4.6387	27.3344
4.0	0.2689	0.765	6.2807	23.3563
3.8	0.4272	1.030	8.4563	19.7947
3.6	0.6750	1.32	10.8372	16.0551
3.4	1.076	1.63	13.3823	12.4371
3.2	1.697	2.05	16.8305	9.9178
3.0	2.689	2.60	21.346	7.9383
2.8	4.272	3.20	26.272	6.1498
2.6	6.750	3.85	31.6085	4.6827
2.4	10.76	4.68	38.4228	3.5709
2.2	16.97	5.60	45.976	2.7093
2.0	26.89	6.78	55.6638	2.0701
1.8	42.72	8.18	67.1578	1.5720
1.6	67.50	9.80	80.4580	1.1920
1.4	107.6	12.0	98.5200	0.9156
1.2	169.7	14.4	118.2240	0.6967
1.0	268.9	17.8	146.1380	0.5435
0.9	339.4	19.5	160.095	0.4717
0.8	427.2	21.7	178.157	0.4170
0.7	537.2	24.1	197.861	0.3683
0.6	675.0	26.5	217.565	0.3223
0.5	851.0	30.0	246.300	0.2894

TABLE D-2. Results for the Weissenberg Rheogoniometer for  
0.25% Polyacrylamide solution at 21°C

G.B.	$\dot{\gamma}$ (sec <sup>-1</sup> )	$\Delta_T$	$\tau_{12}$ (dyne/cm. <sup>2</sup> )	$\eta$ (gr./cm. sec)
5.0	0.02689	0.062	0.50902	18.9297
4.8	0.04272	0.097	0.7964	18.6427
4.6	0.06750	0.147	1.2106	17.9356
4.4	0.1076	0.214	1.7577	16.3354
4.2	0.1697	0.300	2.4769	14.5956
4.0	0.2689	0.425	3.4879	12.9712
3.8	0.4272	0.545	4.4751	10.4755
3.6	0.6750	0.712	5.8480	8.6638
3.4	1.076	0.910	7.4598	6.9329
3.2	1.697	1.150	9.4120	5.5463
3.0	2.689	1.390	11.4131	4.2444
2.8	4.272	1.730	14.1992	3.3238
2.6	6.750	2.150	17.6161	2.6098
2.4	10.76	2.670	21.9579	2.0407
2.2	16.97	3.280	26.9195	1.5863
2.0	26.89	4.060	33.3032	1.2385
1.8	42.72	4.82	39.5928	0.9268
1.6	67.50	5.94	48.8025	0.7230
1.4	107.6	7.30	59.9547	0.5572
1.2	169.7	8.85	72.6316	0.4280
1.0	268.9	11.10	91.1571	0.3390
0.9	339.4	12.43	102.0236	0.3006
0.8	427.2	13.42	110.2176	0.2580
0.7	537.2	15.10	123.9857	0.2308
0.6	675.0	16.50	135.4650	0.2000
0.5	851.0	18.80	154.3480	0.1837

TABLE D-3. Results for the Weissenberg Rheogoniometer for  
0.10% Polyacrylamide solution at 21°C

G.B.	$\dot{\gamma}$ (sec <sup>-1</sup> )	$\Delta_T$	$\tau_{12}$ (dyne/cm. <sup>2</sup> )	$\eta$ (gr./cm. sec)
4.8	0.04272	0.032	0.2617	6.1248
4.6	0.0675	0.050	0.4122	6.1064
4.4	0.1076	0.079	0.6487	6.0286
4.2	0.1697	0.119	0.9783	5.7654
4.0	0.2689	0.167	1.3736	5.1084
3.8	0.4272	0.238	1.9557	4.5781
3.6	0.675	0.322	2.6451	3.9187
3.4	1.076	0.432	3.5480	3.2974
3.2	1.697	0.556	4.5657	2.6905
3.0	2.689	0.737	6.0505	2.2501
2.8	4.272	0.890	7.3187	1.7132
2.6	6.750	1.110	9.1266	1.3521
2.4	10.76	1.400	11.5670	1.0750
2.2	16.97	1.730	14.1750	0.8353
2.0	26.89	2.150	17.6586	0.6567
1.8	42.72	2.610	21.4539	0.5022
1.6	67.50	3.280	26.9190	0.3988
1.4	107.6	4.090	33.5712	0.3120
1.2	169.7	5.130	42.1195	0.2482
1.0	268.9	6.320	51.8977	0.1930
0.9	339.4	7.280	59.7344	0.1760
0.8	427.2	8.230	67.5830	0.1582
0.7	537.2	9.300	76.2824	0.1420
0.6	675.0	10.36	85.0500	0.1260
0.5	851.0	11.73	96.3332	0.1132

TABLE D-4. Results for the Weissenberg Rheogoniometer for  
0.05% Polyacrylamide solution at 21°C

G.B.	$\dot{\gamma}$ ( $\text{sec}^{-1}$ )	$\Delta_T$	$\tau_{12}$ ( $\text{dyne/cm.}^2$ )	$\eta$ ( $\text{gr./cm. sec}$ )
4.4	0.1076	0.034	0.2784	2.5872
4.2	0.1697	0.054	0.4434	2.6128
4.0	0.2689	0.085	0.7012	2.6078
3.8	0.4272	0.127	1.0433	2.4422
3.6	0.675	0.181	1.4868	2.2027
3.4	1.076	0.251	2.0605	1.9150
3.2	1.697	0.329	2.6987	1.5903
3.0	2.689	0.423	3.4688	1.2900
2.8	4.272	0.522	4.2848	1.0030
2.6	6.750	0.675	5.5377	0.8204
2.4	10.76	0.867	7.1145	0.6612
2.2	16.97	1.120	9.1688	0.5403
2.0	26.89	1.440	11.7966	0.4387
1.8	42.72	2.000	16.3916	0.3837
1.6	67.50	2.300	18.8865	0.2798
1.4	107.6	2.880	23.6827	0.2201
1.2	169.7	3.720	30.5120	0.1798
1.0	268.9	4.640	38.0762	0.1416
0.9	339.4	5.400	44.1220	0.1300
0.8	427.2	5.940	48.7862	0.1142
0.7	537.2	6.75	55.4390	0.1032
0.6	675.0	7.670	62.9775	0.09325
0.5	851.0	9.320	76.5049	0.08992

APPENDIX E

SUMMARY OF VISCOMETRIC DATA  
STEADY STATE NORMAL STRESS MEASUREMENT

With

10 cm. platen  
2.0083° cone  
1/16" normal force spring  
 $K_N = 520.0$

TABLE E-1. Results for the Weissenberg Rheogoniometer for  
0.50% Polyacrylamide Solution at 21°C

G.B.	$\dot{\gamma}^{-1}$ (sec <sup>-1</sup> )	$\Delta_N$	$-(\tau_{11}-\tau_{22})$ (dyne/cm <sup>2</sup> )		
			Measurement	Correction	Value
3.0	2.689	0.008	4.160	. .	4.160
2.8	4.272	0.020	10.40	. .	10.40
2.6	6.750	0.046	23.92	. .	23.92
2.4	10.76	0.110	57.21	. .	57.21
2.2	16.97	0.220	114.4	. .	114.4
2.0	26.89	0.390	202.8	. .	202.8
1.8	42.72	0.700	364.0	8.000	372.0
1.6	67.50	1.040	540.8	22.00	562.8
1.4	107.6	1.350	702.0	56.00	758.0
1.2	169.7	1.920	998.4	140.0	1138.4
1.0	268.9	2.420	1258.4	340.0	1598.4
0.9	339.4	2.520	1310.4	540.0	1850.4
0.8	427.2	2.650	1378.0	860.0	2238.0
0.7	537.2	2.440	1268.8	1330.	2598.8
0.6	675.0	1.840	956.80	2150.	3106.8
0.5	851.0	0.800	416.00	3300.	3716.0

TABLE E-2. Results for the Weissenberg Rheogoniometer.

G.B.	$\dot{\gamma}$ (sec <sup>-1</sup> )	$\Delta_N$	$-(\tau_{11}-\tau_{22})$ (dyne/cm <sup>2</sup> )		
			Measurement	Correction	Value
For 0.25 % Polyacrylamide Solution at 21°C					
2.4	10.76	0.019	9.880	. .	9.880
2.2	16.97	0.048	24.96	. .	24.96
2.0	26.89	0.105	54.60	. .	54.60
1.8	42.72	0.191	99.20	8.000	107.2
1.6	67.50	0.340	176.8	22.00	198.8
1.4	107.6	0.585	304.2	56.00	360.2
1.2	169.7	0.790	410.8	140.0	550.8
1.0	268.9	0.925	481.0	340.0	821.0
0.9	339.4	0.805	418.6	540.0	958.6
0.8	427.2	0.750	390.0	860.0	1250.0
0.7	537.2	0.387	201.2	1330.	1531.2
0.6	675.0	-0.750	-390.0	2150.	1760.0
0.5	851.0	-1.800	-936.0	3300.	2364.0
For 0.10 % Polyacrylamide Solution at 21°C					
2.0	26.80	0.020	10.40	. .	10.40
1.8	42.72	0.038	19.60	8.000	27.60
1.6	67.50	0.083	43.20	22.00	65.20
1.4	107.6	0.162	84.40	56.00	140.4
1.2	169.7	0.215	118.8	140.0	251.8
1.0	268.9	0.272	141.2	340.0	481.2
0.9	339.4	0.154	80.20	540.0	620.2
0.8	427.2	-0.070	-36.40	860.0	823.6
0.7	537.2	-0.660	-343.2	1330.	986.8
0.6	675.0	-1.600	-832.0	2150.	1318.
0.5	851.0	-3.250	-1690.	3300.	1610.
For 0.05 % Polyacrylamide Solution at 21°C					
1.8	42.72	. .	. .	8.000	8.000
1.6	67.50	-0.005	-2.600	22.00	19.40
1.4	107.6	-0.006	-3.120	56.00	52.90
1.2	169.7	-0.007	-3.640	140.0	136.4
1.0	268.9	-0.225	-117.0	340.0	223.0
0.9	339.4	-0.280	-145.6	540.0	394.4
0.8	427.2	-0.580	-301.6	860.0	558.4
0.7	537.2	-1.330	-691.6	1330.	638.4
0.6	675.0	-2.580	-1341.6	2150.	808.4
0.5	851.0	-4.500	-2340.0	3300.	960.0

APPENDIX F

SUMMARY OF VISCOMETRIC DATA

$H(\tau)$ , RELAXATION TIME SPECTRUM VS.  $t$ , TIME

TABLE F-1. Results of the Viscometric Experiments for 0.5% Separan Solution at 21°C

t (sec)	$\Delta_T$	$\tau_{12}(t)$ dyne/cm <sup>2</sup>	$d\tau_{12}(t)/d\ln t$	$H(\tau)^1$	m	N	$H^*(\tau)$
$\dot{\gamma}_0 = 0.04272 \text{ sec}^{-1}$							
.03	.180	1.4778	.0739	57.654	.55	.619	35.7455
.05	.175	1.4368	.0928	43.433	.59	.634	27.5365
.07	.172	1.4121	.0952	31.847	.61	.641	20.4139
.10	.168	1.3793	.1199	28.059	.65	.727	20.3988
.15	.160	1.3136	.1314	20.499	.68	.754	15.4562
.30	.148	1.2151	.1494	11.659	.70	.771	8.9890
.50	.140	1.1494	.1683	7.879	.72	.790	6.2244
1.0	.127	1.0427	.2069	4.843	.76	.826	4.0003
1.5	.112	.9195	.2611	4.074	.80	.859	3.4995
2.0	.100	.8210	.2997	3.507	.85	.901	3.1598
3.0	.086	.7061	.2956	2.306	.90	.935	2.1561
5.0	.064	.5254	.2759	1.291	.94	.963	1.2432
7.0	.055	.4516	.2742	.917	1.0	1.00	.9170
10.0	.040	.3284	.2726	.638	1.8	1.042	.6647
15.0	.0285	.2340	.2874	.448	1.17	1.078	.4829
20.0	.0180	.1478	.2627	.308	1.29	1.112	.3424
30.0	.0062	.0509	.1970	.154	1.62	1.116	.1718
50.0	0						
$\dot{\gamma}_0 = 0.2689 \text{ sec}^{-1}$							
.03	.76	6.2396	.3284	40.709	.40	.564	22.9598
.05	.74	6.0754	.4269	31.753	.46	.586	18.6072
.07	.72	5.9112	.5008	26.606	.49	.597	15.8837
.10	.70	5.7470	.6568	24.425	.51	.604	14.7527
.15	.660	5.4186	.8210	20.355	.62	.645	13.1289
.30	.572	4.6961	1.1822	14.655	.70	.771	11.2990
.50	.500	4.1050	1.2216	9.086	.80	.859	7.8048
1.0	.405	3.3251	1.1987	4.458	.95	.969	4.3198
1.5	.342	2.8078	1.1822	2.931	1.00	1.00	2.9310
2.0	.300	2.4630	1.1757	2.186	1.05	1.026	2.2428
3.0	.240	1.9704	1.1248	1.394	1.18	1.082	1.5083
5.0	.173	1.4203	.8210	.611	1.22	1.094	.6684
7.0	.131	1.0765	.8144	.433	1.30	1.114	.4823
10.0	.101	.8292	.7553	.281	1.40	1.127	.3166
15.0	.0692	.5681	.6584	.163	1.50	1.128	.1838
20.0	.0445	.3653	.5419	.101	1.60	1.119	.1130
30.0	.0225	.1847	.3941	.0489	1.68	1.104	.0539
50.0	.0040	.0328	.3153	.0235	1.80	1.074	.0252

Notes:  $H(\tau)$  is experimentally determined relaxation time spectrum.  
 $H^*(\tau)$  is corrected relaxation time spectrum.

TABLE F-2. Results of the Viscometric Experiments for 0.25% Separan Solution at 21°C

t (sec)	$\Delta_T$	$\tau_{12}(t)$ dyne/cm <sup>2</sup>	$d\tau_{12}(t)/d\ln t$	$H(\tau)^1$	m	N	$H^*(\tau)$
$\dot{\gamma}_0 = 0.2689 \text{ sec}^{-1}$							
.03	.313	2.5697	.1642	20.355	.21	.494	10.0553
.05	.305	2.5041	.1888	14.045	.35	.545	7.6545
.07	.293	2.4055	.2135	11.340	.48	.593	6.7246
.10	.286	2.3481	.2742	10.198	.57	.626	6.3839
.15	.270	2.2167	.3612	8.956	.65	.727	6.5110
.30	.230	1.8883	.5254	6.513	.80	.859	5.5946
.50	.194	1.5927	.5419	4.030	.95	.969	3.9050
1.0	.151	1.2397	.5254	1.954	1.02	1.01	1.9735
1.5	.123	1.0098	.5090	1.262	1.15	1.071	1.3516
2.0	.109	.8949	.4762	.885	1.18	1.082	.9575
3.0	.084	.6896	.4105	.509	1.24	1.100	.5599
5.0	.0585	.4803	.3645	.271	1.45	1.128	.3056
7.0	.0455	.3736	.3415	.181	1.50	1.128	.2041
10.0	.0312	.2562	.2874	.107	1.56	1.124	.1202
15.0	.020	.1642	.1855	.046	1.60	1.119	.0514
20.0	.016	.1314	.1543	.0287	1.80	1.074	.0308
30.0	.009	.0739	.1149	.0142	2.50	.753	.0106
$\dot{\gamma}_0 = 0.1697 \text{ sec}^{-1}$							
.03	.207	1.6995	.0903	17.739	.16	.476	8.4437
.05	.201	1.6502	.1289	15.191	.30	.527	8.0056
.07	.197	1.6174	.1560	13.132	.37	.553	7.2619
.10	.189	1.5517	.2036	11.998	.50	.600	7.1988
.15	.177	1.4532	.2808	11.031	.60	.672	7.4128
.30	.150	1.2315	.2734	5.370	.75	.816	4.3819
.50	.139	1.1412	.2504	2.951	.88	.922	2.7208
1.0	.110	.9031	.2750	1.621	1.0	1.00	1.6210
1.5	.095	.7800	.3268	1.284	1.11	1.053	1.3520
2.0	.080	.6568	.3777	1.113	1.15	1.071	1.1920
3.0	.065	.5337	.3284	.645	1.17	1.078	.6953
5.0	.044	.3612	.2915	.345	1.18	1.082	.3732
7.0	.0296	.2430	.2586	.218	1.18	1.082	.2358
10.0	.0208	.1708	.2463	.145	1.22	1.094	.1586
15.0	.0072	.0591	.2463	.0968	1.24	1.100	.1200
20.0	0						

TABLE F-3. Results of the Viscometric Experiments for 0.10% Separan Solution at 21°C

t (sec)	$\Delta_T$	$\tau_{12}(t)$ dyne/cm <sup>2</sup>	$d\tau_{12}(t)/d\ln t$	$H(\tau)^1$	m	N	$H^*(\tau)$
$\dot{\gamma}_0 = 1.076 \text{ sec}^{-1}$							
.03	.2275	1.8678	.2135	6.613	.41	.568	3.7561
.05	.216	1.17734	.2594	4.822	.50	.600	2.8932
.07	.206	1.6913	.3005	3.989	.60	.672	2.6806
.10	.191	1.5681	.3612	3.357	.70	.771	2.5882
.15	.1705	1.3998	.4220	2.615	.77	.834	2.1809
.30	.1328	1.0903	.4516	1.399	.96	.976	1.3654
.50	.107	.8785	.4433	.824	1.05	1.026	.8454
1.0	.0695	.5706	.3908	.363	1.26	1.104	.4007
1.5	.055	.4516	.3350	.208	1.33	1.119	.2327
2.0	.0394	.3235	.2791	.130	1.37	1.124	.1461
3.0	.0278	.2282	.2233	.069	1.44	1.128	.0778
5.0	.0158	.1297	.1855	.0345	1.50	1.128	.0389
7.0	.0098	.0805	.1642	.0218	1.53	1.126	.0245
10.0	0						
$\dot{\gamma}_0 = 2.689 \text{ sec}^{-1}$							
.03	.392	3.2183	.5008	49.799	.30	.527	26.2440
.05	.370	3.0377	.5419	40.302	.37	.553	22.2870
.07	.346	2.8407	.6272	33.323	.45	.582	19.3939
.10	.315	2.5862	.7832	29.127	.52	.608	17.7092
.15	.270	2.2167	1.0180	25.240	.67	.746	18.8290
.30	.172	1.4121	1.1166	13.841	.95	.969	13.4119
.50	.120	.9852	.5714	4.250	1.2	1.089	4.6282
1.0	.082	.6732	.4204	1.563	1.54	1.126	1.7599
1.5	.058	.4762	.3875	.961	1.70	1.100	1.0571
2.0	.048	.3941	.3875	.721	1.83	1.065	.7678
3.0	.026	.2135	.3514	.436	2.05	.978	.4264
5.0	.0067	.0550	.2085	.155	2.54	.732	.1134
7.0	.0025	.0205	.0657	.035	2.89	.552	.0193
10.0	0						

TABLE F-4. Results of the Viscometric Experiments for 0.05% Separan Solution at 21°C

t(sec)	$\Delta_T$	$\tau_{12}(t)$ dyne/cm <sup>2</sup>	$d\tau_{12}(t)/d\ln t$	$H(\tau)^1$	m	N	$H^*(\tau)$
$\dot{\gamma}_0 = 2.689 \text{ sec}^{-1}$							
.03	.140	1.1494	.2709	33.585	.63	.710	23.8453
.05	.126	1.0345	.2956	22.983	.72	.790	18.1565
.07	.115	.9442	.3243	17.229	.80	.859	14.7997
.10	.0975	.8005	.4064	15.113	.90	.935	14.1306
.15	.0735	.6034	.3612	8.956	1.10	1.050	9.4038
.3	.0510	.4187	.2463	3.053	1.26	1.104	3.3705
.5	.0350	.2874	.1970	1.466	1.36	1.123	1.6463
1.0	.0180	.1478	.1535	.571	1.47	1.128	.6440
1.5	.0134	.1100	.1297	.322	1.55	1.127	.3628
2.0	.0067	.0550	.1067	.198	1.55	1.127	.2231
3.0	.0045	.0369	.0961	.119	1.55	1.127	.1341
5.0	0						
$\dot{\gamma}_0 = 10.76 \text{ sec}^{-1}$							
.03	.330	2.7093	1.0180	3.154	.55	.619	1.9523
.05	.250	2.0525	1.3136	2.442	.74	.808	1.9731
.07	.200	1.6420	1.3300	1.766	.97	.982	1.7342
.10	.120	.9852	1.5927	1.480	1.05	1.026	1.5184
.15	.074	.6075	.4926	.305	1.27	1.107	.3376
.30	.050	.4105	.2463	.0763	1.52	1.127	.0859
.50	.0365	.2997	.2135	.0397	1.74	1.089	.0432
1.0	.023	.1888	.1396	.0130	2.05	.978	.0127
1.5	.019	.1560	.0985	.0061	2.20	.908	.0055
2.0	.016	.1314	.0821	.0038	2.24	.887	.0033
3.0	.014	.1149	.0640	.0020	2.28	.867	.0017
5.0	.0080	.0657	.0361	.00067	2.33	.842	.0005
7.0	.0035	.0287					
10.0	0						

APPENDIX G

MODEL INDEPENDENT PARAMETERS

TABLE G-1. Model Independent Parameters for 0.50% Separan Solution at 21°C

$\dot{\gamma}$ (sec <sup>-1</sup> )	$\eta$ ( $\frac{\text{gr}}{\text{cm}^2 \text{ sec}}$ )	$\theta$ (gr/cm)	$\theta/\eta$ (sec)	$\dot{\gamma}$ (sec <sup>-1</sup> )	$\eta$ ( $\frac{\text{gr}}{\text{cm}^2 \text{ sec}}$ )	$\theta$ (gr/cm)	$\theta/\eta$ (sec)
2.689	7.9383	.5753	.0725	107.6	.9156	.0654	.0714
4.272	6.1498	.5698	.0927	169.7	.6967	.0395	.0567
6.75	4.6827	.5249	.1121	268.9	.5435	.0221	.0407
10.76	3.5709	.4941	.1384	339.4	.4717	.0160	.0339
16.97	2.7093	.3972	.1466	427.2	.4170	.0122	.0293
26.89	2.0701	.2804	.1355	537.2	.3683	.0090	.0244
42.72	1.5720	.2038	.1296	675.0	.3223	.0068	.0211
67.50	1.1920	.1235	.1036	851.0	.2894	.0051	.0176

TABLE G-2. Model Independent Parameters for 0.25% Separan Solution at 21°C

$\dot{\gamma}$ (sec <sup>-1</sup> )	$\eta$ ( $\frac{\text{gr}}{\text{cm}^2 \text{ sec}}$ )	$\theta$ (gr/cm)	$\theta/\eta$ (sec)	$\dot{\gamma}$ (sec <sup>-1</sup> )	$\eta$ ( $\frac{\text{gr}}{\text{cm}^2 \text{ sec}}$ )	$\theta$ (gr/cm)	$\theta/\eta$ (sec)
10.76	2.0407	.0853	.0418	537.2	.2308	.0053	.0230
16.97	1.5863	.0866	.0546	675.0	.2000	.0039	.0195
26.89	1.2385	.0755	.0610	851.0	.18137	.0033	.0182
42.72	.9268	.0586	.0632				
67.50	.7230	.0436	.0603				
107.6	.5572	.0311	.0558				
169.7	.4280	.0191	.0446				
268.9	.3390	.0113	.0333				
339.4	.3006	.0083	.0276				
427.2	.2580	.0068	.0264				

TABLE G-3. Model Independent Parameters for 0.10% Separan Solution at 21°C

$\dot{\gamma}$ (sec <sup>-1</sup> )	$\eta$ ( $\frac{\text{gr}}{\text{cm sec}}$ )	$\Theta$ (gr/cm)	$\Theta/\eta$ (sec)	$\dot{\gamma}$ (sec <sup>-1</sup> )	$\eta$ ( $\frac{\text{gr}}{\text{cm sec}}$ )	$\Theta$ (gr/cm)	$\Theta/\eta$ (sec)
42.72	.5022	.0151	.0301	537.2	.1420	.0034	.0239
67.5	.3988	.0143	.0359	675.0	.1260	.0028	.0222
107.6	.3120	.0121	.0388	851.0	.1132	.0020	.0177
169.7	.2482	.0087	.0351				
268.9	.1930	.0066	.0342				
339.4	.1760	.0053	.0301				
427.2	.1582	.0045	.0284				

TABLE G-4. Model Independent Parameters for 0.05% Separan Solution at 21°C

$\dot{\gamma}$ (sec <sup>-1</sup> )	$\eta$ ( $\frac{\text{gr}}{\text{cm sec}}$ )	$\Theta$ (gr/cm)	$\Theta/\eta$ (sec)	$\dot{\gamma}$ (sec <sup>-1</sup> )	$\eta$ ( $\frac{\text{gr}}{\text{cm sec}}$ )	$\Theta$ (gr/cm)	$\Theta/\eta$ (sec)
107.6	.2201	.0045	.0204	675.0	.09325	.0017	.0182
169.7	.1798	.0047	.0261	851.0	.08992	.0013	.0145
268.9	.1416	.0040	.0282				
339.4	.1300	.0035	.0269				
427.2	.1142	.0030	.0263				
537.2	.1032	.0022	.0213				

## APPENDIX H

### MODEL INDEPENDENT STRESS PARAMETERS

$$S_w = \frac{|\tau_{11} - \tau_{22}|}{12}, \text{ Recoverable Shear Strain}$$

$$G_w = \frac{\tau_{12}}{S_w}, \text{ Shear Modulus Weissenberg Ratio}$$

TABLE H-1. Model Independent Stress Parameters for 0.5% Polyacrylamide Solution at 21°C

$\dot{\gamma}$ (sec <sup>-1</sup> )	$\tau_{12}$ (dyne/cm <sup>2</sup> )	$\tau_{11} - \tau_{22}$ (dyne/cm <sup>2</sup> )	$\frac{\tau_{11} - \tau_{22}}{2\tau_{12}}$	$S_w$	$G_w$
2.689	21.346	4.16	0.0974	0.1948	109.5790
4.272	26.272	10.40	0.1979	0.3958	66.3769
6.750	31.6085	23.92	0.3783	0.7566	41.7768
10.76	38.4228	57.21	0.7444	1.4888	25.8087
16.97	45.9760	114.4	1.2441	2.4882	18.4776
26.89	55.6638	202.8	1.8216	3.6432	15.2788
42.72	67.1578	372.0	2.7700	5.5400	12.1223
67.50	80.4580	562.8	3.4974	6.9948	11.5025
107.6	98.5200	758.0	3.8469	7.6938	12.8051
169.7	118.224	1138.4	4.8145	9.6290	12.2779
268.9	146.138	1598.4	5.4688	10.9376	13.3610
339.4	160.095	1850.4	5.7790	11.5580	13.8514
427.2	178.157	2238.0	6.2809	12.5618	14.1824
537.2	197.861	2598.8	6.5672	13.1344	15.0643
675.0	217.565	3106.8	7.1399	14.2798	15.2358
851.0	246.300	3716.0	7.5436	15.0872	16.3250

TABLE H-2. Model Independent Stress Parameters for 0.25% Polyacrylamide Solution at 21°C

$\dot{\gamma}$ ( $\text{sec}^{-1}$ )	$\tau_{12}$ ( $\text{dyne/cm}^2$ )	$\tau_{11} - \tau_{22}$ ( $\text{dyne/cm}^2$ )	$\frac{\tau_{11} - \tau_{22}}{2\tau_{12}}$	$S_w$	$G_w$
10.76	21.9579	9.88	0.2249	0.4498	48.8170
16.97	26.9195	24.96	0.4636	0.9272	29.0331
26.89	33.3032	54.60	0.8197	1.6394	20.3142
42.72	39.5928	107.2	1.3537	2.7074	14.6239
67.50	48.8025	198.8	2.0367	4.0734	11.9807
107.6	59.9547	360.2	3.0039	6.0078	9.9794
169.7	72.6316	550.8	3.7917	7.5834	9.5777
268.9	95.1571	821.0	4.5032	9.0064	10.5654
339.4	102.0236	958.6	4.6979	9.3958	10.8584
427.2	110.2176	1250.0	5.6706	11.3412	9.7183
537.2	123.9857	1531.2	6.1749	12.3498	10.0394
675.0	135.4650	1760.0	6.4961	12.9922	10.4266
851.0	154.3480	2364.0	7.6580	15.3160	10.0775

TABLE H-3. Model Independent Stress Parameters for 0.1% Polyacrylamide Solution at 21°C

$\dot{\gamma}$ (sec <sup>-1</sup> )	$\tau_{12}$ (dyne/cm <sup>2</sup> )	$\tau_{11} - \tau_{22}$ (dyne/cm <sup>2</sup> )	$\frac{\tau_{11} - \tau_{22}}{2\tau_{12}}$	$S_w$	$G_w$
26.89	17.6586	10.4	0.2944	0.5888	29.9908
42.72	21.4539	27.6	0.6432	1.2864	16.6774
67.50	26.9190	65.2	1.2110	2.4220	11.1143
107.6	33.5712	140.4	2.0910	4.1820	8.0275
169.7	42.1195	251.8	2.9891	5.9782	7.0455
268.9	51.8977	481.2	4.6360	9.2720	5.5972
339.4	59.7344	620.2	5.1913	10.3826	5.7533
427.2	67.5830	823.6	6.0932	12.1864	5.5457
537.2	76.2824	986.8	6.4680	12.9360	5.8969
675.0	85.0500	1318.0	7.7483	15.4966	5.4883
851.0	96.3332	1610.0	8.3564	16.7128	5.7640

TABLE H-4. Model Independent Stress Parameters for 0.05% Polyacrylamide Solution at 21°C

$\dot{\gamma}$ (sec <sup>-1</sup> )	$\tau_{12}$ (dyne/cm <sup>2</sup> )	$\tau_{11} - \tau_{22}$ (dyne/cm <sup>2</sup> )	$\frac{\tau_{11} - \tau_{22}}{2\tau_{12}}$	$S_w$	$G_w$
67.50	18.8865	19.4	0.5135	1.0270	18.3899
107.6	23.6827	52.9	1.1168	2.2336	10.6029
169.7	30.5120	136.4	2.2351	4.4702	6.8256
268.9	38.0762	223.0	2.9283	5.8566	6.5014
339.4	44.1220	394.4	4.4694	8.9388	4.9360
427.2	48.7862	558.4	5.7229	11.4458	4.2623
537.2	55.4390	638.4	5.7576	11.5152	4.8144
675.0	62.9775	808.4	6.4181	12.8362	4.9062
851.0	76.5049	960.0	6.2741	12.5482	6.0968

APPENDIX I

SUMMARY OF VISCOMETRIC DATA  
AND ELLIS MODEL CALCULATION

TABLE I-1. Results for the Weissenberg Rheogoniometer for 0.50% Polyacrylamide Solution at 21°C

$\dot{\gamma}_{\text{expt.}}, \text{ sec}^{-1}$	$\tau_{12}, \text{ dyne/cm}^2$	$\eta_{\text{expt.}}, \frac{\text{gr}}{\text{cm sec}}$	$\eta_{\text{calc.}}, \frac{\text{gr}}{\text{cm sec}}$	% error in $\eta_{\text{calc.}}$
.00675	.2948	43.6745	43.1283	-1.27
.01076	.4748	44.1248	42.7362	-3.25
.01697	.7389	43.5415	42.0412	-3.57
.02689	1.1494	42.7445	40.7712	-4.84
.04272	1.6831	39.3972	38.9203	-1.23
.0675	2.4220	35.8807	36.2092	0.91
.1076	3.4072	31.6650	32.6333	2.97
.1697	4.6387	27.3344	28.5325	4.20
.2689	6.2807	23.3563	23.9068	2.30
.4272	8.4563	19.7947	19.1652	-3.28
.6750	10.8372	16.0551	15.3753	-4.42
1.076	13.3823	12.4371	12.4462	0.07
1.697	16.8305	9.9178	9.6750	-2.51
2.689	21.3460	7.9383	7.2990	-8.76
4.272	26.2720	6.1498	5.6260	-9.31
6.75	31.6805	4.6827	4.4221	-5.89
10.76	38.4228	3.5709	3.4045	-4.89
16.97	45.9760	2.7093	2.6628	-1.75
26.89	55.6638	2.0701	2.0405	-1.45
42.72	67.1578	1.5720	1.5658	-0.39
67.50	80.4580	1.1920	1.2105	1.53
107.6	98.5200	.9156	.9051	-1.16
169.7	118.2240	.6967	.6955	-0.17
268.9	146.1380	.5435	.5112	-6.33
339.4	160.095	.4717	.4478	-5.33
427.2	178.157	.4170	.3832	-8.81

TABLE I-2. Results for the Weissenberg Rheogoniometer for 0.25% Polyacrylamide Solution at 21°C

$\dot{\gamma}_{\text{expt.}}, \text{ sec}^{-1}$	$\tau_{12}, \text{ dyne/cm}^2$	$\eta_{\text{expt.}} \frac{\text{gr}}{\text{cm sec}}$	$\eta_{\text{calc.}} \frac{\text{gr}}{\text{cm sec}}$	% error in $\eta_{\text{calc.}}$
.02689	.5090	18.9297	18.7626	-0.89
.04272	.7964	18.6427	17.6314	-5.73
.0675	1.2106	17.9356	16.7803	-6.88
.1076	1.7577	16.3354	15.5999	-4.71
.1697	2.4769	14.5956	14.0790	-3.67
.2689	3.4879	12.9712	12.1459	-6.79
.4272	4.4751	10.4755	10.5416	0.63
.675	5.8480	8.6638	8.7430	0.90
1.076	7.4598	6.9329	7.1439	2.95
1.697	9.4120	5.5463	5.7347	3.29
2.689	11.4131	4.2444	4.6941	9.58
4.272	14.1992	3.3238	3.6772	9.61
6.75	17.6161	2.6098	2.8460	8.30
10.76	21.9579	2.0407	2.1627	5.64
16.97	26.9195	1.5863	1.6625	4.58
26.89	33.3032	1.2385	1.2538	1.22
42.72	39.5928	.9268	.9925	6.61
67.5	48.8025	.7230	.7451	2.97
107.6	59.9547	.5572	.5601	0.51
169.7	72.6316	.4280	.4282	0.05
268.9	91.1571	.3390	.3110	-9.02
339.4	102.0236	.3006	.2652	-13.36
427.2	110.2176	.2580	.2377	-8.56
537.2	123.9857	.2308	.2011	-14.78
675.0	135.4650	.2000	.1773	-12.81
851.0	154.3480	.1837	.1472	-24.78

TABLE I-3. Results for the Weissenberg Rheogoniometer for 0.10% Polyacrylamide Solution at 21°C

$\dot{\gamma}_{\text{expt.}}, \text{ sec}^{-1}$	$\tau_{12}, \text{ dyne/cm}^2$	$\eta_{\text{expt.}} \frac{\text{gr}}{\text{cm sec}}$	$\eta_{\text{calc.}} \frac{\text{gr}}{\text{cm sec}}$	% error in $\eta_{\text{calc.}}$
.04272	.2617	6.1248	5.9326	-3.24
.0675	.4122	6.1064	5.8082	-5.13
.1076	.6487	6.0286	5.5922	-7.80
.1697	.9783	5.7654	5.2750	-9.30
.2689	1.3736	5.1084	4.8961	-4.34
.4272	1.9557	4.5781	4.3740	-4.67
.675	2.6451	3.9187	3.8321	-2.26
1.076	3.5480	3.2974	3.2477	-1.53
1.697	4.5657	2.6905	2.7318	1.51
2.689	6.0505	2.2501	2.1776	-3.33
4.272	7.3187	1.7132	1.8333	6.55
6.750	9.1266	1.3521	1.4758	8.38
10.76	11.5670	1.0750	1.1484	6.39
16.97	14.1750	.8353	.9144	8.65
26.89	17.6586	.6567	.7072	7.14
42.72	21.4539	.5022	.5590	10.15
67.50	26.9190	.3988	.4218	5.46
107.6	33.5712	.3120	.3189	2.17
169.7	42.1195	.2482	.2382	-4.21
268.9	51.8977	.1930	.1815	-6.34
339.4	59.7344	.1760	.1509	-16.61
427.2	67.5830	.1582	.1283	-23.32
537.2	76.2824	.1420	.1093	-29.91
675.0	85.0500	.1260	.0946	-33.15
851.0	96.3332	.1132	.0802	-41.16

TABLE I-4. Results for the Weissenberg Rheogoniometer for 0.05% Polyacrylamide Solution at 21°C

$\dot{\gamma}$ expt., sec <sup>-1</sup>	$\tau_{12}$ , dyne/cm <sup>2</sup>	$\eta$ expt. $\frac{gR}{cm \ sec}$	$\eta$ calc. $\frac{gR}{cm \ sec}$	% error in $\eta$ calc.
.1076	.2784	2.5872	2.4762	-4.48
.1697	.4434	2.6128	2.3903	-9.31
.2689	.7012	2.6078	2.2567	-15.56
.4272	1.0433	2.4422	2.0888	-16.92
.675	1.4868	2.2027	1.8929	-16.37
1.076	2.0605	1.9150	1.6760	-14.26
1.697	2.6987	1.5903	1.4768	-7.68
2.689	3.4688	1.2900	1.2835	-0.51
4.272	4.2848	1.0030	1.1211	10.53
6.750	5.5377	.8204	.9317	11.95
10.76	7.1145	.6612	.7618	13.20
16.97	9.1688	.5403	.6098	11.39
26.89	11.7966	.4387	.4810	8.79
42.72	16.3916	.3837	.3458	-10.94
67.5	18.8865	.2798	.2983	6.21
107.6	23.6827	.2201	.2342	6.03
169.7	30.5120	.1798	.1774	-1.35
268.9	38.0762	.1416	.1385	-2.25
339.4	44.1220	.1300	.1172	-10.91
427.2	48.7862	.1142	.1045	-9.25
537.2	55.4390	.1032	.0903	-14.30
675.0	62.9775	.09325	.0780	-19.62

APPENDIX J

SUMMARY OF VISCOMETRIC DATA AND  
POWER-LAW MODEL CALCULATION

TABLE J-1. Results for the Weissenberg Rheogoniometer for the 0.5% Polyacrylamide Solution at 21°C

$\dot{\gamma}_{\text{expt.}}, \text{ sec}^{-1}$	$\tau_{12}, \text{ dyne/cm}^2$	$\eta_{\text{expt.}} \frac{\text{gr}}{\text{cm sec}}$	$\eta_{\text{calc.}} \frac{\text{gr}}{\text{cm sec}}$	% error in $\eta_{\text{calc.}}$
.00675	.2948	43.6745	291.9567	85.04
.01076	.4748	44.1248	221.1795	80.05
.01697	.7389	43.5415	168.6294	74.18
.02689	1.1494	42.7445	128.2058	66.66
.04272	1.6831	39.3972	97.3213	59.52
.0675	2.4220	35.8807	74.1171	51.60
.1076	3.4072	31.6650	56.1494	43.61
.1697	4.6387	27.3344	42.8088	36.15
.2689	6.2807	23.3563	32.5467	28.24
.4272	8.4563	19.7947	24.7063	19.88
.675	10.8372	16.0551	18.4217	14.67
1.076	13.3823	12.4371	14.2543	12.75
1.697	16.8305	9.9178	10.8676	8.74
2.689	21.3460	7.9383	8.2624	3.92
4.272	26.2720	6.1498	6.2720	1.95
6.75	31.6085	4.6827	4.7766	1.97
10.76	38.4228	3.5709	3.6186	1.32
16.97	45.9760	2.7093	2.7589	1.80
26.89	55.6638	2.0701	2.0975	1.31
42.75	67.1578	1.5720	1.5922	1.27
67.50	80.4580	1.1920	1.2126	1.70
107.6	98.5200	.9156	.9186	0.33
169.7	118.2240	.6967	.7004	0.53
268.9	146.1380	.5435	.5325	-2.07
339.4	160.095	.4717	.4636	-1.76
427.2	178.157	.4170	.4042	-3.16

TABLE J-2. Results for the Weissenberg Rheogoniometer for the 0.25% Polyacrylamide Solution at 21°C

$\dot{\gamma}_{\text{expt.}}, \text{ sec}^{-1}$	$\tau_{12}, \text{ dyne/cm}^2$	$\eta_{\text{expt.}} \frac{\text{gr}}{\text{cm sec}}$	$\eta_{\text{calc.}} \frac{\text{gr}}{\text{cm sec}}$	% error in $\eta_{\text{calc.}}$
.02689	.5090	18.9297	75.1995	74.83
.04272	.7964	18.6427	57.2376	67.43
.0675	1.2106	17.9356	43.7063	58.96
.1076	1.7577	16.3354	33.2005	50.80
.1697	2.4769	14.5956	25.3794	42.49
.2689	3.4879	12.9712	19.3471	32.95
.4272	4.4751	10.4755	14.7259	28.86
.675	5.8480	8.6638	11.2446	22.95
1.076	7.4598	6.9329	8.5417	18.83
1.697	9.4120	5.5463	6.5295	15.06
2.689	11.4131	4.2444	4.9775	14.73
4.272	14.1992	3.3238	3.7886	12.27
6.75	17.6161	2.6098	2.8930	9.79
10.76	21.9579	2.0407	2.1976	7.14
16.97	26.9195	1.5863	1.6799	5.57
26.89	33.3032	1.2385	1.2806	3.29
42.72	39.5928	.9268	.9747	4.92
67.50	48.8025	.7230	.7443	2.86
107.6	59.9547	.5572	.5654	1.45
169.7	72.6316	.4280	.4322	0.97
268.9	91.1571	.3390	.3295	-2.89
339.4	102.0236	.3006	.2872	-4.66
427.2	110.2176	.2580	.2508	-2.88
537.2	123.9857	.2308	.2191	-5.35
675.0	135.4650	.2000	.1925	-4.44
851.0	154.3480	.1837	.1670	-9.97

TABLE J-3. Results for the Weissenberg Rheogoniometer for 0.10% Polyacrylamide Solution at 21°C

$\dot{\gamma}_{\text{expt.}}, \text{ sec}^{-1}$	$\tau_{12}, \text{ dyne/cm}^2$	$\eta_{\text{expt.}}, \frac{\text{gr}}{\text{cm sec}}$	$\eta_{\text{calc.}}, \frac{\text{gr}}{\text{cm sec}}$	% error in $\eta_{\text{calc.}}$
.04272	.2617	6.1248	28.8962	78.80
.0675	.4122	6.1064	22.2220	72.52
.1076	.6487	6.0286	17.0029	64.54
.1697	.9783	5.7654	13.0896	55.95
.2689	1.3736	5.1084	10.0498	49.17
.4272	1.9557	4.5781	7.7044	40.58
.675	2.6451	3.9187	5.9249	33.86
1.076	3.5480	3.2974	4.5334	27.26
1.697	4.5657	2.6905	3.4900	22.91
2.689	6.0505	2.2501	2.6795	16.03
4.272	7.3187	1.7132	2.0542	16.60
6.750	9.1266	1.3521	1.5797	14.41
10.76	11.5670	1.0750	1.2087	11.06
16.97	14.1750	.8353	.9305	10.23
26.89	17.6586	.6567	.7144	8.08
42.72	21.4539	.5022	.5477	8.31
67.5	26.9190	.3988	.4212	5.32
107.6	33.5712	.3120	.3223	3.19
169.7	42.1195	.2482	.2481	-0.04
268.9	51.8977	.1930	.1905	-1.32
339.4	59.7344	.1760	.1660	-5.61
427.2	67.5830	.1582	.1460	-8.33
537.2	76.2824	.1420	.1280	-10.91
675.0	85.0500	.1260	.1123	-12.19
851.0	96.3332	.1132	.0983	-15.14

TABLE J-4. Results for the Weissenberg Rheogoniometer for 0.05% Polyacrylamide Solution at 21°C

$\dot{\gamma}_{\text{expt.}}, \text{ sec}^{-1}$	$\tau_{12}, \text{ dyne/cm}^2$	$\eta_{\text{expt.}} \frac{\text{gr}}{\text{cm sec}}$	$\eta_{\text{calc.}} \frac{\text{gr}}{\text{cm sec}}$	% error in $\eta_{\text{calc.}}$
.1076	.2784	2.5872	10.0902	74.36
.1697	.4434	2.6128	7.8773	66.83
.2689	.7012	2.6078	6.1340	57.49
.4272	1.0433	2.4422	4.7698	48.80
.675	1.4868	2.2027	3.7200	40.79
1.076	2.0605	1.9150	2.8874	33.68
1.697	2.6987	1.5903	2.2541	29.45
2.689	3.4688	1.2900	1.7553	26.51
4.272	4.2848	1.0030	1.3649	26.51
6.750	5.5377	.8204	1.0645	22.93
10.76	7.1145	.6612	.8262	19.97
16.97	9.1688	.5403	.6450	16.24
26.89	11.7966	.4387	.5023	12.66
42.72	16.3916	.3837	.3906	1.76
67.5	18.8865	.2798	.3046	8.14
107.6	23.6827	.2201	.2364	6.91
169.7	30.5120	.1798	.1846	2.59
268.9	38.0762	.1416	.1437	1.48
339.4	44.1220	.1300	.1266	-2.65
427.2	48.7862	.1142	.1118	-2.18
537.2	55.4390	.1032	.0987	-4.58
675.0	62.9775	.09325	.0872	-6.98

APPENDIX K

SUMMARY OF VISCOMETRIC DATA AND  
SPRIGGS MODEL CALCULATION

TABLE K-1. Results for the Weissenberg Rheogoniometer for 0.50% Polyacrylamide Solution at 21°C

$\dot{\gamma}$ (sec <sup>-1</sup> )	$(c\lambda\dot{\gamma})^2$ (dimensionless)	$\eta_{eq. 1}^{\dagger}$ (gr./cm.sec)	$\eta_{eq. 2}^{\dagger\dagger}$ (gr./cm.sec)	$\eta_{expt.}$ (gr./cm.sec)	% error in $\eta_{calc.}$
0.00675	0.0003	43.5119	252.0818	43.6745	-0.37
0.01076	0.0010	43.4901	192.4103	44.1248	-1.45
0.01697	0.0025	43.4428	147.7755	43.5415	-0.22
0.02689	0.0062	43.3274	113.1866	42.7445	1.35
0.04272	0.0159	43.0289	86.5630	39.3972	8.45
0.0675	0.0399	42.3139	66.4112	35.8807	15.21
0.1076	0.1015	40.6202	50.6907	31.6650	22.05
0.1697	0.2526	37.1655	38.9316	27.3344	26.45
0.2689	0.6342	31.2573	29.8191	23.3563	21.68
0.4272	1.6007	23.9446	22.8051	19.7947	13.21
0.675	3.9964	17.7157	17.4961	16.0551	8.24
1.076	10.155	13.3144	13.3545	12.4371	6.87
1.697	25.261	10.2561	10.2566	9.9178	3.31
2.689	63.425	7.8609	7.8559	7.9383	-1.04
4.272	160.081	6.0082	6.0080	6.1498	-2.36
6.750	399.656	4.6089	4.6094	4.6827	-1.59
10.76	1015.56	3.5174	3.5183	3.5709	-1.49
16.97	2526.07	2.7012	2.7021	2.7093	-0.26
26.89	6342.55	2.0687	2.0696	2.0701	-0.02
42.72	16008.27	1.5819	1.5828	1.5720	0.69
67.50	39965.89	1.2135	1.2143	1.1920	1.84
107.6	101556.24	0.9263	0.9269	0.9156	1.22
169.7	252607.16	0.7118	0.7119	0.6967	2.14
268.9	634254.71	0.5467	0.5452	0.5435	0.32
339.4	1010428.8	0.4793	0.4764	0.4717	0.99
427.2	1600827.7	0.4220	0.4170	0.4170	0.00
537.2	2531361.2	0.3732	0.3652	0.3683	-0.84
675.0	3996590.7	0.3324	0.3199	0.3223	-0.75
851.0	6352449.9	0.2985	0.2797	0.2894	-3.46

$\dagger$ Viscosity was calculated with series expression:  $\eta_{eq. 1} = \eta_0 - \frac{\eta_0 (c\lambda\dot{\gamma})^2}{2(\alpha)} \sum_{p=1}^{\infty} \frac{p^{-\alpha}}{2\alpha + (c\lambda\dot{\gamma})^2}$

$\dagger\dagger$ Viscosity was calculated with asymptotic expression:  $\eta_{eq. 2} = \frac{\eta_0 \pi}{2\alpha \cos \frac{\pi}{2\alpha}} \frac{(c\lambda\dot{\gamma})^{\frac{1}{\alpha}} - 1}{2(\alpha)}$

$\dagger\dagger\dagger$ Average % error is calculated as: % error =  $\frac{\eta_{calc} - \eta_{exp}}{\eta_{calc}} \times 100$ .

TABLE K-2. Results for the Weissenberg Rheogoniometer for 0.25% Polyacrylamide Solution at 21°C

$\dot{\gamma}$ (sec <sup>-1</sup> )	$(c\dot{\gamma})^2$ (dimensionless)	$\eta_{\text{eq. 1}}$ (gr./cm.sec)	$\eta_{\text{eq. 2}}$ (gr./cm.sec)	$\eta_{\text{expt.}}$ (gr./cm.sec)	% error in $\eta$ calc.
0.02689	0.0032	18.7444	57.7308	18.9297	-0.98
0.04272	0.0082	18.6769	44.5580	18.6427	0.20
0.0675	0.0206	18.5219	34.4959	17.9356	3.17
0.1076	0.0524	18.1341	26.5745	16.3354	9.92
0.1697	0.1305	17.2733	20.5948	14.5956	13.50
0.2689	0.3277	15.5456	15.5187	12.9712	16.57
0.4272	0.8273	12.8161	12.2864	10.4755	14.74
0.675	2.0655	9.8125	9.5119	8.6638	8.92
1.076	5.2491	7.3555	7.3276	6.9329	5.39
1.697	13.0566	5.6707	5.6788	5.5463	2.34
2.689	32.7824	4.3929	4.3894	4.2444	3.31
4.272	82.7426	3.3897	3.3879	3.3238	1.90
6.750	206.573	2.6239	2.6228	2.6098	0.50
10.76	524.923	2.0214	2.0205	2.0407	-0.99
16.97	1305.68	1.5666	1.5659	1.5863	-1.30
26.89	3278.34	1.2111	1.2103	1.2385	-2.33
42.72	8274.38	0.9349	0.9342	0.9268	0.80
67.50	20657.6	0.7240	0.7232	0.7230	0.03
107.6	52492.6	0.5581	0.5571	0.5572	0.00
169.7	130568.	0.4331	0.4318	0.4280	0.89
268.9	327835.	0.3361	0.3337	0.3390	-1.58
339.4	522273.	0.2963	0.2930	0.3006	-2.59
427.2	827439.	0.2623	0.2576	0.2580	-0.15
537.2	1308415.	0.2334	0.2266	0.2308	-1.85
675.0	2065767.	0.2092	0.1994	0.2000	-0.30
851.0	3283468.	0.1890	0.1752	0.1814	-3.53

TABLE K-3. Results for the Weissenberg Rheogoniometer for 0.10% Polyacrylamide Solution at 21°C

$\dot{\gamma}$ (sec <sup>-1</sup> )	( $c\dot{\gamma}$ ) <sup>2</sup> (dimensionless)	$\eta$ (gr./cm <sup>2</sup> .sec)	$\eta$ (gr./cm <sup>2</sup> .sec)	$\eta$ (gr./cm <sup>2</sup> .sec)	$\eta$ expt. (gr./cm <sup>2</sup> .sec)	% error in $\eta$ calc.
0.04272	0.0026	6.0768	18.6852	6.1248	6.1248	-0.78
0.0675	0.0066	6.0613	14.7328	6.1064	6.1064	-0.74
0.1076	0.0168	6.0222	11.5633	6.0286	6.0286	-0.10
0.1697	0.0420	5.9288	9.1262	5.7654	5.7654	2.76
0.2689	0.1054	5.7124	7.1852	5.1084	5.1084	10.66
0.4272	0.2663	5.2591	5.6493	4.5781	4.5781	12.95
0.675	0.6648	4.5069	4.4544	3.9187	3.9187	12.03
1.076	1.6897	3.5708	3.4961	3.2974	3.2974	5.69
1.697	4.2029	2.7695	2.7592	2.6905	2.6905	2.49
2.689	10.5527	2.1679	2.1724	2.2501	2.2501	-3.57
4.272	26.6359	1.7057	1.7080	1.7132	1.7132	-0.30
6.750	66.4975	1.3443	1.3467	1.3521	1.3521	-0.40
10.76	168.977	1.0545	1.0570	1.0750	1.0750	-1.70
16.97	420.307	0.8317	0.8342	0.8353	0.8353	-0.13
26.89	1055.33	0.6542	0.6568	0.6567	0.6567	0.02
42.72	2663.59	0.5138	0.5164	0.5022	0.5022	2.75
67.50	6649.86	0.4047	0.4072	0.3938	0.3938	2.07
107.6	16897.8	0.3172	0.3196	0.3120	0.3120	2.38
169.7	42030.9	0.2501	0.2522	0.2482	0.2482	1.59
268.9	105532.	0.1972	0.1986	0.1930	0.1930	2.82
339.4	168124.	0.1753	0.1760	0.1760	0.1760	0.00
427.2	266359.	0.1565	0.1561	0.1582	0.1582	-1.34
537.2	421190.	0.1405	0.1386	0.1420	0.1420	-2.45
675.0	664887.	0.1271	0.1231	0.1260	0.1260	-2.35
851.0	1056975.	0.1160	0.1091	0.1132	0.1132	-3.75

TABLE K-4. Results for the Weissenberg Rheogoniometer for 0.05% Polyacrylamide Solution at 21°C

$\dot{\gamma}$ (sec <sup>-1</sup> )	(cA $\dot{\gamma}$ ) <sup>2</sup> (dimensionless)	$\eta_{eq. 1}$ (gr./cm.sec)	$\eta_{eq. 2}$ (gr./cm.sec)	$\eta_{expt.}$ (gr./cm.sec)	% error in $\eta_{calc.}$
0.1076	0.0075	2.5913	5.7627	2.5872	0.16
0.1697	0.0187	2.5748	4.6500	2.6128	-1.47
0.2689	0.0471	2.5345	3.7438	2.6078	-2.89
0.4272	0.1190	2.4414	3.0105	2.4422	0.00
0.675	0.2972	2.2541	2.4271	2.2027	2.29
1.076	0.7553	1.9424	1.9486	1.9150	1.42
1.697	1.8790	1.5821	1.5723	1.5903	-0.51
2.689	4.7180	1.2632	1.2659	1.2900	-1.90
4.272	11.909	1.0137	1.0180	1.0030	1.48
6.750	29.931	0.8170	0.8207	0.8204	0.00
10.76	75.549	0.6553	0.6589	0.6612	-0.34
16.97	187.917	0.5281	0.5317	0.5403	-1.61
26.89	471.832	0.4245	0.4281	0.4387	-2.47
42.72	1190.88	0.3407	0.3442	0.3837	-11.47
67.50	2973.14	0.2741	0.2775	0.2798	-0.82
107.6	7554.95	0.2195	0.2228	0.2201	1.22
169.7	18791.9	0.1769	0.1798	0.1798	0.00
268.9	47183.4	0.1428	0.1447	0.1416	2.15
339.4	75167.7	0.1287	0.1297	0.1300	-0.23
427.2	119098.	0.1167	0.1164	0.1142	1.90
537.2	188313.	0.1066	0.1045	0.1032	1.25
675.0	297314.	0.0983	0.0938	0.0933	0.54
851.0	472571.	0.0917	0.0841	0.0899	-6.89

TABLE K-5. Results for the Weissenberg Rheogoniometer for  
0.50% Polyacrylamide Solution at 21°C

$\dot{\gamma}$ (sec <sup>-1</sup> )	$(c\lambda\dot{\gamma})^2$ (dimensionless)	$\theta_{\text{eq. 1}}^{\dagger}$ (gr./cm.)	$\theta_{\text{eq. 2}}^{\dagger\dagger}$ (gr./cm.)	$\theta_{\text{expt}}$ (gr./cm.)
0.04272	0.0159	233.0892	-690.7946	
0.0675	0.0399	227.9358	265.9631	
0.1076	0.1015	215.7351	369.0469	
0.1697	0.2526	190.8820	274.3498	
0.2689	0.6342	148.5389	170.8110	
0.4272	1.6007	96.7450	97.4375	
0.675	3.9964	54.3549	53.3249	
1.076	10.1550	28.0731	27.9503	
1.697	25.2606	14.5395	14.5583	
2.689	63.4252	7.4180	7.4186	0.5753
4.272	160.081	3.7225	3.7234	0.5698
6.750	399.656	1.8670	1.8680	0.5249
10.76	1015.557	0.9175	0.9186	0.4941
16.97	2526.068	0.4557	0.4568	0.3972
26.89	6342.545	0.2235	0.2246	0.2804
42.72	16008.27	0.1085	0.1097	0.2038
67.50	39965.89	0.0527	0.0538	0.1235
107.6	101556.24	0.0249	0.0260	0.0654
169.7	252607.16	0.0117	0.0128	0.0395
268.9	634254.71	0.0051	0.0062	0.0221
339.4	1010428.8	0.0033	0.0043	0.0160
427.2	1600827.7	0.0020	0.0030	0.0122
537.2	2531361.2	0.0012	0.0021	0.0090
675.0	3996590.7	0.0006	0.0015	0.0068
851.0	6352449.9	0.0002	0.0010	0.0051

$$\theta_{\text{eq. 1}}^{\dagger}(\dot{\gamma}) = \frac{2\lambda\eta_0}{Z(\alpha)} \sum_{p=1}^{\infty} \frac{1}{p^{2\alpha} + (c\lambda\dot{\gamma})^2}$$

$$\theta_{\text{eq. 2}}^{\dagger\dagger}(\dot{\gamma}) = \frac{2\lambda\eta_0}{Z(\alpha)} \left[ \frac{(c\lambda\dot{\gamma})^{\frac{1}{\alpha}-2}}{2\alpha \sin \frac{\pi}{2\alpha}} - \frac{(c\lambda\dot{\gamma})^{-2}}{2} \right]$$

TABLE K-6. Results for the Weissenberg Rheogoniometer for  
0.25% Polyacrylamide Solution at 21°C

$\dot{\gamma}$ (sec <sup>-1</sup> )	$(c\lambda\dot{\gamma})^2$ (dimensionless)	$\theta_{\text{eq. 1}}$ (gr./cm.)	$\theta_{\text{eq. 2}}$ (gr./cm.)	$\theta_{\text{expt}}$ (gr./cm.)
0.04272	0.0082	70.6617	-1003.3735	
0.0675	0.0206	69.8451	-126.1869	
0.1076	0.0524	67.8388	85.9018	
0.1697	0.1305	63.3893	99.7701	
0.2689	0.3277	54.4792	71.8532	
0.4272	0.8273	40.4914	44.1515	
0.675	2.0655	25.4010	25.2873	
1.076	5.2491	13.8534	13.6894	
1.697	13.0566	7.3088	7.3024	
2.689	32.7824	3.7927	3.7939	
4.272	82.7426	1.9364	1.9356	
6.750	206.573	0.9856	0.9849	
10.76	524.923	0.4913	0.4907	0.0853
16.97	1305.680	0.2475	0.2469	0.0866
26.89	3278.341	0.1233	0.1227	0.0755
42.72	8274.376	0.0612	0.0606	0.0586
67.50	20657.65	0.0306	0.0300	0.0436
107.6	52492.58	0.0153	0.0147	0.0311
169.7	130568.18	0.0079	0.0073	0.0191
268.9	327834.92	0.0042	0.0036	0.0113
339.4	522272.74	0.0032	0.0025	0.0083
427.2	827439.29	0.0024	0.0017	0.0068
537.2	1308415.5	0.0020	0.0012	0.0053
675.0	2065766.6	0.0016	0.0009	0.0039
851.0	3283468.3	0.0014	0.0006	0.0033

TABLE K-7. Results for the Weissenberg Rheogoniometer for  
0.10% Polyacrylamide Solution at 21°C

$\dot{\gamma}$ (sec <sup>-1</sup> )	$(c\lambda\dot{\gamma})^2$ (dimensionless)	$\theta_{\text{eq. 1}}$ (gr./cm.)	$\theta_{\text{eq. 2}}$ (gr./cm.)	$\theta_{\text{expt}}$ (gr./cm.)
0.04272	0.0026	12.2333	-1008.8406	
0.0675	0.0066	12.1878	-291.9209	
0.1076	0.0168	12.0752	-58.7015	
0.1697	0.0420	11.8003	3.9375	
0.2689	0.1054	11.1681	15.3766	
0.4272	0.2663	9.8470	12.9606	
0.675	0.6648	7.6700	8.5827	
1.076	1.6897	5.0192	5.0761	
1.697	4.2029	2.8929	2.8733	
2.689	10.5527	1.5611	1.5619	
4.272	26.6359	0.8237	0.8265	
6.750	66.4975	0.4328	0.4336	
10.76	168.977	0.2212	0.2220	
16.97	420.307	0.1136	0.1144	
26.89	1055.327	0.0574	0.0582	0.0151
42.72	2663.592	0.0286	0.0293	0.0151
67.50	6649.864	0.0141	0.0148	0.0143
107.6	16897.79	0.0066	0.0074	0.0121
169.7	42030.94	0.0030	0.0037	0.0087
268.9	105532.72	0.0011	0.0019	0.0066
339.4	168123.86	0.0006	0.0013	0.0053
427.2	266359.52	0.0004	0.0009	0.0045
537.2	421189.71	0.0003	0.0007	0.0034
675.0	664987.24		0.0005	0.0028
851.0	1056975.4		0.0003	0.0022

TABLE K-8. Results for the Weissenberg Rheogoniometer for  
0.05% Polyacrylamide Solution at 21°C

$\dot{\gamma}$ (Sec <sup>-1</sup> )	$(c\lambda\dot{\gamma})^2$ (dimensionless)	$\theta_{\text{eq. 1}}$ (gr./cm.)	$\theta_{\text{eq. 2}}$ (gr./cm.)	$\theta_{\text{expt}}$ (gr./cm.)
0.1076	0.0075	3.1955	-73.7850	
0.1697	0.0187	3.1634	-16.5665	
0.2689	0.0471	3.0850	0.1175	
0.4272	0.1190	2.9042	3.4627	
0.675	0.2972	2.5420	3.1118	
1.076	0.7553	1.9461	2.1081	
1.697	1.8790	1.2798	1.2904	
2.689	4.7180	0.7440	0.7410	
4.272	11.9087	0.4076	0.4091	
6.750	29.7308	0.2224	0.2222	
10.76	75.5491	0.1174	0.1173	
16.97	187.917	0.0621	0.0621	
26.89	471.832	0.0323	0.0324	
42.72	1190.885	0.0166	0.0168	0.0043
67.5	2973.139	0.0086	0.0087	0.0042
107.6	7554.947	0.0043	0.0046	0.0045
169.7	18791.91	0.0022	0.0023	0.0047
268.9	47183.40	0.0011	0.0012	0.0040
339.4	75167.71	0.0007	0.0008	0.0035
427.2	119088.56	0.00002	0.0006	0.0030
537.2	188312.69		0.0004	0.0022
675.0	297313.92		0.0003	0.0017
851.0	472570.73		0.0002	0.0013

APPENDIX L

SUMMARY OF THE VISCOMETRIC DATA AND  
BIRD-CARREAU MODEL CALCULATION

TABLE L-1. Results for the Weissenberg Rheogoniometer for 0.50% Polyacrylamide Solution at 21°C

$\dot{\gamma}$ expt., sec <sup>-1</sup>	$\eta$ eq. 1† g/cm.sec.	$\eta$ eq. 2†† g/cm.sec.	$\eta$ expt g/cm.sec.	% error in $\eta$ calc.†††	$\eta$ calc g/cm.	$\eta$ expt g/cm.	% error in $\eta$ calc.
.00675	43.4947		43.6745	-0.41			
.01076	43.4537		44.1248	-1.54			
.01697	43.3538		43.5415	-0.43			
.02689	43.1050		42.7445	0.84			
.04272	42.4975	18.0135	39.3972	7.30			
.0675	41.1178	45.4493	35.8807	12.74			
.1076	38.2190	43.6388	31.6650	17.15			
.1697	33.4945	36.0052	27.3344	18.39			
.2689	27.5556	28.5978	23.3563	15.24			
.4272	21.8199	22.2829	19.7947	9.28			
.675	17.0331	17.2562	16.0551	5.74			
1.076	13.1140	13.2305	12.4371	5.16			
1.697	10.1270	10.1883	9.3178	2.07			
2.689	7.8086	7.8164	7.9383	-1.66	6.8285	.5753	91.58
4.272	6.0873	5.9842	6.1498	-1.03	3.7515	.5699	84.91
6.75	5.2018	4.5915	4.6827	-1.99	2.2481	.5249	76.65
10.76		3.5035	3.5709	-1.92	1.2608	.4941	60.81
16.97		2.6940	2.7093	-0.57	.7144	.3972	44.40
26.89		2.0629	2.0701	-0.35	.4017	.2804	30.20
42.72		1.5755	1.5720	-0.22	.2247	.2038	9.30
67.5		1.2099	1.1920	1.48	.1265	.1235	2.37
107.6		.9237	.9156	0.77	.0703	.0654	6.97
169.7		.7094	.6967	1.79	.0397	.0395	0.50
268.9		.5440	.5435	0.09	.0222	.0221	0.45
339.4		.4774	.4717	1.19	.0166	.0160	3.61
427.2		.4135	.4170	-0.85	.0123	.0122	0.81
537.2		.3656	.3683	-0.74	.0093	.0090	3.23
675.0		.3177	.3223	-1.45	.0070	.0068	2.86
851.0		.2785	.2894	-3.91	.0052	.0051	1.92

†Viscosity was calculated with series expression for the low shear rates as:  $\eta_{eq. 1} = \eta_0 - \frac{\eta_0(2^{1/2}\dot{\gamma})^2}{z(\dot{\gamma})^2 - 1} - \frac{\eta_0}{z(\dot{\gamma})^2 - 1} \frac{p}{p - 2\alpha_1 \dot{\gamma}^2}$

††Viscosity was calculated with asymptotic expression for the high shear rates as:  $\eta_{eq. 2} = \frac{\eta_0}{z(\dot{\gamma})^2 - 1} \left[ \frac{\pi(2^{1/2}\dot{\gamma})^2 \frac{\alpha_1}{\sigma_1}}{2\alpha_1 \sin\left(\frac{\pi \alpha_1}{2\sigma_1} \pi\right)} - \frac{1 + \frac{1}{\sigma_1}}{(\alpha_1 + 1)(2^{1/2}\dot{\gamma})^2 - 2[1 + (2^{1/2}\dot{\gamma})^2]} \right]$

†††Average % error is calculated as % error =  $\frac{\eta_{calc} - \eta_{expt}}{\eta_{calc}} \times 100$

TABLE L-2. Results for the Weissenberg Rheogoniometer for 0.25% Polyacrylamide Solution at 21°C

$\gamma_{\text{expt.}}, \text{sec}^{-1}$	$\eta_{\text{eq. 1}}$ $\frac{\text{gr}}{\text{cm. sec.}}$	$\eta_{\text{eq. 2}}$ $\frac{\text{gr}}{\text{cm. sec.}}$	$\eta_{\text{expt}}$ $\frac{\text{gr}}{\text{cm. sec.}}$	% error in $\eta_{\text{calc.}}$	$\theta_{\text{calc}}$ $\frac{\text{gr}}{\text{cm.}}$	$\theta_{\text{expt}}$ $\frac{\text{gr}}{\text{cm.}}$	% error in $\theta_{\text{calc}}$
.02689	18.7001		18.9297	-1.23			
.04272	18.5715		18.6427	-0.38			
.0675	18.2662		17.9356	1.81			
.1076	17.5689	19.6917	16.3354	7.02			
.1697	16.2017	18.0780	14.5956	9.91			
.2689	14.0527	14.8993	12.9712	-6.02			
.4272	11.5200	11.8729	10.4755	9.07			
.675	9.1861	9.3405	8.6638	5.69			
1.076	7.1851	7.2534	6.9329	3.51			
1.697	5.6016	5.6471	5.5463	-0.81			
2.689	4.3596	4.3734	4.2444	2.64			
4.272	3.3939	3.3796	3.3283	1.93			
6.750	2.6875	2.6169	2.6098	0.27			
10.76	2.3069	2.0176	2.0407	-1.14	.6350	.0853	77.74
16.97		1.5630	1.5863	-1.49	.3832	.0867	64.25
26.89		1.2000	1.2385	-3.21	.2425	.0755	48.64
42.72		.9337	.9268	0.74	.1470	.0587	33.90
67.5		.7214	.7230	-0.22	.0888	.0436	19.11
107.6		.5561	.5572	-0.20	.0324	.0311	4.01
169.7		.4321	.4280	0.95	.0197	.0191	3.05
268.9		.3325	.3390	-1.95	.0119	.0113	5.04
339.4		.2931	.3006	-2.56	.0092	.0083	9.78
427.2		.2574	.2580	-0.23	.0072	.0068	5.56
537.2		.2254	.2308	-2.40	.0056	.0053	5.36
675.0		.1991	.2000	-0.45	.0043	.0038	11.63
851.0		.1747	.1814	-3.84	.0034	.0032	5.88

TABLE L-3. Results for the Weissenberg Rheogoniometer for 0.10% Polyacrylamide Solution at 21°C

$\dot{\gamma}$ expt., sec <sup>-1</sup>	$\eta$ eq. 1 gr/cm.sec.	$\eta$ eq. 2 gr/cm.sec.	$\eta$ expt gr/cm.sec.	% error in $\eta$ calc	$\theta$ calc gr/cm.	$\theta$ expt gr/cm.	% error in $\theta$ calc
.04272	6.0671		6.1248	-0.95			
.0675	6.0377		6.1064	-1.14			
.1076	5.9649		6.0286	-1.07			
.1697	5.8005	3.4941	5.7654	0.61			
.2689	5.4571	5.1162	5.1084	4.69			
.4272	4.8687	5.3596	4.5781	5.97			
.675	4.1185	4.8760	3.9187	4.85			
1.076	3.3494	4.1354	3.2974	1.55			
1.697	2.6879	3.3689	2.6905	-0.01			
2.689	2.1319	2.7078	2.2501	-4.57			
4.272	1.6800	2.1518	1.7132	-0.78			
6.750	1.3237	1.6998	1.3434	-0.65			
10.76	1.0363	1.0557	1.0750	-1.83	.1437		
16.97	.8150	.8337	.8353	-0.19	.0919	.0151	74.41
26.89	.6396	.6566	.6567	-0.02	.0590	.0151	61.48
42.72		.5163	.5022	2.73	.0392	.0143	43.38
67.50		.4071	.3988	2.04	.0253	.0121	24.84
107.6		.3196	.3120	2.38	.0161	.0087	16.35
169.7		.2522	.2482	1.59	.0104	.0066	1.49
268.9		.1968	.1930	1.93	.0067	.0053	0.00
339.4		.1759	.1760	-0.06	.0053	.0045	-4.56
427.2		.1561	.1582	-1.35	.0043	.0034	0.00
537.2		.1386	.1420	-2.45	.0034	.0028	0.00
675.0		.1231	.1260	-2.36	.0028	.0022	0.00
851.0		.1091	.1132	-3.76	.0022	.0022	0.00

TABLE L-4. Results for the Weissenberg Rheogoniometer for 0.05% Polyacrylamide Solution at 21°C

$\dot{\gamma}_{\text{expt.}}, \text{sec}^{-1}$	$\frac{\eta_{\text{eq. 1}}}{\text{cm. sec.}}$	$\frac{\eta_{\text{eq. 2}}}{\text{cm. sec.}}$	$\frac{\eta_{\text{expt}}}{\text{cm. sec.}}$	% error in $\eta_{\text{calc}}$	$\frac{\theta_{\text{calc}}}{\text{cm.}}$	$\frac{\theta_{\text{expt}}}{\text{cm.}}$	% error in $\theta_{\text{calc}}$
.1076	2.5828		2.5872	-0.17			
.1697	2.5548	2.0774	2.6128	-2.27			
.2689	2.4888	2.6385	2.6078	1.16			
.4272	2.3519	2.5547	2.4422	4.44			
.675	2.1223	2.2411	2.2027	1.71			
1.076	1.8187	1.8749	1.9150	-2.14			
1.697	1.5145	1.5426	1.5903	-3.09			
2.689	1.2380	1.2539	1.2900	-2.88			
4.272	1.0003	1.0132	1.0030	1.01			
6.75	.8075	.8188	.8204	-0.20			
10.76	.6495	.6582	.6612	-0.46			
16.97	.5276	.5315	.5403	-1.66	.0513		
26.87		.4281	.4387	-2.48	.0336		
42.72		.3443	.3837	-11.44	.0231		
67.5		.2774	.2798	-0.87	.0153	.0043	81.39
107.6		.2228	.2201	1.21	.0101	.0042	72.55
169.7		.1798	.1798	0.00	.0067	.0045	55.45
268.9		.1447	.1416	2.14	.0044	.0047	29.85
359.4		.1296	.1300	-0.31	.0036	.0040	9.09
427.2		.1163	.1142	1.81	.0029	.0035	2.78
537.2		.1044	.1032	1.15	.0024	.0030	-3.45
675.0		.0940	.0933	0.74	.0019	.0022	8.33
851.0		.0841	.0899	-6.90	.0016	.0017	10.53
						.0013	18.75

**APPENDIX M**

**SUMMARY OF THE CONSTANT FLOW RATE EXPERIMENT  
DATA AND NEWTONIAN FLUID CALCULATION**

TABLE M-1. Results for the Constant Flow Rate Experiments for Newtonian (Distilled Water) Fluid at 21°C

Q, cc min	G <sub>o</sub> gr cm <sup>2</sup> sec	ΔP, Psia	N <sub>Re</sub>	f* calc.	f* expt.	% error
Bed Properties: D <sub>p</sub> = .0597 cm, L = 45.72 cm, ε = .394, M = 1.0257						
34.7	.1137	.216	1.1712	128	147	-15.11
32.1	.1052	.194	1.0836	138	155	-11.74
29.0	.0950	.168	.9785	153	164	-7.16
27.2	.0891	.142	.9178	163	159	3.43
24.0	.0786	.123	.8096	185	176	5.18
22.7	.0744	.117	.7663	196	187	4.71
20.0	.0655	.112	.6747	222	230	-3.6
18.0	.0590	.103	.6077	247	261	-5.78
14.6	.0478	.082	.4924	305	317	-3.95
12.5	.0410	.065	.4223	355	341	3.93
10.0	.0328	.055	.3379	444	451	-1.61
8.5	.0278	.048	.2864	524	548	-4.62
7.4	.0242	.041	.2493	602	618	-2.66
6.2	.0203	.032	.2091	717	685	4.48
4.0	.0131	.021	.1349	1112	1080	2.86
Bed Properties: D <sub>p</sub> = .0432 cm, L = 45.72 cm, ε = .3744, M = 1.0359						
10.3	.1350	.575	.9844	152	166	-8.81
9.4	.1232	.521	.8984	167	180	-8.00
8.6	.1127	.454	.8218	183	189	-2.91
8.0	.1048	.420	.7642	196	201	-2.38
7.5	.0983	.397	.7168	209	216	-3.17
6.8	.0891	.340	.6497	231	225	2.52
6.0	.0786	.298	.5731	262	253	3.15
5.6	.0734	.280	.5352	280	273	2.55
5.0	.0655	.272	.4776	314	333	-6.08
4.6	.0603	.247	.4397	341	357	-4.64
4.1	.0537	.215	.3916	383	392	-2.28
3.6	.0472	.181	.3442	436	427	2.04
3.2	.0419	.172	.3055	491	515	-4.87
3.0	.0393	.160	.2866	523	544	-4.00
2.6	.0341	.131	.2487	603	592	1.86
2.2	.0288	.118	.2100	714	748	-4.67
2.0	.0262	.106	.1910	785	811	-3.35
1.8	.0236	.090	.1721	872	849	2.58

## APPENDIX N

### SUMMARY OF THE CONSTANT FLOW RATE EXPERIMENT DATA AND POWER-LAW MODEL CALCULATION

$$f^*_{\text{expt}} = \left( \frac{\rho \Delta p}{M G_o^2} \right) \left( \frac{D_p}{L} \right) \left( \frac{\epsilon^3}{1 - \epsilon} \right)$$

$$f^*_{\text{calc}} = \frac{150}{N_{\text{Re,eff}}} + 1.75$$

$$\frac{1}{\eta_{\text{eff}}}^* = \frac{1}{M^2 K} \left[ \frac{4n}{3n+1} \left( \frac{\tau_w^*}{K} \right)^{\frac{1}{n} - 1} \right]$$

$$\frac{1}{\eta_{\text{eff}}}^{**} = \frac{150 (1 - \epsilon)}{M D_p G_o \left[ \left( \frac{\rho \Delta p}{M G_o^2} \right) \left( \frac{D_p}{L} \right) \left( \frac{\epsilon^3}{1 - \epsilon} \right) - 1.75 \right]}$$

: Calculated based on the Ergun equation

TABLE N-1. Results for the Constant Flow Rate Experiments for 0.50% Polyacrylamide Solution at 21°C

Q, $\frac{CC}{min}$	$G \frac{gr}{cm^2 sec}$	$\Delta P, Psia$	$\frac{l^*}{\eta_{eff}} \cdot (\frac{cm \ sec}{gr})$	$\frac{l^{**}}{eff} \cdot (\frac{cm \ sec}{gr})$	$N_{Re,eff}$	$v_{w,sec}^{-1}$	f* calc.	f* expt.	% error
45.4	.1493	5.650	.4651	.4369	.0210	52.1170	7152	7615	-6.47
38.6	.1270	5.324	.4262	.3944	.0163	44.3326	9177	9917	-8.07
31.0	.1020	4.807	.3667	.3508	.0113	35.6057	13279	13881	-4.34
23.2	.0927	4.498	.3326	.3407	.0993	32.3592	16111	15726	4.39
22.3	.0733	3.967	.2764	.3055	.0061	25.5872	24511	22182	9.50
17.0	.0559	3.521	.2320	.2625	.0039	19.5133	38306	33853	11.52
16.0	.0526	3.425	.2227	.2539	.0035	18.3614	42398	37191	12.23
13.2	.0434	3.298	.2107	.2175	.0028	15.1499	54324	52605	3.16
10.8	.0355	3.050	.1878	.1924	.0020	12.3922	74507	72710	2.41
10.4	.0342	2.980	.1815	.1897	.0019	11.9384	80027	76545	4.35
9.6	.0316	2.788	.1645	.1874	.0016	11.0308	95527	83882	12.19
6.8	.0224	2.400	.1320	.1543	.00089	7.8193	168002	143703	14.46
6.1	.0201	2.366	.1292	.1404	.00078	7.0164	191197	175944	7.98
4.0	.0132	2.010	.1017	.1086	.00041	4.6078	370077	346577	6.35
3.0	.0099	1.764	.0839	.0928	.00025	3.4558	597922	540730	9.57
2.8	.0092	1.654	.0763	.0919	.00021	3.2215	707345	587100	17.00
2.4	.0079	1.542	.0688	.0847	.00016	2.7577	913254	742305	18.72
2.0	.0066	1.483	.0650	.0736	.00013	2.3039	1157716	1022834	11.65
1.5	.0049	1.284	.0526	.0631	.000078	1.7105	1927577	1606663	16.65
1.0	.0033	1.065	.0399	.0512	.00004	1.1519	3768582	2938148	22.04

Bed Properties:  $D_p = .1621 \text{ cm}$ ,  $L = 45.72 \text{ cm}$ ,  $\epsilon = .4237$ ,  $M = 1.0738$

TABLE N-2. Results for the Constant Flow Rate Experiments for 0.25% Polyacrylamide Solution at 21°C

$Q, \frac{CC}{min}$	$G_0, \frac{gr}{cm^2sec}$	$\Delta P, Paia$	$\frac{l^*}{\eta_{eff}}, (\frac{cm \ sec}{gr})$	$\frac{l^{**}}{r_{eff}}, (\frac{cm \ sec}{gr})$	$N_{Re,eff}$	$\dot{\gamma}_w, sec^{-1}$	$f^* \text{ calc.}$	$f^* \text{ expt.}$	% error
170.2	.5588	5.984	1.6766	1.5510	.2829	194.1635	530	575	-8.42
145.0	.4761	5.645	1.5418	1.3998	.2217	165.4281	677	747	-10.39
130.0	.4268	5.285	1.4026	1.3399	.1808	148.2981	830	870	-4.87
110.0	.3612	4.895	1.2563	1.2237	.1370	125.5644	1095	1125	-2.81
92.4	.3034	4.498	1.1125	1.1182	.1019	105.4209	1471	1466	0.40
76.2	.2502	4.152	.9917	.9987	.0749	86.9358	2002	1989	0.63
70.1	.2302	3.968	.9292	.9614	.0646	79.9865	2322	2246	3.29
67.3	.2210	3.720	.8469	.8845	.0565	76.7898	2654	2284	13.92
62.0	.2036	3.614	.8124	.9335	.0500	70.7439	3003	2615	12.92
58.8	.1931	3.552	.7925	.9007	.0462	67.0955	3246	2857	11.97
48.0	.1576	3.410	.7474	.7656	.0356	54.7605	4217	4118	2.35
41.5	.1363	3.164	.6711	.7136	.0276	47.3595	5430	5108	5.92
32.0	.1051	2.642	.5180	.6589	.0164	36.5186	9124	7174	21.32
23.8	.0781	2.463	.4683	.5251	.0110	27.1370	13580	1211	10.82
20.1	.0660	2.258	.4134	.4840	.0082	22.9327	18206	15347	14.61
17.0	.0558	2.030	.3547	.4552	.0060	19.3886	25093	19554	22.07
14.8	.0486	1.921	.3277	.4189	.0048	16.8868	31187	24393	21.79
14.0	.0460	1.874	.3162	.4065	.0044	15.9834	34144	26562	22.20
12.2	.0401	1.848	.3100	.3593	.0038	13.9333	39962	34469	13.75
8.0	.0263	1.525	.2352	.2856	.0019	9.1383	80297	66126	17.65
6.0	.0197	1.286	.1841	.2537	.0011	6.8451	136945	99385	27.43
4.5	.0148	1.175	.1617	.2086	.00072	5.1425	207527	160889	22.47
3.8	.0125	1.050	.1376	.1971	.00052	4.3433	288807	201550	30.21
3.0	.0098	.945	.1183	.1717	.00035	3.4052	428579	295116	31.14
2.2	.0072	.864	.1040	.1380	.00023	2.5017	663496	499875	24.66

Bed Properties:  $D_p = .1621 \text{ cm}$ ,  $L = 45.72 \text{ cm}$ ,  $c = .4237$ ,  $M = 1.0738$



TABLE N-3. Results for the Constant Flow Rate Experiments for 0.10% Polyacrylamide Solution at 21°C

$Q, \frac{cc}{min}$	$G_0, \frac{gr}{cm^2 \cdot sec}$	$\Delta P, Psia$	$\frac{l^*}{\eta_{eff}}, (\frac{cm \cdot sec}{gr})$	$\frac{l^{**}}{\eta_{eff}}, (\frac{cm \cdot sec}{gr})$	$N_{Re,eff}$	$\dot{\gamma}_w, sec^{-1}$	$f^* \text{ calc.}$	$f^* \text{ expt.}$	$\% \text{ error}$
Bed Properties: $D_p = .1621 \text{ cm}, L = 45.72 \text{ cm}, \epsilon = .4237, M = 1.0738$									
268.0	.8796	4.412	4.1289	3.3367	1.0968	300.7700	137	171	-25.01
200.0	.6564	3.765	3.3342	2.9074	.6609	224.4491	227	262	-15.44
172.2	.5652	3.465	2.9811	2.7167	.5088	193.2642	294	325	-10.31
158.4	.5199	3.251	2.7356	2.6620	.4295	177.7744	349	361	-3.25
135.7	.4454	2.916	2.3625	2.5403	.3178	152.2999	472	441	6.64
112.0	.3676	2.612	2.0367	2.3384	.2261	125.6970	663	580	12.65
91.0	.2987	2.489	1.9084	1.9921	.1722	102.1373	871	836	4.01
60.5	.1986	2.050	1.4692	1.6066	.0881	67.9092	1702	1558	8.46
45.8	.1503	1.693	1.1351	1.4718	.0515	51.3935	2911	2247	22.82
32.1	.1054	1.528	.9886	1.1431	.0315	36.0404	4767	4124	13.49
18.2	.0597	1.154	.6771	.8571	.0122	20.4138	12287	9707	20.99
12.8	.0420	.926	.5033	.7514	.0064	14.3615	23499	15738	33.03
10.5	.0345	.854	.4512	.6693	.0047	11.7969	31906	21511	32.58
9.1	.0299	.815	.4237	.6078	.0038	10.2240	39209	27331	30.29
6.0	.0197	.672	.3266	.4856	.0019	6.7362	77187	51913	32.74
5.2	.0171	.604	.2829	.4690	.0015	5.8472	102677	61928	39.69
3.1	.0102	.486	.2110	.3477	.00065	3.4878	230745	140047	39.31
2.3	.0075	.406	.1656	.3060	.00038	2.5645	399918	216393	45.89
2.0	.0066	.395	.1596	.2768	.00032	2.2568	471596	271862	42.35
1.8	.0059	.380	.1515	.2572	.00027	2.0174	555812	327279	41.12
Bed Properties: $D_p = .1621 \text{ cm}, L = 45.72 \text{ cm}, \epsilon = .4237, M = 1.1476$									
65.2	.8559	4.382	3.2748	3.2696	.9048	312.7804	166	168	-1.22
58.0	.7614	4.182	3.0749	3.0422	.7558	278.2463	198	202	-1.96
54.4	.7142	3.980	2.8764	2.9965	.6631	260.9975	226	219	3.23
45.8	.6013	3.642	2.5521	2.7520	.4954	219.7393	303	283	6.68
39.6	.5199	3.368	2.2967	2.5699	.3854	189.9924	389	350	10.18
36.0	.4726	3.065	2.0226	2.3196	.3076	172.7071	486	385	20.81
30.4	.3991	2.960	1.9297	2.2410	.2486	145.8472	603	521	13.60
26.8	.3518	2.638	1.6522	2.2156	.1876	128.5619	799	598	25.21
22.0	.2888	2.412	1.4643	1.9877	.1365	105.5392	1099	811	26.17
18.0	.2363	2.315	1.3855	1.6934	.1057	86.3536	1419	1163	18.06
15.7	.2061	2.156	1.2588	1.5855	.0837	75.3173	1791	1424	20.51
14.0	.1838	2.020	1.1529	1.5088	.0684	67.1679	2193	1677	23.51
11.4	.1497	1.782	.9736	1.3927	.0470	54.7064	3188	2231	30.03
8.0	.1050	1.488	.7635	1.1694	.0259	38.3712	5796	3786	34.68
6.8	.0893	1.389	.6959	1.0654	.0201	32.6338	7478	4886	34.66
5.1	.0670	1.274	.6193	.8714	.0134	24.4845	11198	7961	28.91
4.0	.0525	1.086	.4994	.8009	.0085	19.1856	17723	11053	37.64
3.1	.0407	.992	.4420	.6797	.0058	14.8734	25830	16799	34.96
2.2	.0289	.844	.3555	.5673	.0033	10.5612	45228	28348	37.32

TABLE N-4. Results for the Constant Flow Rate Experiments for 0.05% Polyacrylamide Solution at 21°C

$Q, \frac{CC}{min}$	$G_0 \frac{gr}{cm^2sec}$	$\Delta P, Psia$	$\frac{1^*}{\eta_{eff}} (\frac{cm \ sec}{gr})$	$\frac{1^{**}}{\eta_{eff}} (\frac{cm \ sec}{gr})$	$N_{Re, eff}$	$\dot{\gamma}_w, sec^{-1}$	$f^* \text{ calc.}$	$f^* \text{ expt.}$	% error
Bed Properties: $D_p = .1621 \text{ cm}, L = 45.72 \text{ cm}, \epsilon = .4237, M = 1.0738$									
200.0	.6562	2.715	4.3244	4.0423	.8570	217.8215	175	189	-7.97
148.5	.4872	2.272	3.4983	3.5750	.5147	161.7230	291	287	1.56
130.4	.4278	2.065	3.1223	3.4506	.4034	142.0055	372	338	9.05
100.0	.3281	1.682	2.4459	3.2444	.2424	108.9108	619	468	24.34
80.5	.2641	1.575	2.2618	2.7857	.1804	87.6663	831	677	18.60
70.2	.2303	1.402	1.9693	2.7279	.1370	76.4466	1095	792	27.66
58.4	.1916	1.288	1.7802	2.4690	.1030	63.6004	1456	1052	27.78
50.2	.1647	1.254	1.7245	2.1791	.0858	54.6711	1749	1386	20.77
40.5	.1329	1.120	1.5074	1.9680	.0605	44.1153	2479	1901	23.34
30.8	.1011	.961	1.2563	1.7443	.0384	33.5555	3910	2818	27.94
25.4	.0833	.826	1.0492	1.6719	.0264	27.6509	5683	3568	37.22
20.0	.0656	.718	.8880	1.5145	.0176	21.7755	8526	5001	41.35
17.4	.0571	.705	.8689	1.3424	.0150	18.9540	10011	6481	35.26
9.8	.0322	.495	.5704	1.0780	.0055	10.6886	27043	14309	47.09
6.0	.0197	.407	.4519	.8021	.0027	6.5393	55798	31432	43.67
Bed Properties: $D_p = .1621 \text{ cm}, L = 45.72 \text{ cm}, \epsilon = .4237, M = 1.1476$									
50.6	.6641	2.965	3.8848	3.7461	.8328	253.5945	180	189	-4.68
49.2	.6457	2.882	3.7557	3.7463	.7828	229.0670	192	194	-1.17
46.8	.6142	2.790	3.6135	3.6788	.7164	217.8921	209	207	0.94
44.0	.5775	2.675	3.4369	3.6053	.6407	204.8725	234	225	3.92
38.2	.5013	2.346	2.9399	3.5645	.4757	177.8400	315	262	16.97
32.0	.4200	2.105	2.5840	3.3235	.3503	148.9982	428	335	21.84
28.8	.3780	2.050	2.5039	3.0687	.3055	134.0984	491	402	18.05
20.4	.2677	1.800	2.1148	2.4705	.1853	94.9896	809	704	12.96
14.2	.1864	1.466	1.6800	2.1100	.1011	66.1268	1484	1183	20.26
12.6	.1654	1.390	1.5768	1.9741	.0842	58.6769	1782	1425	20.03
10.8	.1417	1.196	1.3185	1.9653	.0603	50.2691	2487	1670	32.84
9.4	.1234	1.174	1.2897	1.7431	.0514	43.7771	2920	2162	25.95
9.0	.1181	1.158	1.1580	1.6912	.0484	41.8969	3101	2328	24.92
8.4	.1102	1.065	1.1485	1.7158	.0409	39.0943	3672	2459	33.02
6.0	.0787	.882	.9176	1.4792	.0233	27.9194	6435	3994	37.94
4.6	.0604	.803	.8207	1.2467	.0160	21.4274	9375	6173	34.15
3.1	.0407	.654	.6428	1.0314	.0084	14.4386	17762	11072	37.66
2.0	.0262	.512	.4803	.8480	.0041	9.2946	36925	20917	43.35

APPENDIX O

SUMMARY OF THE CONSTANT FLOW RATE EXPERIMENT  
DATA AND ELLIS MODEL CALCULATION

$$f_{\text{expt}}^* = \left( \frac{\rho \Delta p}{M G_o^2} \right) \left( \frac{D_p}{L} \right) \left( \frac{\epsilon^3}{1 - \epsilon} \right)$$

$$f_{\text{calc}}^* = \frac{150}{N_{\text{Re,eff}}} + 1.75$$

$$^+ \frac{1}{\eta_{\text{eff}}} = \frac{1}{M^2 \eta_o} \left[ 1 + \frac{4}{\alpha + 3} \left( \frac{\tau_w^*}{\tau_{\frac{1}{2}}} \right)^{\alpha - 1} \right]$$

$$^{++} \frac{1}{\eta_{\text{eff}}} = \frac{150(1 - \epsilon)}{M D_p G_o \left[ \left( \frac{\rho \Delta p}{M G_o^2} \right) \left( \frac{D_p}{L} \right) \left( \frac{\epsilon^3}{1 - \epsilon} \right) - 1.75 \right]}$$

: Calculated from the Ergun equation

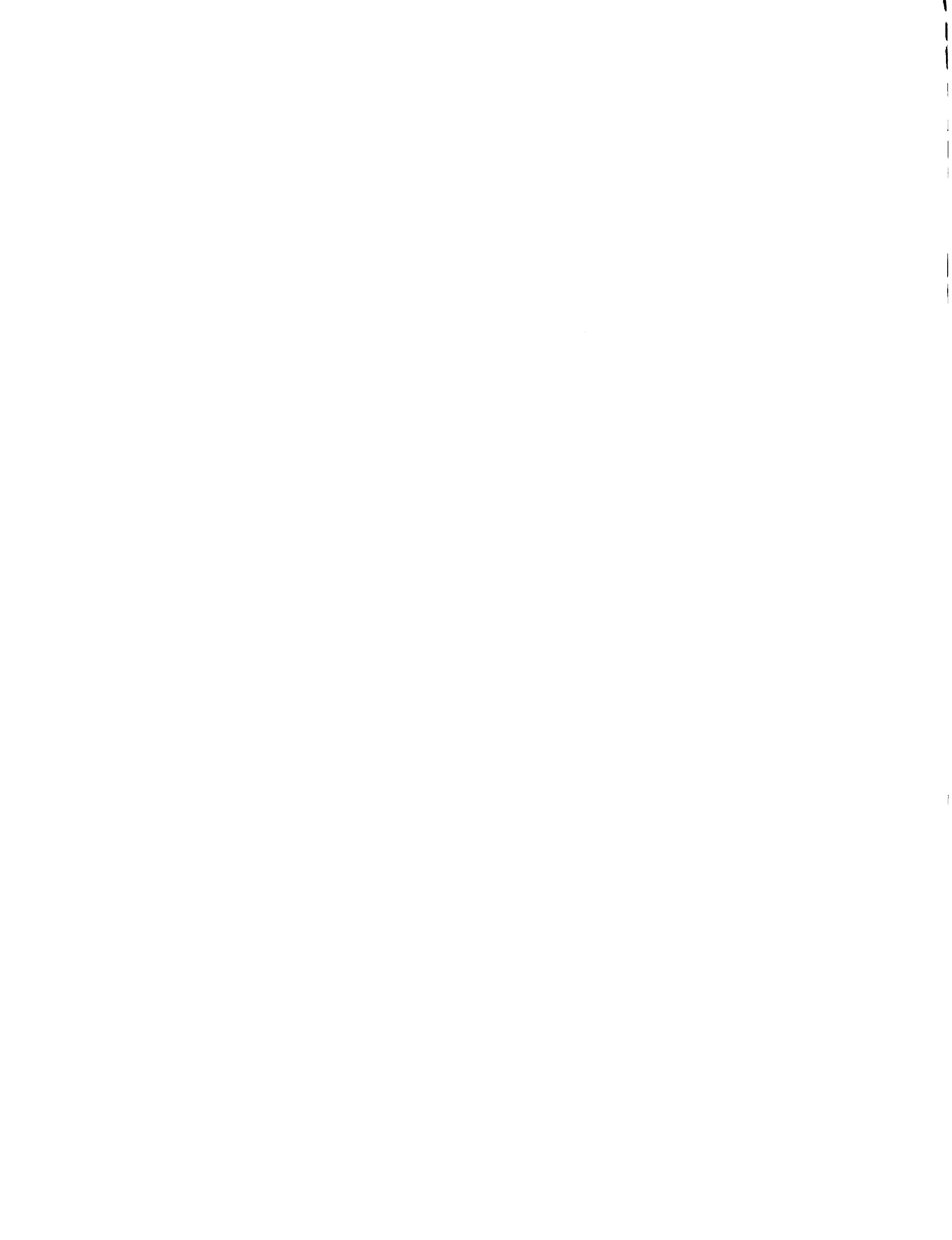


TABLE 0-1. Results for the Constant Flow Rate Experiments for 0.5% Polyacrylamide Solution at 21°C

$\frac{Q, \text{cc}}{\text{min}}$	$G \frac{\text{gr}}{\text{cm}^2 \text{sec}}$	$\Delta P, \text{Pisia}$	$\dagger \frac{1}{\eta_{\text{eff}}} \left( \frac{\text{cm. sec}}{\text{gr}} \right) \dagger \dagger \frac{1}{\eta_{\text{eff}}} \left( \frac{\text{cm. sec}}{\text{gr}} \right)$	$N_{\text{Re, eff}}$	$\dot{\gamma}_w, \text{sec}^{-1}$	$f^* \text{ calc.}$	$f^* \text{ expt.}$	$\% \text{ error}$
45.4	.1493	5.650	.4851	.4369	61.6427	6859	7615	-11.03
38.6	.1270	5.324	.4461	.3944	52.4355	8767	9917	-13.12
31.0	.1020	4.807	.3866	.3508	42.1135	12594	13881	-10.22
28.2	.0927	4.498	.3525	.3407	38.2738	15200	15726	-3.46
22.3	.0733	3.967	.2964	.3055	30.2639	22863	22182	2.98
17.0	.0559	3.521	.2519	.2625	23.0799	35275	33853	4.03
16.0	.0526	3.425	.2426	.2539	21.7174	38916	37191	4.43
13.2	.0434	3.298	.2306	.2175	17.9189	49629	52605	-6.00
10.8	.0355	3.050	.2077	.1924	14.6572	67359	72710	-7.94
10.4	.0342	2.980	.2014	.1897	14.1204	72109	76545	-6.15
9.6	.0316	2.788	.1845	.1874	13.0469	85208	83882	1.56
6.8	.0224	2.400	.1519	.1543	9.2485	145964	143703	1.55
6.1	.0201	2.366	.1492	.1404	8.2988	165656	175944	-6.20
4.0	.0132	2.010	.1216	.1086	5.4500	309432	346577	-12.00
3.0	.0099	1.764	.1038	.0928	4.0875	483173	540730	-11.90
2.8	.0092	1.654	.0963	.0919	3.7985	560901	587100	-4.67
2.4	.0079	1.542	.0888	.0847	3.2617	708247	742305	-4.81
2.0	.0066	1.483	.0849	.0736	2.7250	886080	1022834	-15.43
1.5	.0049	1.284	.0725	.0631	2.0231	1397865	1606663	-14.94
1.0	.0033	1.065	.0599	.0512	1.3625	2514144	2938148	-16.86

Bed Properties:  $D_p = 0.1621 \text{ cm}$ ,  $L = 45.72 \text{ cm}$ ,  $\epsilon = .4237$ ,  $M = 1.0738$

TABLE O-2. Results for the Constant Flow Rate Experiments for 0.25% Polyacrylamide Solution at 21°C

$Q, \frac{cc}{ml \cdot hr}$	$G, \frac{gr}{cm^2 \cdot sec}$	$\Delta P, Paia$	$\frac{1}{\eta_{eff}}, (\frac{cm \cdot sec}{gr})$	$+\frac{1}{\eta_{eff}}, (\frac{cm \cdot sec}{gr})$	$N_{Re, eff}$	$\dot{\gamma}_w, sec^{-1}$	$f^* \text{ calc.}$	$f^* \text{ expt.}$	$\% \text{ error}$
170.2	.5588	5.984	1.7228	1.5510	.2907	229.8770	516	575	-11.40
145.0	.4761	5.645	1.5880	1.3998	.2283	195.8562	657	747	-13.70
130.0	.4268	.5285	1.4487	1.3399	.1867	175.5753	803	870	-8.33
110.0	.3612	4.895	1.3025	1.2237	.1421	148.5890	1056	1125	-6.59
92.4	.3034	4.498	1.1587	1.1182	.1062	124.8115	1413	1466	-3.73
76.2	.2502	4.152	1.0379	.9987	.0784	102.9263	1913	1989	-4.00
70.1	.2302	3.968	.9753	.9614	.0678	94.6988	2212	2246	-1.52
67.3	.2210	3.720	.8930	.9845	.0596	90.9141	2517	2284	9.23
62.0	.2036	3.614	.8586	.9335	.0528	83.7562	2841	2615	7.97
58.8	.1931	3.552	.8386	.9007	.0489	79.4367	3067	2857	6.85
48.0	.1576	3.410	.7935	.7656	.0378	64.8329	3972	4118	-3.68
41.5	.1356	3.164	.7173	.7136	.0295	56.0706	5080	5108	-.55
32.0	.1051	2.642	.5641	.6589	.0179	43.2356	8377	7174	14.37
23.8	.0781	2.463	.5145	.5251	.0121	32.1285	12361	12111	2.03
20.1	.0660	2.258	.4595	.4840	.0092	27.1508	16377	15547	5.07
17.0	.0558	2.030	.4009	.4552	.0068	22.9548	22203	19554	11.93
14.8	.0486	1.921	.3739	.4189	.0055	19.9929	27336	24393	10.77
14.0	.0460	1.874	.3624	.4065	.0050	18.9233	29794	26562	10.85
12.2	.0401	1.848	.3561	.3593	.0043	16.4962	34781	34469	0.90
8.0	.0263	1.525	.2814	.2856	.0022	10.8192	67122	66126	1.48
6.0	.0197	1.286	.2303	.2537	.0014	8.1041	109490	99385	9.23
4.5	.0148	1.176	.2079	.2086	.00093	6.0084	161440	160889	0.34
3.8	.0125	1.050	.1837	.1971	.00069	5.1422	216247	201550	6.80
3.0	.0098	0.045	.1644	.1717	.00049	4.0315	308246	295116	4.26
2.2	.0072	0.064	.1501	.1380	.00033	2.9619	459479	499875	-8.73

Bed Properties:  $D_p = .1621 \text{ cm}$ ,  $L = 45.72 \text{ cm}$ ,  $\epsilon = .4237$ ,  $M = 1.0738$

TABLE O-3. Results for the Constant Flow Rate Experiments for 0.10% Polyacrylamide Solution at 21°C

$Q_{\text{min}}$	$G_0 \frac{\text{gr}}{\text{cm}^2 \text{sec}}$	$\Delta P, \text{Psia}$	$t \frac{1}{\eta_{\text{eff}}} (\frac{\text{cm sec}}{\text{gr}})$	$t + \frac{1}{\eta_{\text{eff}}} (\frac{\text{cm sec}}{\text{gr}})$	$N_{\text{Re,eff}}$	$\dot{\gamma}_w, \text{sec}^{-1}$	$f^* \text{ calc.}$	$f^* \text{ expt.}$	% error
268.0	.8796	4.412	4.2713	3.3367	1.1346	357.0087	132	171	-29.32
200.0	.6564	3.765	3.4766	2.9074	.6892	266.4171	218	262	-20.37
172.2	.5652	3.465	3.1235	2.7167	.5332	229.4012	281	325	-15.59
158.4	.5199	3.251	2.8781	2.6620	.4519	211.0150	332	361	-8.63
135.7	.4454	2.916	2.5050	2.5403	.3370	180.7773	445	441	1.01
112.0	.3676	2.612	2.1791	2.3384	.2419	149.2001	620	580	6.54
91.0	.2987	2.489	2.0509	1.9921	.1850	121.2352	811	836	-3.16
60.5	.1986	2.050	1.6117	1.6066	.0967	80.6070	1552	1558	-0.42
45.8	.1503	1.693	1.2776	1.4718	.0580	61.0032	2587	2247	13.13
32.1	.1054	1.528	1.1431	1.1431	.0360	42.7794	4166	4124	1.03
18.2	.0597	1.154	.8196	.8571	.0597	24.2308	10151	9707	4.37
12.8	.0420	.926	.6457	.7514	.0082	17.0468	18314	15738	14.07
10.5	.0345	.854	.5937	.6693	.0062	14.0027	24249	21511	11.29
9.1	.0299	.815	.5662	.6078	.0051	12.1357	29341	27331	6.85
6.0	.0197	.672	.4691	.4856	.0028	7.9958	53744	51913	3.41
5.2	.0171	.604	.4254	.4690	.0022	6.9405	68285	61928	9.31
3.1	.0102	.486	.3535	.3477	.0011	4.1399	137746	140047	-1.67
2.3	.0075	.406	.3081	.3060	.00070	3.0441	214964	216393	-0.66
2.0	.0066	.395	.3021	.2768	.00060	2.6788	249146	271862	-9.12
1.8	.0059	.380	.2939	.2572	.00052	2.3947	286399	327279	-14.27
Bed Properties: $D_p = .1621 \text{ cm}$ , $L = 45.72 \text{ cm}$ , $\epsilon = .4237$ , $M = 1.0738$									
65.2	.8559	4.382	3.3996	3.2696	.9392	371.2648	160	168	-5.07
58.0	.7614	4.182	3.1997	3.0422	.7864	330.2734	191	202	-6.09
54.4	.7142	3.980	3.0012	2.9965	.6919	309.7994	217	219	-0.96
45.8	.6013	3.642	2.6768	2.7520	.5196	260.8266	289	283	2.12
39.6	.5199	3.368	2.4214	2.5699	.4064	225.5177	369	350	5.30
36.0	.4726	3.065	2.1473	2.3196	.3276	205.0003	458	385	15.93
30.4	.3991	2.960	2.0545	2.2410	.2647	173.1181	567	521	8.01
26.8	.3518	2.638	1.8151	2.2156	.2061	152.6007	728	598	16.43
22.0	.2888	2.412	1.5890	1.9877	.1481	125.2731	1013	811	19.88
18.0	.2363	2.315	1.5102	1.6934	.1152	102.5001	1302	1163	10.68
15.7	.2061	2.156	1.3835	1.5855	.0920	89.4002	1630	1424	12.63
14.0	.1838	2.020	1.2776	1.5088	.0758	79.7271	1979	1677	15.23
11.4	.1497	1.782	1.0984	1.3927	.0531	64.9356	2826	2231	21.07
8.0	.1050	1.488	.8883	1.1694	.0301	45.5460	4982	3786	24.01
6.8	.0893	1.389	.8206	1.0654	.0237	38.7358	6341	4886	22.95
5.1	.0670	1.274	.7441	.8714	.0161	29.0627	9321	7961	14.59
4.0	.0525	1.086	.6241	.8009	.0106	22.7730	14181	11053	22.06
3.1	.0407	.992	.5668	.6797	.0074	17.6545	20145	16799	16.61
2.2	.0289	.844	.4803	.5673	.0045	12.5360	33480	28348	15.33
Bed Properties: $D_p = .1621 \text{ cm}$ , $L = 45.72 \text{ cm}$ , $\epsilon = .4237$ , $M = 1.1476$									

TABLE O-4. Results for the Constant Flow Rate Experiments for 0.05% Polyacrylamide Solution at 21°C

$Q, \frac{cc}{min}$	$G, \frac{gr}{cm^2sec}$	$\Delta P, Psia$	$t \frac{1}{\eta_{eff}}, (\frac{cm \ sec}{gr})$	$t + \frac{1}{\eta_{eff}}, (\frac{cm \ sec}{gr})$	$N_{Re, eff}$	$\dot{\gamma}_w, sec^{-1}$	$f^* \text{ calc.}$	$f^* \text{ expt.}$	% error
Bed Properties: $D_p = .1621 \text{ cm}, L = 45.72 \text{ cm}, \epsilon = .4237, M = 1.0738$									
200.0	.6562	2.715	4.6577	4.0423	.9230	259.7893	163	189	-16.29
148.5	.4872	2.272	3.8315	3.5750	.5637	192.8823	266	287	-7.82
130.4	.4278	2.065	3.4555	3.4506	.4464	169.3659	336	338	-0.65
100.0	.3281	1.682	2.7791	3.2444	.2754	129.8947	545	468	14.03
80.5	.2641	1.575	2.5951	2.7857	.2070	104.5571	725	677	6.61
70.2	.2303	1.402	2.3026	2.7279	.1601	91.1757	937	792	15.41
58.4	.1916	1.288	2.1135	2.4690	.1223	75.8544	1227	1052	14.27
50.2	.1647	1.254	1.8467	2.1791	.1023	65.2047	1466	1386	5.46
40.5	.1329	1.120	1.5895	1.9680	.0739	52.6151	2030	1901	6.40
30.8	.1011	.961	1.3824	1.7443	.0485	40.0255	3091	2818	9.83
25.4	.0833	.826	1.2212	1.6719	.0348	32.9784	4313	3568	17.28
20.0	.0656	.718	1.2021	1.5145	.0242	25.9710	6200	5001	19.34
17.4	.0571	.705	.9036	1.3424	.0207	22.6059	7236	6481	10.44
9.8	.0322	.495	.7851	1.0780	.0088	12.7480	17070	14309	16.18
6.0	.0197	.407	.8021	.8021	.0047	7.7992	32115	31432	2.13
Bed Properties: $D_p = .1621 \text{ cm}, L = 45.72 \text{ cm}, \epsilon = .4237, M = 1.1476$									
50.6	.6641	2.965	4.1766	3.7461	.8953	280.9867	168	189	-12.54
49.2	.6457	2.882	4.0475	3.7463	.8436	273.2015	178	194	-9.03
46.8	.6142	2.790	3.9052	3.6788	.7743	259.8735	194	207	-7.06
44.0	.5775	2.675	3.7286	3.6053	.6951	244.3454	216	225	-4.23
38.2	.5013	2.346	3.2316	3.5645	.5229	212.1045	287	262	8.73
32.0	.4200	2.105	2.8758	3.3235	.3899	177.7058	385	335	13.01
28.8	.3780	2.050	2.7956	3.0687	.3411	159.9352	440	402	8.50
20.4	.2677	1.800	2.4366	2.4705	.2106	113.2663	712	704	1.12
14.2	.1864	1.466	1.9717	2.1100	.1186	78.8675	1274	1183	6.41
12.6	.1654	1.390	1.8686	1.9741	.0998	69.9822	1504	1425	5.23
10.8	.1417	1.196	1.6103	1.9653	.0737	59.9545	2037	1670	17.98
9.4	.1234	1.174	1.5814	1.7431	.0630	52.2116	2381	2162	9.20
9.0	.1181	1.158	1.5605	1.6912	.0595	49.9692	2521	2328	7.65
8.4	.1102	1.065	1.4402	1.7158	.0512	46.6266	2928	2459	16.00
6.0	.0787	.882	1.2094	1.4792	.0307	33.2987	4882	3994	18.20
4.6	.0604	.803	1.1124	1.2467	.0217	25.5558	6916	6173	10.75
2.0	.0262	.512	.7721	1.0314	.0065	11.0855	22972	20917	8.94
3.1	.0407	.654	.9345	.8480	.0123	17.2205	12217	11072	9.37

## APPENDIX P

### SUMMARY OF THE CONSTANT FLOW RATE EXPERIMENT DATA AND SPRIGG'S MODEL CALCULATION

$$f_{\text{expt}}^* = \left( \frac{\rho \Delta p}{M G_o} \right)^2 \left( \frac{D_p}{L} \right) \left( \frac{\epsilon^3}{1 - \epsilon} \right)$$

$$f_{\text{calc}}^* = \frac{150}{N_{\text{Re,eff}}} + 1.75$$

$$^+ \frac{1}{\eta_{\text{eff}}} = \frac{1}{M^2 \eta_o} \left[ 1 + \frac{4}{\alpha + 3} \frac{[2\alpha \cos \frac{\pi}{2\alpha} z(\alpha)]^2}{\pi^\alpha} \left( \frac{c \lambda \tau_w^*}{\eta_o} \right)^{\alpha - 1} \right]$$

$$^{++} \frac{1}{\eta_{\text{eff}}} = \frac{150(1 - \epsilon)}{M D_p G_o \left[ \left( \frac{\rho \Delta p}{M G_o} \right)^2 \left( \frac{D_p}{L} \right) \left( \frac{\epsilon^3}{1 - \epsilon} \right) - 1.75 \right]}$$

: Calculated from the Ergun equation

TABLE P-1. Results for the Constant Flow Rate Experiments for 0.50% Polyacrylamide Solution at 21°C

$Q, \frac{CC}{min}$	$G_0 \frac{GR}{cm^2 sec}$	$\Delta P, Paia$	$\frac{1}{\eta_{eff}} \left( \frac{cm \cdot sec}{gr} \right) + \frac{1}{\eta_{eff}} \left( \frac{cm \cdot sec}{gr} \right)$	$N_{Re, eff}$	$\dot{\gamma}, w, sec^{-1}$	$f^* \text{ calc.}$	$f^* \text{ expt.}$	% error
45.4	.1493	5.650	.4758	.0215	51.2197	6993	7615	-8.90
38.6	.1270	5.324	.4384	.0168	43.5693	8921	9917	-11.16
31.0	.1020	4.807	.3809	.0117	34.9927	12786	13881	-8.57
28.2	.0927	4.498	.3476	.0097	31.8022	15416	15725	-2.01
22.3	.0733	3.967	.2923	.0065	25.1467	23178	22182	4.30
17.0	.0559	3.521	.2481	.0042	19.1774	35818	33853	5.49
16.0	.0526	3.425	.2388	.0038	18.0452	39542	37191	5.94
13.2	.0434	3.298	.2267	.0030	14.8890	50483	52604	-4.20
10.8	.0355	3.050	.2036	.0022	12.1788	68732	72710	-5.79
10.4	.0342	2.980	.1972	.0020	11.7328	73662	76545	-3.91
9.6	.0316	2.788	.1799	.0017	10.8409	87830	83882	4.00
6.8	.0224	2.400	.1463	.0010	7.6847	151519	143703	5.16
6.1	.0201	2.366	.1435	.00087	6.8956	172208	175944	-2.17
4.0	.0132	2.010	.1146	.00046	4.5285	328241	346577	-5.59
3.0	.0099	1.764	.0928	.00029	3.3963	523846	540730	-3.22
2.8	.0092	1.654	.0919	.00024	3.1562	615965	587099	4.67
2.4	.0079	1.542	.0847	.00019	2.7012	790038	742305	6.04
2.0	.0066	1.483	.0754	.00015	2.2642	997842	1022834	-2.50
1.5	.0049	1.284	.0619	.000092	1.6810	1638993	1606663	1.97
1.0	.0033	1.065	.0478	.000048	1.1321	3148421	2938143	6.68

Bed Properties:  $D_p = .1621 \text{ cm}$ ,  $L = 45.72 \text{ cm}$ ,  $\epsilon = .4237$ ,  $M = 1.0738$

TABLE P-2. Results for the Constant Flow Rate Experiments for 0.25% Polyacrylamide Solution at 21°C

Q, cc min	G, gr cm <sup>2</sup> sec	ΔP, Psia	$t \frac{1}{\eta_{eff}} (\frac{cm \cdot sec}{gr})$	$t + \frac{1}{\eta_{eff}} (\frac{cm \cdot sec}{gr})$	N <sub>Re,eff</sub>	$\dot{\gamma}_w, sec^{-1}$	f* calc.	f* expt.	% error
170.2	.5588	5.984	1.7075	1.5510	.2882	188.2136	521	575	-10.41
145.0	.4761	5.645	1.5856	1.3998	.2280	160.3588	658	747	-13.52
130.0	.4268	5.285	1.4583	1.3399	.1880	143.7537	798	870	-9.00
110.0	.3612	4.895	1.3230	1.2237	.1443	121.6585	1039	1125	-8.26
92.4	.3034	4.498	1.1882	1.1182	.1089	102.1904	1378	1466	-6.37
76.2	.2502	4.152	1.0734	.9987	.0811	84.2717	1849	1989	-7.56
70.1	.2302	3.968	1.0133	.9614	.0704	77.5354	2129	2246	-5.47
67.3	.2210	3.720	.9336	.9845	.0623	74.4367	2407	2284	5.11
62.0	.2036	3.614	.8999	.9335	.0553	68.5760	2711	2615	3.54
58.8	.1931	3.552	.8604	.9007	.0512	65.0395	2922	2857	2.21
48.0	.1576	3.410	.8359	.7656	.0398	53.0824	3770	4118	-9.21
41.5	.1363	3.164	.7601	.7136	.0313	45.9082	4794	5108	-6.54
32.0	.1051	2.642	.6045	.6589	.0192	35.3995	7818	7174	8.24
23.8	.0781	2.463	.5530	.5251	-.130	26.3054	11501	12111	-5.30
20.1	.0660	2.258	.4952	.4840	.0099	22.2300	15198	15547	-2.30
17.0	.0558	2.030	.4326	.4552	.0073	18.7944	20578	19554	4.97
14.8	.0486	1.921	.4033	.4189	.0059	16.3693	25342	24393	3.74
14.0	.0460	1.874	.3908	.4065	.0054	15.4936	27630	26562	3.86
12.2	.0401	1.848	.3839	.3593	.0046	13.5064	32263	34469	-6.84
8.0	.0263	1.525	.3008	.2856	.0024	8.8583	62785	66126	-5.32
6.0	.0197	1.286	.2422	.2537	.0014	6.6353	104080	99385	4.51
4.5	.0148	1.175	.2160	.2086	.00097	4.9849	155369	160889	-3.55
3.8	.0125	1.050	.1872	.1971	.00071	4.2102	212207	201550	5.02
3.0	.0098	0.945	.1638	.1717	.00048	3.3008	309428	295116	4.63
2.2	.0072	0.864	.1462	.1380	.00032	2.4251	471936	499875	-5.92

Bed Properties: D<sub>p</sub> = .1621 cm, L = 45.72 cm, ε = .4273, M = 1.0738

TABLE P-3. Results for the Constant Flow Rate Experiments for 0.10% Polyacrylamide Solution at 21°C

$Q, \frac{cc}{min}$	$G_0, \frac{gr}{cm^2 sec}$	$\Delta P, Psia$	$\frac{1}{\eta_{eff}} \left( \frac{cm \ sec}{gr} \right)$	$\frac{1}{\eta_{eff}} \left( \frac{cm \ sec}{gr} \right) + \frac{1}{\eta_{eff}} \left( \frac{cm \ sec}{gr} \right)$	$N_{Re, eff}$	$\dot{\gamma}_w, sec^{-1}$	$f^* \text{ calc.}$	$f^* \text{ expt.}$	$\% \text{ error}$
Bed Properties: $D_p = .1621 \text{ cm}, L = 45.72 \text{ cm}, \epsilon = .4237, M = 1.0738$									
268.0	.8796	4.412	3.8359	3.3367	1.0190	285.7599	147	171	-16.14
200.0	.6564	3.765	3.2315	2.9074	.6406	213.2479	234	262	-11.88
172.2	.5652	3.465	2.9540	2.7167	.5042	183.6193	297	326	-9.31
158.4	.5199	3.251	2.7572	2.6620	.4329	168.9024	346	361	-4.07
135.7	.4454	2.916	2.4514	2.5403	.3297	144.6993	455	441	3.13
112.0	.3676	2.612	2.1763	2.3384	.2416	119.4240	621	580	6.66
91.0	.2987	2.489	2.0657	1.9921	.1863	97.0401	805	836	-3.90
60.5	.1986	2.050	1.6748	1.6066	.1004	64.5201	1493	1558	-4.35
45.8	.1503	1.693	1.3618	1.4718	.0618	48.8287	2427	2247	7.41
32.1	.1054	1.528	1.2189	1.1431	.0388	34.2418	3866	4124	-6.66
18.2	.0597	1.154	.8998	.8571	.0162	19.3950	9246	9707	-4.98
10.5	.0345	.854	.6498	.6693	.0068	13.6447	16674	15738	5.62
9.1	.0299	.815	.6178	.6078	.0056	9.7138	26890	21511	2.91
6.0	.0197	.672	.5015	.4856	.0030	6.4000	50279	27331	-1.64
5.2	.0171	.604	.4468	.4690	.0023	5.5554	65005	61928	4.73
3.1	.0102	.486	.3532	.3477	.0011	3.3137	137851	140047	-1.59
2.3	.0075	.406	.2908	.3060	.0006	2.4366	227720	216392	4.97
2.0	.0066	.395	.2823	.2768	.00056	2.1442	266573	271862	-1.98
1.8	.0059	.380	.2707	.2572	.00048	1.9168	310948	327279	-5.25
Bed Properties: $D_p = .1621 \text{ cm}, L = 45.72 \text{ cm}, \epsilon = .4237, M = 1.1476$									
65.2	.8559	4.382	3.5604	3.2696	.9837	297.1709	152	168	-10.04
58.0	.7614	4.182	3.3851	3.0422	.8320	264.3602	180	202	-12.24
54.4	.7142	3.980	3.2086	2.9955	.7397	247.9723	203	219	-7.94
45.8	.6013	3.642	2.9151	2.7520	.5658	208.7731	265	283	-6.59
39.6	.5199	3.368	2.6787	2.5699	.4495	180.5108	334	350	-4.76
36.0	.4726	3.065	2.4191	2.3196	.3690	164.0881	406	385	5.29
30.4	.3991	2.960	2.3296	2.2410	.3001	138.5687	500	521	-4.31
26.8	.3518	2.638	2.0569	2.2156	.2336	122.1460	642	598	6.89
22.0	.2888	2.412	1.8670	1.9877	.1741	100.2722	862	811	5.87
18.0	.2363	2.315	1.7860	1.6934	.1362	82.0440	1101	1163	-5.63
15.7	.2061	2.156	1.6537	1.5855	.1100	71.5585	1363	1424	-4.44
14.0	.1838	2.020	1.5413	1.5088	.0914	63.8159	1640	1677	-2.26
11.4	.1497	1.782	1.3459	1.3927	.0650	51.9763	2306	2231	3.28
8.0	.1050	1.488	1.1075	1.1694	.0375	36.4563	3996	3786	5.25
6.8	.0893	1.389	1.0281	1.0654	.0296	31.0052	5062	4886	3.47
5.1	.0670	1.274	.9363	.8714	.0206	23.2626	7407	7961	-7.48
4.0	.0525	1.086	.7879	.8009	.0134	18.2281	11234	11053	1.61
3.1	.0407	.992	.7144	.6797	.0094	14.1312	15981	16799	-5.12
2.2	.0289	.844	.5999	.5673	.0056	10.0342	26802	28348	-5.77

TABLE P-4. Results for the Constant Flow Rate Experiments for 0.05% Polyacrylamide Solution at 21°C

$Q, \frac{cc}{min}$	$G_0 \frac{gf}{cm^2 sec}$	$\Delta P, \text{Psia}$	$\frac{l}{\eta_{eff}} (\frac{cm \text{ sec}}{gr})$	$\frac{l}{\eta_{eff}} (\frac{cm \text{ sec}}{gr})$	$N_{Re, eff}$	$\dot{\gamma}_w, \text{sec}^{-1}$	$f^* \text{ calc.}$	$f^* \text{ expt.}$	% error
Bed Properties: $D_p = .1621 \text{ cm}, L = 45.72 \text{ cm}, \epsilon = .4237, M = 1.0738$									
200.0	.6562	2.715	4.6263	4.0423	.9168	205.2228	164	189	-15.50
148.5	.4872	2.272	3.9480	3.5750	.5809	152.3690	258	287	-11.10
130.4	.4278	2.065	3.6262	3.4506	.4685	133.7920	320	338	-5.62
100.0	.3281	1.682	3.0211	3.2444	.2993	102.6114	501	468	6.54
80.5	.2641	1.575	2.8494	2.7857	.2273	82.5957	660	677	-2.54
70.2	.2303	1.402	2.5691	2.7279	.1787	72.0250	839	792	5.62
58.4	.1916	1.288	2.3823	2.4690	.1378	59.9218	1088	1052	3.36
50.2	.1647	1.254	2.3263	2.1791	.1157	51.5090	1296	1386	-6.88
40.5	.1329	1.120	2.1037	1.9680	.0844	41.5637	1777	1900	-6.98
30.8	.1011	.961	1.8357	1.7443	.0560	31.6184	2676	2818	-5.29
25.4	.0833	.826	1.6043	1.6719	.0404	26.0516	3717	3568	4.00
20.0	.0656	.718	1.4162	1.5145	.0281	20.5160	5346	5000	6.47
17.4	.0571	.705	1.3934	1.3424	.0240	17.8577	6243	6481	-3.81
9.8	.0322	.495	1.0171	1.0780	.0099	10.0704	15165	14309	5.65
6.0	.0197	.407	.8545	.8021	.0051	6.1611	29505	31432	-6.53
Bed Properties: $D_p = .1621 \text{ cm}, L = 45.72 \text{ cm}, \epsilon = .4237, M = 1.1476$									
50.6	.6641	2.965	4.1291	3.7461	.8852	221.9678	169	189	-11.26
49.2	.6457	2.882	4.0261	3.7463	.8392	215.8178	179	194	-8.45
46.8	.6142	2.790	3.9115	3.6788	.7755	205.2893	193	207	-7.23
44.0	.5775	2.675	3.7676	3.6053	.7024	193.0227	214	225	-5.32
38.2	.5013	2.346	3.3523	3.5646	.5425	167.5537	277	262	5.32
32.0	.4200	2.105	3.0440	3.3235	.4127	140.3802	363	335	7.93
28.8	.3870	2.050	2.9731	3.0687	.3628	126.3421	413	402	2.69
20.4	.2677	1.800	2.6482	2.4705	.2288	89.4756	655	704	-7.46
14.2	.1864	1.466	2.2060	2.1100	.1327	62.3020	1130	1183	-4.71
12.6	.1654	1.390	2.1039	1.9741	.1123	55.2830	1335	1425	-6.71
10.8	.1417	1.196	1.8405	1.9653	.0842	47.3616	1782	1670	6.25
9.4	.1234	1.174	1.8103	1.7431	.0721	41.2450	2080	2162	-3.94
9.0	.1181	1.158	1.7884	1.6912	.0682	39.4736	2200	2328	-5.83
8.4	.1102	1.065	1.6599	1.7158	.0590	36.8331	2540	2459	3.18
6.0	.0787	.882	1.4035	1.4792	.0357	26.3046	4207	3994	5.07
4.6	.0604	.803	1.2911	1.2467	.0252	20.1880	5959	6173	-3.59
2.0	.0262	.512	.8650	1.0314	.0073	8.7570	20504	20917	-2.01
3.1	.0407	.654	1.0755	.8480	.0141	13.6035	10615	11072	-4.30

APPENDIX Q

SUMMARY OF VISCOMETRIC DATA AND  
METER MODEL CALCULATION

TABLE Q-1. Results for the Weissenberg Rheogoniometer for 4.0% P V P Solution at 21°C

G.B.	$\dot{\gamma}_{exp}$ (sec <sup>-1</sup> )	$\Delta\tau$	$\tau_{12}$ (gr/cm sec <sup>2</sup> )	$\eta_{expt}$ (poise)	$\eta_{cal}$ (poise)	% error in $\eta_{cal}$
5.0	0.0269	0.0050	0.0411	1.5285	1.5182	0.67
4.8	0.0427	0.0078	0.0643	1.5074	1.4997	0.36
4.6	0.0675	0.0122	0.1003	1.4871	1.4655	1.37
4.4	0.1076	0.0182	0.1501	1.3956	0.4115	-1.18
4.2	0.1697	0.0265	0.2176	1.2828	0.3321	-3.88
4.0	0.2689	0.0380	0.3122	1.1613	0.2189	-4.99
3.8	0.4272	0.0532	0.4370	1.0231	0.0786	-5.44
3.6	0.6750	0.0741	0.6088	0.9020	0.9129	-1.21
3.4	1.076	0.0969	0.7952	0.7390	0.7697	-4.15
3.2	1.697	0.1240	1.0202	0.6012	0.6384	-6.20
3.0	2.689	0.1630	1.3394	0.4981	0.5072	-1.82
2.8	4.272	0.2070	1.7007	0.3981	0.4080	-2.49
2.6	6.750	0.2650	2.1742	0.3221	0.3239	-0.55
2.4	10.76	0.3330	2.7352	0.2542	0.2613	-2.79
2.2	16.97	0.4200	3.4466	0.2031	0.2123	-4.51
2.0	26.89	0.5510	4.5229	0.1682	0.1695	-0.77
1.8	42.72	0.7200	5.9082	0.1383	0.1397	-1.00
1.6	67.50	0.9224	7.5735	0.1122	0.1200	-6.99
1.4	107.6	1.2600	10.3403	0.0961	0.1032	-7.44
1.2	169.7	1.7820	14.6281	0.0862	0.0915	06.11
1.0	268.9	2.6824	22.0229	0.0819	0.0834	-1.77
0.9	339.4	3.3000	27.0841	0.0798	0.0808	-1.19
0.8	427.2	4.0530	33.2788	0.0779	0.0788	-1.20
0.7	537.2	4.9730	40.8272	0.0760	0.0774	-1.88
0.6	675.0	6.0840	49.9500	0.0740	0.0765	-3.24
0.5	851.0	7.8200	64.1654	0.0750	0.0755	-0.10
0.4	1076.	9.9870	81.9912	0.0762	0.0748	1.78

<sup>a</sup>Average % error is calculated as:  $\frac{\eta_{cal} - \eta_{expt}}{\eta_{cal}} \times 100$

TABLE Q-2. Results for the Weissenberg Rheogoniometer for 3.0% P V P Solution at 21°C

G.B.	$\dot{\gamma}_{\text{exp}}$ ( $\text{sec}^{-1}$ )	$\Delta_T$	$\tau_{12}$ ( $\text{gr/cm sec}^2$ )	$\eta_{\text{expt}}$ (poise)	$\eta_{\text{cal}}$ (poise)	% error in $\eta_{\text{cal}}$
4.8	0.0427	0.0039	0.0326	0.7645	0.7545	1.12
4.6	0.0675	0.0060	0.0505	0.7491	0.7406	1.00
4.4	0.1076	0.0094	0.0776	0.7217	0.7177	0.48
4.2	0.1697	0.0140	0.1154	0.6801	0.6843	-0.63
4.0	0.2689	0.0210	0.1702	0.6331	0.6363	-0.54
3.8	0.4272	0.0295	0.2422	0.5671	0.5775	-1.87
3.6	0.6750	0.042	0.3429	0.5080	0.5063	0.34
3.4	1.076	0.056	0.4612	0.4287	0.4393	02.27
3.2	1.697	0.075	0.6138	0.3617	0.3710	-2.56
3.0	2.689	0.099	0.8150	0.3031	0.3071	-1.34
2.8	4.272	0.130	1.0637	0.2490	0.2530	-1.62
2.6	6.750	0.170	1.3986	0.2072	0.2055	0.81
2.4	10.76	0.223	1.8345	0.0705	0.1672	1.95
2.2	16.97	0.292	2.3961	0.1412	0.1375	2.63
2.0	26.89	0.382	3.1326	0.1165	0.1147	1.53
1.8	42.72	0.498	4.0883	0.0957	0.0978	-2.18
1.6	67.50	0.676	5.5485	0.0822	0.0838	-1.95
1.4	107.6	0.958	7.8655	0.0731	0.0730	0.14
1.2	169.7	1.340	10.9965	0.0648	0.0662	-2.18
1.0	268.9	1.962	16.1071	0.0599	0.0613	-2.33
0.9	339.4	2.414	19.8210	0.0584	0.0595	-1.84
0.8	427.2	2.997	24.6067	0.0576	0.0580	-0.75
0.7	537.2	3.684	30.2443	0.0563	0.0570	-1.22
0.6	675.0	4.530	37.1925	0.0551	0.0562	-1.96
0.5	851.0	5.784	47.4858	0.0558	0.0555	0.58
0.4	1076.	7.390	60.6864	0.0564	0.0550	2.55

TABLE Q-3. Results for the Weissenberg Rheogoniometer for 1.0% P V P Solution at 21°C

G.B.	$\dot{\gamma}^{\text{exp}}$ ( $\text{sec}^{-1}$ )	$\Delta T$	$\tau_{12}^{\text{exp}}$ ( $\text{gr/cm sec}^2$ )	$\eta^{\text{exp}}$ (poise)	$\eta^{\text{cal}}$ (poise)	% error in $\eta^{\text{cal}}$
4.4	0.1076	0.0026	0.0215	0.2002	0.1994	0.22
4.2	0.1697	0.0040	0.0330	0.1945	0.1952	-0.36
4.0	0.2689	0.0061	0.0506	0.1882	0.1887	-0.28
3.8	0.4272	0.0094	0.0777	0.1821	0.1790	1.56
3.6	0.6750	0.0136	0.1122	0.1663	0.1677	-0.86
3.4	1.076	0.0200	0.1658	0.1541	0.1522	1.22
3.2	1.697	0.028	0.2328	0.1372	0.1364	0.59
3.0	2.689	0.038	0.3143	0.1169	0.1212	-3.70
2.8	4.272	0.053	0.4314	0.1010	0.1050	-3.99
2.6	6.750	0.073	0.6000	0.0889	0.0891	-0.21
2.4	10.76	0.098	0.8048	0.0748	0.0764	-2.19
2.2	16.97	0.133	1.0894	0.0642	0.0654	-1.82
2.0	26.89	0.185	1.5192	0.0565	0.0556	1.57
1.8	42.72	0.248	2.0334	0.0476	0.0490	-2.91
1.6	67.50	0.344	2.8282	0.0419	0.0433	-3.41
1.4	107.6	0.499	4.0995	0.0381	0.0388	-1.89
1.2	169.7	0.719	5.9055	0.0348	0.0358	-2.88
1.0	268.9	1.084	8.9005	0.0331	0.0336	-1.42
0.9	339.4	1.319	10.8268	0.0319	0.0328	-2.86
0.8	427.2	1.629	13.3713	0.0313	0.0322	-2.76
0.7	537.2	2.015	16.5457	0.0308	0.0317	-2.76
0.6	675.0	2.582	21.1950	0.0314	0.0312	0.67
0.5	851.0	3.379	27.7426	0.0326	0.0308	4.57
0.4	1076.	4.377	35.9384	0.0334	0.0306	8.52

TABLE Q-4. Results for the Weissenberg Rheogoniometer for 0.5% P V P Solution at 21°C

G.B.	$\dot{\gamma}_{\text{exp}}$ (sec <sup>-1</sup> )	$\Delta T$	$\tau_{12 \text{ exp}}$ (gr/cm sec <sup>2</sup> )	$\eta_{\text{exp}}$ (poise)	$\eta_{\text{cal}}$ (poise)	% error in $\eta_{\text{cal}}$
4.2	0.1697	0.0018	0.0153	0.0906	0.0917	-1.70
4.0	0.2689	0.0028	0.0238	0.0886	0.0897	-1.36
3.8	0.4272	0.0044	0.0367	0.0860	0.0868	-1.04
3.6	0.6750	0.0066	0.0549	0.0814	0.0830	-2.01
3.4	1.076	0.0100	0.0830	0.0772	0.0776	-0.65
3.2	1.697	0.0145	0.1191	0.0702	0.0718	-2.25
3.0	2.689	0.0210	0.1723	0.0641	0.0647	-0.97
2.8	4.272	0.0294	0.2417	0.0566	0.0576	-1.81
2.6	6.750	0.0410	0.3348	0.0496	0.0506	-2.03
2.4	10.76	0.0580	0.4723	0.0439	0.0435	0.88
2.2	16.97	0.0780	0.6414	0.0378	0.0378	0.04
2.0	26.89	0.1070	0.8793	0.0327	0.0327	0.15
1.8	42.72	0.1500	1.2303	0.0288	0.0282	2.25
1.6	67.50	0.200	1.6335	0.0242	0.0251	-3.73
1.4	107.6	0.277	2.2703	0.0211	0.0223	-5.82
1.2	169.7	0.400	3.2922	0.0194	0.0200	-5.17
1.0	268.9	0.576	4.7326	0.0176	0.0184	-4.61
0.9	339.4	0.695	5.7019	0.0168	0.0178	-5.84
0.8	427.2	0.858	7.0488	0.0165	0.0172	-4.20
0.7	537.2	1.054	8.6489	0.0161	0.0167	-3.94
0.6	675.0	1.300	10.6650	0.0158	0.0164	-3.50
0.5	851.0	1.700	13.9564	0.0164	0.0160	2.63
0.4	1076.	2.270	18.6148	0.0173	0.0157	9.47

APPENDIX R

SUMMARY OF THE CONSTANT FLOW RATE EXPERIMENT  
DATA AND METER'S MODEL CALCULATION

$$f_{\text{expt}}^* = \left( \frac{\rho \Delta p}{M G_o^2} \right) \left( \frac{D_p}{L} \right) \left( \frac{\epsilon^3}{1 - \epsilon} \right)$$

$$f_{\text{calc}}^* = \frac{150}{N_{\text{Re,eff}}} + 1.75$$

$$\begin{aligned} \frac{1}{\eta_{\text{eff}}} = \frac{1}{M^2 \eta_o} & \left[ 1 + \frac{4}{\alpha+3} \left( \frac{\tau_w^*}{\tau_m} \right)^{\alpha-1} - \left( \frac{\eta_\infty}{\eta_o} \right) \left( \frac{\tau_w^*}{\tau_m} \right)^{\alpha-1} \left[ \frac{4}{\alpha+3} \right. \right. \\ & \left. \left. + \frac{2}{\alpha+1} \left( \frac{\tau_w^*}{\tau_m} \right)^{\alpha-1} \right] + \left( \frac{\eta_\infty}{\eta_o} \right)^2 \left( \frac{\tau_w^*}{\tau_m} \right)^{2\alpha-2} \left( \frac{2}{\alpha+1} + \frac{4}{3\alpha+1} \left( \frac{\tau_w^*}{\tau_m} \right)^{\alpha-1} \right) \right] \end{aligned}$$

$$\frac{1}{\eta_{\text{eff}}} = \frac{150(1 - \epsilon)}{M D_p G_o \left[ \left( \frac{D_p}{L} \right) \left( \frac{\epsilon^3}{1 - \epsilon} \right) - 1.75 \right]}$$

: Calculated from the Ergun equation

TABLE R-1. Results for the Constant Flow Rate Experiments for 4.0% P V P Solution at 21°C

$Q, \frac{CC}{min}$	$G_o, \frac{gr}{cm^2 sec}$	$\Delta P, Psia$	$\frac{1}{\eta_{eff}}, (\frac{cm \ sec}{gr})$	$\frac{1}{\eta_{eff}}, (\frac{cm \ sec}{gr})$	$\frac{1}{\eta_{eff}}, (\frac{cm \ sec}{gr})$	$N_{Re, eff}$	$f^* \text{ calc.}$	$f^* \text{ expt}$	% error
350.0	1.1566	1.570	20.4664	13.9294	7.0451	21.29	33.03	-55.15	
285.2	.9425	1.524	16.5148	11.4905	4.6326	32.38	48.29	-49.13	
265.4	.8771	1.508	15.2940	10.7562	3.9924	37.57	55.17	-46.85	
252.0	.8325	1.495	14.3573	10.2712	3.5586	42.15	60.67	-43.93	
218.4	.7217	1.461	12.1293	9.0459	2.6053	57.57	78.95	-37.13	
205.6	.6794	1.442	11.0169	8.6080	2.2277	67.33	87.93	-30.58	
183.5	.6064	1.405	9.1036	7.8563	1.6430	91.30	107.54	-17.79	
163.0	.5387	1.386	8.2426	7.0516	1.3215	113.50	134.43	-18.43	
110.6	.3655	1.314	5.6460	5.0125	.6142	244	277	-13.35	
67.5	.2231	1.215	3.5016	3.2964	.2325	645	687	-6.49	
56.4	.1864	1.188	3.1462	2.8147	.1745	859	962	-11.98	
54.0	.1785	1.162	2.8808	2.7554	.1530	980	1026	-4.73	
48.8	.1613	1.095	2.4905	2.6416	.1196	1255	1185	5.58	
43.5	.1438	.912	2.7992	2.8274	.1198	1252	1241	0.86	
46.2	.1527	.710	3.7858	3.8590	.1721	872	857	1.70	
42.4	.1401	.635	4.0046	3.9583	.1670	898	911	-1.36	
40.0	.1322	.602	4.0531	3.9394	.1595	941	970	-3.07	
34.3	.1133	.490	3.9653	4.1472	.1337	1122	1074	4.23	
31.0	.1024	.448	3.8281	4.0989	.1167	1286	1203	6.47	
25.2	.0833	.412	3.7106	3.5467	.0920	1631	1708	-4.73	
22.6	.0747	.392	3.5599	3.4153	.0791	1895	1977	-4.33	
18.0	.0595	.316	3.0569	3.3740	.0541	2771	2512	9.33	
12.5	.0413	.264	2.6393	2.8024	.0324	4624	4356	5.78	

Bed Properties:  $D_p = .1621 \text{ cm}$ ,  $L = 45.72 \text{ cm}$ ,  $\epsilon = .4157$ ,  $M = 1.0728$

TABLE R-2. Results for the Constant Flow Rate Experiments for 3.0% P V P Solution at 21°C

$Q$ , $\frac{cc}{min}$	$G_0$ , $\frac{gr}{cm^2sec}$	$\Delta P$ , $\frac{psia}{cm}$	$t \frac{1}{n_{eff}} \left( \frac{cm \cdot sec}{gr} \right)$	$t + \frac{1}{n_{eff}} \left( \frac{cm \cdot sec}{gr} \right)$	$N_{Re,eff}$	$f^*$ calc.	$f^*$ expt	% error
453.8	1.4967	.625	105.1154	55.3190	46.8238	3.2035	7.8373	-144.65
407.2	13.430	.605	92.6289	48.9135	37.0244	4.0514	9.4223	-132.57
348.0	1.1477	.582	79.8104	41.1897	27.2617	5.5022	12.4114	-125.57
303.2	1.000	.558	68.0530	36.1957	20.2541	7.4059	15.6743	-111.65
248.5	.8196	.523	53.5725	30.5631	13.0680	11.4784	21.8701	-90.53
215.0	.7091	.500	45.5959	27.1464	9.6227	15.5881	27.9324	-79.19
191.4	.6313	.481	39.9021	24.8304	7.4835	20.0440	33.9021	-69.14
166.5	.5491	.460	34.2423	22.3294	5.5960	26.8047	42.8557	-59.88
148.8	.4908	.441	29.8339	20.6718	4.3579	34.42	51.43	-49.41
103.5	.3414	.400	22.1427	15.5968	2.2499	66.67	96.40	-44.60
82.4	.2718	.362	16.8656	13.6450	1.3643	110	138	-25.20
66.7	.2200	.329	13.4248	12.1088	.8790	171	191	-11.89
60.5	.1995	.320	12.6389	11.2732	.7504	200	226	-12.99
48.5	.1600	.274	9.4323	10.5385	.4492	334	301	9.97
33.2	.1095	.251	8.2326	7.8507	.2683	559	588	-5.18
25.5	.0841	.213	6.6559	7.0989	.1666	900	846	6.05
23.0	.0759	.204	6.3376	6.6873	.1432	1048	995	5.06
19.2	.0633	.195	6.0354	5.8318	.1137	1319	1367	-3.63
16.5	.0544	.183	5.6536	5.3390	.0915	1639	1737	-6.00
12.2	.0402	.148	4.6390	4.8768	.0555	2703	2573	4.81
9.3	.0307	.127	4.0731	4.3392	.0372	4031	3785	6.09
6.6	.0218	.112	3.6788	3.4932	.0239	6284	6620	-5.34
5.4	.0178	.099	3.3411	3.2266	.0177	8475	8777	-3.57

Bed Properties:  $D_p = .1621$  cm,  $L = 45.72$  cm,  $\epsilon = .4157$ ,  $M = 1.0728$

TABLE R-3. Results for the Constant Flow Rate Experiments for 1.0% P V P Solution at 21°C

$Q, \frac{cc}{min}$	$G_0, \frac{gr}{cm^2 sec}$	$\Delta P, Psia$	$t \frac{l}{\eta_{eff}}, (\frac{cm \cdot sec}{gr})$	$t + \frac{l}{\eta_{eff}}, (\frac{cm \cdot sec}{gr})$	$N_{Re, eff}$	$f^* \text{ calc.}$	$f^* \text{ expt}$	% error
368.0	1.2087	.312	219.6165	98.7078	79.0041	1.8986	5.9742	-214.66
312.4	1.0261	.292	175.0472	81.7477	53.4578	2.8060	7.7583	-176.50
249.6	.8198	.275	143.1126	63.3995	34.9182	4.2958	11.4468	-166.47
215.0	.7062	.264	125.0972	54.6508	26.2931	5.7049	14.8086	-159.58
197.5	.6487	.256	113.2065	50.8844	21.8565	6.8629	17.0184	-147.97
158.2	.5196	.237	88.7241	42.5288	13.7207	10.932	24.557	-124.63
134.6	.4421	.221	71.8132	38.1506	9.4491	15.875	31.631	-99.26
107.8	.3541	.203	56.3238	32.6888	5.9359	25.27	45.29	-79.23
93.4	.3068	.191	47.8249	29.8591	4.3669	34.35	56.77	-65.26
73.6	.2417	.178	40.0634	24.9759	2.8820	52.05	85.24	-63.77
66.5	.2184	.170	35.9564	23.5586	2.3372	64.18	99.70	-55.35
58.7	.1928	.165	33.6255	21.3522	1.9295	77.74	124.18	-59.73
47.3	.1554	.147	26.5685	19.2431	1.2288	122	170	-39.50
41.2	.1353	.135	22.8657	18.2104	.9208	163	206	-26.64
36.8	.1209	.123	19.8196	17.8409	.7132	210	236	-11.92
31.2	.1025	.114	17.8956	16.2924	.5459	275	304	-10.48
20.5	.0673	.091	14.0455	13.3654	.2813	533	562	-5.42
16.4	.0539	.075	11.9890	12.9789	.1923	780	722	7.40
12.0	.0394	.063	10.6392	11.2845	.1248	1202	1135	5.57
7.4	.0243	.050	9.2719	8.7622	.0671	2237	2369	-5.89
5.0	.0164	.036	7.8324	8.2111	.0382	3924	3744	4.57

Bed Properties:  $D_p = .1621 \text{ cm}$ ,  $L = 45.72 \text{ cm}$ ,  $\epsilon = .4157$ ,  $M = 1.0728$

TABLE R-4. Results for the Constant Flow Rate Experiments for 0.50% P V P Solution at 21°C

$Q, \frac{CC}{min}$	$G_0 \frac{gr}{cm^2 sec}$	$\Delta P, \text{Pisia}$	$\tau \frac{l}{n_{eff}} (\frac{cm \text{ sec}}{gr})$	$\tau \frac{l}{n_{eff}} (\frac{cm \text{ sec}}{gr})$	$N_{Re, eff}$	$f^* \text{ calc.}$	$f^* \text{ expt}$	$\% \text{ error}$
389.7	1.2787	.268	320.3018	139.2395	121.8972	1.2305	4.5807	-272.25
366.5	1.2026	.261	295.3861	127.2464	105.7249	1.4188	5.0435	-255.48
315.4	1.0349	.250	259.3506	102.0220	79.8825	1.8778	6.5234	-247.41
280.0	.9188	.241	232.5632	88.0716	63.5957	2.3586	7.9783	-238.26
247.2	.8111	.229	200.3949	77.8860	48.3757	3.1007	9.7279	-213.73
226.0	.7416	.219	176.4961	72.4635	38.9557	3.8505	11.1285	-189.01
202.4	.6641	.209	155.0648	66.0278	30.6487	4.8942	13.2438	-170.60
189.5	.6218	.204	145.2235	62.3702	26.8753	5.5813	14.7456	-164.20
151.4	.4968	.193	125.5012	50.4619	18.5565	8.0834	21.8538	-170.35
134.7	.4420	.182	108.2565	46.9527	14.2411	10.5329	26.0352	-147.18
110.0	.3609	.166	87.1654	41.2334	9.3626	16.0212	35.6179	-122.32
98.4	.3229	.153	73.1240	39.7564	7.0274	21.3451	41.0099	-92.13
93.2	.3058	.146	66.5850	39.3507	6.0601	24.7521	43.6326	-76.28
78.5	.2576	.135	57.6022	35.5042	4.4162	33.97	56.86	-67.39
66.8	.2192	.127	51.9654	31.8816	3.3902	44.25	73.87	-56.95
63.0	.2067	.124	50.0287	30.7243	3.0777	48.74	81.11	-66.42
57.4	.1883	.118	46.4235	29.3298	2.6017	57.66	93.00	-61.32
47.5	.1559	.108	41.1383	26.4044	1.9088	78.58	124.18	-58.03
34.4	.1129	.092	34.2604	22.3245	1.1512	130.30	201.7	-54.81
28.0	.0919	.078	29.4662	21.3927	.8059	186	258	-38.68
22.8	.0748	.061	24.6628	22.2415	.5490	273	305	-11.53
18.6	.0610	.048	21.4098	23.0299	.3887	386	361	6.58
15.0	.0492	.041	19.7168	21.7210	.2887	520	473	8.89
12.2	.0400	.039	19.2343	18.5440	.2290	655	716	-3.99

Bed Properties:  $D_p = .1621 \text{ cm}$ ,  $L = 45.72 \text{ cm}$ ,  $\epsilon = .4157$ ,  $M = 1.0728$

APPENDIX S

SUMMARY OF VISCOMETRIC DATA AND  
HERSCHEL-BULKLEY MODEL CALCULATION

TABLE S-1. Results for the Weissenberg Rheogoniometer for 0.05% P M C 400 Solution at 21°C

G.B.	$\dot{\gamma}$ (sec <sup>-1</sup> )	$\Delta_T$	$\tau_{12}$ (gr/cm sec <sup>2</sup> )	$\eta_{\text{expt}}$ (gr/cm sec)	$\eta_{\text{calc.}}$ (gr/cm sec)	% error in <sup>a</sup> $\eta_{\text{calc.}}$
3.8	0.4272	0.83	6.7809	15.8730		
3.6	0.675	0.67	5.4834	8.1235		
3.4	1.076	0.78	6.4038	5.9515	6.0977	2.40
3.2	1.697	0.82	6.7900	4.0012	4.0782	1.89
3.0	2.689	0.90	7.3321	2.7267	2.7491	0.82
2.8	4.272	0.07	7.9512	1.8612	1.8750	0.73
2.6	6.75	1.10	9.0543	1.3414	1.3032	-2.85
2.4	10.76	1.20	9.8650	0.9168	0.9160	-0.10
2.2	16.97	1.37	11.2573	0.6634	0.6596	-0.57
2.0	26.89	1.60	13.1321	0.4884	0.4816	-1.42
1.8	42.72	1.88	15.4451	0.3615	0.3569	-1.29
1.6	67.5	2.24	18.3524	0.2719	0.2696	-0.85
1.4	107.6	2.69	22.0512	0.2049	0.2055	0.31
1.2	169.7	3.34	27.4543	0.1618	0.1596	-1.35
1.0	268.9	4.10	33.6387	0.1251	0.1250	-0.05
0.9	339.4	4.36	35.7756	0.1054	0.1109	4.96
0.8	427.2	5.18	42.5538	0.0996	0.0987	-0.90
0.7	537.4	5.61	46.0517	0.0857	0.0881	2.69
0.6	675.0	6.47	53.1019	0.0787	0.0787	0.06
0.5	851.0	7.44	61.0687	0.0718	0.0704	-1.99

<sup>a</sup>Average % error is calculated as:  $\frac{\eta_{\text{calc}} - \eta_{\text{expt}}}{\eta_{\text{calc}}} \times 100$

TABLE S-2. Results for the Weissenberg Rheogoniometer for 0.3% P M C 400 Solution at 21°C

G.B.	$\dot{\gamma}$ (sec <sup>-1</sup> )	$\Delta_T$	$\tau_{12}$ (gr/cm sec <sup>2</sup> )	$\eta_{\text{expt}}$ (gr/cm sec)	$\eta_{\text{calc.}}$ (gr/cm sec)	% error in $\eta_{\text{calc.}}$
3.8	0.4272	0.32	2.6272	6.1498	2.8942	-0.12
3.6	0.675	0.31	2.5451	3.7705	1.9521	-0.94
3.4	1.076	0.38	3.1185	2.8982	1.3303	-0.98
3.2	1.697	0.41	3.3439	1.9705	0.9200	-0.27
3.0	2.689	0.44	3.6123	1.3434	0.6508	-2.80
2.8	4.272	0.48	3.9408	0.9225	0.4664	-0.46
2.6	6.75	0.55	4.5155	0.6690	0.3435	-0.68
2.4	10.76	0.61	5.0412	0.4685	0.2570	-1.97
2.2	16.97	0.71	5.8689	0.3458	0.1956	0.58
2.0	26.89	0.86	7.0487	0.2621	0.1519	-0.68
1.8	42.72	1.02	8.3100	0.1945	0.1191	2.33
1.6	67.5	1.26	10.3210	0.1529	0.0951	-1.84
1.4	107.6	1.52	12.5100	0.1163	0.0765	2.21
1.2	169.7	2.00	16.4200	0.0968	0.0688	-0.20
1.0	268.9	2.45	20.1145	0.0748	0.0620	3.40
0.9	339.4	2.85	23.3985	0.0689	0.0560	4.53
0.8	427.2	3.12	25.6006	0.0599	0.0507	3.42
0.7	537.4	3.50	28.7350	0.0535	0.0459	-1.47
0.6	675.0	4.03	33.0487	0.0490		
0.5	851.0	4.83	39.6200	0.0466		

TABLE S-3. Results for the Weissenberg Rheogoniometer for 0.5% P M C 25 Solution at 21°C

G.B.	$\dot{\gamma}$ (sec <sup>-1</sup> )	$\Delta_T$	$\tau_{12}$ (gr/cm sec <sup>2</sup> )	$\eta_{\text{expt}}$ (gr/cm sec)	$\eta_{\text{calc.}}$ (gr/cm sec)	% error in $\eta_{\text{calc.}}$
3.8	0.4272	0.12	0.9852	2.3062	0.8705	0.71
3.6	0.675	0.10	0.8210	1.2163	0.5944	2.32
3.4	1.076	0.113	0.9300	0.8643	0.4112	-3.88
3.2	1.697	0.12	0.9852	0.5806	0.2894	0.39
3.0	2.689	0.14	1.1494	0.4274	0.2087	-4.88
2.8	4.272	0.15	1.2315	0.2883	0.1528	-4.85
2.6	6.75	0.18	1.4778	0.2189	0.1150	-0.98
2.4	10.76	0.21	1.7241	0.1602	0.0880	6.32
2.2	16.97	0.24	1.9704	0.1161	0.0684	1.03
2.0	26.89	0.27	2.2167	0.0824	0.0542	0.72
1.8	42.72	0.35	2.8912	0.0677	0.0433	1.65
1.6	67.5	0.44	3.6323	0.0538	0.0352	3.64
1.4	107.6	0.56	4.5871	0.0426	0.0288	0.94
1.2	169.7	0.70	5.7470	0.0339	0.0261	1.76
1.0	268.9	0.93	7.6620	0.0285	0.0237	-0.13
0.9	339.4	1.06	8.6720	0.0256	0.0215	1.10
0.18	427.2	1.23	10.1310	0.0237	0.0196	2.18
0.7	537.4	1.40	11.4600	0.0213	0.0179	1.57
0.6	675.0	1.58	12.9330	0.0192		
0.5	851.0	1.83	15.0050	0.0176		

TABLE S-4. Results for the Weissenberg Rheogoniometer for 0.3% P M C 25 Solution at 21°C

G.B.	$\dot{\gamma}$ (sec <sup>-1</sup> )	$\Delta_T$	$\tau_{12}$ (gr/cm sec <sup>2</sup> )	$\eta_{\text{expt}}$ (gr/cm sec)	$\eta_{\text{calc.}}$ (gr/cm sec)	% error in $\eta_{\text{calc.}}$
3.8	0.4272	0.029	0.2401	0.5621	0.2586	0.70
3.6	0.675	0.029	0.2399	0.3554	0.1844	-0.51
3.4	1.076	0.034	0.2763	0.2568	0.1340	-2.56
3.2	1.697	0.038	0.3145	0.1853	0.0995	-1.64
3.0	2.689	0.045	0.3695	0.1374	0.0758	-1.45
2.8	4.272	0.053	0.4217	0.1011	0.0587	0.70
2.6	6.75	0.063	0.5190	0.0769	0.0466	1.30
2.4	10.76	0.076	0.6270	0.0583	0.0375	1.63
2.2	16.97	0.095	0.7812	0.0460	0.0306	0.57
2.0	26.89	0.12	0.9915	0.0369	0.0253	-0.57
1.8	42.72	0.16	1.2994	0.0304	0.0210	-1.08
1.6	67.5	0.21	1.7137	0.0254	0.0176	2.33
1.4	107.6	0.28	2.2847	0.0212	0.0148	-0.42
1.2	169.7	0.35	2.9111	0.0172	0.0136	3.14
1.0	268.9	0.49	3.9992	0.0149	0.0125	3.51
0.9	339.4	0.55	4.4878	0.0132	0.0116	-2.14
0.8	427.2	0.63	5.1633	0.0121	0.0107	3.31
0.7	537.4	0.77	6.3457	0.0118	0.0098	1.18
0.6	675.0	0.85	6.9517	0.0103		
0.5	851.0	1.00	8.2620	0.0097		

APPENDIX T

SUMMARY OF THE CONSTANT FLOW RATE EXPERIMENT  
DATA AND HERSCHEL-BULKLEY MODEL  
CALCULATION

$$f_{\text{expt}}^* = \left( \frac{\rho \Delta p}{M G_o} \right) \left( \frac{D_p}{L} \right) \left( \frac{\epsilon^3}{1 - \epsilon} \right)$$

$$f_{\text{calc}}^* = \frac{150}{N_{\text{Re,eff}}} + 1.75$$

$$\begin{aligned} \dagger \frac{1}{\eta_{\text{eff}}} = & \frac{4 \tau_y^{m+3}}{M^2 \mu_o (\tau_w^*)^4} \left( \frac{\tau_w^*}{\tau_y} - 1 \right)^{m+1} \left[ \frac{\left( \frac{\tau_w^*}{\tau_y} - 1 \right)^2}{m+3} \right. \\ & \left. + \frac{\left( \frac{\tau_w^*}{\tau_y} - 1 \right)}{m+2} + \frac{1}{m+1} \right] \end{aligned}$$

$$\dagger \dagger \frac{1}{\eta_{\text{eff}}} = \frac{150(1 - \epsilon)}{M D_p G_o \left[ \left( \frac{\Delta \rho p}{M G_o} \right) \left( \frac{D_p}{L} \right) \left( \frac{\epsilon^3}{1 - \epsilon} \right) - 1.75 \right]}$$

: Calculated from the Ergun equation

TABLE T-1. Results for the Constant Flow Rate Experiments for 0.50% P M C 400 Solution at 21°C

$Q, \frac{cc}{min}$	$G_0, \frac{gr}{cm^2 \cdot sec}$	$\Delta P, Psia$	$\frac{1}{\eta_{eff}} \left( \frac{cm \cdot sec}{gr} \right) + \frac{1}{\eta_{eff}} \left( \frac{cm \cdot sec}{gr} \right)$	$N_{Re,eff}$	$f^* \text{ calc.}$	$f^* \text{ expt}$	% error
Bed Properties: $D_p = .1621 \text{ cm}, L = 45.72 \text{ cm}, \epsilon = .4157, M = 1.0728$							
151.6	.4986	1.457	7.4121	1.0999	139.9	163.9	-17.18
136.4	.4486	1.418	6.5243	.8711	176	197	-12.13
112.0	.3684	1.365	5.4445	.5970	255	281	-10.30
95.7	.3148	1.320	4.6346	.4342	349	372	-6.60
84.4	.2776	1.264	3.7529	.3101	487	459	5.79
76.3	.2510	1.242	3.4422	.2571	587	551	6.12
20.2	.2309	1.230	3.2808	.2255	669	645	3.54
63.0	.2072	1.225	3.2151	.1940	777	833	-7.25
55.7	.1832	1.204	2.9498	.1608	936	1003	-7.12
48.6	.1599	1.167	2.5212	.1200	1254	1276	-1.79
44.2	.1454	1.134	2.1785	.0943	1594	1500	5.91
40.4	.1329	1.121	2.0532	.0812	1851	1774	4.15
37.8	.1243	1.118	2.0250	.0749	2006	2023	-0.84
33.5	.1102	1.110	1.9513	.0640	2347	2555	-8.85
30.1	.0990	1.088	1.7584	.0518	2899	3104	-7.06
27.5	.0905	1.050	1.4580	.0393	3820	3584	6.19
24.2	.0796	1.045	1.4214	.0337	4454	4611	-3.51
19.8	.0651	1.020	1.2483	.0242	6202	6729	-8.50
16.6	.0546	.970	.9480	.0154	9744	9097	6.64
12.4	.0408	.946	.8240	.0100	15004	15888	-5.90
10.5	.0345	.925	.7253	.0074	20274	21728	-7.17
8.9	.0293	.886	.5649	.0049	30616	28854	5.75
7.2	.0237	.860	.4968	.0033	45458	42806	5.83
6.5	.0214	.856	.4507	.0029	51728	52258	-1.03
5.0	.0164	.830	.3808	.0019	78951	86278	-9.28
Bed Properties: $D_p = .0579 \text{ cm}, L = 45.72 \text{ cm}, \epsilon = .3940, M = 1.0259$							
106.3	.3496	2.800	23.1840	.8398	182	198	-8.72
95.0	.3125	2.736	20.3568	.6591	231	242	-4.72
92.1	.3029	2.670	17.7074	.5557	273	251	8.20
84.0	.2673	2.635	16.4068	.4697	323	298	7.70
73.5	.2418	2.586	14.7017	.3683	411	381	9.25
65.8	.2164	2.574	14.3041	.3207	471	474	-0.59
60.2	.1980	2.500	12.0186	.2466	612	550	10.10
51.8	.1704	2.445	10.4966	.1853	813	726	10.70
45.4	.1493	2.418	9.8017	.1516	993	935	5.84
41.3	.1358	2.410	9.6022	.1351	1114	1127	-1.19
35.2	.1158	2.376	8.7861	.1054	1427	1528	-7.10
30.1	.0990	2.275	6.6500	.0682	2203	2001	9.17
23.9	.0786	2.215	5.5704	.0454	3307	3091	6.54
17.4	.0572	2.165	4.7697	.0283	5304	5706	-7.58
13.5	.0444	2.100	3.8536	.0177	8478	9185	-8.34
8.6	.0283	1.965	2.3538	.0069	21743	21156	2.70

TABLE T-2. Results for the Constant Flow Rate Experiments for 0.30% P M C 400 Solution at 21°C

$Q_{\text{min}}$	$G \frac{gf}{O \text{ cm}^2 \text{ sec}}$	$\Delta P, \text{Psia}$	$t \frac{1}{n_{\text{eff}}} (\frac{\text{cm sec}}{gr})$	$t + \frac{1}{n_{\text{eff}}} (\frac{\text{cm sec}}{gr})$	$N_{\text{Re,eff}}$	$f^* \text{ calc.}$	$f^* \text{ expt}$	% error
Bed Properties: $D_p = .1621 \text{ cm}$ , $L = 45.72 \text{ cm}$ , $\epsilon = .4157$ , $M = 1.0728$								
133.6	.4392	1.265	7.1881	6.3229	.9396	163	183	-12.17
119.4	.3925	1.180	5.4280	6.0492	.6341	240	214	10.85
100.2	.3294	1.165	5.1534	5.1300	.5052	300	300	0.14
91.4	.3005	1.158	5.0287	4.7037	.4497	337	358	-6.21
83.5	.2745	1.132	4.5847	4.3923	.3746	404	420	-3.98
74.2	.2439	1.115	4.3101	3.9588	.3129	483	524	-8.51
66.4	.2183	1.060	3.5027	3.7252	.2276	663	622	6.12
52.0	.1709	1.000	2.7529	3.0883	.1400	1075	957	10.97
41.4	.1361	.965	2.3733	2.5470	.0961	1564	1456	6.93
33.6	.1105	.952	2.2424	2.0953	.0737	2039	2179	-6.88
27.7	.0911	.914	1.8896	1.7989	.0512	2933	3077	-4.90
20.0	.0657	.846	1.3606	1.4012	.0266	5643	5476	2.95
15.1	.0496	.818	1.1775	1.0939	.0174	8624	9290	-7.72
12.9	.0424	.772	.9160	.9908	.0116	12935	11999	7.23
9.4	.0309	.749	.8023	.7442	.0074	20274	21919	-8.12
7.0	.0230	.706	.6173	.5877	.0042	35718	37290	-4.40
5.7	.0187	.678	.5147	.4975	.0029	51728	54174	-4.73
Bed Properties: $D_p = .0597 \text{ cm}$ , $L = 45.72 \text{ cm}$ , $\epsilon = .3940$ , $M = 1.0259$								
109.2	.3590	2.100	36.3074	29.0741	1.3505	115	14140	-22.20
100.0	.3287	2.040	31.9052	27.3570	1.0866	142	163	-15.16
87.8	.2886	1.980	27.8989	24.6936	.8342	183	205	-11.83
72.3	.2377	1.911	23.7517	21.0203	.5849	260	291	-11.94
68.6	.2255	1.872	21.6133	20.3471	.5050	301	317	-5.48
61.4	.2018	1.832	19.5666	18.5879	.4091	370	388	-4.82
55.5	.1824	1.751	15.8511	17.5669	.2996	504	454	9.95
50.9	.1673	1.730	14.9767	16.2991	.2596	581	533	8.31
42.4	.1394	1.722	14.6528	13.6308	.2116	712	764	-7.25
35.7	.1174	1.684	13.1821	11.7314	.1603	939	1053	-12.11
29.8	.0980	1.620	10.9470	10.1751	.1112	1352	1454	-7.51
26.7	.0878	1.541	8.5762	9.5817	.0780	1927	1723	10.57
22.1	.0726	1.532	8.3316	7.9670	.0627	2396	2505	-4.56
18.9	.0621	1.460	6.5488	7.1496	.0421	3566	3362	8.54
16.0	.0526	1.415	5.5828	6.2476	.0304	4938	4407	10.75
13.5	.0444	1.384	4.9789	5.3912	.0229	6554	6050	7.69
11.6	.0381	1.376	4.8308	4.6528	.0191	7857	8169	-3.97
8.4	.0276	1.321	3.8957	3.5105	.0111	13517	14944	-10.56

TABLE T-3. Results for the Constant Flow Rate Experiments for 0.50% P M C 25 Solution at 21°C

$Q, \frac{cc}{min}$	$G, \frac{gr}{cm^2sec}$	$\Delta P, \text{Psia}$	$\frac{1}{\eta_{eff}} \left( \frac{cm \cdot sec}{gr} \right)$	$\frac{1}{\eta_{eff}} \left( \frac{cm \cdot sec}{gr} \right) + \frac{1}{\eta_{eff}} \left( \frac{cm \cdot sec}{gr} \right)$	$N_{Re, eff}$	$f^*_{calc.}$	$f^*_{expt}$	% error
Bed Properties: $D_p = .1621 \text{ cm}$ , $L = 45.72 \text{ cm}$ , $\epsilon = .4157$ , $M = 1.0728$								
90.4	.2973	.695	9.5194	7.7739	.8423	182	220	-21.16
82.8	.2723	.672	8.385	7.3561	.6795	224	253	-12.82
70.3	.2312	.644	7.1395	6.5062	.4913	309	337	-9.13
64.5	.2121	.631	6.6091	6.0872	.4172	363	392	-7.98
55.2	.1815	.612	5.8858	5.3648	.3179	475	519	-9.18
47.4	.1559	.570	4.4915	4.9442	.2084	723	656	9.30
41.0	.1348	.552	3.9739	4.4117	.1594	945	849	10.11
35.6	.1171	.541	3.6796	3.9085	.1282	1174	1103	6.01
29.4	.0967	.532	3.4508	3.2806	.0993	1514	1590	-5.01
24.0	.0789	.514	3.0241	2.7695	.0710	2116	2308	-9.06
18.4	.0605	.470	2.1421	2.3218	.0386	3889	3590	7.70
14.0	.0460	.438	1.6295	1.8940	.0223	6730	5787	14.01
11.2	.0368	.429	1.5468	1.5468	.0165	9094	8856	2.62
9.0	.0296	.420	1.3836	1.2707	.0122	12299	13401	-8.96
6.7	.0220	.392	1.0558	1.0119	.0069	21743	22641	-4.13
4.9	.0161	.360	.7541	.8063	.0036	41670	38825	6.83
Bed Properties: $D_p = .0597 \text{ cm}$ , $L = 45.72 \text{ cm}$ , $\epsilon = .3940$ , $M = 1.0259$								
82.2	.2703	1.315	47.1321	34.9000	1.3199	117	155	-32.31
74.8	.2460	1.254	39.1832	33.2589	.9987	154	179	-16.46
72.0	.2368	1.168	29.6784	34.3707	.7281	209	180	14.09
63.3	.2082	1.152	28.1135	30.5757	.6064	251	229	8.71
56.2	.1848	1.130	26.0599	26.1153	.4990	304	285	6.28
46.7	.1536	1.118	24.9863	23.1669	.3976	381	408	-7.15
40.1	.1319	1.095	23.0181	20.2908	.3146	480	543	-13.06
35.3	.1161	1.020	17.3704	19.1633	.2089	722	652	9.64
28.2	.0927	.985	15.1098	15.8305	.1451	1037	988	4.75
24.2	.0796	.976	14.5645	13.7127	.1201	1252	1328	-6.03
18.3	.0602	.925	11.7375	10.9369	.0732	2053	2201	-7.23
13.4	.0441	.850	8.3266	8.7160	.0380	3951	3768	4.63
10.9	.0358	.815	7.0080	7.3784	.0260	5773	5483	5.02
9.5	.0312	.801	6.5252	6.5423	.0211	7113	7094	0.26
7.8	.0257	.784	5.9714	5.5054	.0159	9437	10234	-8.44
6.1	.0201	.740	4.6952	4.5615	.0098	15310	15792	-3.15
4.7	.0155	.695	3.6050	3.7452	.0058	25867	24941	3.57

TABLE T-4. Results for the Constant Flow Rate Experiments for 0.30% P M C 25 Solution at 21°C

$Q_{\min}$	$\frac{CC}{\min}$	$G_0$	$\frac{gr}{cm^2sec}$	$\Delta P, Psia$	$t \frac{1}{n_{eff}} (\frac{cm \ sec}{gr})$	$t + \frac{1}{n_{eff}} (\frac{cm \ sec}{gr})$	$N_{Re, eff}$	$f^* \text{ calc.}$	$f^* \text{ expt}$	% error
Bed Properties: $D_p = .1621 \text{ cm}$ , $L = 45.72 \text{ cm}$ , $\epsilon = .4157$ , $M = 1.0728$										
94.5		.3106		.562	12.8010	10.0771	1.1833	130	163	-25.13
85.9		.2824		.540	11.1047	9.5210	.9333	164	189	-15.09
73.8		.2426		.518	9.5756	8.5083	.6914	220	246	-11.59
68.6		.2255		.504	8.6847	8.1217	.5829	261	277	-6.20
63.7		.2094		.475	7.9302	7.9980	.4381	346	303	12.40
54.7		.1798		.464	6.4663	7.0202	.3460	437	401	8.24
44.4		.1460		.454	5.9823	5.8177	.2599	581	595	-2.47
37.7		.1239		.442	5.4365	5.0673	.2005	752	805	-7.10
24.2		.0796		.385	3.3174	3.7332	.0786	1912	1698	11.19
17.7		.0582		.374	2.9901	2.8085	.0518	2899	3085	-6.41
13.7		.0450		.340	2.1239	2.3882	.0284	5285	4691	11.24
10.8		.0355		.324	1.7860	1.9768	.0189	7940	7183	9.53
8.2		.0270		.315	1.6139	1.5463	.0130	11542	12073	-4.60
6.8		.0224		.306	1.4539	1.3205	.0097	15467	17040	-10.17
5.6		.0184		.284	1.1109	1.1687	.0061	24594	23438	4.70
Bed Properties: $D_p = .0597 \text{ cm}$ , $L = 45.72 \text{ cm}$ , $\epsilon = .3940$ , $M = 1.0259$										
63.1		.2074		.952	47.3910	36.9314	1.0184	151	191	-26.67
55.7		.1831		.910	40.2887	34.0523	.7643	200	234	-17.14
48.5		.1594		.871	34.4072	30.9247	.5682	267	295	-10.28
43.4		.1427		.845	30.8450	28.5078	.4560	332	357	-7.39
34.6		.1137		.774	22.4638	24.7615	.2646	570	516	9.54
29.8		.0980		.756	20.6301	21.8332	.2095	719	678	5.77
22.8		.0749		.734	18.5372	17.1697	.1439	1046	1127	-7.76
19.0		.0625		.685	14.4270	15.3461	.0934	1609	1511	6.12
15.3		.0503		.652	12.0561	12.9710	.0628	2392	2221	7.15
12.2		.0401		.639	11.2037	11.0961	.0465	3229	3424	-6.03
10.0		.0329		.612	9.5722	9.0347	.0326	4605	4872	-5.80
9.0		.0296		.580	7.8671	8.5765	.0261	6228	5705	8.39
8.0		.0263		.568	7.2877	7.7809	.0199	7541	7076	6.17
6.8		.0224		.548	6.3908	6.8685	.0148	10139	9412	7.17
5.2		.0171		.534	5.8120	5.3805	.0103	14566	15737	-8.03

MICHIGAN STATE UNIV. LIBRARIES



31293017478755